Condition monitoring of crossbonded transmission cable systems

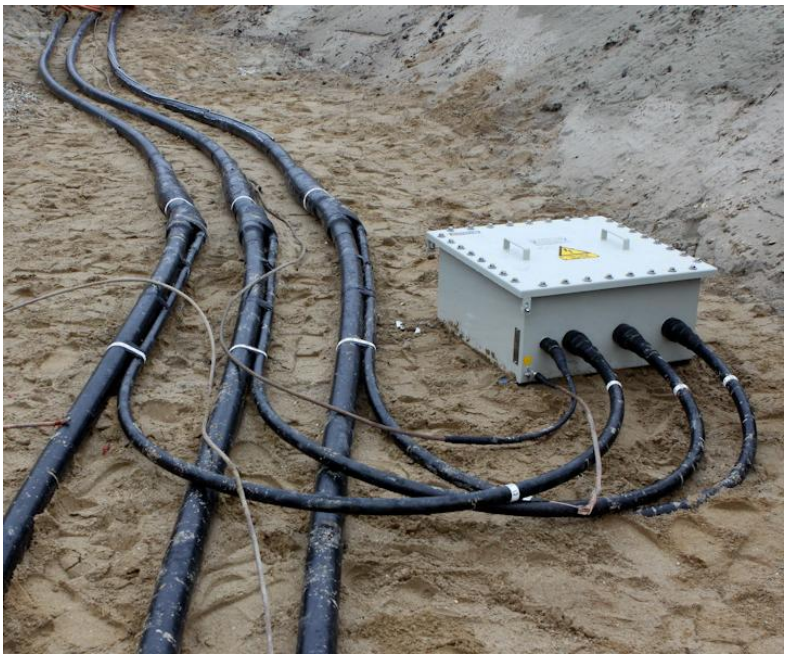

MASTER THESIS, AUTUMN 2011 - SPRING 2012

GROUP EPSH3-4: 933-1031

BOARD OF STUDIES OF ENERGY

AALBORG UNIVERSITY
STUDENT PROJECT

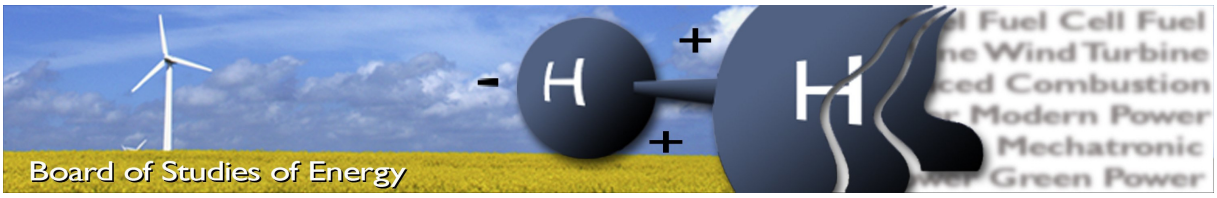

Title:	Condition monitoring of crossbonded transmission cable systems
Semester:	9th and 10th.
Project period:	01.09.11 to 31.05.12
ECTS:	50
Supervisors:	Claus Leth Bak (AAU), Christian Flytkjær (Energinet.dk / AAU) Peter Rønne-Hansen (N1)
Project group:	933-1031

Morten Thule Hansen

Kasper Schultz Pedersen

Copies: 4
Pages, total: 281
Appendix: A-H
Supplements: Attached DVD

SYNOPSIS:

This report study the possibility of monitoring the condition of the link boxes in a cross bonded cable line. The study is focused on how the condition can be determined from an impedance measurement, in order to make the method available, line impedance measuring equipment is used. The measuring technique is improved to gain high sensitivity in respect to screen circuit faults. This is achieved, using ungrounded voltages sources and increased measuring frequency. A DIgSILENT simulation model of the cable line FRT-NOR is developed and verified against field measurements. The simulation model is used for simulation of four study cases, which represent possible link box faults. From the study cases the largest detectable fault resistances are determined to $39 - 68\Omega$ according to the type of fault. Finally there are given suggestions of how the impedance method could be used at cable lines consisting of more than one major section. It is recommended to make strategic chosen link boxes easy accessible, when construction new cable lines.

By signing this document, each member of the group confirms that all participated in the project work and thereby all members are collectively liable for the content of the report.

Preface

This report is written as documentation of the project work made by the group EPSH-1031 at Aalborg University, Institute for Energy Technology. The project was performed in corporation with the Danish transmission company N1. The contact person from N1 was Peter Rønne Hansen.

The project period comprises the last two semesters of the master programme in Electrical Power Systems and High Voltage Engineering (EPSH) and covers a total work of 50 ECTS points.

The thesis comprises XX main parts and an appendix part.

A CD is attached, containing the report in digital format (PDF), developed MATLAB scripts, a network model of the 150kV transmission line FRT-NOR in DigSILENT Power Factory.

Literature references are shown as [**i, p.k**], where **i** is the number of the literature in the reference list, which can be found after the main report at page 135. **k** is the page number in the given literature, the page number is omitted when there are referred to general conclusions.

References to figures, tables and equations are given as figure **X.Y**, table **X.Y**, and equation **X.Y** where **X** refers to the chapter number and **Y** refers to the figure, table or equation number, respectively.

The authors would like to thank Peter Rønne Hansen from N1 for sharing relevant information and for providing the possibility of performing measurements at the new cable line FRT-NOR. Also thanks are given to Ph.D. student Christian Flytkjær Jensen, for a number of useful discussions and professional support regarding cable lines. Professor Claus Leth Bak for professional discussions, regarding cable lines and measuring technique. Engineering assistant Henrik Koch from the Section of Environmental Engineering at Aalborg University for providing information concerning conductivity of rain water and for providing conductivity measuring equipment.

Summary

On the 4th of November 2008, the Danish government decided, that all transmission lines with a voltage level of 150kV must be undergrounded gradually, in order to reduce the visual pollution caused by overhead lines (OHL). The undergrounding should be performed during the next 30 years. Also it was decided that all new 400kV lines will be performed as cable lines.

Approximately 3000km of underground cables are going to be installed. In connection with the restructuring, the grid is re-designed to be better suited for further implementation of renewable energy.

Under-grounding a large transmission grid has never been performed before and therefore operation and maintenance experiences do not exist. New maintenance strategies shall be developed, in order to ensure a reliable power supply. High voltage cables are provided with a metallic screen, which provides a low resistance path for charging current, to flow back to the source. The bonding of the screens may be performed in different ways, but for long cross country cables, cross bonding is typical used. Cross bonding requires that the cable screen is cross connected, every 1-3 kilometer along the line. The cross connection is performed in link boxes, which for many cases, are placed underground next to the cables. Maintenance experience has shown defects such as damaged arresters, corroded connections, and leaky boxes. A survey in a certain area has shown that up to 80% of the link boxes were faulty.

As mentioned most of the boxes are placed underground, next to the cables, hence the boxes are not easy to access. The cooperation company N1 has estimated the cost of 40,000 Dkk, for accessing one line box. The manufacture has prescribed visual inspection of the boxes every second year.

Visual inspection is costly and therefore it is of great interest to be able to determine the condition of the link boxes without having physical access to the boxes. Therefore the initial problem is:

Can the condition of the link boxes can be determined without having physical access to the boxes?

This study is based on a state of the art analysis, of what literature there may be found, within the area. The analysis showed that there is a very little experience within the specific area. For this reason this study will be based on known fault detection and localization methods. It is decided to base this work on impedance measurements, because this makes the developed methods, easy to implement for the transmission companies.

The screen circuit of cross bonded cable lines is studied, in respect to screen to screen faults and to Screen to ground faults. It was found that main challenge is to detect, a large fault resistance, in a low impedance screen circuit. It was found that the detectability increases if the frequency of the measuring voltage is increased, due to the increase of reactance.

The earthing resistance at the cross bonding points, were found to cause large difficulties for detection of screen to ground faults. In order to suppress the importance of the ground resistance it was favorable to use ungrounded measuring voltage. Thereby a ground fault will provide a potential displacement of the entire screen circuit, which increases the detectability. Also it was found that the detectability of ground fault is dependent on the earthing resistance at the end of the major section.

Four study cases, representing possible screen circuit fault are chosen in cooperation with N1. In order to analyze the study cases, there is made a DIgSILENT simulation model. The simulation model is validated according to field measurements performed on the new established 150kV cable line FRT-NOR. The validation compared simulated and measured impedances, both for healthy screen circuit and for two different fault scenarios. The faults were measured and simulated by applying a 2.5Ω resistance in the first and second link box accordingly. Furthermore the model is validated for three different frequencies. The validation showed that, by increasing the distance between the cables, the model represents the actual cable line within $\approx 3\%$, for both healthy and fault cases.

The validated simulation model is used to perform the following four study cases:

- Screen-screen fault
- Screen-ground fault
- Disconnected screen conductor
- Three screen to ground short circuit

For the two first study cases, the largest detectable fault resistances are determined to 55 and 68Ω.

The disconnected conductor provided a large increase of apparent screen impedance. Thereby this is detectable, but furthermore it is possible to locate this fault based on the charging current, which is proportional to the distance to the fault.

The three screens to ground fault, is to represent a water filled link box. The largest detectable fault resistance is determined. In order to study if a water filled link box is detectable there is performed a full scale link box test. A link box identical to the used link boxes, at the FRT-NOR cable line is filled with water and the resistance between the connection points are measured to $\approx 35\Omega$.

Finally cable lines with several major sections are considered. It was found that for cable lines with more than two major sections; at least one line box should be accessed, in order to measure the entire screen circuit. Furthermore there is suggested a method where the screen circuit of the major sections are series connected. For the series connection a significantly larger fault resistance is detectable.

The findings and recommendations are summarizes in the following:

- There is developed a measuring technique, suitable for measuring screen circuit faults up to 9 times the detectable fault resistance of one major section.
- Largest detectable fault resistances are determined.
- It is highly recommended to place strategically chosen link boxes at accessible locations.

As mentioned in the state of the art analysis, the subject of this study has until now, not been given much attention. Therefore this project may be seen as the preliminary work, within the area.

Contents

Chapter 1

Introduction

The 4th of November 2008 published the Danish government guidelines for the future development of the Danish electrical power grid. The main purpose of the guidelines is to meet the growing interest of keeping the nature untouched by technical installations [8].

In order to meet the guidelines requirements it has been decided to put all 132kV and 150kV transmission lines into the ground as high voltages cables. This will be done over the next 30 years. Approximately 3000km of underground-cables are going to be established and the transmission grid at these voltage levels are going to be re-designed so that the grid will be better suited for further implementation of renewable energy sources such as wind power [8]. In the past the load flow of electric power in Jutland was north and south where it nowadays is more west to east. The present and the future layout of the transmission grid in Denmark is illustrated in figure 1.1.

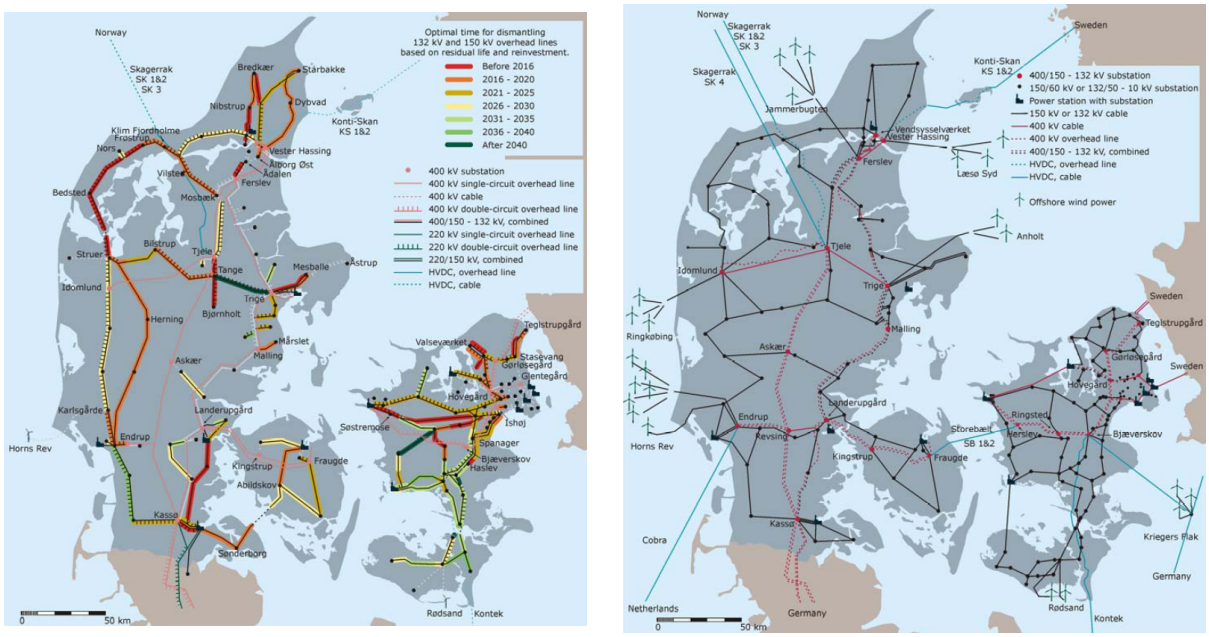

Figure 1.1: To the left is the Danish transmission grid as it is today. To the right is the future Danish transmission grid [8].

Under-grounding a large transmission grid has never been done before and therefore operation and maintenance experiences do not exist. It is therefore of great interest to develop new maintenance strategies

when making such a large conversion of the existing transmission grid and still ensure a high reliability of supplying electric power.

High Voltage cables (HV cables) are provided with a metallic screen. The metallic screen provides a low resistance path for charging and fault currents to flow back to the source [50, p.119]. Long cable transmission-lines are normally cross bonded. This is done to minimize the induced voltage and losses in the screen [45, p.61]. Figure 1.2 illustrates a cross bonded section of a cable line. The cross bonding is done in four link boxes where the screen is transposed in link box B and C. These link boxes are also provided with surge arrestors which protects the screen against transient over-voltages at fault conditions. The grounding of the screen is done in link box A and D.

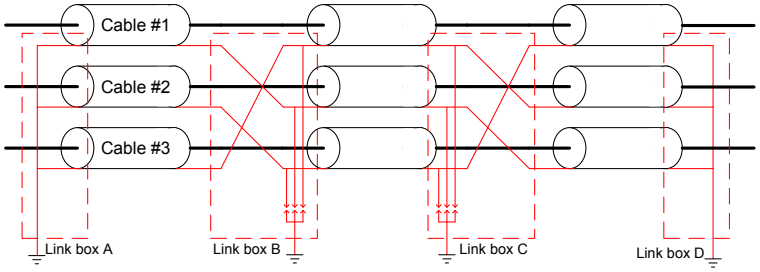

Figure 1.2: Cross bonded cable section. Red marked lines illustrates connections inside the link boxes.

The link boxes are for cross country cable lines normally located underground near the cable system, as shown in figure 1.3. Maintenance experience has shown different defects such as damaged surge arresters, corroded screen connections and leaky link boxes. A survey in a certain area has shown that up to 80% of the link boxes at a cross bonded transmission cable system was faulty [35].

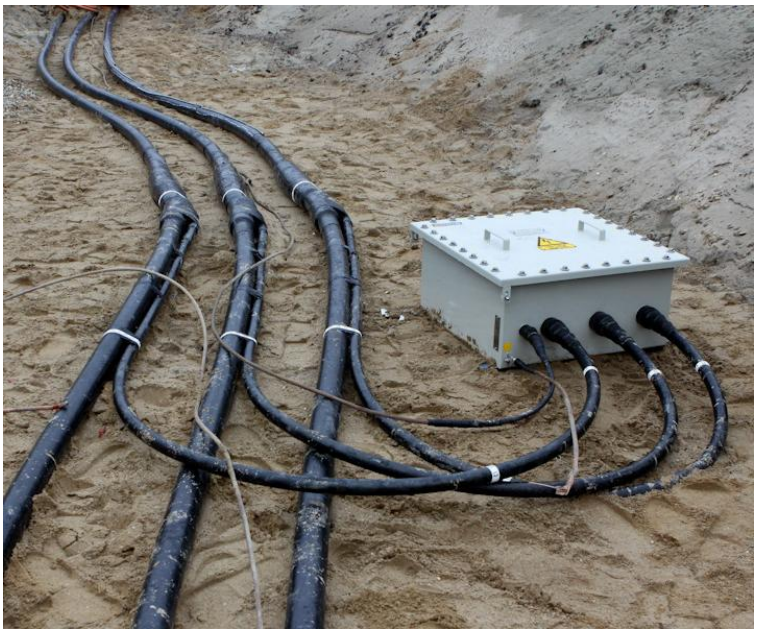

Figure 1.3: Link box placed approx 1.5m underground, next to the cable system.

It is important to ensure that the cross bonding points (Link box A-D i figure 1.2) are in good condition,

in order to keep a high reliability of the transmission system. To investigate the condition of the cross bonding points the cable manufacture prescribes visual inspection of the link boxes [37]. This method is time consuming and very expensive. The Danish Transmission company N1 expects that it will cost approx. 40,000 Dkk and take about 4 working days to do a visual inspection of a single link box. The expenses include, among other things, compensation to the landowner for field damage, rental excavator and etc.. This is the reasons why it is the, by far the most preferred method to be able to determine the condition of the link boxes only from measurements at the end of the cable line.

Several hundred link-boxes are going to be installed the coming years in order to fulfill the earlier mentioned guidelines. N1 have no cost and time effective way to determine the condition of the cross bonding points in a cross bonded transmission cable system. Therefore are N1 and other TSO's interested to develop measuring techniques that can monitor the condition of cross bonded transmission cable systems. This leads to the following initiating problem:

"Can the condition of the link boxes in a cross bonded transmission cable system be determined without having physical access to them?"

Chapter 2

System description of the cable line FRT-NOR

The system description presents physical and electrical data for the cable system under consideration. All data is provided by the co-operating company N1. The cable system is used for field measurements 1, 2 and 3, for which the test reports are given in Appendix D, E and F.

The system that has been used for field measurement is described in this section. The cable line is located in the North Western part of Jutland i Denmark as shown in figure 2.1. The cable line connects the two 150kV substations Frøstrup (FRO) and Nors(NOR). The cable line is established in the autumn 2011, and replaces the excising overhead line (OHL) shown in figure 2.2. The measurements are performed in January 2012, before the cable line is taking into service.

Figure 2.1: Geographical placing of the cable line at which measurements are performed.

The cable line has a total length of 15.1km shown in figure 2.2.

The system is considered for an estimated earth temperature of $5°C$. This is because the cable system is measured before the line is taken into service. The operation temperature is $60°C$ for the conductor and $52°C$ for the cable screen according to the data sheet.

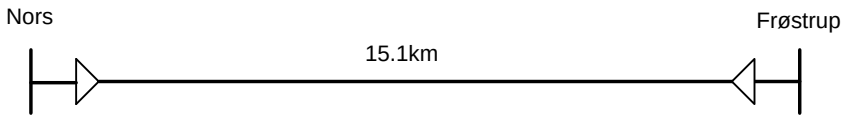

Figure 2.2: The 150kV cable line between Frøstrup and Nors.

2.1 The cable

Physical placing of the cables

The cable line consist of three parallel coaxial cables placed in flat formation 1.2m below the ground surface. The horizontal distance between the cables is 0.3m as shown in figure 2.3.

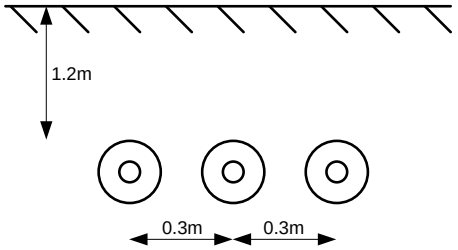

Figure 2.3: Cross section layout of the cable line between Frøstrup and Nors. The three coaxial cables are placed in flat formation with 0.3m between the cables and 1.2m below the ground surface.

The line represents one major cross bonded section, followed by two sections using single point bounding. The three minor sections of the cross bonded section is 3840m each. The two sections using single point grounding are 1280m and 2300m accordingly. The line is transposed and the phases shift position at four places, next to joint number 3,6,10 and 11 see figure 2.4. The cross bonded screen is also transposed, meaning that the cable screen besides shifting phase also shifting physical placing at the cross bonding points at joint 3 and 6 as shown in figure 2.4.

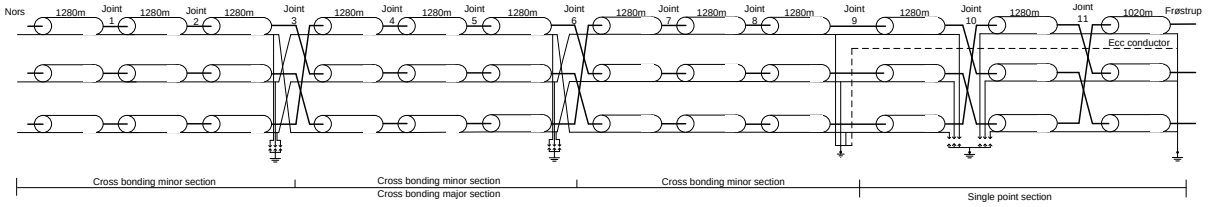

Figure 2.4: Bonding schematic for the cable line.

The two single point bounding sections are placed one after another next to substation FRT. For this part the system is also equipped with a earth continuity conductor (ecc). This is performed by a non-insulated 95mm^2 copper wire placed in the ground between the cables. The purpose of this is providing a low impedance return path for ground faults and minimize possible earth potential rise during ground faults [23, p.11].

Cable parameters

The coaxial cables is produced by the French company Nexans and is a XLPE 150kV power cable. The cable is made of a number of layers as shown in figure 2.5.

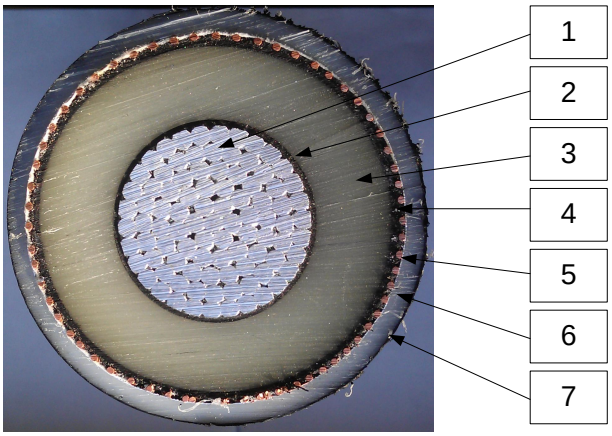

Figure 2.5: Coaxial cable made of a number of layers. 1: Conductor, 2: Inner semi-conducting layer, 3: Insulation, 4: Outer semi-conducting layer, 5: Copper wired screen, 6: Aluminum foil, 7: Outer covering.

The insulation is made of Cross-linked polyethylene(XLPE). At both the inner and outer surface of the insulation there is a semi-conductive layer to ensure homogeneous radial electric field distribution [45, p.31]. The copper wired screen is made of 63 copper wires each with a diameter of 1.39mm, in total performing a cross section area of 95mm^2. The aluminum foil is separated from the copper wires by semi conductive swelling tape. The aluminum foil and the copper wires are connected at the joints and at the terminations of the cables[16, p.36]. The aluminum foil and the swelling tape prevent moisture and water from penetrating into the cable radial and longitudinal accordingly [45]. The outer covering is made high-density polyethylene(HDPE) which provide protection from the surrounding environment and can withstand high temperature. The outer most layers are a black semi conductive layer.

Cable parameters are obtained from the data sheet provided from the manufacture by the co-operating company N1. Relevant values are presented in table 2.1.

Layer	Parameter	Value	Material
Conductor	Thickness	21mm	Al
Inner semi-conducting layer	Thickness	1.0mm	extruded semi-conduction XLPE
Insulation	Thickness	16.0mm	XLPE
Outer semi-conduction layer	Thickness	2.1mm	extruded semi-conduction XLPE
Copper wire screen	Cross section	95mm^2	Cu
Aluminium screen	Thickness	0.2mm	Al
Outer covering	Thickness	3.8mm	HDPE

Table 2.1: Cable parameters from data sheet.

2.2 Bonding cable

The bonding cable is the connection between the joints and the link boxes. It is a coaxial cable with a center conductor of 240mm^2 copper and a screen of 240mm^2 copper. The cable is shown in figure 2.6.

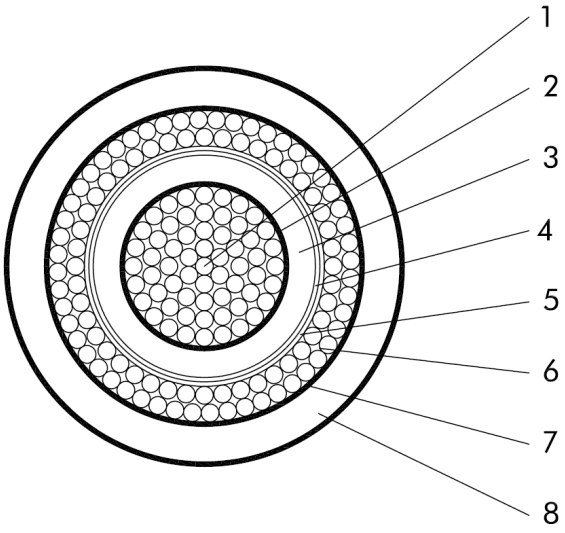

Figure 2.6: Coaxial bonding cable made of a number of layers. 1: Conductor, 2: Inner semi-conducting layer, 3: Insulation, 4: Outer semi-conducting layer, 5: Bedding/sealing, 6: Copper wired screen, 7: Bedding/sealing, 8: Outer covering.

The layers of which the is made is listed in table 2.2.

Layer	Parameter	Value	Material
Conductor	Thickness	8.5mm	Cu
Inner semi-conducting layer	Thickness	≥ 0.3mm	extruded semi-conduction XLPE
Insulation	Thickness	3.4mm	XLPE
Outer semi-conduction layer	Thickness	$0.3-0.6$mm	extruded semi-conduction XLPE
Bedding/Sealing	Thickness	-	semi-conduction swelling tape
Copper wire screen	Cross section	*nom*.240mm^2	2 layers Cu
Bedding/sealing	Thickness	-	Swelling Tape
Outer sheath	Thickness	4.0mm	HDPE

Table 2.2: Bonding cable parameters from data sheet.

2.3 Link box

The link box is a painted metallic box as shown in figure 2.7 and 2.8. The box is placed in the ground next to the cables as shown in figure 1.3 in chapter 1.

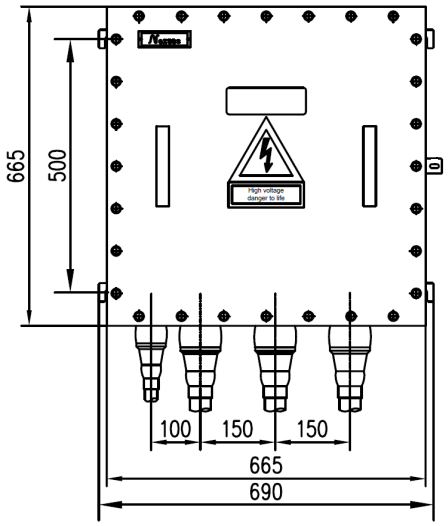

Figure 2.7: Engineering drawing of a Link box, all measurements are in cm.

Figure 2.8: Installed link box from the considered cable line, placed at joint no.10.

The connections from the cable screens to the link boxes are performed by bonding cables, which is the coaxial cables shown in figure 2.6. The bonding cable is connected to the cables by premolded Sectionalizing Straight Joints shown in figure 2.9. From the joint to the link box center conductor of the bonding cable forms connection to the cable screen at one side of the joint and the screen of the bonding cable form connection to the cable screen at the other side of the joint.

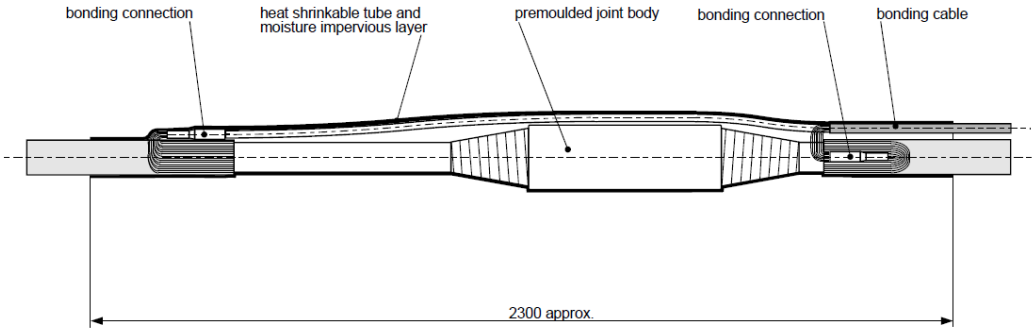

Figure 2.9: Premolded Sectionalizing Straight Joints, used for connection of cables and cross bonding of screen.

For the considered line three different link box types are used: Cross bonding link box, solid grounding link box and single point bounding link box. These may be seen in figure 2.10, 2.11 and 2.12 accordingly.

1 Cabinet
2 Surge arrester
3 Support insulators
4 Gland for coaxial cable
5 Gland for earthing cable
6 Fixing clamp
7 Cable end fixing clamp
8 Bus bars
9 Disconnectable crossing bar
10 Earthing bar bridge type
11 Protection cover
12 Box earthing bar
13 Blocking rod of incorrect pos.
14 Heat shrinkable tube

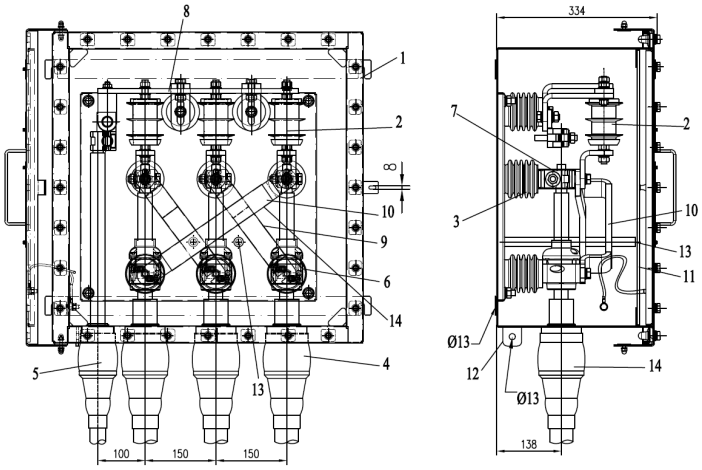

Figure 2.10: Cross bonding link box placed at joint 3 and 6.

1 Cabinet
2 Support insulators
3 Gland for coaxial cable
4 Gland for earthing cable
5 Fixing clamp
6 Cable end fixing clamp
7 Earthing bus bar
8 Disconnectable earthing bar
9 Protection cover
10 Box earthing bar
12 Heat shrinkable tube

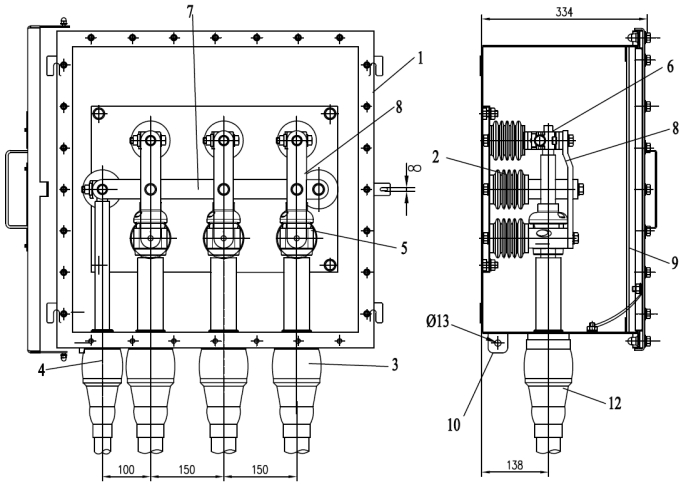

Figure 2.11: Solid earthing link box placed at joint 9.

1 Cabinet
2 Surge arrester
3 Support insulators
4 Gland for coaxial cable
5 Gland for earthing cable
6 Cable end fixing clamp
7 Bus bars
8 Support bar
9 Adjustable support bar
10 Coaxial fixing clamp
11 Protection cover
12 Box earthing bar
13 Door fixing bolts

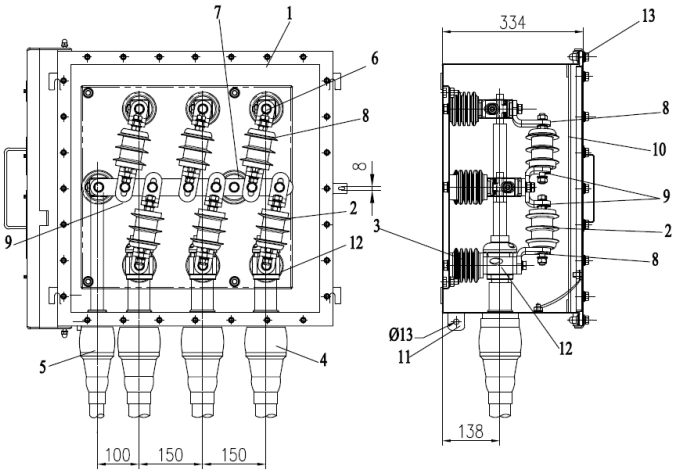

Figure 2.12: Single point bounding link box placed at joint 10.

During the installation the link boxes are filled by compound, as shown in figure 2.13. The compound prevents water or moisture in the link box from penetrating into the cables.

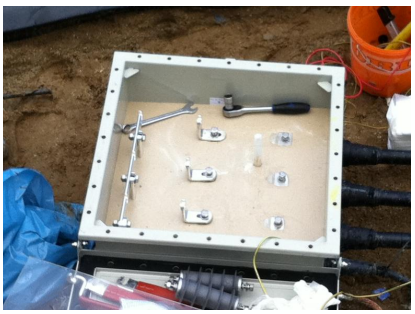

Figure 2.13: Link box during installation. It may be seen that the bottom is covered by compound.

2.4 Screen voltage Limiters

The screen voltage limiters(SVL) are placed inside the link boxes. The purpose of the SVL is limitation of the screen voltage from lightning impulses and switching surges [44] and not power frequency. The system under consideration uses the Zink Oxide(ZnO) SVL type, housed in gray silicon. The used SVL is shown in figure 2.14.

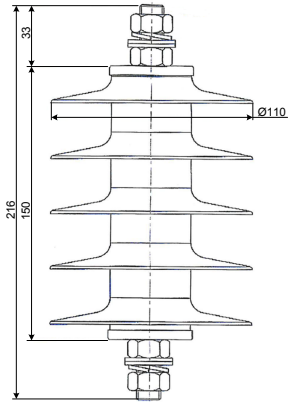

Figure 2.14: Engineering drawing of a SVL, all measurements are in [mm].

Ratings of the SVL from the data sheet is given in table 2.3.

Parameter	Value
Rated voltage(U_r)	10.0kV
Continuous operating voltage(U_c)	8.5kV
Rated current(I_r)	10.0kA

Table 2.3: SVL parameters.

U_r is the maximum permissible r.m.s. value of power-frequency voltage between its terminals at which it is designed to operate correctly under temporary overvoltage conditions. U_c is the maximum designated permissible R.M.S. value of power-frequency voltage that may be applied continuously between the arrester terminals [22, p.23].

2.5 Earthing points

The co-operations company N1 has provided earthing resistances for three points of the cable line see table 2.4. The earthing resistances are measures in May 2011 by HEF (Himmerlands elforsyning).

Position	Resistance [Ω]
Joint 3	0.2
Joint 6	7.0

Table 2.4: Earthing resistances for some specific points of the cable line, measured by HEF.

The joint numbers are shown in figure 2.4.

Chapter 3

Analysis of cross bonded cable systems

This chapter will first provide a state of the art analysis, where it is studied what literature there might be found in the area of this project. This is followed by a review of different bonding schemes used for HV cable lines, a special focus is given to the cross bonding method, which is typically used for long cross country cable lines. The link boxes in cross bonded cable systems are divided into two categories, and possible link box faults are presented for both types. In the final part three measuring techniques, and their ability to be used for screen circuit determination is discussed.

3.1 State of the art analysis of link box condition monitoring

From the introduction it was explained that the purpose of this study is to determined the condition of the link boxes, without having physical access to them.

A literature study is carried out, in order to find the available literature within specific field of: *Determination of the condition of link boxes, without having physical access to them.* To the authors knowledge, there exist very little literature on the specific area, of link box condition determination. There was found literature of three areas which relation to the subject of this study:

- Sheath voltage profile and maximum sheath voltage.
- Dimensioning of, and environmental influences of SVLs.
- Fault location on OHL and cable systems.

Sheath voltage profile and maximum sheath voltage
In the literature there may be found studies of screen voltage profiles for different bonding schemes and earthing resistances [14].

The IEEE guide for bounding consider the maximum sheath voltage [23]. This must not exceed $65-90$V throughout the whole length of the cables under normal operating conditions. In this contest, according to the IEEE guide for substation grounding [25] the maximum sheath voltage at the cable ends should not exceed 50V.

The IEEE Std. 575 suggested the application of approximate equations in order to calculate the induced voltages and currents at cable sheaths. In the new revised form IEEE Std. 575-1988 [23] suggests that

the induced voltages must be calculated for each case using proper simulations.

The IEEE design guide for installation of cable systems in substations suggest that, metallic sheath/armor should be solidly grounded at one or more points so that they operate at or near ground voltage at all times [24].

Environmental impact on the SVL
The functionallity of the SVLs according to environmental affection such as moisture, are considered in [33][44]. Important parameters according to accurate dimensioning of SVL are considered in [38] [40]. The sheath voltage at the cross bonding points are considered in relation to lightning transients of combined OHL and cable lines in [41] [39].

Fault location on OHL and cable systems
Several articles consider how to determine the location of a fault in an OHL system. [1] [9] consider what there exist of fault location techniques.

An IEEE guide provide and discusses impedance and travelling wave based methods for detection and location [26]. Another IEEE guide provide techniques for fault location techniques on shielded power cables [27].

A Cigré guide considers standing screen voltage under normal and faulty condition [2]. Special bounding are discussed and SVL type and placing are considered.

Summary state of the art
None of the references consider the condition of the link boxes in which the cross bondings are performed and the SVLs are placed. The Cigré report states that the SVL are placed in housing sealed from environmental affections.

3.2 Screen bounding and grounding methods for cable lines

The screen circuit is of vital importance of any underground cable system. Are the screen circuit not in proper condition, the protection equipment such as SVL, might not work properly causing serious risk of cable damage. Also the ampacity might be reduced due to possible increased screen current and enlarged heat dissipation in the cable. If the cable temperature is not monitored, there is a risk of overheating the cable, causing rapid aging and possible risk of cable damage.

3.2.1 Single point grounding

The most simple is to connect one end of the screen to ground and leave the other end open. In this case voltage is induced in the cable screen, because the screen conductor is located in a magnetic field, produced by the conductor current. The magnetic field generates force acting on the electrons in the cable screen, and cause a displacement of the electrons in the cable screen. The displacement of the electrons generate a voltage difference between the two ends of the screen conductor [10, p.855].

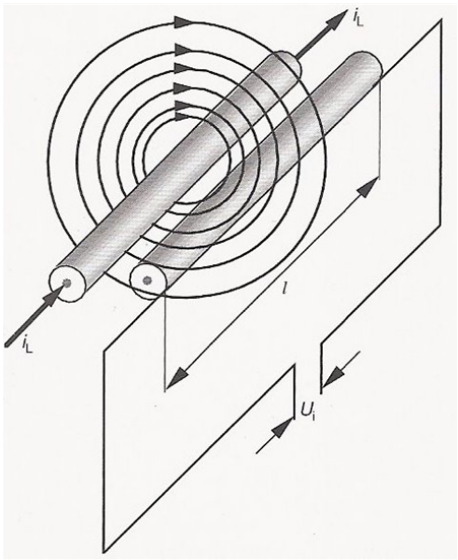

Figure 3.1: Magnetic field from conductor, induce voltage into the screen [45, p.60].

One end of the screen conductor is kept at zero potential, due to the ground connection. The induced voltage is therefore present at the not grounded end of the screen connector. The screen voltage is induced by the flux from the load current (I_L) in the conductor. This forms the relation that the screen voltage (U_i) is proportional to both the cable length and the load current, as shown in figure 3.2.[50, p.218]

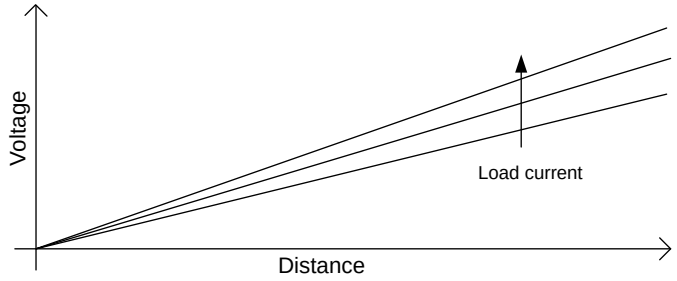

Figure 3.2: Principle sketch of the magnitude of the induced screen voltage [45, p.60].

I order not to cause any damage to the outer insulation of the cable, the screen voltage should be limited. Therefore single point grounding may not be used for long cable lines.

3.2.2 Multipoint ground

In order to decrease the voltage of the screen it is desirable to connect both ends of the screen to ground. Grounding both ends creates the circuit shown in figure 3.3. In this case the induced voltage generates a current flowing in the screen because of the closed earth loop. The voltage across the total cable screen is zero [50, p.218].

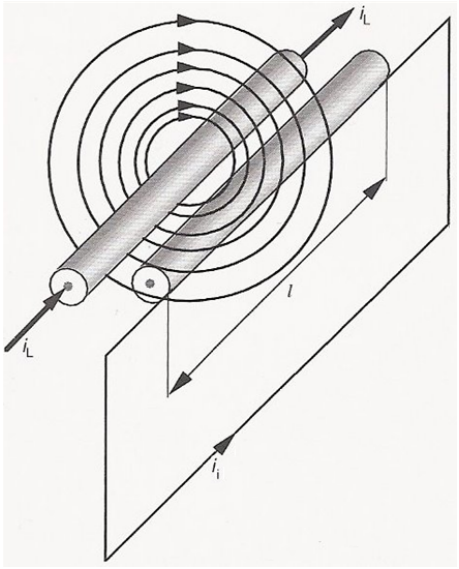

Figure 3.3: Screen current when the screen in multi point grounded [45].

The screen current will, because of the resistance of the cable screen, contribute to heating of the cable and thereby reducing the ampacity of the cable and cause screen losses [50, p.218]. Multipoint ground is used for submarine cables where it is not possible to ground the screen for the underwater distance. This will lead to screen losses and heat up the screen, but the screen voltage is kept low.

3.2.3 Cross bonding

As described in the previous section, it is desirable to have low screen voltage and at the same time keep the screen current at a minimum. To obtain both criteria cross bonding may be used. Cross bonding is a certain way of connecting the cable screens at a three phase cable system. The cable line is divided into major sections, each major section is subdivided into three minor sections of equal length, as shown in figure 3.4.

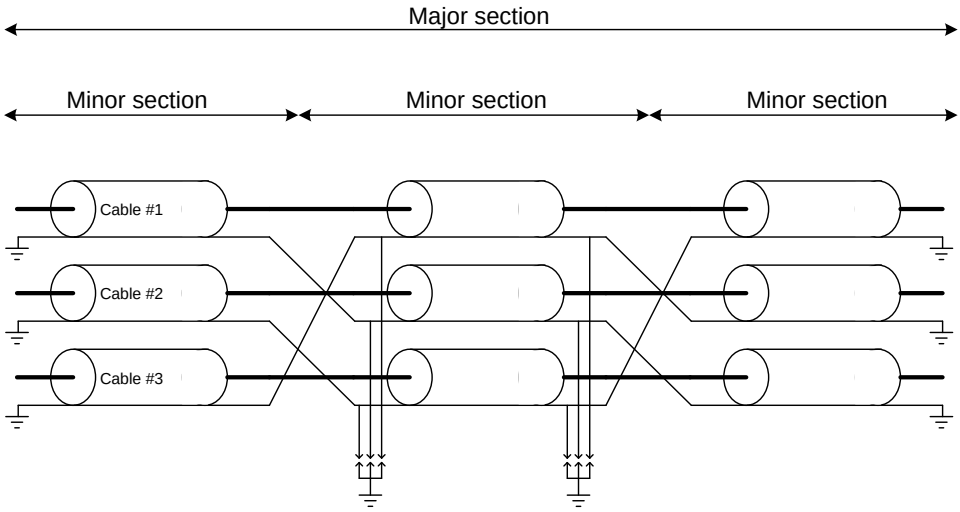

Figure 3.4: Practical implementation of series connection of the three cable screens. The figure shows a major section with cross bonded screens.

The cable screens are switched within a major section as shown in figure 3.4, hence the induced screen voltage at one minor section is electrical displaced by 120° according to the induced voltage of the next minor section. The vectorial sum of the total screen voltage of one major section will become zero, in case the magnitude of the induced screen voltages are equal, as shown in figure 3.5.

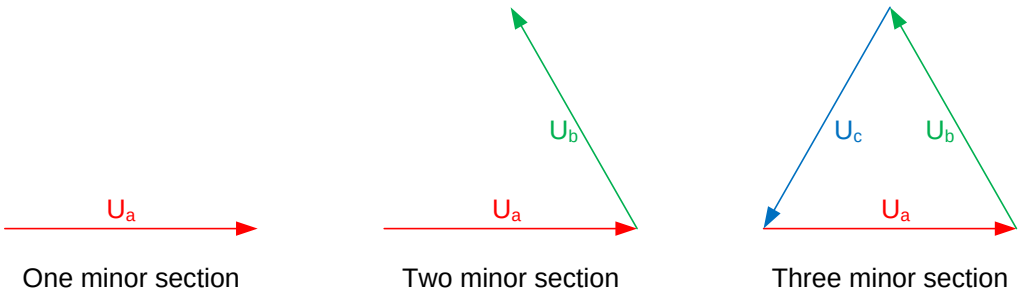

Figure 3.5: Induced screen voltage of a cross bonded major cable section.

The induced screen voltage for a major section is shown figure 3.6.

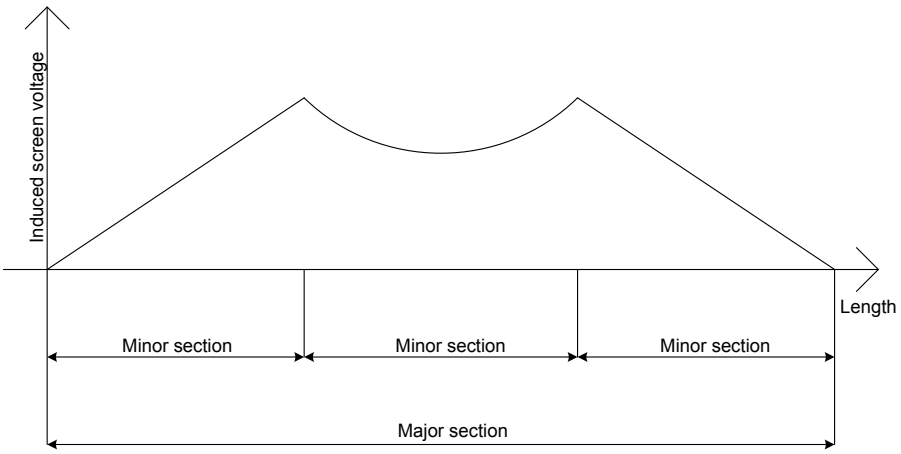

Figure 3.6: Induced screen voltage as a function of distance, over a complete major cable section.

For practical implementation is the cable line divided into a number of major sections. The length of the major section is limited by the maximum allowed screen voltage. All three cable screens are grounded in both ends of the major section. Where two minor sections are connected, there are placed screen voltage limiters (SVL), to limit the screen voltage during fault conditions. The circulating screen current through ground is eliminated and screen losses are minimized [45, p.62].

Cross bonding can be done in different ways. If the cable line is lead in flat formation the centre conductor and maybe also the screen may be transposed. I general transposing describes whenever the conductor shifts physical place according to the two other phases. Cross bonding is the screen shifting between the three different phases. The different scenarios are illustrated in the following figures.

Figure 3.7 shows one major section of a cable line, where the screen is cross bonded and transposed.

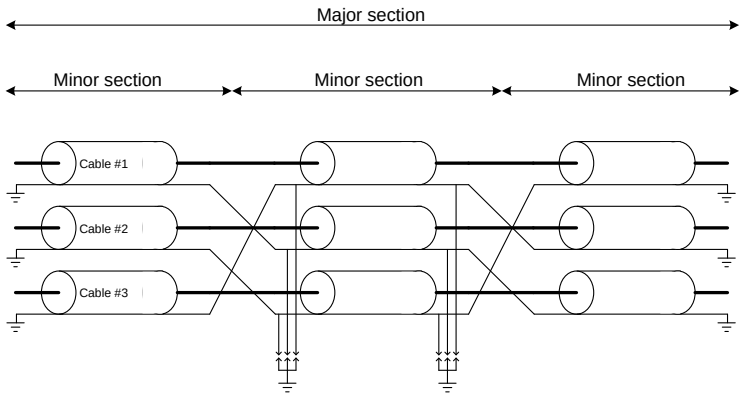

Figure 3.7: One major section of a cable line, screen cross bonded and transposed.

Figure 3.8 shows one major section of a cable line. The line is transposed and cross bonded, but the screen is not transposed. For this implementation it should be considered how to do the cable crossing, and still obtain distance between the cables to ensure proper heat dissipation. In case the cables are closer to each other at the point of crossing there is introduced a bottleneck for the ampacity of the line.

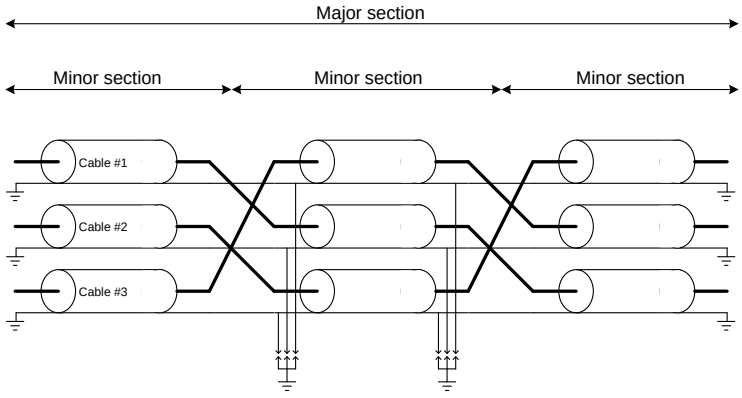

Figure 3.8: One major section of a cable line, transposed and cross bonded but the screen is not transposed.

Figure 3.9 shows a third implementation where the line is transposed, cross bonded and also the screens are transposed.

There is a third way of performing cross bonding af a cable line, were both the cables are transposed and the cross bonding is done by transposing the screens, as shown in figure 3.9. Also for this implementation the crossing point should be considered, for heat dissipation.

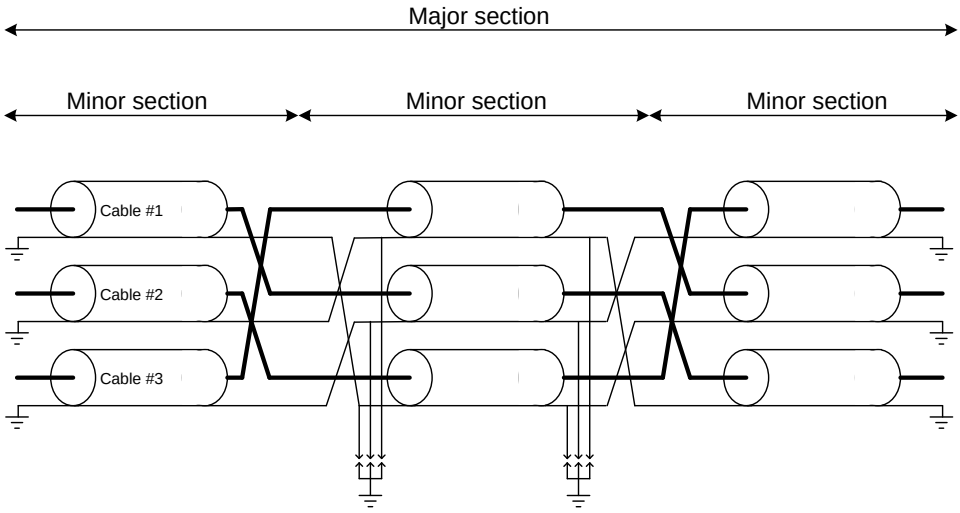

Figure 3.9: Another implementation of cross bonding. In this case the line is both transposed and cross bonded. Also both the conductor and the screen changes place between each minor section.

In general the term transposed is used when the physical position is changed and cross bonded is used whenever the screen is shifted between the three phases.

3.2.4 Screen circuit, for cross bonding

The cable screens of a cross bonded cable system forms a electrical circuit, as shown in figure 3.10, the phase conductors are not transposed. In top of the figure is a cross bonded cable system consisting of eight minor sections, named A-H. The six minor sections at the left forms two major sections. The three single phase cables named 1-3. It may be observed that the cable screens are grounded where two major sections are connected and the SVL are placed at the points, where minor sections are connected.

In the middle of the figure only the screen circuit is shown. The screen conductor from each minor section is named: Z_{Xy}.

Where:
- X Refers to the minor section of the impedance.
- y Refers to the phase conductor of the screen.
- Z_e is the earthing impedance at the cross bonding points. This is further explained in section 3.2.6.

In the button of the figure the screen circuit seen from the cable end is shown. Typical for cross country cable lines are the connections between minor and major sections placed underground. The impedance $Z_{majorsection}$ is the equivalent impedance of the complete major section.

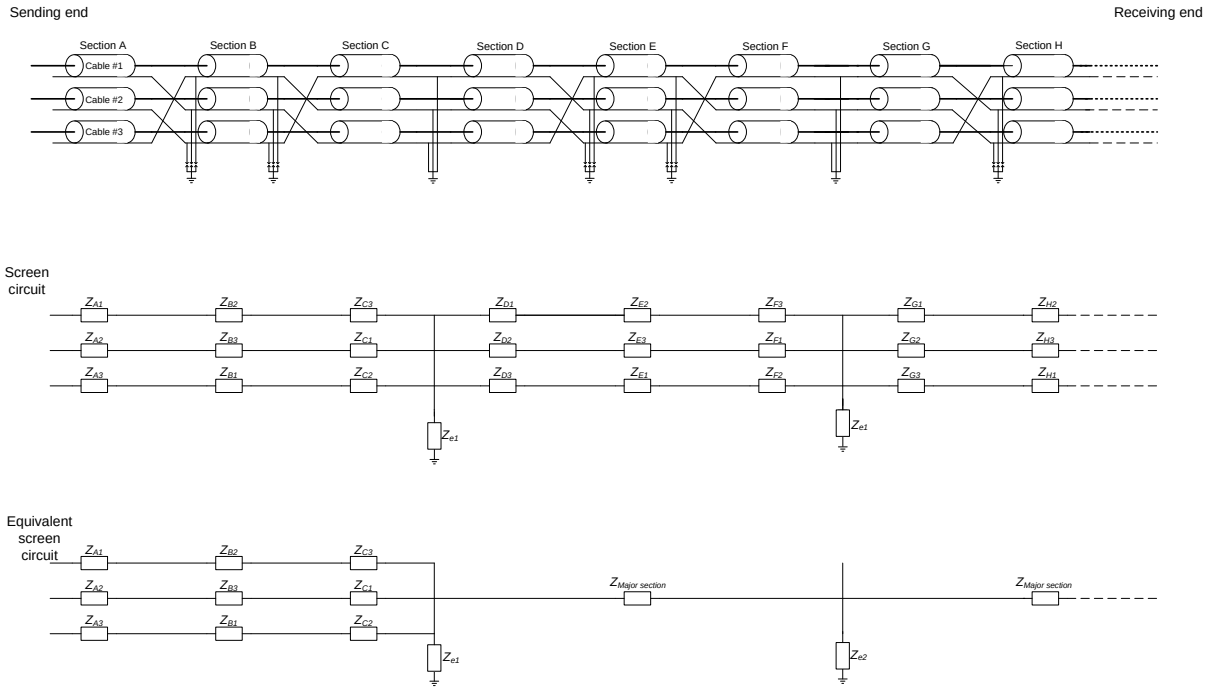

Figure 3.10: At the top a cross bonded cable system, consisting of 8 minor sections. In the middle the electrical circuit formed by the cable screens are shown. At the bottom the screen circuit is shown seen from one end. $Z_{majorsection}$ is the equivalent impedance of the major section.

3.2.5 Cross bonding points

From figure 3.10 it is clear that the link boxes can be divided into two types. For this project these are named A and B.

- Type A: This type is used in the end of each major section. The screen is directly connected to ground in the A type boxes. Figure 3.11 show the principle of this box.

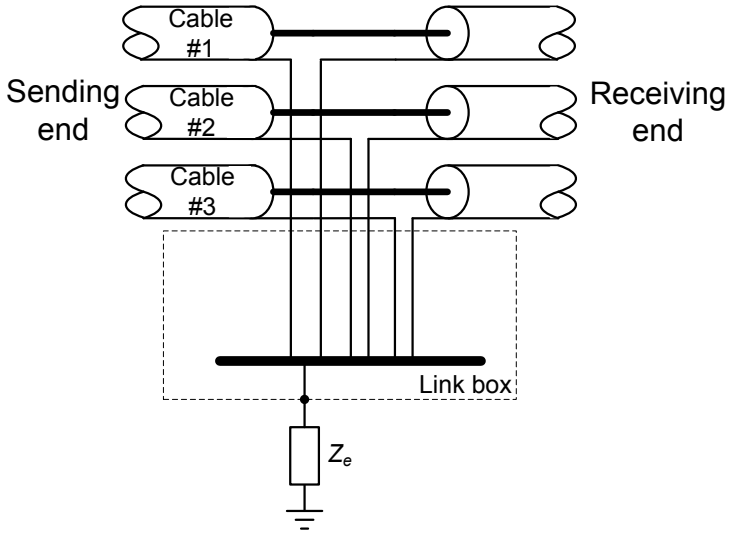

Figure 3.11: Electrical connection in type A link box.

- Type B: This type is used at the point where two minor sections are connected. The cable screen from the individual screens are cross connected. Screen voltage limiters (SVL) are placed at each cross connection. The SVL protects the cable screen from damage during high frequency over-voltages. Figure 3.12 shown the principle of this box.

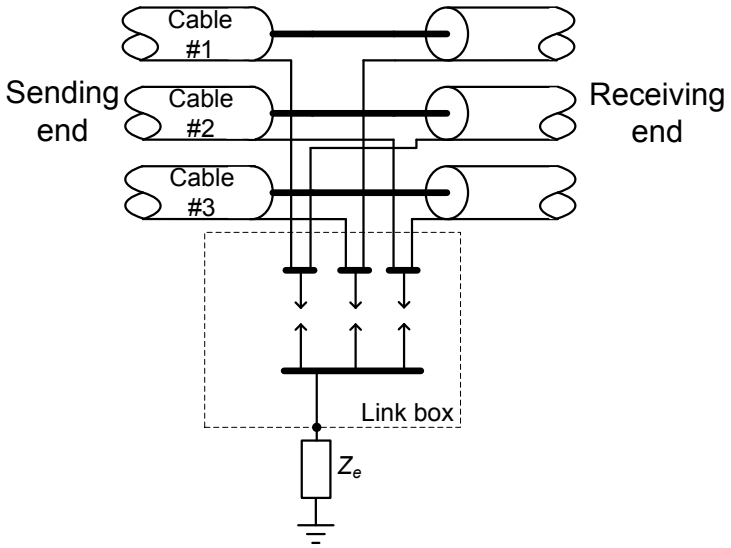

Figure 3.12: Electrical connection in type B link box.

3.2.6 Earthing resistance

The earthing impedance can be split up into a earth resistance and a earth inductance equation 3.1.

$$Z_e = R_e + j\omega L_e \quad [\Omega] \quad (3.1)$$

The earth resistance R_e is defined as the resistance between the points of earthing on the system to an area designated as neutral ground. Neutral ground is defined by an area which potential will not change due to any surrounding electrical circuit. [53, p.366].

The earth inductance L_e is very difficult to determine accurate, but because of the fact that the impedance is dependent on the loop of the current. AC current through the earth will not be distributed on all of the available area, but because of skin effect propagates deeper into the ground. The depth of the current can be equivalent by using Carson equation 3.2.

$$d = 660\sqrt{\frac{\rho}{f}} \quad [\mathrm{m}] \quad (3.2)$$

From the depth it is possible to estimate the inductance equation 3.3.

$$L = 2 \cdot 10^{-7} \cdot \frac{d}{D_s} \quad [\mathrm{H/m}] \quad (3.3)$$

Where D_s is the geometrical average area of the conductor, typically determined from tables [53, p.109]. The impedance calculations are based on ideal conditions where the earth is considered homogeneous and the earth surface is parallel to conductor [53, p.118].

The earthing resistance is dependent on several things [11, p.4]:

- Length/depth of the ground electrode
- Diameter of the ground electrode
- Number of ground electrodes
- Design of the ground system
- Soil type and temperature

As indicated above, the earthing resistance is dependent on the physical design of the ground electrode. Besides the design the resistance is also dependent on the resistivity of the surrounding soil and the temperature. The resistivity of the soil give an indication of the needed extent of the grounding system, the resistivity may be determined by the Wenner method [11, p.6]. Soil resistivity of very moist soil is around 30Ωm, for clay soil it is around 100Ωm and for sandy clay it is around 150Ωm.[11, p.5] In Denmark the soil has a large contain of sand and clay, for this reason a value between 100 and 150Ω may be expected [16, p.31]. The earthing resistance may also change with the seasons, due to changes in the surrounding environment. The condition of the earth electrodes may change over time due to corrosion and change of soil conditions. For these reasons it is required that the earthing resistance is checked

regularly. In case the earthing resistance is increased more than 20% the installation should be correction to lower the resistance by a technician. This also indicates that the value is expected to vary.

The size of the earthing resistances is required not to exceed certain limits depending on the system, it should protect. For cross bonding point the value is normally between $10 - 20\Omega$ [29].

3.3 Faults in link boxes

As described in the introduction, link boxes are subject to faults in the HV cable transmission systems[35]. The connections inside the boxes are affected from intrusion of moisture. Moisture may, dependent on the extent and duration, leads to unwanted connections inside the box. Figure 3.13 shows a link box under inspection. From the figure it is clear that the conductors are corroded due to a presence of moisture.

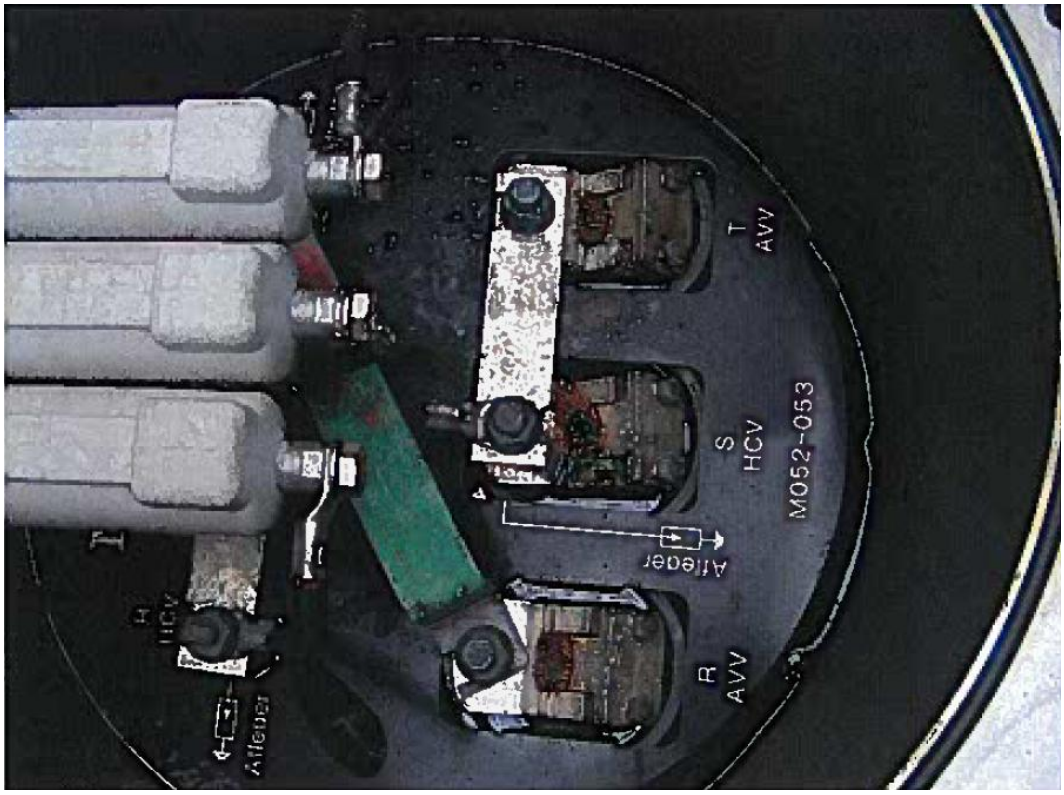

Figure 3.13: Link box under inspection. The electrical connections and conductors are corroded.[35]

The corrosion leads to several unwanted phenomena. Connections points may change to high impedance fault due to poor connections. The moisture may also constitute unwanted connections between different screen circuits inside the link box. Is moisture present in the box for a long time, the impact of corroded connections may increase significantly. If nothing is done to prevent the intrusion of moisture the risk of material to vanish also becomes present. The influences on the electrical connection are dependent on the amount of moisture and water inside the box. The amount of moisture and water that enters the box is dependent on several things. E.g. the encapsulation of the box and the environment in which the box is present. If the box is not airtight there is risk of the condensation due to temperature changes. The surroundings may change with the seasons, during rain periods the risk of intrusion of moisture is significantly larger than during dry periods.
In general the presence of moisture and water inside the link box may cause some of the following three phenomenons:

- Impedanse between connections changes
- Unwanted connections may appear
- Disconnection of conductors.

It is not possible to foresee the placing of the moisture and water, any combination of the three listed phenomenons may occur. In order to analyze the above mentioned phenomenon, a number of fault causes are set up. These are subdivided according the two link box types.

The fault condition for type A link boxes will be:

- **Case #1A:** Disconnected screen conductor
- **Case #2A:** Unwanted short circuited between screen conductors
- **Case #3A:** Unwanted ground connection of a single screen conductor
- **Case #4A:** Disconnected ground conductor at star point connection

The fault condition for type B link boxes will be:

- **Case #1B:** Disconnected screen conductor
- **Case #2B:** Short circuit between screen conductors
- **Case #3B:** Ground connection of a single screen conductor
- **Case #4B:** Short circuit SVL
- **Case #5B:** Disconnected ground connection at SVL's star point connection

For each case the electrical circuit for a complete major section is shown. This will later be used for the measuring method analysis.

Type A Link Box failure types

Case #1A

This fault condition have the screen conductor at cable #1 disconnected. The ground connections are intact, as shown in figure 3.14.

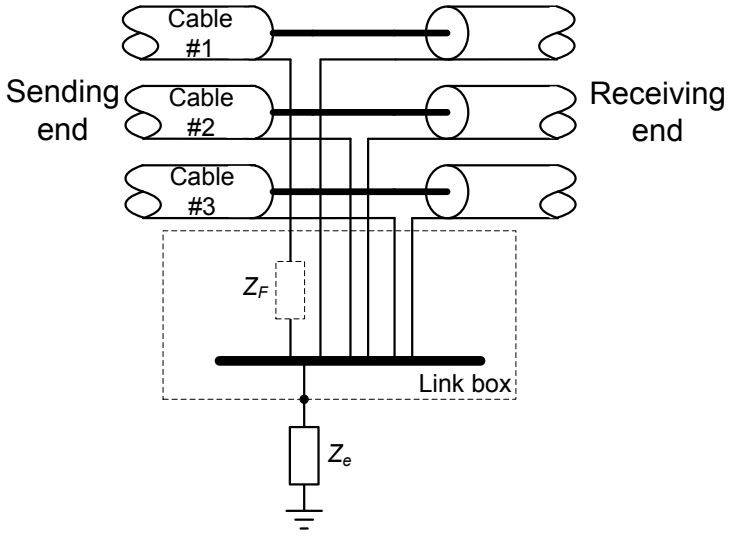

Figure 3.14: Type A link box with a disconnected screen conductor at cable #1.

Seen from the sending end two of the screens will still be connected to ground whereas the last screen conductor will be open-ended. Seen from the receiving end the three screen conductors will still be connected to ground. In case of a corroded connection the faulty screen conductor should be represented as series fault impedance with a finite value. Equivalent screen circuit of the faulty major cable section is shown in figure 3.15.

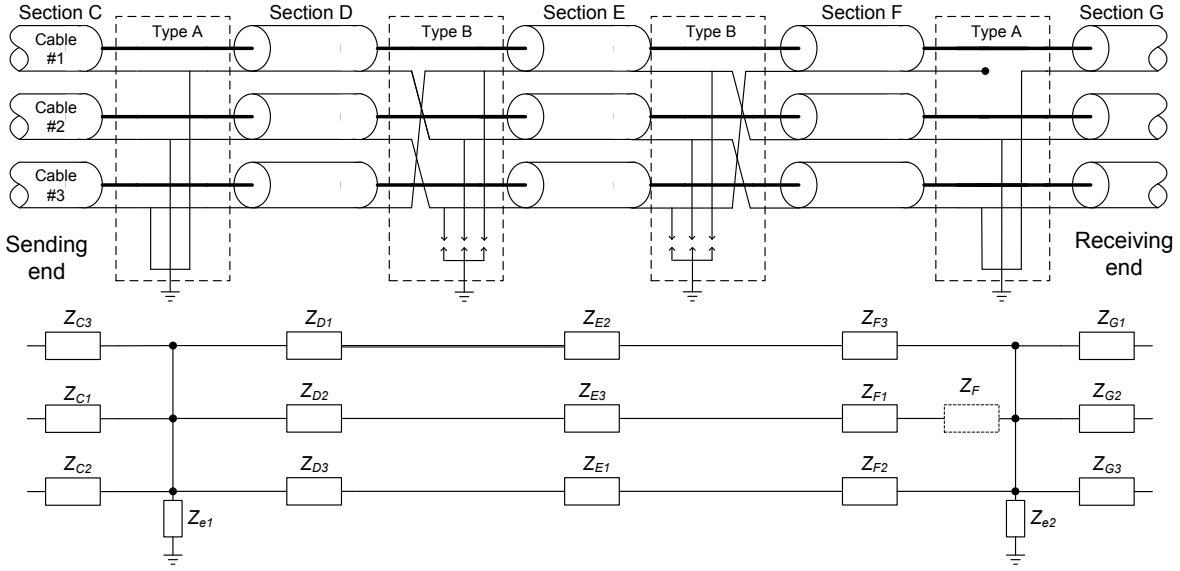

Figure 3.15: An major section with a disconnected screen conductor at cable #1 in a type A link box. Equivalent screen circuit of the major section with the disconnection.

Case #2A

This fault condition have an unwanted connection between the screen conductors of cable #1 and #2. The ground connections are all intact, as shown in figure 3.16.

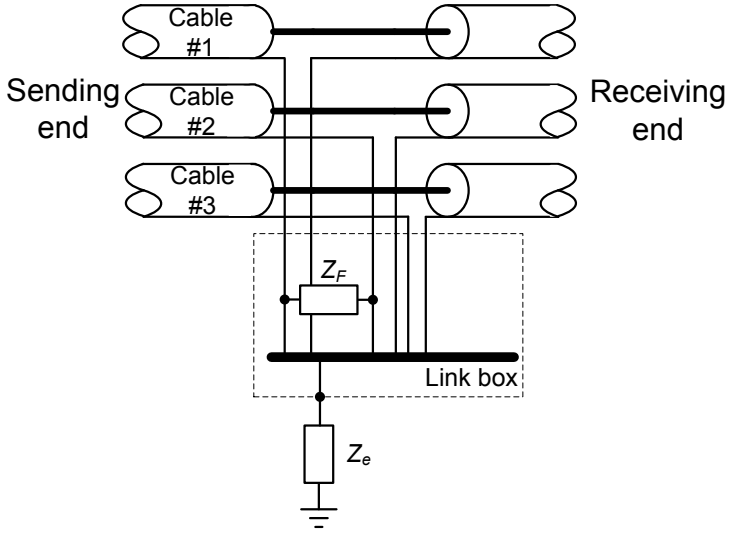

Figure 3.16: Type A link box with a unwanted connection between the cable screens at cable #1 and #2.

The unwanted connection between the screen conductors may most likely have higher impedance compared with the star connection. Therefore the short circuited between the screen conductor at cable #1 and #2 represented as a fault impedance Z_F. Equivalent screen circuit of the faulty major cable section is shown in figure 3.17.

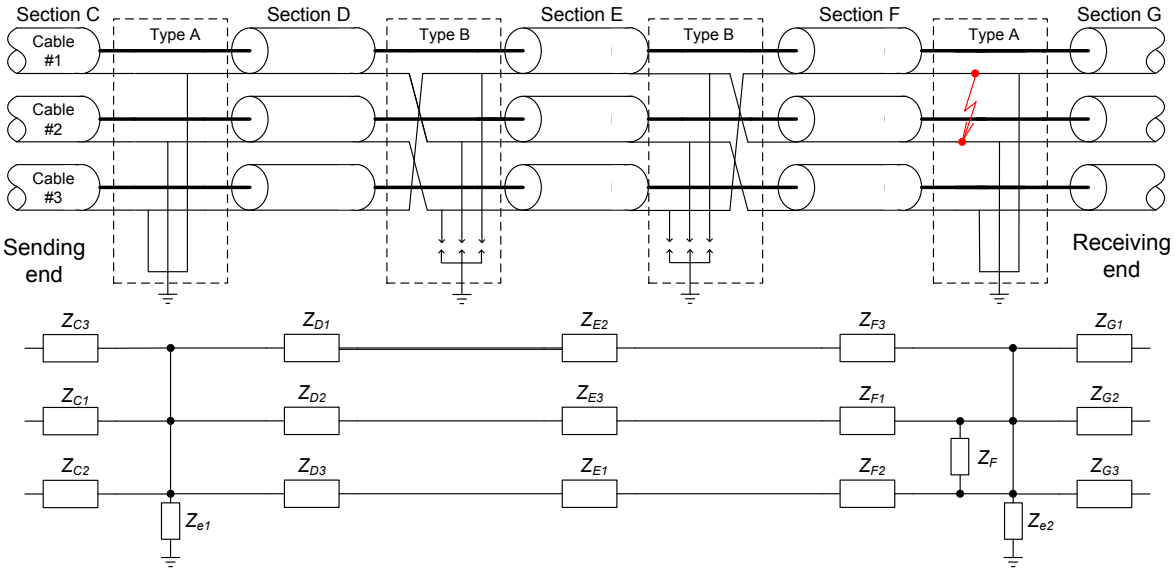

Figure 3.17: An major section with a unwanted connection between the screen conductors of cable #1 and cable #2 in a type A link box. Equivalent screen circuit of the major section with the unwanted connection.

Case #3A

This fault condition have an single screen connection to ground at cable #1 . The connections to ground are all intact, as shown in figure 3.18.

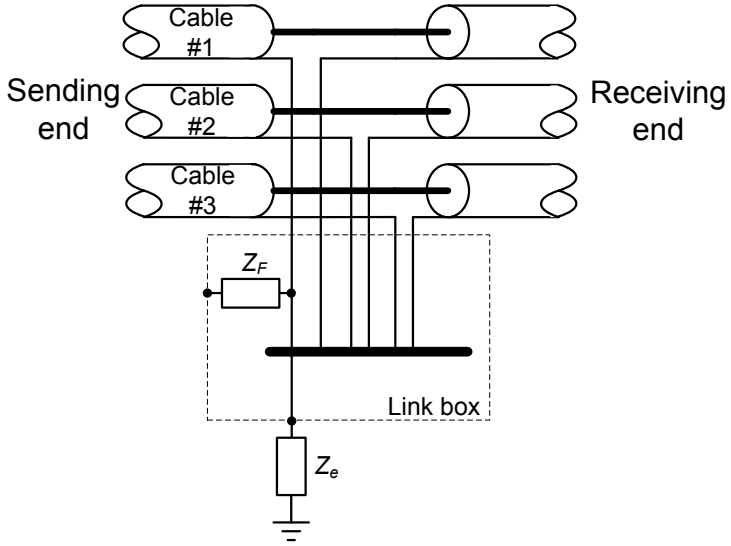

Figure 3.18: Type A link box with a unwanted ground connection. The ground connection is located at the sending end of cable #1's screen conductor.

The unwanted ground connection may most likely have higher impedance than the conductor connection to the star point. Therefore is the faulty connection represented as the fault impedance Z_F. Equivalent screen circuit of the faulty major cable section is shown in figure 3.19.

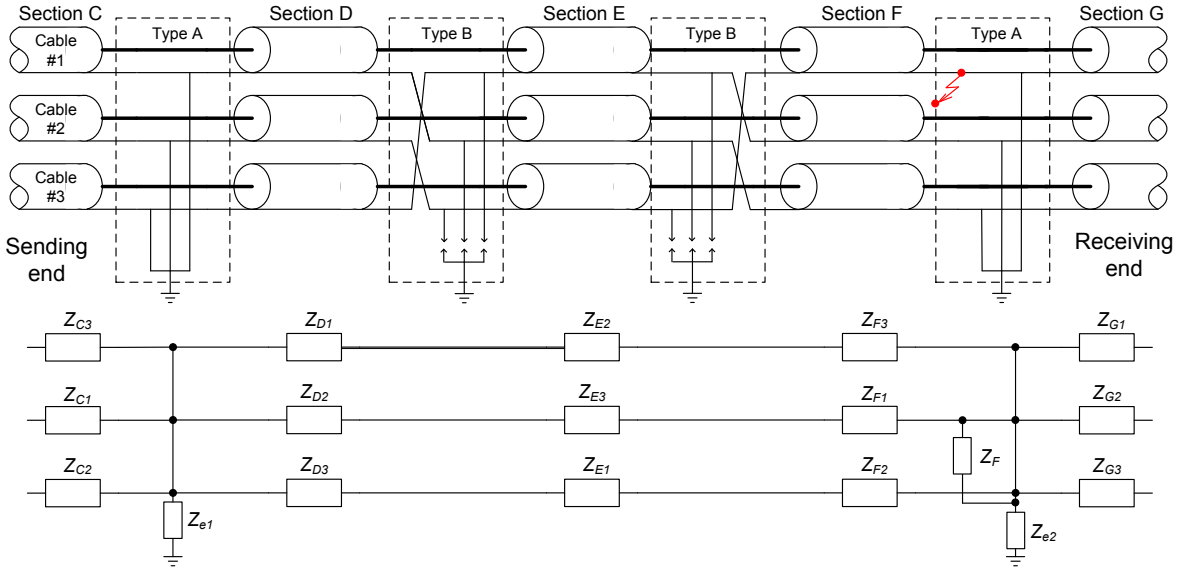

Figure 3.19: An major section with an unwanted ground connection at the screen conductor of cable #1 in a type A link box. Equivalent screen circuit of the major section with the unwanted ground connection.

Case #4A

This fault condition has total disconnection of the ground conductor at the star point. All six screen conductors have intact connections to the star point, as shown in figure 3.20.

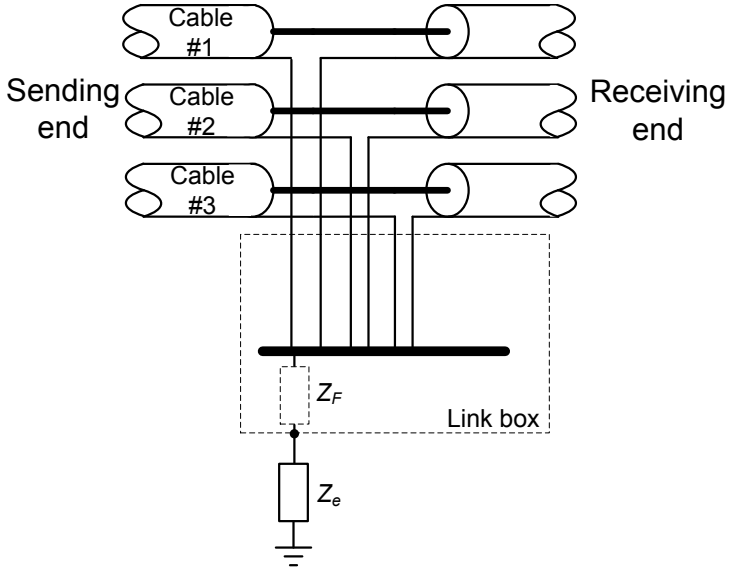

Figure 3.20: Disconnected grounding at the star point connection.

In case of a corroded connection the faulty ground conductor should be represented as series fault impedance with a finite value. This fault condition will affect all of the six screen conductors due to the star point connection. Equivalent screen circuit of the faulty major cable section is shown in figure 3.21.

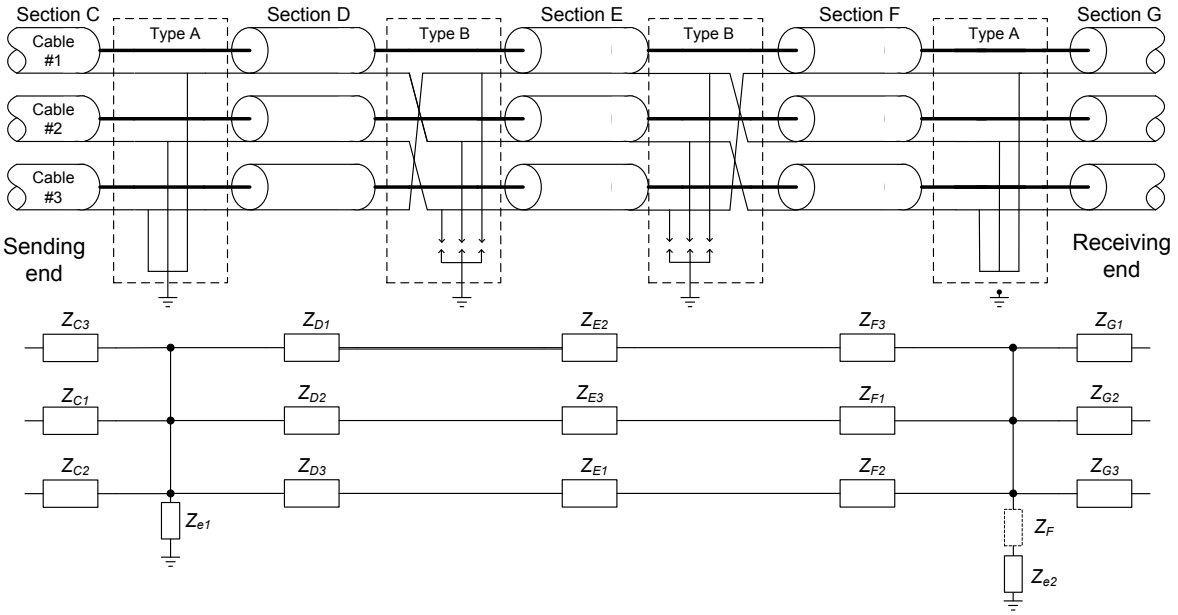

Figure 3.21: An major section with a disconnected ground connection at the star point connection in a type A link box. Equivalent screen circuit of the major section with the disconnected ground connection.

Type B Link Box failure types

Case #1B

Fault condition where the screen conductor at cable #1 disconnected. All other connections are intact, as shown in figure 3.22.

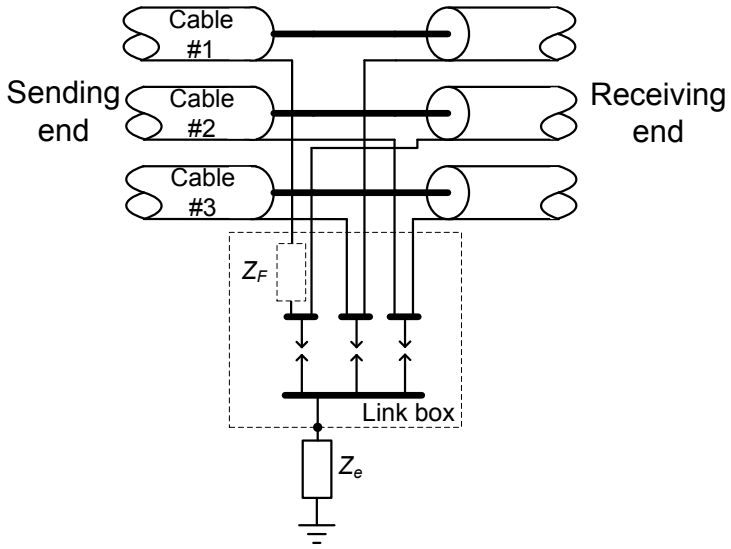

Figure 3.22: Disconnected cross bonding between cable # 1 and #2.

At the sending end of the major section the screen conductor of cable #1 is disconnected. At the receiving end the disconnection will occur at the screen conductor of cable #3. Equivalent screen circuit of the faulty major cable section is shown in figure 3.23. In case of a corroded connection the faulty screen conductor should be represented as series fault impedance with a finite value.

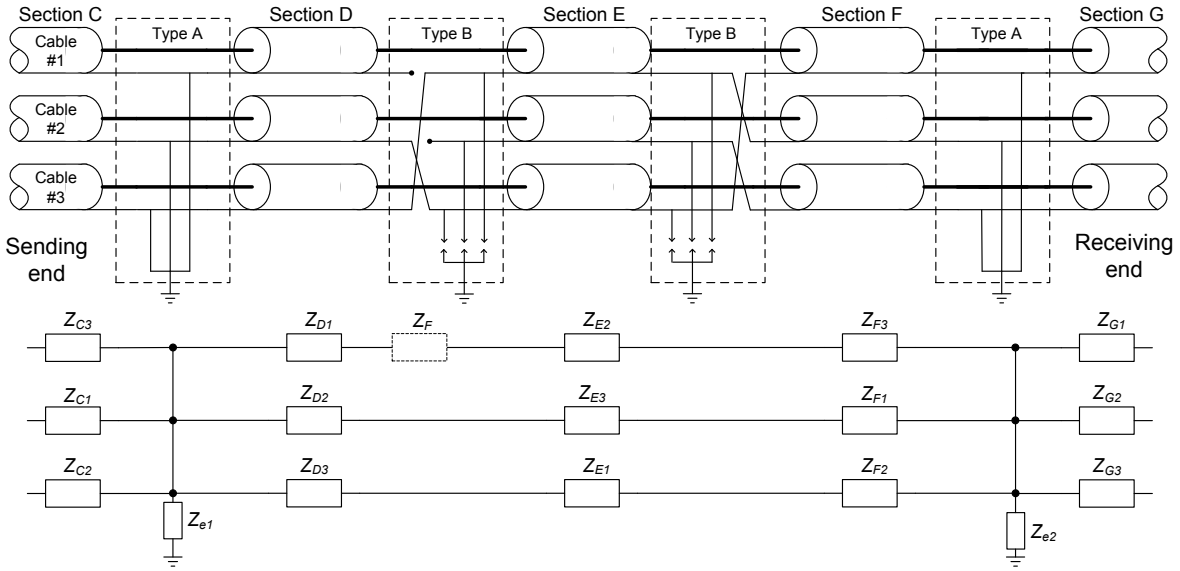

Figure 3.23: An major section with a disconnected screen conductor at cable #1 in a type B link box. Equivalent screen circuit of the major section with the disconnection.

Case #2B

Fault condition at the sending end where the screen conductors of cable #1 and #2 are short circuited. All other connections are intact, as shown in figure 3.24.

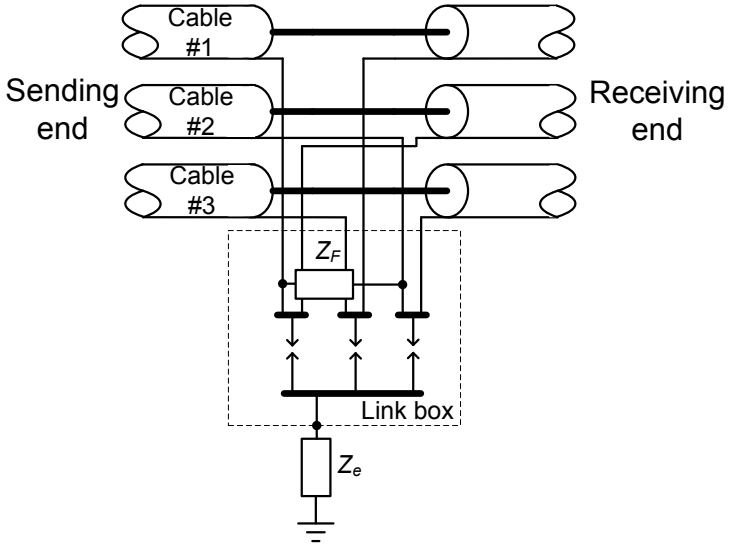

Figure 3.24: Short circuited screen conductors at sending end.

At the sending end of the major section the screen conductors of cable #1 and #2 is short circuited. At the receiving end the short circuit will occur between cable #1 and #3. Equivalent screen circuit of the faulty major cable section is shown in figure 3.25. The short circuit is represented as the fault impedance Z_F.

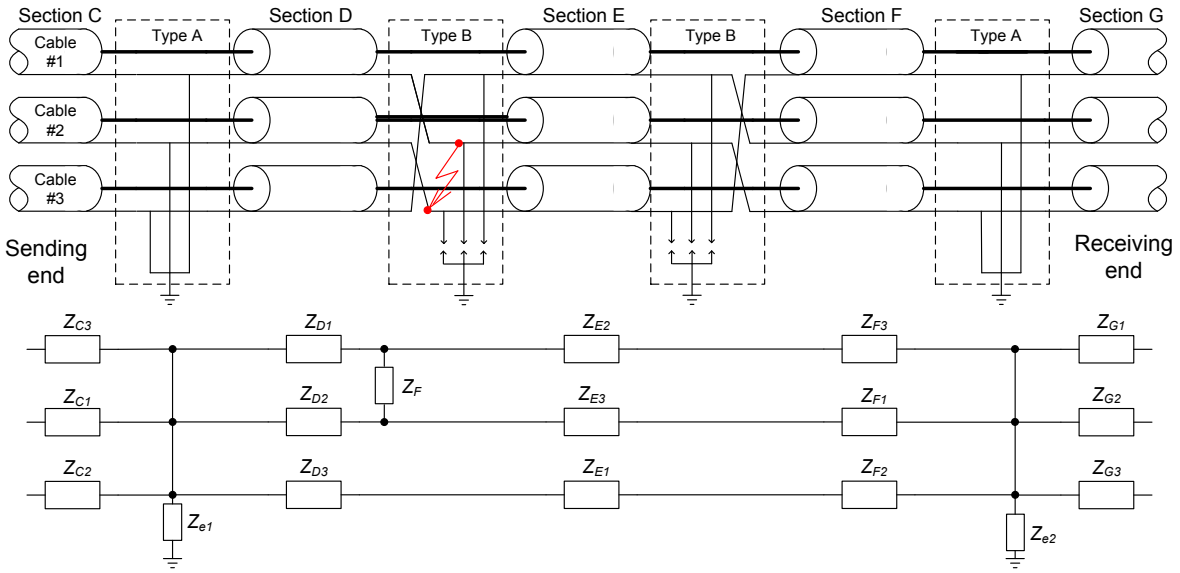

Figure 3.25: An major section with short circuit between the screen conductors of cable #1 and #2 at sending end in a type B link box. Equivalent screen circuit of the major section with the short circuit.

Case #3B

Fault condition at the sending end where the screen conductor of cable #1 is grounded. All other connections are intact, as shown in figure 3.26.

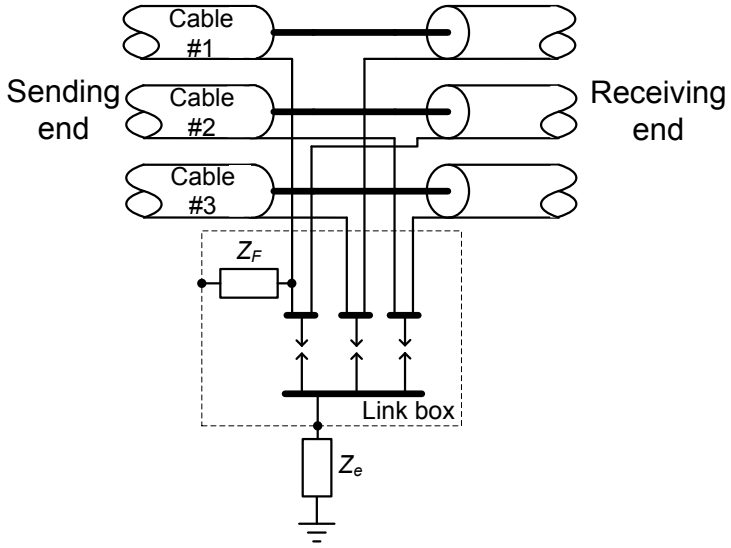

Figure 3.26: Ground connected screen conductor at sending end.

At the sending end of the major section the screen conductor of cable #1 is grounded. At the receiving end the screen conductor of cable #3 will be grounded. Equivalent screen circuit of the faulty major cable section is shown in figure 3.27. The grounding is represented as the fault impedance Z_F.

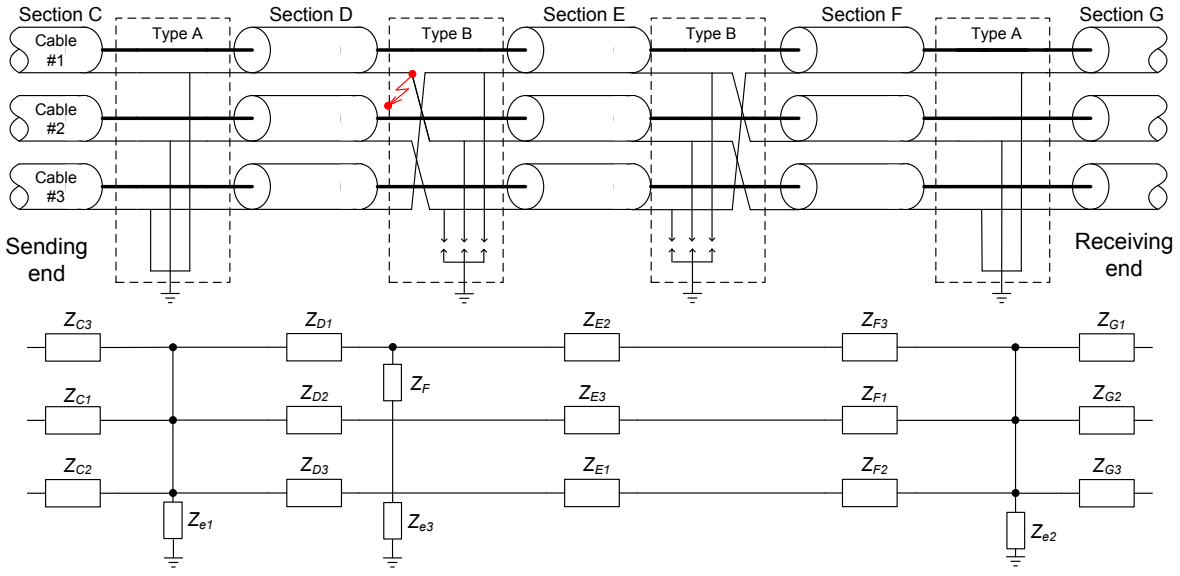

Figure 3.27: An major section with ground connected screen conductor at cable #1. The grounding is located in a type B link box at the sending end. Equivalent screen circuit of the major section with the ground connection.

Case #4B

Fault condition where a SVL is short circuited. All other connections are intact, as shown in figure 3.28.

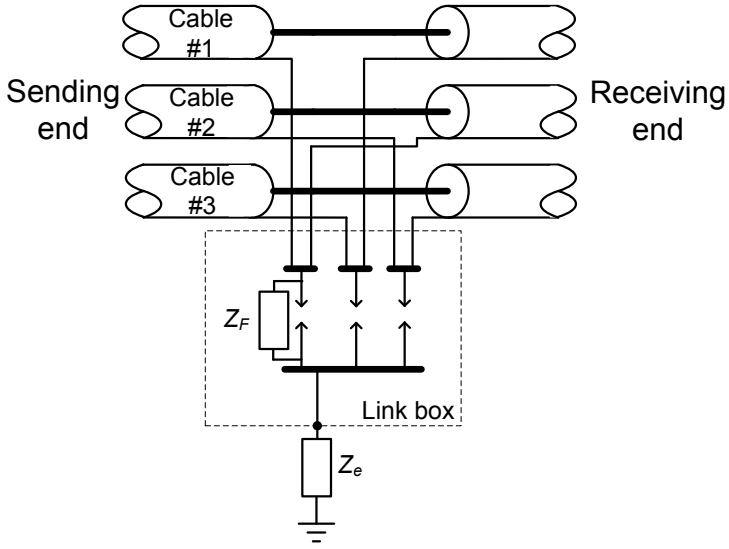

Figure 3.28: Short circuited SVL.

There are direct connection between the potential of the screen, at cable #1(sending end) and cable #2(receiving end), and ground potential. Equivalent screen circuit of the faulty major cable section is shown in figure 3.29. The short circuit is represented as the fault impedance Z_F. It may be seen that case #3 and #4 is identical if the casing is grounded.

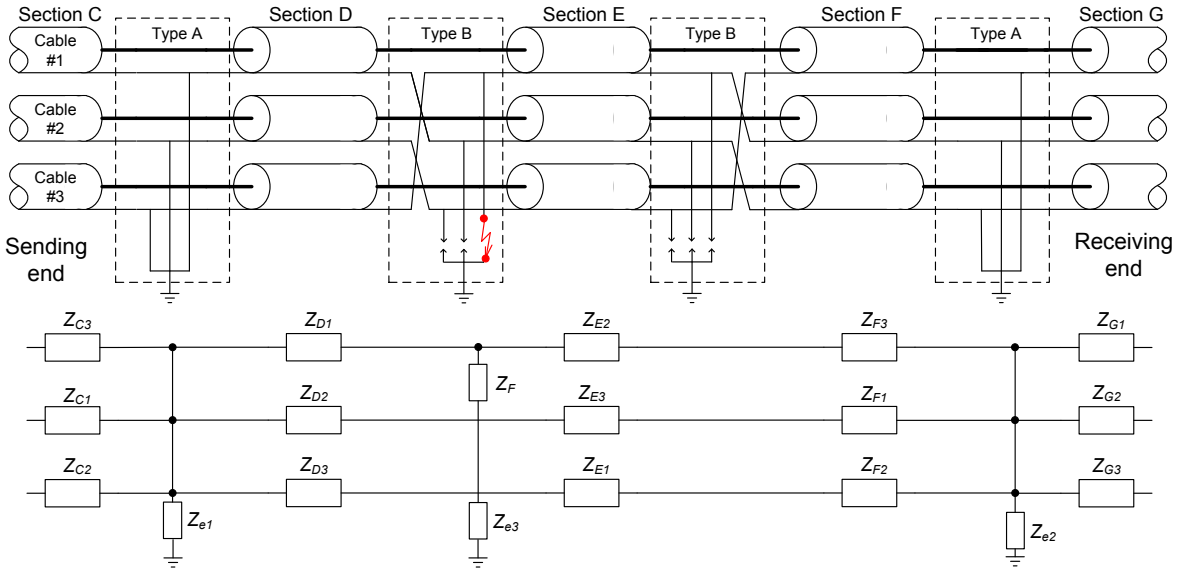

Figure 3.29: An major section with a short circuited SVL. Equivalent screen circuit of the major section with the ground connection.

Case #5B

This fault condition has total disconnection of the ground connection at the star point of the SVL's. The cross bonding is intact, as shown in figure 3.30.

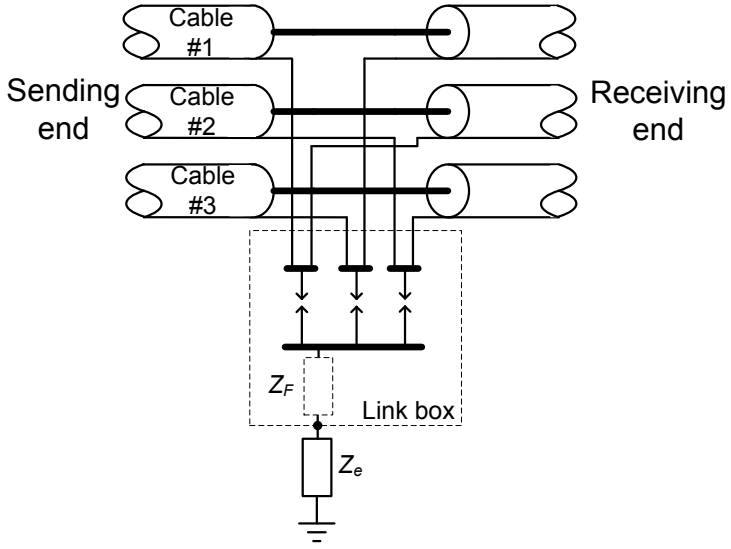

Figure 3.30: Disconnected grounding at the star connection of the SVL's.

In case of a corroded connection the faulty ground conductor should be represented as series fault impedance with a finite value. This fault condition will not affect the cross bonded system in normal operation mode. Equivalent screen circuit of the faulty major cable section is shown in figure 3.31.

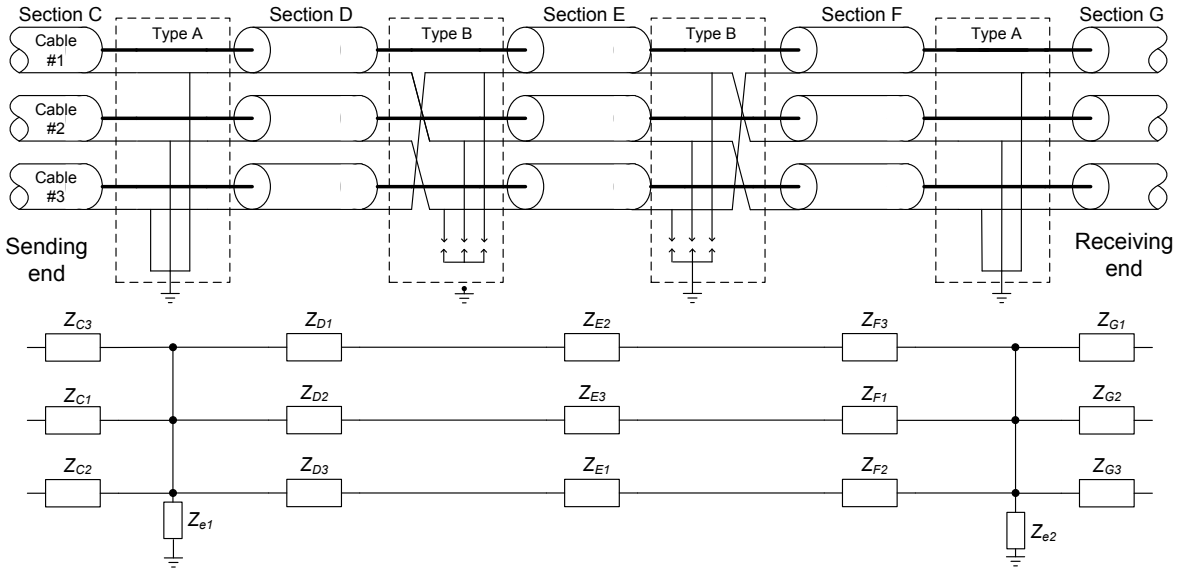

Figure 3.31: An major section with a disconnected ground connection in a type B link box. Equivalent screen circuit of the major section without the ground connection.

In Table 3.1 and 3.2 it is determined whereas the above cases have an unintended effect on the cross bonding during normal operation. The tables are only valid for one fault condition per major section.

Case	Affects the cross bonding at normal operation condition
#1A	(YES)
#2A	NO
#3A	NO
#4A	(YES)

Table 3.1: Fault conditions in type A link boxes

Case #1A and #4A in Table 3.1 will affect the cross bonding if the cable line is exposed to unbalanced faults or unbalanced load conditions.

Case	Affects the cross bonding at normal operation condition
#1B	YES
#2B	YES
#3B	YES
#4B	YES
#5B	NO

Table 3.2: Fault conditions in type B link boxes

All the fault cases in table 3.2 affects the cross bonding, except for case #5B. The condition of type B link boxes should have a high priority in order to ensure that the cross bonding serves as intended.

3.4 Measuring techniques for cross bonded cable systems

The state of the art analysis, showed that there existed no methods in respect to determine the condition of a cross bonded screen circuit. This section will analyze three known fault detection methods:

- Resistance (DC source)
- Impedance (AC source)
- Travelling wave (Impulse)

The methods will be evaluated in relation to their ability to determine the condition of the link boxes and to locate a faulty link box.

3.4.1 Resistance method

Screen to screen measurement

A simple technique to determine if the screen circuit is faulty is to apply a low voltage DC source to the cable screen at the end of the line. From figure 3.10 on page 22 it can be seen that any combination formed by two cable screen ends should be electrical connected through the third cross bonding point and the resistance might be estimated by direct resistance calculations 3.4. [46, p.30]

$$R = \frac{\rho \cdot l}{q} \quad [\Omega] \quad (3.4)$$

Where ρ is the resistivity of the screen material, l is the total length of the measuring loop and q is the cross section area of the screen. The connections points represent a fraction of the measured resistance. In the calculations this is not included, in order to simplify the analysis. The measuring circuit is shown in figure 3.32.

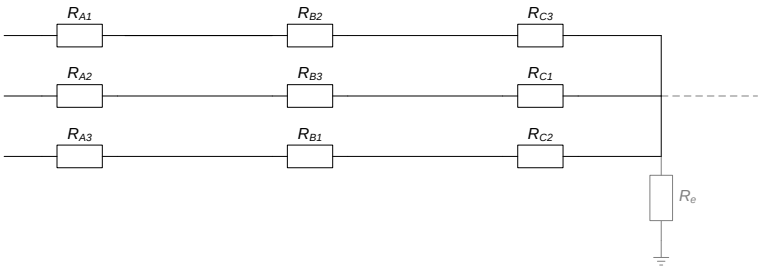

Figure 3.32: Measurement circuit for screen to screen measurement.

By measuring the resistance between two screen conductors it is desirable to determine if the cross bonding is faulty or not. If the cross bonding is faulty the measured resistance should revile at which link box the fault is located.

In case of a short circuit between two cross bonding points inside one of the two first link boxes the following equations can be derived. The screen circuits may be seen in figure 3.33. At the figure is also shown a healthy screen circuit which is use as a reference.

$$R_{eq1} = \left(\frac{(R_{B2} + R_{C3} + R_{B3} + R_{C1}) \cdot R_F}{R_{B2} + R_{C3} + R_{B3} + R_{C1} + R_F} \right) + R_{A1} + R_{A2} \quad [\Omega] \quad (3.5)$$

$$R_{eq2} = \left(\frac{(R_{C3} + R_{C1}) \cdot R_F}{R_{C3} + R_{C1} + R_F} \right) + R_{A1} + R_{A2} + R_{B2} + R_{B3} \quad [\Omega] \quad (3.6)$$

Where:
R_{Ax}, R_{Bx}, R_{Cx} is the resistance of the screen conductors. Where x specifies the cable number and A, B and C specifies the minor section.

To analyze this measuring technique the fault resistance R_F will be changed in value. The simulation results shows that a fault resistance with values higher than 100Ω have little or no influence on the measured resistance, it is therefore decided to change the fault resistance in the span $0-100\Omega$, in steps of 1Ω. All screen conductors have a resistance of 1Ω. Calculation results may be seen in figure 3.33.

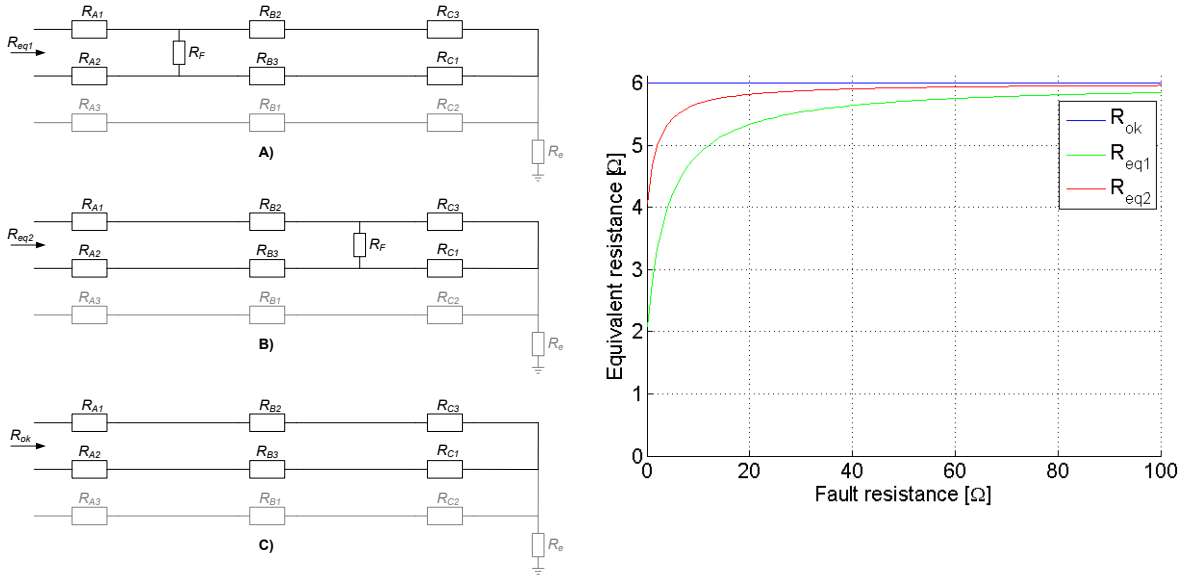

Figure 3.33: Circuit **A)** fault in first link box. Circuit **B)** fault in second link box. Circuit **C)** no fault present. Simulation results is shown to the right.

The above figures illustrate the difficulty in locating or even determine whether there is a short circuit or not. If a fault is present and the measured resistance in the screen circuit is below 4Ω it is possible to locate the fault in the first link box. If the measured resistance have a value between four and 6Ω it is not possible to locate the fault it is only possible to say that the screen circuit is faulty. A measured resistance of five ohms could either mean a fault resistance in the first link box with a value of 12Ω or a fault resistance in the second link box with a value of 3.3Ω. In case of a high resistance fault it would be very difficult to determine the condition of the cross bonding.

Because of the short circuiting of the three cable screens at the third cross bonding point, the method is unable to detect the condition of the cross bonding points located after the short circuit point.

The resistance measurement determines the resistance between two cable screens. The measure path does not include any part of the earth circuit and do not achieve any information on the condition of the earth connection.

Screen to ground measurement

The resistance method has been used for fault location on Cable systems [34]. The method is today applied for location of a detected fault on a HV line. This means that the method is applied when a fault is detected by the line relay protection, for determination of the location of the fault. The method is relative uncomplicated to implement due to the fact that the necessary equipment already exist, and is used in the industry. The method is based on resistance measurement performed by applying DC voltage. This section describes the principle of the resistance method, this is followed by a discussion of how the method may be converted for measuring the condition of the screen circuit.

Principle of the resistance method

There are several ways of performing this technique, one way is to use the setup shown in figure 3.34, this setup is called a improved Murray Bridge [34]. On the figure the two parallel horizontal lines are one healthy and the faulty conductor, the two conductors are short circuited at the far end. R_0 is the resistance of the healthy conductor, R_1 and R_2 are the resistance of the faulty conductor from the near and the far end accordingly, to the fault location.

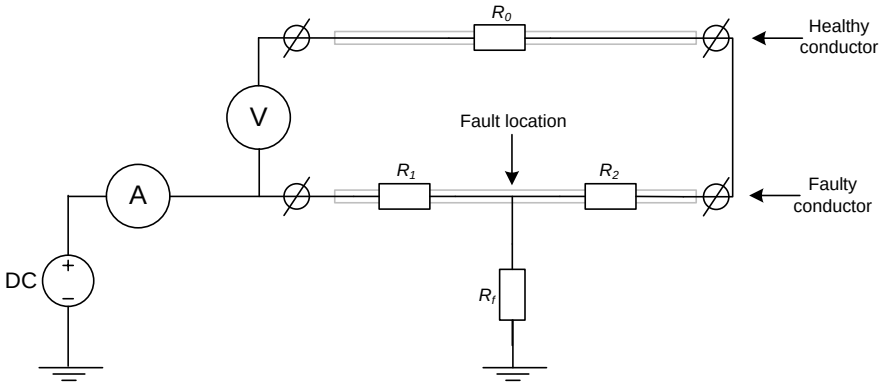

Figure 3.34: Test circuit for the improved bridge measuring.

Due to the high internal resistance in the voltmeter, the measured voltage is equal to the voltage drop across R_1. The measured current is the current passing through the same resistance R_1. When both voltage and current are known the size of the resistance is easily calculated. The distance is then determined by comparing the resistance to fault location and resistance of the whole line. As the figure shows the method uses the ground as return path for the measurement.

Conversion to screen fault measurement

The resistance method is developed for localization of conductor to earth faults. Because of the circuit formed by the cable screens of a three phase cross bonded cable system include earth connection, the method cannot be used directly on the cable screens. The three cable screens are short circuited and connected to ground at the third cross bonding point, as shown in figure 3.10 on page 22.

Although the above method cannot be used for fault location on the screen conductors, it is interesting to analyze whether the principle of the method can used to detect ground faults in the link boxes of type B.

The equivalent resistance for the four fault scenarios in figure 3.35. Each are calculated from equation 3.7 - 3.10.

$$R_{eq1} = \left(\frac{(R_{B2} + R_{C3} + R_e + R_{g2} + R_{g3}) \cdot (R_F + R_e)}{R_{B2} + R_{C3} + R_e + R_{g2} + R_{g3} + R_F + R_e} \right) + R_{A1} + R_{g1} + R_e \quad [\Omega] \quad (3.7)$$

$$R_{eq2} = \left(\frac{(R_{C3} + R_e + R_{g3}) \cdot (R_F + R_e)}{R_{C3} + R_e + R_{g3} + R_F + R_e} \right) + R_{A1} + R_{B2} + R_{g1} + R_{g2} + R_e \quad [\Omega] \quad (3.8)$$

$$R_{eq3} = \left(\frac{(R_e + R_{g2} + R_{g3}) \cdot (R_F + R_e + R_{B3} + R_{C1})}{R_e + R_{g2} + R_{g3} + R_F + R_e + R_{B3} + R_{C1}} \right) + R_{A1} + R_{B2} + R_{C3} + R_{g1} + R_e \quad [\Omega] \quad (3.9)$$

$$R_{eq4} = \left(\frac{(R_e + R_{g3}) \cdot (R_F + R_e + R_{C1})}{R_e + R_{g3} + R_F + R_e + R_{C1}} \right) + R_{A1} + R_{B2} + R_{C3} + R_{g1} + R_{g2} + R_e \quad [\Omega] \quad (3.10)$$

Where:
R_{eqy} is the equivalent resistance. Where y specifies the scenario number.
R_{Ax}, R_{Bx}, R_{Cx} is the resistance of the screen conductors. Where x specifies the cable number and A, B and C specifies the minor section.
R_e is the earthing resistance.

The fault resistance R_F is changed in value. The simulation results shows that a fault resistance with values higher than 1000Ω have little or no influence on the measured resistance, it is therefore decided to change the fault resistance in the span $0 - 1000\Omega$, in steps of 1Ω. All screen conductors have a resistance of 1Ω. The earth resistance R_e have a value of 10Ω. Simulation results may be seen in figure 3.35.

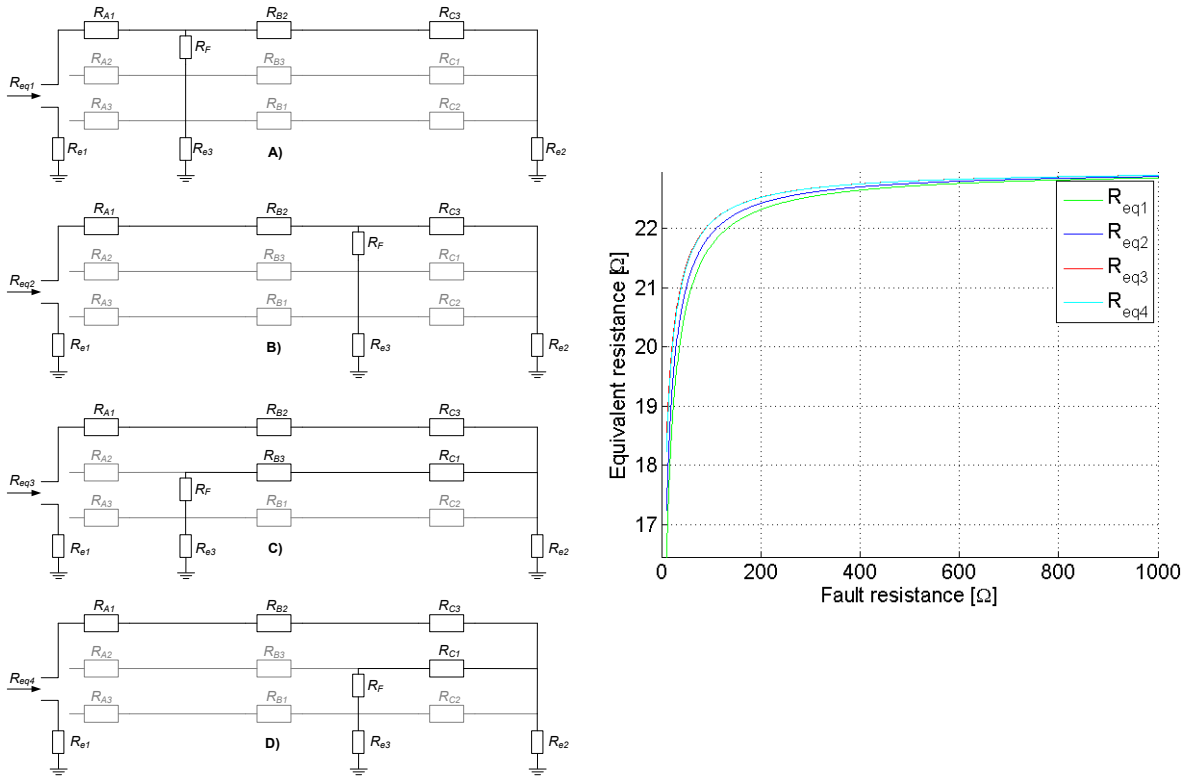

Figure 3.35: Circuit **A)** fault in first link box. Circuit **B)** fault in second link box. Circuit **C)** fault in first link box at a "non-measured" phase. **D)** fault in second link box at a "non-measured" phase. Simulation results is shown to the right.

Using this measuring method the condition of entire major section is determined by only one measurement because the equivalent resistance for the four fault scenarios is more or less the same, as illustrated in figure 3.35. It is possible to measure the presence of a ground fault, if the fault is low resistance meaning less than $\approx 50\Omega$. In case of a ground fault with a high resistance this method is not suitable because the equivalent resistance will become close to the healthy screen circuit resistance and it will therefore be difficult to distinguish between a faulty and a healthy screen circuit. It is not possible with this method to distinguish between a fault in the first and second link box due to the very small deviation between the four equivalent resistances. A significant uncertainty of this method is the grounding resistance it is known that this will change over time[11]. This will have an influence on the measured circuit resistance both in healthy condition and faulty condition.

Sensitivity on fault and earth resistance.

As explained in the above section the earthing resistance will change over time. It is therefore interesting to analyze what effect a change in the earth resistance has. The analysis will take both the fault and earth resistance into consideration. The earth resistance is on the span of $5 - 15\Omega$. The fault resistance is on the span of $0 - 1000\Omega$. The evaluated screen circuit is the first one from the top, shown in figure 3.35.

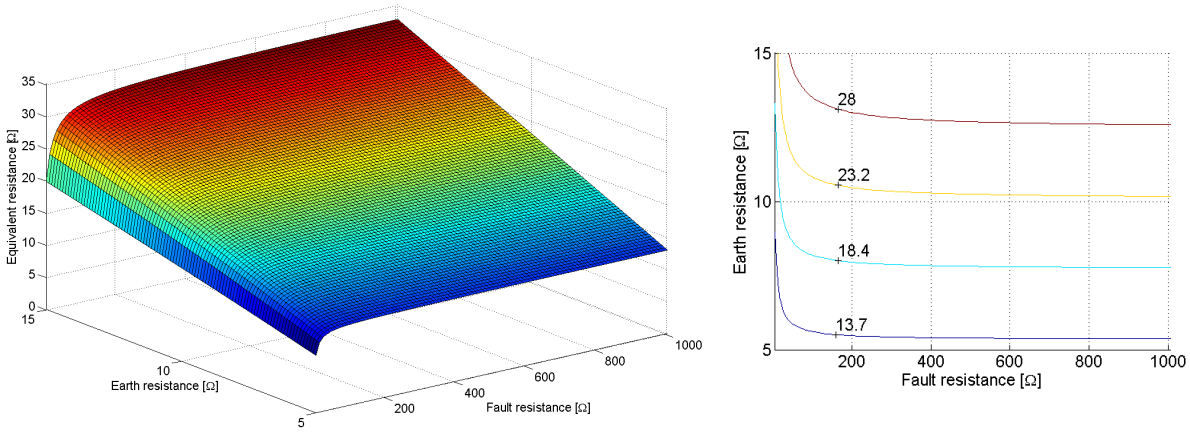

Figure 3.36: To the left is a 3D plot of the equivalent resistance as a function of the earth resistance and fault resistance. To the right is a contour plot of the equivalent resistance

As shown at the contour plot above shows that the equivalent resistance may have the same value with numerous combinations of fault resistances and earth resistances this means that if is very difficult to determine the condition of the link boxes.

The equivalent resistance will at low resistive fault be most sensitive to the fault itself. This means that the fault would be difficult to locate but should be possible to determine that the section is faulty, see figure 3.36. This is true if the earth resistance does not increase in value. At high resistance fault the equivalent resistance will be sensitive to the earth resistance as shown in figure 3.36. It should be mentioned that there at a healthy major section could be measured a resistance that indicate that the section is faulty. This is the case if the earth resistance has changed to a lower value however, if the earth resistance increases the section might look healthy but it is faulty.

Summary of the resistance method

The resistance method is simply and cheap to implement, because measuring equipment are easy accessible. The limitation of the method is one major section, due to the short circuit connection of the screen circuit.

Screen to screen measurement
Disadvantages:

- High resistance faults can not be detected
- Low resistance faults can not be located.

Advantages:

- Disconnections can be detected
- Low resistance short circuit between cross bonding points in first and second link box, can be detected.

Screen to ground measurement
Disadvantages

- Sensitive to the earthing resistance, at the cross bonding points
- High resistance faults cannot be detected.

Advantages

- Low resistive earth faults may be detected.

In order to use this method it is necessary to access at least one end of each major section.

3.4.2 Impedance method

This section first describes the principles of the impedance method. This is followed by two study cases with faults in the first link box and two study cases with faults in the second link box. Finally there will be a discussion about additional opportunities with the impedance method.

Principle of the impedance method

The impedance measurements are used for fault localization on OHL and cable systems [54, p.74]. When the distance protection detects a fault and disconnected the line, by the circuit breakers, it calculates the fault location by the measured voltage and current at the end of the line, as shown in figure 3.37.

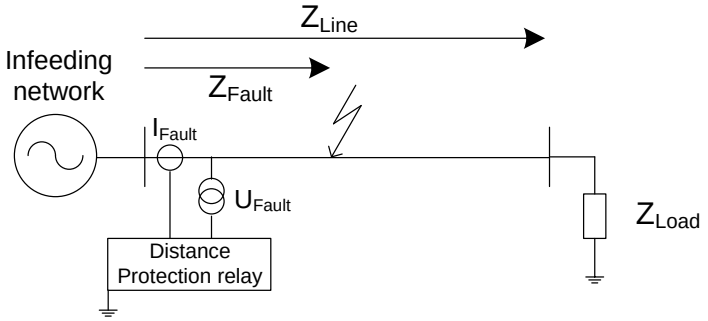

Figure 3.37: Principle of distance protection and measurement of fault impedance.

Using the measured voltage and current, the fault impedance $\mathbf{Z_{Fault}}$ is calculated by equation 3.11 [54] where bold letters indicate vectors. The fault impedance is compared to the impedance of the line $\mathbf{Z_{Line}}$. By this impedance comparison, the distance to the fault is determined.

$$\mathbf{Z_{Fault}} = \frac{\mathbf{U_{Fault}}}{\mathbf{I_{Fault}}} \quad [\Omega] \quad (3.11)$$

Definition

The above mentioned fault impedance $\mathbf{Z_{Fault}}$ will, in the following sections be referred to, as an *apparent impedance*. The apparent impedance is calculated per screen, based on the line-ground voltage at the infeeding voltage source and the respective screen current. The notation of the apparent impedance will be $\mathbf{Z_A}$, $\mathbf{Z_B}$ and $\mathbf{Z_C}$, where the subscript letter referees to screen A, B and C.

In this section the term *equivalent impedance* $\mathbf{Z_{eq}}$ is used. This impedance represents a three phased electrical circuit where a given number of impedances are lumped together to one impedance per screen. The notation of the equivalent impedance will be $\mathbf{Z_{eqA}}$, $\mathbf{Z_{eqB}}$ and $\mathbf{Z_{eqC}}$, where the subscript letter referees to screen A, B and C.

Conversion to screen fault measurement

The following study will analyze different ways of using the impedance method, for screen condition determination. The analysis is based on applying AC voltage to the screen circuit. When AC is applied to the screen circuit, the ratio between current and voltage be governed by the circuit impedance. Where

the impedance consist of a resistive contribution, and a reactive contribution.
The resistance is determined by the conductivity and the additional losses (eddy currents, skin effect, and proximity effect) of the current patch.
The reactance of the screen circuit is determined by the physical lying of the cable system. The screen of a coaxial cable forms a hollow conductor. The inductance of a three screend cable system can be determined by equation 3.12 [53, p.113].

$$L = 2 \cdot 10^{-7} \ln\left(\frac{D}{D_S}\right) \quad [\mathrm{H/m}] \quad (3.12)$$

In equation 3.12, D is the mutual geometrical mean distance and is determined from the equation shown in figure 3.38. The self geometrical mean distance D_S is determined from figure 4.5 in [53, p.110]. It is assumed that the current only flow in the three conductors, and that the material between the forward and return patch is non magnetic.

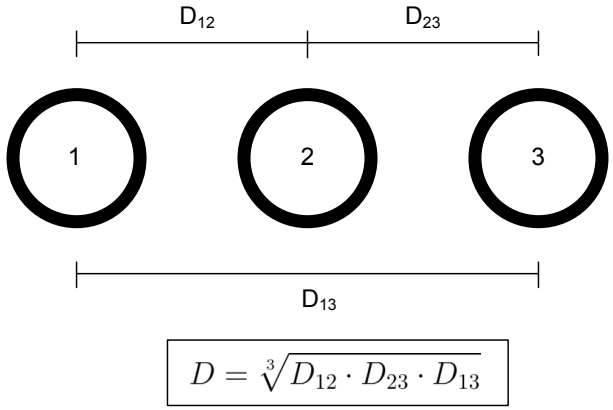

Figure 3.38: Calculation of the mutual geometrical mean distance of a cable system is layed in flat formation.

As explained above the impedance depend on the geometry of the current patch, therefore the impedance is dependent on how the cables are placed in the ground. For cross bonded cable lines, the cables may be placed in two ways. In threefold formation or in flat formation, as shown in figure 3.39.

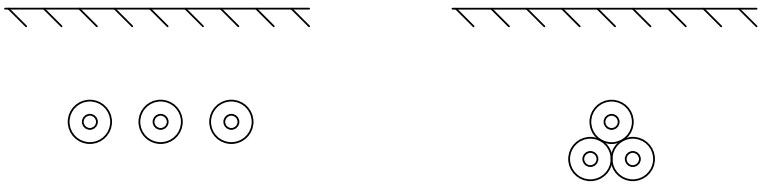

Figure 3.39: A HV cable transmission line, consisting of three separate cables placed in the ground. On the left side of the figure the cables are placed in flat formation. On the right side they are placed in tight triangle.

For the threefold formation the impedances of the three cable screens do not differ because the distance between each of the three cables are equal. Using flat formation the distance between the cables are no

longer equal. To compensate for this inequality the cables may be transposed, as a transposed OHL. In relation to the screen circuit, it is important to distinguish between transposing and cross bonding. A cable line may be cross bonded, without the cable screens being transposed as shown in figure 3.8, in section 3.2.

As described in section 3.2.4, the cross bonded cable screens are connected to ground in every third link box. This forms a return path for the current through the ground. Under normal operating conditions will the screen circuit be symmetrical, hence no ground current. In case of a fault in the screen circuit this will become asymmetrical and thereby will a current flow through ground back to the sources. In order to calculate the voltages and currents in such a system it is decided to model the cable system in DIgSILENT, due to the complexity of the entire system.
The model consists of one major section since this measurement technique is limited by the star point connection in the third link box this is illustrated in the equivalent circuit shown in figure 3.40.

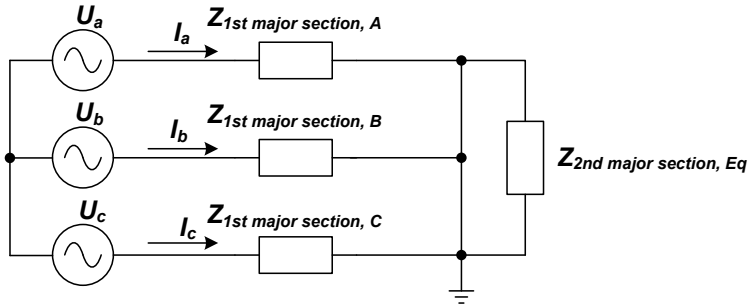

Figure 3.40: Equivalent screen circuit representation of two major sections.

The DIgSILENT model will be used to analyze two fault conditions:

- Screen to screen fault in the first and second link box.
- Screen to ground fault in the first and second link box.

DIgSILENT simulation model

A overview of the simulation model is shown in figure 3.41. The top of the figure is the conductor circuit and the screen circuit is shown in the bottom. The model is based on cable data from an existing 150kV cable line [42]. The simulation model is explained in appendix C. The appendix also provides data used for the model. The DIgSILENT simulation model may be found on the attached CD in the folder '*DIgSILENT*'.

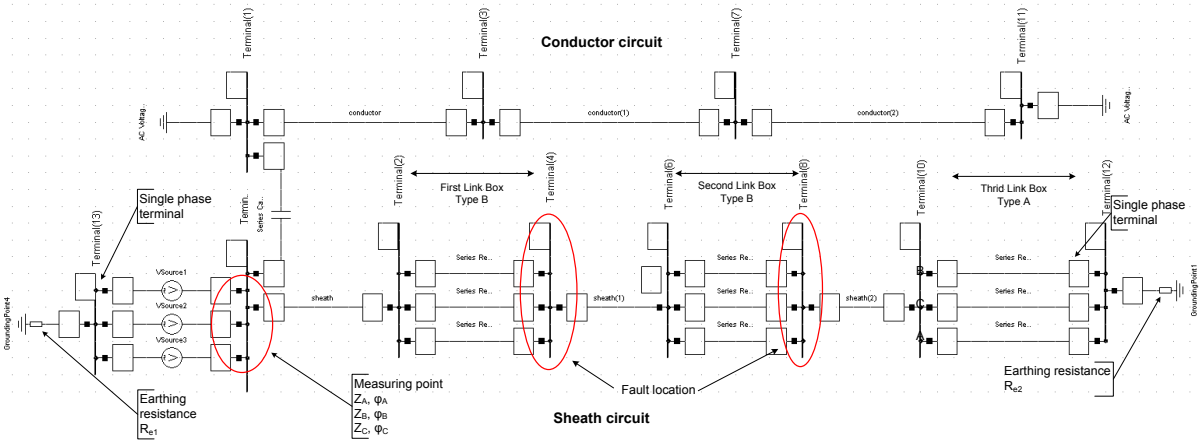

Figure 3.41: DIgSILENT model used for impedance method simulations.

The screen faults are applied at the first and the second cross bonding point in the first and second link box accordingly. In the figure this is terminal 4 and 8. The impedances are measured at the measuring point in figure 3.41. Before any faults are applied the three apparent impedances at a healthy state is simulated. Simulation results are shown in table 3.3.

Screen impedance	$\|\mathbf{Z}\|[\Omega]$	ϕ [°]
$\mathbf{Z_A}$	0.796	44.23
$\mathbf{Z_B}$	0.796	44.18
$\mathbf{Z_C}$	0.796	44.18

Table 3.3: Apparent screen impedances of the healthy screen circuit.

Screen to screen fault at terminal 4

This section consider a screen to screen short circuit at terminal 4 in figure 3.41. The simulated results provides apparent impedances at the measuring point shown in figure 3.41. The short circuit is applied between screen ***a*** and ***b***. Due to the cross bonding at the first link box, the faulty screens at the measuring point will be screen ***c*** and ***a***, as shown in figure 3.42.

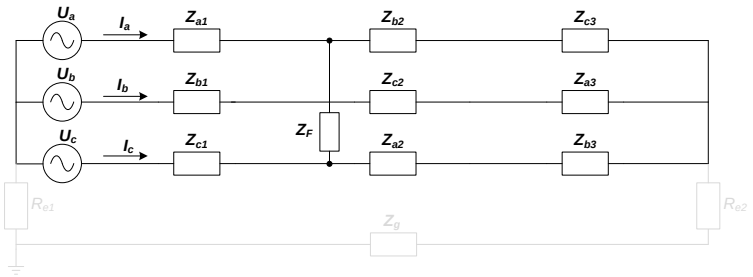

Figure 3.42: Equivalent screen circuit of a major section. Fault is applied in the first link box.

In figure 3.42 vectors are denoted with boldfaced letters. Subscript letters denotes screen *a*, *b* or *c*. The subscript number *1-3* denotes the section. Where the first section is between the measuring point and first link box, second section is between first and second link box and the third section is between the second and third link box. The screen voltages $\mathbf{U_a}$, $\mathbf{U_b}$ and $\mathbf{U_c}$ and the screen currents $\mathbf{I_a}$, $\mathbf{I_b}$ and $\mathbf{I_c}$ is the measured quantities used to calculate the screen impedances $\mathbf{Z_A}$, $\mathbf{Z_B}$ and $\mathbf{Z_C}$ which is done by equation 3.11. The ground loop is represented by two resistances $\mathbf{R_{e1}}$ and $\mathbf{R_{e2}}$ which are the ground resistance at respectively the substation and the third link box and an impedance $\mathbf{Z_g}$ which represent the ground current return path. This impedance may be determined by Carson equations [53, p.118].

In order to study the influence of the fault impedance between screen *a* and *b* a number of simulations have been carried out. The fault impedance have been changed in value in the span $0-50\Omega$ in steps of 0.05Ω. The fault impedance is purely resistive. Simulation results may be seen in figure 3.43 and 3.44.

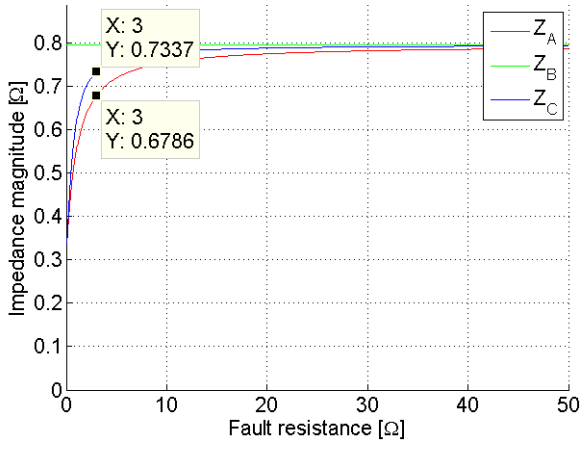

Figure 3.43: Apparent impedance magnitude where a screen to screen fault is applied in the first link box.

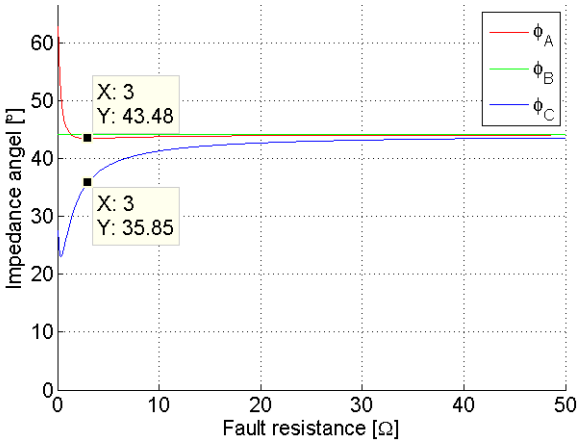

Figure 3.44: Apparent impedance angle where a screen to screen fault is applied in the first link box.

The impedance of screen *b* is not affected by the fault. Whereas the impedances of screen *a* and *c* drops

significant in magnitude for low fault impedances. With a fault impedance of 3Ω the screen *a* impedance magnitude drops by ≈ 8% and screen *c* by ≈ 15%. As the fault impedance gain higher values the two screen impedances becomes less affected. At fault impedances $\mathbf{Z_F} > 30\Omega$ it become very difficult to distinguish between a healthy major section and a faulty one.

The simulations showed that the screen impedance of screen *a* and *c* was not with equal magnitude and angle at low impedance faults. It was expected that these impedances were more or less the same. It is believed that two things could cause this difference: The asymmetrical condition caused by the applied fault and/or the flat formation of the cable system.
It is therefore decided to analysis the fault condition more in details to determine what causes the difference in the two faulty screen impedances.

The analysis is based on the screen circuit shown in figure 3.45. The screen circuit is simplified by excluding the ground return path. The return path through the ground may be omitted, since earthing resistance at the third link box is relatively large compared to the screen circuit impedance. The screen circuit impedance is less than one ohm whereas the earthing resistance is several ohms [11, p. 5]. All nine screen conductors are given equal impedance values, which is $\frac{1}{3}\mathbf{Z_A}$, where $\mathbf{Z_A}$ is screen *a* healthy screen impedance as shown in table 3.3. The fault impedance $\mathbf{Z_F}$ is set to 3Ω

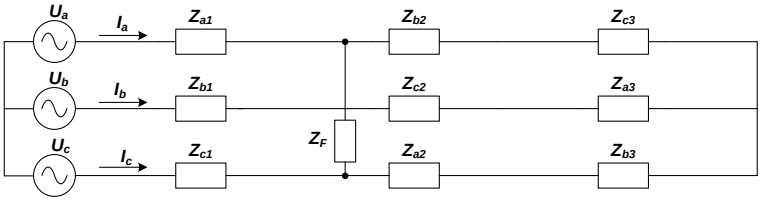

Figure 3.45: Equivalent screen circuit of a major section with a screen to screen fault in first link box.

The three voltage sources are set to 1V RMS and each phase shifted by 120°.

$$\begin{aligned} \mathbf{U_a} &= \quad 1\angle 0 \\ \mathbf{U_b} &= 1\angle -120 \\ \mathbf{U_c} &= \quad 1\angle 120 \end{aligned} \qquad [\mathrm{V}] \quad (3.13)$$

The detailed calculations are shown in appendix A and the results are presented here.

The screen circuit shown in figure 3.45 is rearranged to the circuit shown in figure 3.46. The screen impedances have the given values listed in table 3.4.

Equivalent impedance	$\|\mathbf{Z}\|$ [Ω]	ϕ [°]
$\mathbf{Z_{eqA}}$	0.678	37.41
$\mathbf{Z_{eqB}}$	0.859	46.93
$\mathbf{Z_{eqC}}$	0.678	37.41

Table 3.4: Equivalent impedances.

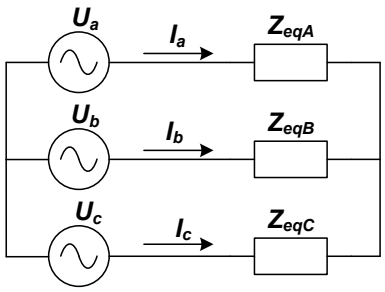

Figure 3.46: Simplified equivalent screen circuit of a major section.

The screen currents becomes asymmetrical despite the two faulty screens have equal impedances ($\mathbf{Z_{eqA}} = \mathbf{Z_{eqC}}$), as shown in table 3.4. The asymmetrical currents are caused by the 120° phase shift of the voltage sources. The voltages are symmetrical, hence the apparent impedances will be asymmetrical, as shown in table 3.5.

	Calculated		Deviation	
Apparent impedance	$\|\mathbf{Z}\|$ [Ω]	ϕ [°]	$\|\mathbf{Z}\|$[%]	ϕ[%]
$\mathbf{Z_A}$	0.672	42.79	0.9	3.4
$\mathbf{Z_B}$	0.796	44.23	≈ 0	≈ 0
$\mathbf{Z_C}$	0.738	34.84	0.6	2.8

Table 3.5: Apparent screen impedances and there deviation to simulated results.

As shown in above table the three apparent impedances have different values and differs less than 1% in magnitude compared to the simulated results. The deviation may be caused by the simplified screen circuit. Reason for the difference in the faulty screens are due to the asymmetrical screen circuit caused by fault impedance and not the flat formation of the cable system. Furthermore this type of fault is characterized with balanced voltages and unbalanced currents.

Screen to ground fault at terminal 4

It is now studied how the circuit is influenced by an earth connection in the first link box. The earth connection is applied by making a single screen to ground short circuit at terminal 4 in figure 3.41. The fault is applied to screen *a* meaning that at the measuring point the faulty screen is screen *c*, as shown in figure 3.47.

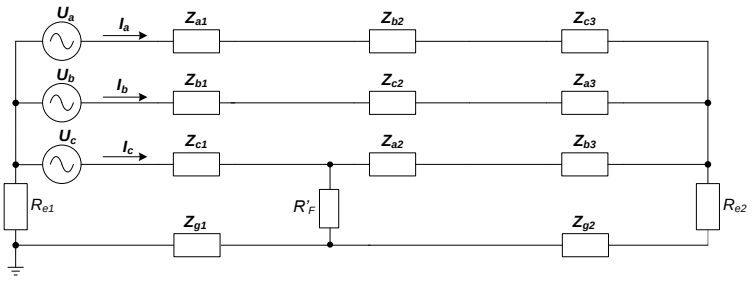

Figure 3.47: Screen circuit of one major section including ground loop. $R_F^{'}$ indicate screen to ground fault in the first link box.

The fault resistance $R_F^{'}$ is the serial connection of the earthing resistance R_e at the star connection of the SVL's and the actual fault resistance R_F between the cross bonding connection and the housing of the link box as shown in figure 3.48.

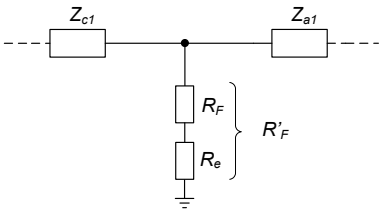

Figure 3.48: Screen to ground fault in link box. R_F is the fault resistance and R_e is the earthing resistance from the fault to ground potential.

$$R_F^{'} = R_e + R_F \qquad [\Omega] \quad (3.14)$$

Grounded voltage source

The fault resistance $R_F^{'}$ is changed in the span $5-50\Omega$ in order to study if it is possible to distinguish between a healthy and faulty cross bonding. As a reference the healthy screen impedances in table 3.3 is used. The voltage sources are placed in a substation therefore it is believed that the earthing resistance R_{e1} is very low 0.1Ω or less [2, p. 32]. The voltage sources grounding resistance is therefore set to 0.1Ω. The earthing resistance at the link boxes can have value in the span of $5-15\Omega$ [18][2]. The earthing resistance at the star point grounding R_{e2} in the third link box is set to 10Ω. Simulation results of the measured impedances may be seen in figure 3.49 and 3.50.

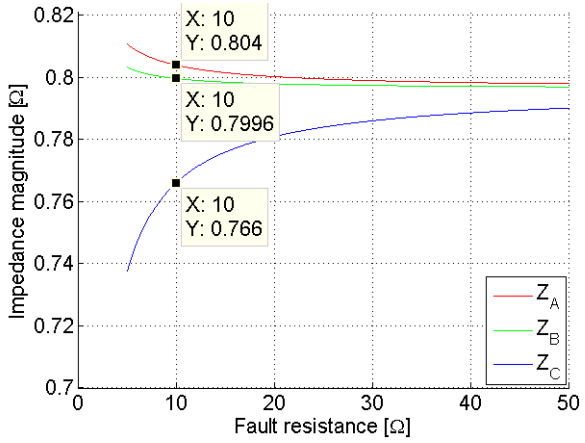

Figure 3.49: Apparent impedance magnitude where a screen to ground fault is applied in the first link box.

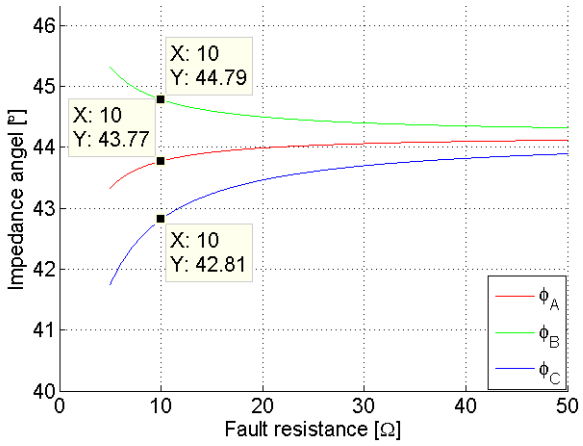

Figure 3.50: Apparent impedance angle where a screen to ground fault is applied in the first link box.

In the above figures simulation results with a fault resistance $R_F^{'} = 10\Omega$ are pointed out. If the earthing resistance is 10Ω at the first and third link box and a ground fault is present in the first link box the deviation between the faulty and healthy cross bonding is low, as shown in table 3.6. Determining the condition of the cross bonding would be difficult due to measurement errors.
If a similar fault happens in the second link box the maximum deviation between healthy and faulty condition is $\approx 1.3\%$ in impedance magnitude and $\approx 1.5\%$ for the angle. Based on the very small deviation this measuring technique is not a very good solution.

Apparent impedance	$\lvert\mathbf{Z}\rvert$ [%]	ϕ [%]
$\mathbf{Z_A}$	≈ 0.7	≈ 0.4
$\mathbf{Z_B}$	≈ 0.2	≈ 0.7
$\mathbf{Z_C}$	≈ 3.2	≈ 3.0

Table 3.6: Apparent impedances deviation compared to healthy screen conductor impedances.

Ungrounded voltage source

In order to improve the measuring technique the effect of the grounding is studied. From a practical point of view the voltage source grounding is the simplest one to disconnect. Removing this grounding the voltage sources will become ”floating” as shown in figure 3.51. The current path in the ground is now reduced only to be between the faulty link box and the solid grounded star point connection in the third link box.

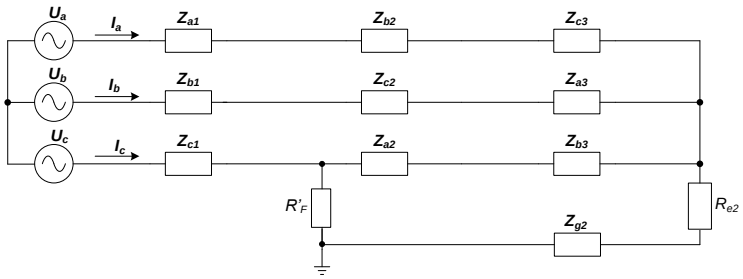

Figure 3.51: Screen circuit of one major section. Screen to ground fault in the first link box.

A simulation with floating voltage sources are carried out. The simulation results are shown in figure 3.52 and 3.53. Simulation parameters are identical to the previous simulation in section 3.4.2.

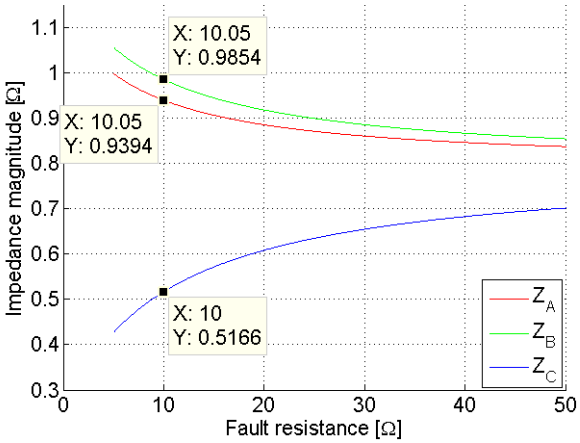

Figure 3.52: Apparent impedance magnitude where a screen to ground fault is applied in the first link box.

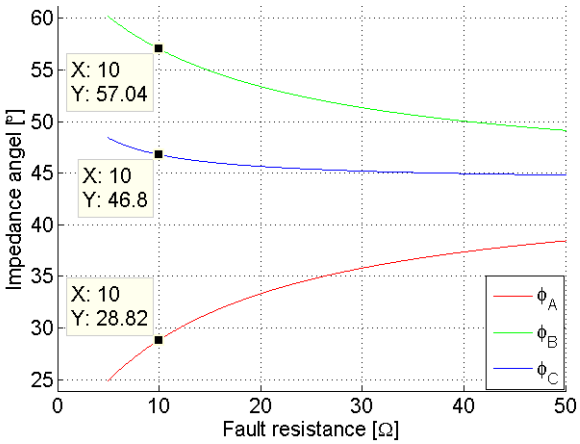

Figure 3.53: Apparent impedance angle where a screen to ground fault is applied in the first link box.

The simulation results are significantly different when the ground connection is removed at the voltage sources. As shown in table 3.7 the faulty screen has decreased more than 30% in magnitude from the value of a healthy value. This improvement should make the measuring technique suitable for detection of a fault in the screen circuit and it may even be possible to determine the location of the fault.

Apparent impedance	$\lvert\mathbf{Z}\rvert$ [%]	ϕ [%]
$\mathbf{Z_A}$	≈ 19.9	≈ -33.5
$\mathbf{Z_B}$	≈ 22.6	≈ 31.1
$\mathbf{Z_C}$	≈ -35.7	≈ 1.7

Table 3.7: Apparent impedances deviation relative to healthy state. With floating voltage sources.

The impedance magnitude of the two non-faulty screens are increased approximately 20% above health value, which was not expected. This phenomenon is therefore analyzed.

The simulation results showed that the screen currents were not affected by the ground fault and was still balanced as shown in table 3.8. The symmetrical currents indicate that only a very small part of the current will flow through the ground.

screen current	$\lvert\mathbf{I}\rvert$ [A]	ϕ [°]
$\mathbf{I_a}$	1.27	-43.8
$\mathbf{I_b}$	1.26	-164.3
$\mathbf{I_c}$	1.26	76.1

Table 3.8: Measured currents during a single screen fault to ground in first link box. $R_F^{'} = 10\Omega$.

Based on the above observations the screen circuit shown in figure 3.51 reduced so the ground loop now consist of two earthing resistances, as shown in figure 3.54.

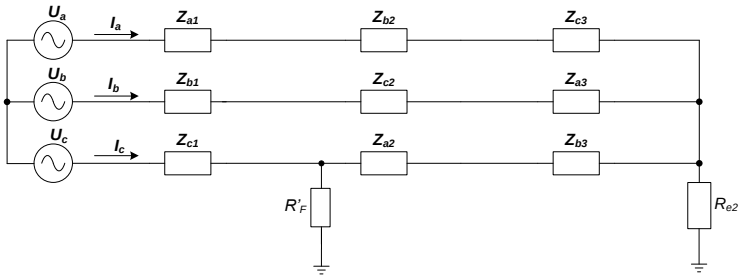

Figure 3.54: Screen circuit of one major section. Ground fault in the first link box, earth impedance neglected.

The following calculations are based on the screen circuit above. All nine screen conductors are given equal impedance values, which is $\frac{1}{3}\mathbf{Z_A}$, where $\mathbf{Z_A}$ is screen *a* healthy screen impedance as shown in table 3.3. The earthing resistance in the third link box R_{e2} is set to 10Ω and fault resistance $R_F^{'}$ to 10Ω.

The three voltage sources are set 1V RMS and each phase shifted by 120°.

$$\begin{aligned} \mathbf{U_a} &= \quad 1\angle 0 \\ \mathbf{U_b} &= 1\angle -120 \\ \mathbf{U_c} &= \quad 1\angle 120 \end{aligned} \quad [\mathrm{V}] \quad (3.15)$$

The detailed calculations are shown in appendix B and the results are presented here.

The screen circuit shown in figure 3.54 is rearranged to the circuit shown in figure 3.55.

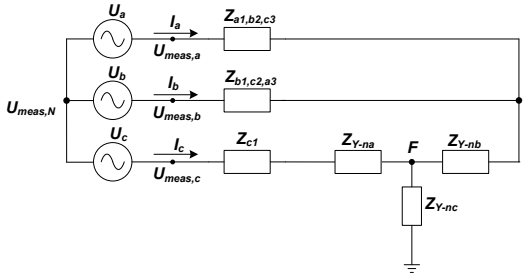

Figure 3.55: Reduced screen circuit.

The voltage is zero at point **F** in figure 3.55, due to the ground connection. The voltage at $U_{meas,N}$ increases in magnitude and is phase shifted 180° relative to phase c. This decreases the voltage at $U_{meas,c}$ so that the screen current is unaffected as simulation results showed in table 3.8.

The voltage at the measuring point at screen a and b will increase since these voltage is the vectorial sum of the sources and the neutral voltage. This explain the increase in the measured impedances at the non faulty screens since the screen currents are the same as for the healthy screen circuit, as illustrated in figure 3.56.

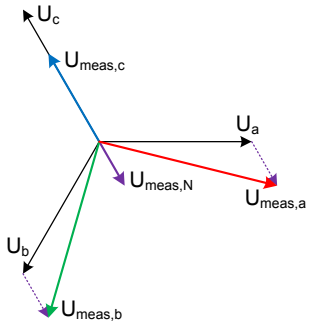

Figure 3.56: Vector representation of the voltages at the measuring point and the sources during at screen to ground fault.

In table 3.9 is the calculated results and there deviation relative to the simulated results. The deviation may be cause by the simplified screen circuit use for the analysis. Furthermore this type of fault is characterized with unbalanced voltages and balanced currents.

	Calculated		Deviation	
Apparent impedance	$\lvert\mathbf{Z}\rvert$ [Ω]	ϕ [°]	$\lvert\mathbf{Z}\rvert$[%]	ϕ[%]
$\mathbf{Z_A}$	0.952	30.42	0.3	3.4
$\mathbf{Z_B}$	0.958	57.35	1.8	1.0
$\mathbf{Z_C}$	0.526	43.72	2.7	2.7

Table 3.9: Apparent impedances and there deviations to simulated results.

Screen to screen fault at terminal 8

This section considers a screen to screen short circuit at terminal 8, hence a fault in the second link box. The simulation results provides apparent impedances at the measuring point shown in figure 3.41. The short circuit is applied at terminal 8 between screen ***b*** and ***c***. Due to the cross bonding at the two link boxes the faulty screens at the measuring point will be screen ***c*** and ***a***, as shown in figure 3.42.

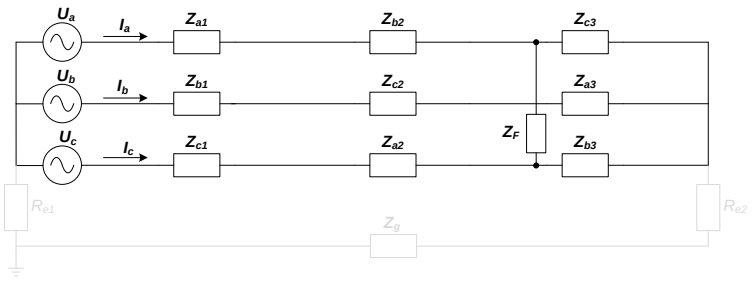

Figure 3.57: Equivalent screen circuit of a major section. Fault is applied in the second link box.

In order to study the influence of the fault impedance between screen ***b*** and ***c*** in the second link box, a number of simulations have been carried out. The fault impedance have been changed in the span $0-50\Omega$ in steps of 0.05Ω. The fault impedance is purely resistive. Simulation results may be seen in figure 3.58 and 3.59.

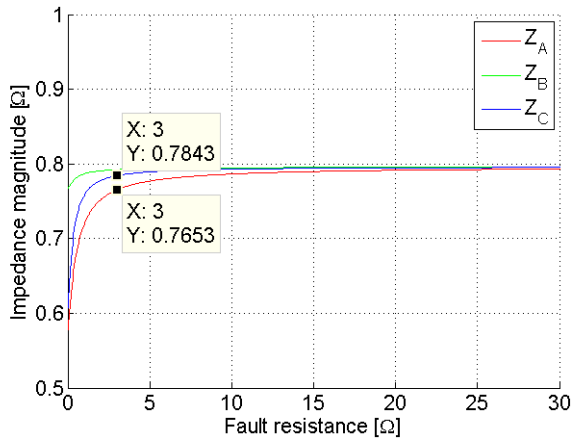

Figure 3.58: Impedance magnitude where a screen to screen fault is applied in the second link box.

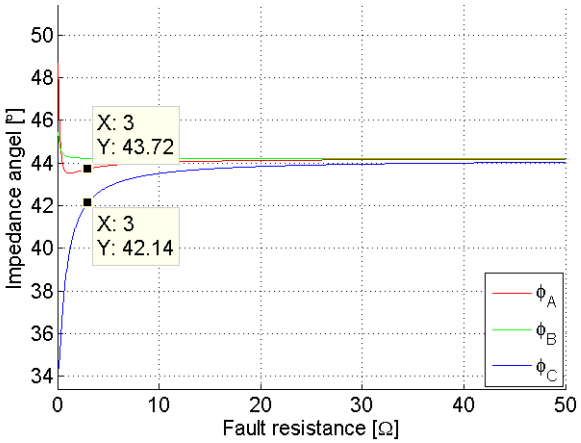

Figure 3.59: Impedance angle where a screen to screen fault is applied in the second link box.

As the above figures illustrates the simulated fault impedances have similar characteristics as the simulations performed in section 3.4.2. This make the fault localization difficult, it is not possible to distinguish between a low resistance fault in the second link box and a high resistance fault in the first link box.

Apparent screen impedance	Simulated $\lvert\mathbf{Z}\rvert$ [Ω]	Simulated ϕ [°]	Deviation $\lvert\mathbf{Z}\rvert$[%]	Deviation ϕ[%]
Simulation results first link box				
$\mathbf{Z_A}$	0.679	43.48	-14.7	≈ 0
$\mathbf{Z_B}$	0.796	44.18	≈ 0	≈ 0
$\mathbf{Z_C}$	0.734	35.85	-7.8	-18.9
Simulation results second link box				
$\mathbf{Z_A}$	0.765	43.72	3.9	1.2
$\mathbf{Z_B}$	0.792	44.22	0.5	≈ 0
$\mathbf{Z_C}$	0.784	42.14	1.5	4.6

Table 3.10: Apparent screen impedances and there deviation to healthy state.

A screen to screen fault is more pronounced when applied in the first link box, as shown in table 3.10.

Screen to ground fault at terminal 8

This study case considers a screen to ground fault applied at terminal 8. The fault was applied between screen conductor ***b*** and ground potential. Due to the cross bonding the faulty screen at the measuring point is screen ***c*** as shown in figure 3.60. The voltage sources are chosen to be floating as the analysis in section 3.4.2 concluded as the most useful source connection.

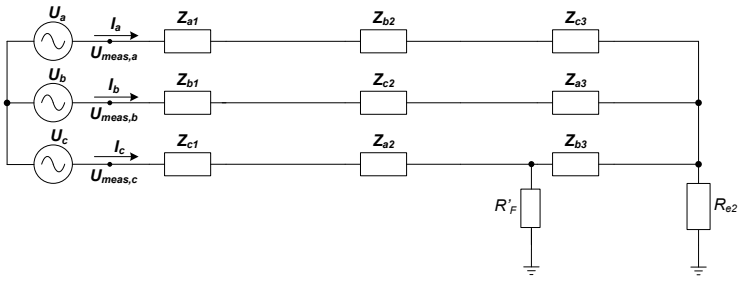

Figure 3.60: Equivalent screen circuit of a major section. The screen to ground fault is applied in the third link box.

In order to study the influence of the fault impedance between ground and the screen conductor, a number of simulations have been carried out. The fault impedance has been changed in the span $0-50\Omega$ in steps of 0.05Ω. The fault impedance is purely resistive. Simulation results may be seen in figure 3.61 and 3.62.

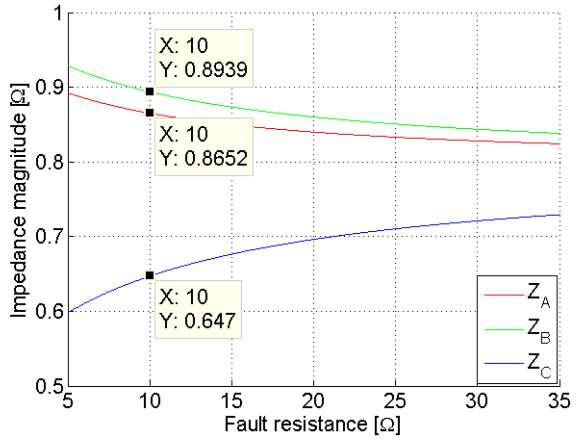

Figure 3.61: Apparent impedance magnitude where a screen to ground fault is applied in the second link box.

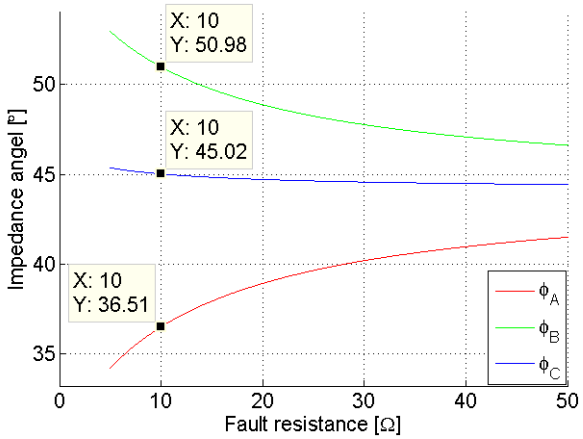

Figure 3.62: Apparent impedance angle where a screen to ground fault is applied in the second link box.

As the above figures illustrate the simulated fault impedances have similar characteristics as the simulations done in section 3.4.2. This does fault localization difficult it is not possible to distinguish between a low resistance fault in the second link box and a high resistance fault in the first link box.

Apparent screen impedance	Simulated $\lvert\mathbf{Z}\rvert$ [Ω]	ϕ [°]	Deviation $\lvert\mathbf{Z}\rvert$[%]	ϕ[%]
Simulation results first link box				
$\mathbf{Z_A}$	0.939	28.82	17.9	-34.8
$\mathbf{Z_B}$	0.985	57.04	23.7	29.1
$\mathbf{Z_C}$	0.517	46.80	-35.1	5.9
Simulation results second link box				
$\mathbf{Z_A}$	0.865	36.51	8.7	-17.5
$\mathbf{Z_B}$	0.894	50.98	12.3	15.4
$\mathbf{Z_C}$	0.647	45.02	-18.7	1.9

Table 3.11: Apparent screen impedances and there deviation to healthy state.

A screen to ground fault is more pronounced when applied in the first link box, as shown in table 3.11.

Additional options with the impedance method

By increasing the screen circuit impedance a larger fault resistance will become detectable. This could be done by:

- Increasing the measuring frequency
- Series connection of cable systems consisting of several major section

Increasing the measuring frequency
The screen circuit is inductive and the impedance of an inductor is proportional to the frequency as shown in equation 3.16 [46, p. 387].

$$Z_L = 2\pi \cdot f \cdot L \quad [\Omega] \quad (3.16)$$

Where:
L is the inductance of the screen.
f is the measuring frequency.

The advantage of this option is that no further changes of the screen circuit must be made, it require however a voltage source with adjustable frequency which may be difficult to purchase.

Series connection of cable systems consisting of several major section
Considering a cable system with three major sections, as shown in figure 3.63. The total screen circuit impedance is increased three times by series connecting the major sections.

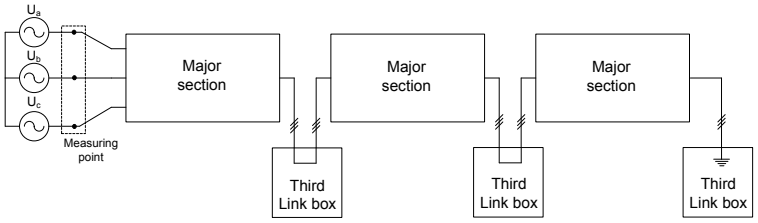

Figure 3.63: Principle for a impedance measuring setup where three major section are connected in series in every third link box.

In order to do so, every third link must be accessed to do the series connection of the sections. If these boxes are difficult to access this option may be time and cost ineffective.

Section summary

In this section, two scenarios has been studied. Screen to screen fault and screen to ground fault. There have been made simulations of both cases using the simulation software DIgSILENT. The simulation results were further studied, by detailed calculations to find the origin of the obtained simulation results.

Screen to screen fault

The screen to screen fault is characterized by balanced voltages and unbalanced screen currents. The two faulty screens impedances decreases with unequal magnitudes due to the 120° phase shift between the source voltages. The non faulty screen remains unaffected. Fault localization of this fault type is difficult.

Screen to ground fault

The voltage sources should be floating in order to detect screen to ground faults. The screen to ground fault is characterized by balanced screen current and unbalanced voltages, hence an increase of the neutral voltage at the star point connected voltage sources. The increase at the neutral voltage leads to an increase of the voltage at the two non-faulty screens, hence these impedances will increase compared to the impedance at healthy state. The voltage at the faulty screen will decrease and the screen impedance too. Fault localization of this fault type is difficult.

Additional options with the impedance method

The impedance method may be improved in order to detect larger fault resistances by increasing the measuring frequency or by series connection major sections at cable systems consisting of several major sections.

3.4.3 Travelling wave method

This section will briefly describe how the travelling wave theory, can be used to determine the condition of the link boxes.

Travelling wave theory
Any transmission line may be modeled in two ways, either as lumped parameters or as distributed parameters. The lumped parameter representation is typically used for load flow analysis. The problems concerning the use of lumped parameter representation, is further explained in Appendix H. Figure 3.64 shows a sketch of a two wire transmission line represented by lumped parameters.

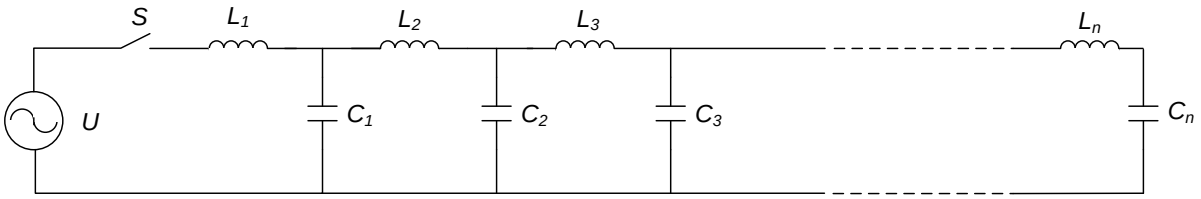

Figure 3.64: Transmission line represented as lumped parameters [15].

The system is energizes by closing the breaker (S). The energization starts with a current flowing through (L1) , charging (C1). As voltage is established across (C1) current will start to flow through (L2) and so on. From this explanation it may be seen that from the time the breaker closes, the voltage in the end of the line is delayed.

To analyze the energization the line is assumed loss less, and thereby no resistance is included the analysis is based on [15]. As explained currents starts to flow, charging (C1). Δt after the energization has started Δx of the line is charged, see equation 3.17.

$$Q = CU \triangle x \tag{3.17}$$

Due to the definition of current $I = {}^{\Delta Q}/_{\Delta t}$, equation 3.17, may be expressed as equation 3.18.

$$I = CU \frac{\triangle x}{\triangle t} \tag{3.18}$$

Obtaining the limit condition of equation 3.18.

$$\lim_{\triangle x \to 0} I = \lim_{\triangle x \to 0} CU \frac{\triangle x}{\triangle t} = CU \frac{dx}{dt} \tag{3.19}$$

Since ${}^{dx}/_{dt}$ is the speed of propagation, this may be substituted by the propagation speed v.

$$I = CUv \tag{3.20}$$

As the current flows there is created a magnetic flux round the conductor. The magnetic flux induces an emf, in the loop formed by the conductors and the wave front. The flux linkage may be determined by equation 3.21 [15].

$$\Phi = L\Delta xI = L\Delta xCUv \tag{3.21}$$

The induced emf is, the rate of change of the flux linkage, per rate of time.

$$\frac{d\Phi}{dt} = LCUv\frac{\Delta x}{\Delta t} \tag{3.22}$$

The limit of the right side of equation 3.22, is shown in equation 3.23.

$$\lim_{\triangle x \to 0} LCUv\frac{\Delta x}{\Delta t} = LCUv^2 \tag{3.23}$$

$^{d\Phi}/_{dt}$ is the voltage, thereby equation 3.23 may be written in terms of the propagation speed v, see equation 3.24.

$$v = \frac{1}{\sqrt{LC}} \quad [^{\mathrm{m}}/_{\mathrm{s}}] \tag{3.24}$$

It may now be seen that the speed of propagation is dependent on the media of the surrounding medium [15, p.236].

The propagation voltage and current wave are associated according to the surge impedance of the line. The velocity may be derived from equation 3.20.

$$I = CUv = \frac{CU}{\sqrt{LC}} \Longrightarrow \frac{U}{I} = Z_0 = \sqrt{\frac{L}{C}} \tag{3.25}$$

The typical surge impedances for OHL is about 400Ω, and for cables this is typically about $30 - 80\Omega$. Because the closer spacing makes the capacitance larger and the inductance smaller [15, p.237].

Reflection and refraction

When the current and voltage waves meet a discontinuous point, a part of the wave is refracted and a part is reflected. This is illustrated in figure 3.65.

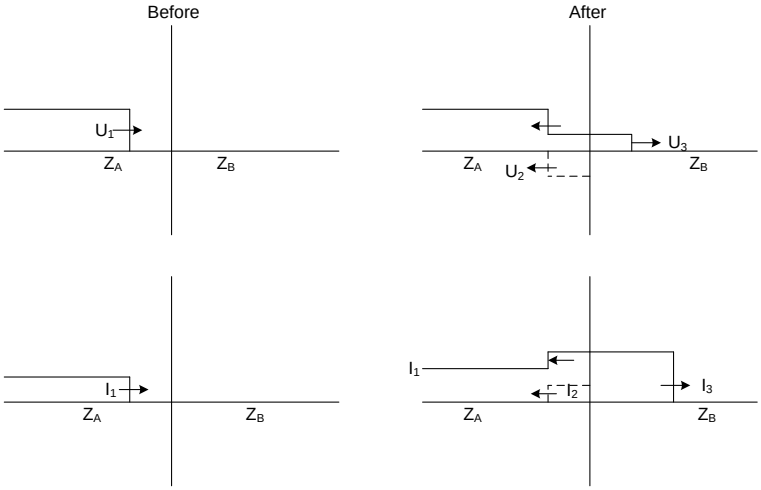

Figure 3.65: Voltage and current wave reflected and refracted at the junction between Z_A and Z_B.[15]

At the discontinuous point the energy of the reflected and refracted wave equals the energy of the incident wave, due to energy conservation.
The reflection and refraction coefficients are given by equation 3.26 and 3.27 [15, p.244].

Reflection:

$$U_2 = U_1 \cdot \frac{Z_B - Z_A}{Z_A + Z_B} \quad [\mathrm{V}] \quad (3.26)$$

Refraction:

$$U_3 = U_1 \cdot \frac{2 \cdot Z_B}{Z_A + Z_B} \quad [\mathrm{V}] \quad (3.27)$$

In equation 3.26 and 3.27, Z_B is the surge impedance of the media the wave is propagation into and Z_A is the surge impedance of the media the wave is coming from.

3.4.4 Section summary

Due to the above stated reflections, it is expected that these will change during fault conditions. The travelling wave method may be used to evaluate if the surge impedances in the link boxes have changed.

3.5 Chapter summary

The analysis of cross bonded cable systems with a number of interesting conclusions. The most important conclusions are listed below.

- **State of the art analysis**. There was found no literature that describes methods that can be used to determine the condition of cross bonded cable systems.

- **Faults in link box**. Faults in Type B link boxes will most likely lead to the cross bonding does not work as intended.

- **Resistance method**. The conclusion was that, it is a simple and well known measuring technique that can detect both screen to screen fault and screen to ground fault. However the screen to ground measurements are sensitive to the earthing resistance at both the fault location but also at the third link box. This is a problem because the earthing resistance most likely will change over time, hence the healthy state resistance will change which is not desirable. Localization of a fault is difficult using this method.

- **Impedance method**. This method is simple and well known and can detect both screen to screen faults and screen to ground faults. By using floating voltage sources is the healthy state screen impedances not sensitive to the earthing resistance at the third link box. The method may be improved, in order to detected a larger fault resistance, by increasing the measuring frequency or by series connecting major sections for cable systems consisting of several major sections. Localization of a fault is difficult using this method.

- **Travelling wave method**. This method is well known but complex. Screen to screen faults and screen to ground faults may be detectable due to the change in surge impedance and thereby changes the reflection/refraction coefficients. Localization of the fault may be possible using this method.

Chapter 4

Problem statement

As described in the problem analysis, problems concerning determination and localization of link box faults may be difficult. Due to the lack of experience within the specific area, this study is based on how impedance measurements can be used for link box condition determination.

Distance protection is widely used as network protection on transmission lines. Distance relays measure the line impedance online and compared this to a preconfigured line impedance. The transmission companies therefore have to measure precisely the line impedance in order to configure the distance relays. Therefore it would be preferable if the measuring equipment already owned by the transmission companies, could be used for condition monitoring of the link boxes. The main focus of this study will therefore be a condition evaluation based on impedance measurements.

The use of impedance measurements for link box condition determination will be validated according to field measurements of the 150kV cable line FRT-NOR. The validation will include a comparison between simulations and measurements. The validated simulation model will further be used to consider study cases. The study cases will be selected in collaboration with N1, to represent possible screen circuit faults, at the cable line FRT-NOR.

The problem formulation is divided into three main topics.

1 General use of impedance measurements, for link box condition determination, including suggestions of how to perform measurements.
2 The above mentioned study cases selected in collaboration with N1.
3 To come up with suggestions on how to perform impedance measurements at lines consisting of several major sections.

Questions regarding general use and measurements:

- How can the measuring strategy be improved in order to increase the sensitivity according to link box faults?
- To what extent can line impedance measuring equipment be used for detection of a faulty link box?

Questions regarding study cases:

- The study cases will provide the largest detectable fault resistances for different fault conditions at the line FRT-NOR.

Questions regarding lines consisting of several sections:

- How may the impedance measurements be used at lines consisting of several sections?
- To what extent is fault localisation possible, when third link box is accessible?

To answer the general questions, the screen circuit will be studied analytically regarding Sc-Sc and Sc-Gr fault. It will also be studied analytically if line impedance measuring equipment can be used for measuring of the apparent screen impedances defined in section 3.4.2 on page 46. A simulation model of the cable line FRT-NOR will be made. The model will be validated according to measurements as earlier mentioned, and used for study cases.

The detectable resistance from the study cases will be compared to test results form a link box test. The link box test will be performed using a link box similar to the used boxes at the line FRT-NOR. The link box will be filled with water and the resistance between the connection points will be measured.

4.1 Delimitations

The condition of the screen circuit is affected by several things e.g. broken conductors as well as unwanted connections. The apparent screen impedances, defined in section 3.4.2, are affected in different ways according to the type of fault. The possibility of localizing a link box fault may depend on how the apparent impedances are affected and thereby the type of fault, therefore the condition determination is divided into two main subjects:

- Detection of whether the screen circuit is healthy or faulty
- Determination of the location of a given fault.(in which link box)

Detection of whether the screen circuit is healthy or faulty is the primary task, and the secondary task is the localisation of a given fault.

The general analysis of the screen circuit regarding improvement of the measuring technique is limited only to include Sc-Sc and Sc-Gr faults.

The cable modelling will be done in the simulation software DIgSILENT power factory.

The problem analysis provided a short introduction to the travelling wave measuring technique. In cooperation with the supervisors it is decided that the impedance method is the main focus of this project. When the field measurements are performed, and time is allow, there will be made travelling wave measurements. The measuring results will be included as a test report. Only if time allows it will an analysis of the measuring results be performed.

The functionality of the SVLs is not considered.

4.2 Method

The project is based on an initial state of the art analysis given in the problem analysis. From the initial study, it became clear that there is very little knowledge and experience within the area. Therefore the following study is based on already used fault detection techniques. To study the screen circuit, a representative simulation model will be made. The model will be validated by comparing simulation results to full scale test of the transmission line FRT-NOR. The model will be adjusted to represent the actual circuit for both steady state and for applied screen circuit faults. The adjusted simulation model will used to analyze the study cases. Parallel to the screen circuit analysis and modeling the electric characteristic of the water filled link box will examined by performing a full scale test.

4.3 Report structure

The report is divided into seven chapter and an appendix part, as illustrated in figure 4.1.

Chapter 1 - Introduction
The first chapter is the introduction, which explains the background of the project.

Chapter 2 - System description
Physical and electrical parameters of the 150kV cable line FRT-NOR are presented.

Chapter 3 - Problem analysis
The second chapter describe different bonding techniques, followed by an analysis of the possible implementations of already used fault detection techniques to determination the condition of the screen circuit.

Chapter 4 - Problem statement
Chapter three provide the general questions for the project to answer.

Chapter 5 - Analysis and measuring techniques
The fourth chapter is a study of how the screen circuit is influenced by sc-sc and sc-gr faults. The screen circuit is evaluated to achieve large sensitivity according to screen circuit faults. Different measuring techniques are considered.

Chapter 6 - Validation of simulation model
Chapter five is to compare simulation results to measurements, deviations are studied and the model is corrected.

Chapter 7 - Study cases
Chapter six is to present simulation of specific screen circuit faults. The largest detectable fault resistances are determined.

Chapter 8 - Cable systems with several major sections
Chapter seven is to consider how the impedance measurements may be used for cable lines consisting of several major sections.

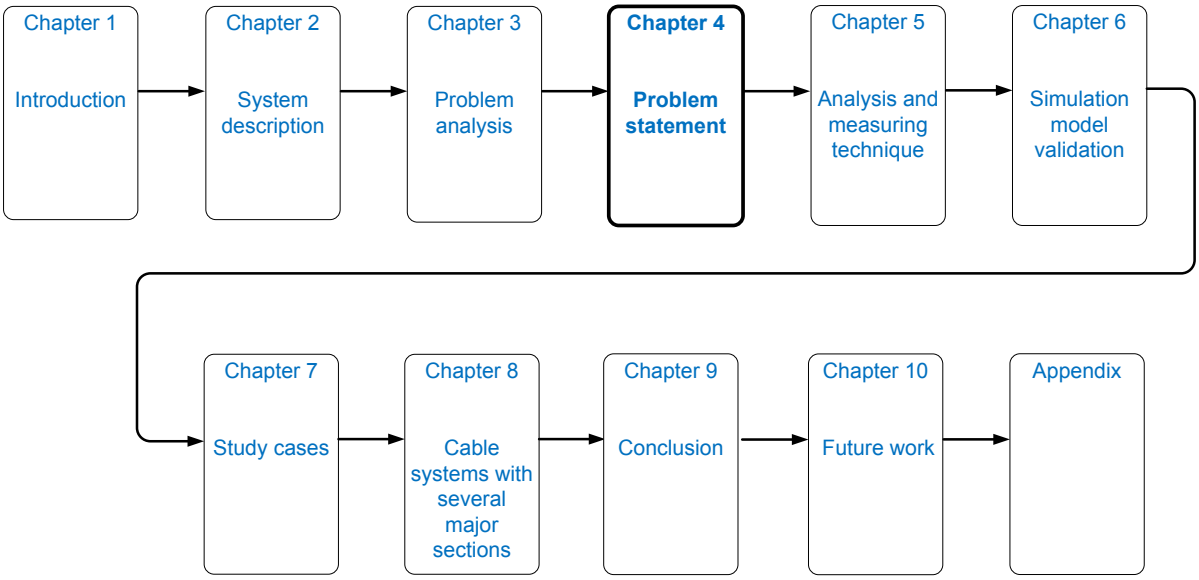

Figure 4.1: Structure of the report.

Chapter 5

Further analysis of screen circuit faults and measuring technique

This chapter is divided into two main sections. The first part considers how the screen circuit is affected by a Sc-Sc fault and a Sc-Gr fault. Methods for analyzing three phased circuits are used to explain characteristic and it is shown how to affect the circuit to obtain larger influence of a Sc-Sc and a Sc-Gr fault. The second part describes and discusses the choice of measuring technique, mentioned in the problem analysis. Finally it is described how the technique is used for practical measurements.

5.1 Analysis of screen circuit faults

The problem analysis showed that a Sc-Sc and a Sc-Gr fault affects the apparent screen impedances. It was shown that the screen circuit impedance is relative low and therefore only affected by low screen fault resistances. In order to detect a fault in the screen circuit, using an impedance measurement, the apparent screen impedances have be to be affected by the fault. It will therefore be studied how to achieved high sensitivity according to screen circuit faults.

Expressions in this chapter are set up for faults in the second link box (SLB). The same approach could be used for fault in the first link box (FLB). This is chosen because the analysis shows that faults in SLB affects the screen circuit at least, and therefore determines how large an error resistance can be detected. This study will first consider how a Sc-Sc fault affects the circuit; this is followed by a study of a Sc-Gr fault.

Definition
Simulations in this chapter are based on a representative MATLAB model with the following parameters: $R = 0.145^{\Omega}/_{\mathrm{km}}$, $L = 0.462^{\mathrm{mH}}/_{\mathrm{km}}$ corresponding to $0.205\Omega\angle 45^{\circ}$@50Hz. AC losses, the mutual coupling between the three screen conductors and the shunt capacitances are not considered. The minor sections are 1km each. The fault resistance is considered pure resistive. The MATLAB scripts may be found on the attached CD, in the folder: *Matlab*.

5.1.1 Sc-Sc fault

A **Sc-Sc fault** forms an additional current path in the screen circuit, illustrated by the red arrow in figure 5.1. Depending on the resistance of the fault, the currents from source U_a and U_b are, for the example shown below, divided between the fault resistance and the screen element of the third minor section. The current deviation is based on the relation on the fault and screen resistance.

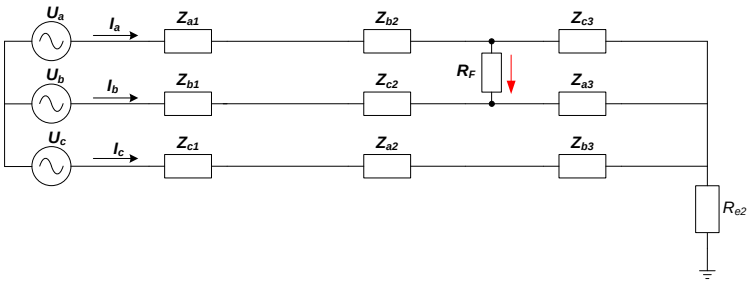

Figure 5.1: Principle sketch of one major section of cross bonded screen circuit. Including Sc-Sc fault in the SLB.

As explained the impedance of the screen circuit is relatively low and therefore the fault resistance also has to be relatively low to affect the circuit. In order to increase the influence of the fault it may be useful to increase the impedance of the screen circuit.

By increasing the frequency, both the resistive and reactive part of the screen circuit increases. The resistance due to increased AC losses from skin and proximity effect [30, p.145] and the reactance proportional to the applied frequency $X_l \propto f$ see equation 5.1 [46, p.387]. As mentioned, AC losses are not considered in this model.

$$X_l = 2 \cdot \pi \cdot f \cdot L \qquad [\Omega] \quad (5.1)$$

It is therefore studied how an increased measuring frequency increases the detectability of a given fault resistance.

There is made a mathematical, in order to study how the increased frequency affects the screen circuit, in respect to screen circuit faults.

To study how the screen circuit is affected in respect to screen circuit faults, by increasing the screen impedance and how fault affects the screen circuit at different screen circuit impedances it is chosen to make a mathematical model of the circuit.
The delta connection between the points A, B and C in figure 5.1 is converted to a star connection. The conversion is performed at shown in figure 5.2, using equation 5.2, 5.3 and 5.4 [46, p. 392].

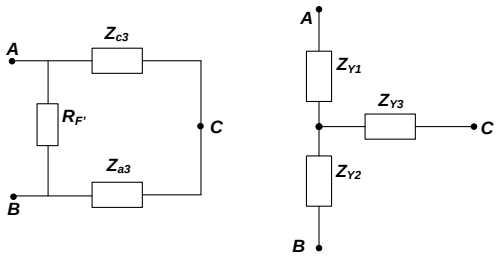

Figure 5.2: Delta to star conversion.

$$Z_{Y1} = \frac{R_{F'} \cdot Z_{c3}}{Z_{a3} + Z_{c3} + R_{F'}} \tag{5.2}$$

$$Z_{Y2} = \frac{R_{F'} \cdot Z_{a3}}{Z_{a3} + Z_{c3} + R_{F'}} \tag{5.3}$$

$$Z_{Y3} = \frac{Z_{c3} \cdot Z_{c3}}{Z_{a3} + Z_{c3} + R_{F'}} \tag{5.4}$$

Using the delta to star conversion, the screen appear as shown in figure 5.3.

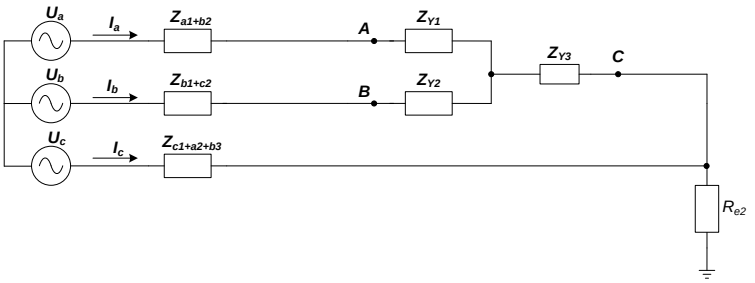

Figure 5.3: Screen circuit of one major section. Including Sc-Sc fault in the second link box.

The impedances Z_{Y1}, Z_{Y2} and Z_{Y3} are dependent on the screen impedance and the fault resistance.

The three impedances of the star conversion are shown as a function of fault resistance in figure 5.4. In figure 5.4(a) the screen circuit is calculated for an applied frequency of 50Hz and in figure 5.4(b) the screen circuit is calculated for 360Hz.

The 50Hz frequency is chosen because this is the power frequency and only needs to be transformed to a lower voltage to be applied as measuring voltage. The 360Hz is chosen to be within the range which may be supplied by line impedance measuring equipment. The choice of the largest frequency will be further explained at the end of this section.

The impedances of the star connection Z_{Y1}, Z_{Y2} and Z_{Y3}, are calculated using equation 5.2, 5.3 and 5.4. When Z_{Y1} and Z_{Y2} reaches the horizontal green line, and Z_{Y3} reaches the horizontal red line, the screen circuit equals the healthy circuit.

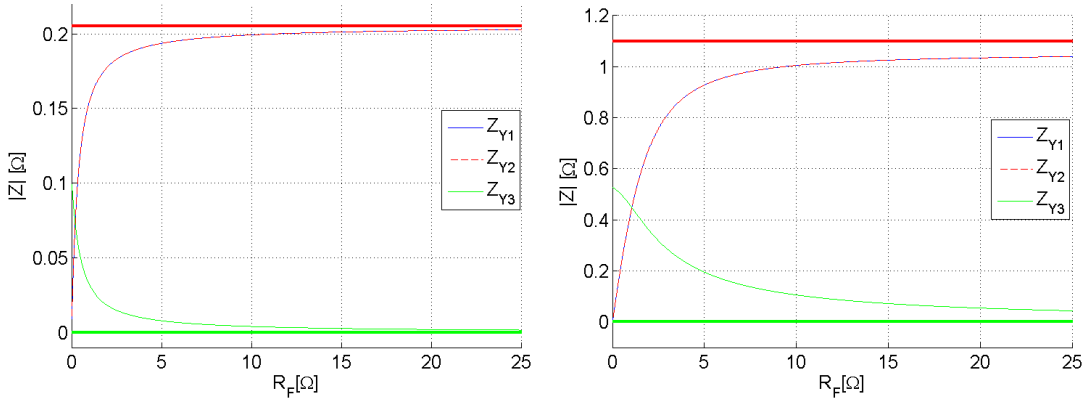

(a) (b)

Figure 5.4: Values of the star connection impedances in figure 5.3 as a function of fault resistance, for an applied frequency of 360Hz.

From figure 5.4 it may be seen that Z_{Y1} and Z_{Y2} equals for all values of R_F. It may also be seen that when the fault resistance R_F is 0Ω the two impedances Z_{Y1} and Z_{Y2} are zero and Z_{Y3} is half the value of one minor section, due to the parallel connection by the fault.
It is seen that both cases approaches healthy state for increasing the fault resistance. For the situation where the frequency and thereby the screen impedances is increased the fault resistance affect the impedance of the delta connection for a larger fault resistance.

To study how the apparent screen impedances are affected, the impedances of the star connection are implemented in the remaining screen circuit see figure 5.3. Using the super position principle explained in Appendix A, the apparent screen impedances are calculated and plotted for 50Hz and 360Hz accordingly in figure 5.5.

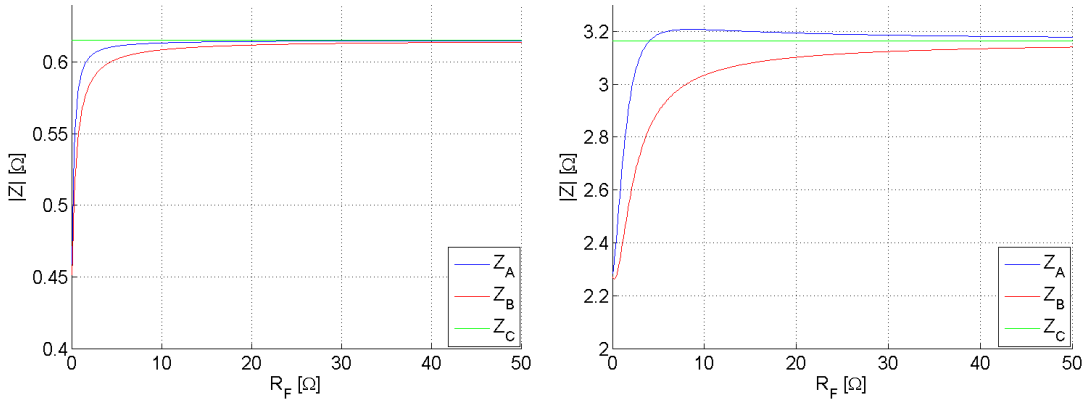

(a) (b)

Figure 5.5: Apparent screen impedances as a function of fault resistance. (a) 50Hz applied measuring voltage. (b) 360Hz applied measuring voltage.

The relative deviations from healthy screen circuit are calculated and shown in figure 5.6.

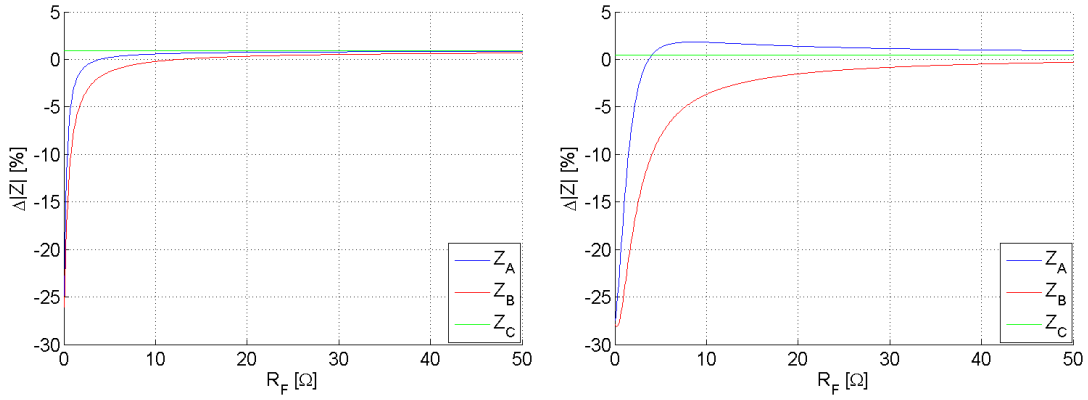

Figure 5.6: Apparent screen impedances as a function of fault resistance. (a) 50Hz applied measuring voltage. (b) 360Hz applied measuring voltage.

From figure 5.6 it may be seen that the relative deviations of the screen impedances for 0Ω fault resistance are identical for 50Hz and 360Hz accordingly. As the fault resistance is increased the deviation decreases, and the circuit approaches healthy state. It is observed that the deviations are present for significantly larger fault resistances (R_F) when the applied frequency is 360Hz than for 50Hz.

It is found that a larger fault resistance is detectable if the impedance of the screen circuit is increased. It would therefore be reasonable to increase the measuring frequency further, in order to gain larger sensitivity in respect to screen circuit faults. But the limitation may be the resonance points of the screen circuit. At the resonance points the apparent screen impedances increases very rapidly, and only a small change of frequency may cause a large impedances change. It may therefore be difficult the measure close to the resonance points. The resonance points are proportional to both the inductance and the capacitance of the screen circuit. However the inductance and capacitance are both proportional to the length of the section. Therefore the resonance points appear at lower frequency for larger sections. This is further explained in section 5.1.3 on page 80.

The impedance of the screen circuit is, beside the applied frequency, also dependent in the length of the major section, the cross section area and material of the screen. The impedance of the screen circuit is larger for long sections and small cross section areas. This also means that large sections provides larger detectability than short sections. However there is a tradeoff between the length of the section, and the limitation of frequency increase.

The increase of frequency makes the screen circuit affected by a larger fault resistance, and thereby the detectability of larger fault resistance is increased.

5.1.2 Sc-Gr fault

A ground fault affects the screen circuit in two ways:

- There is created a **parallel current path** through the ground between the two ground connections
- The ground connection which act as **reference for voltage measurement** is displaced.

Parallel current path

Applying an additional ground connection in one of the link boxes will form a current path through the ground. The current path is shown by the red line in figure 5.7.

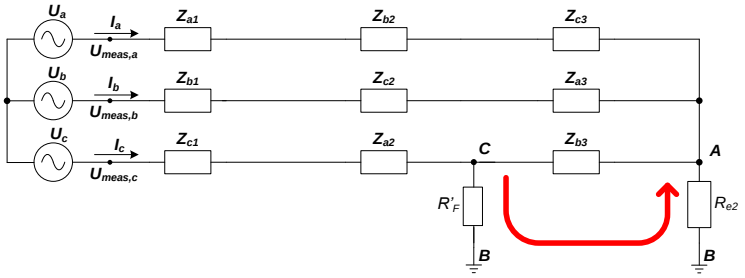

Figure 5.7: Principle sketch of one major section of the screen circuit, including ground fault in the SLB.

The parallel current path through the ground do not lead to any significant decrease of impedance, because the impedance of the ground path is much higher than the metallic screen conductor equation 5.5. This is due to the current loop through the ground, which is many times larger. The depth of which the current will return through the ground may be calculated by Carsons equation 5.6 [53, p.118]. At 50Hz and ground resistivity of 100Ωm the equivalent depth is ≈ 1km.

$$Z_{b3} \ll Z_{groundpath} \tag{5.5}$$

$$d = 660 \cdot \sqrt{\frac{\rho}{f}} \tag{5.6}$$

Where:
d is the depth of the equivalent conductor.
ρ is the resistivity of the soil.
f is the frequency of the applied voltage.

Reference for voltage measurement

By applying floating measuring voltages(U_a, U_b, U_c) will the symmetry of the voltages at the measuring points($U_{meas,a}$, $U_{meas,b}$, $U_{meas,c}$) in figure 5.7, depends on the screen circuit symmetry, since the reference of the measured voltages is ground potential.
If the grounding point at the end of the major section is displaced by adding another grounding point e.g. by a ground fault, the reference point for the voltage measuring is displaced and the voltages at the

measuring point become unsymmetrical according to ground.

If the measured voltages are unsymmetrical, the apparent screen impedances appear unsymmetrical, despite the circuit has not changed, but only the potential of the entire screen circuit is displacement, according to ground. Same characteristic as an earth fault in an ungrounded system, where the voltage of the faulty phase is displaced to ground potential, making a voltage rise at the two healthy phases. Line voltage become present at the healthy phases according to ground while the system remain operation [4].

The voltage reference is displaced from the grounding point in the end of the major section towards the faulty ground connection in one of the link boxes e.g. from point A towards point C in figure 5.7.

Assuming that the two grounding points in figure 5.7 are at the same potential, the two earthing resistances in combination with the screen impedance are forming a delta connection. The delta connection is converted to a star connection as shown in figure 5.8 using equation 5.7, 5.8 and 5.9 [46, p. 392].

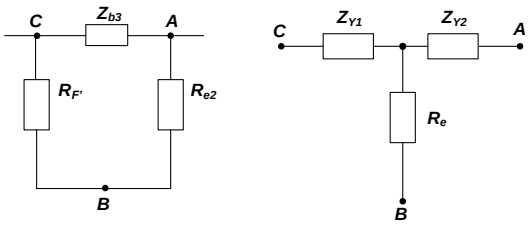

Figure 5.8: Delta to star conversion.

$$Z_{Y1} = \frac{R_{F'} \cdot Z_{b3}}{Z_{b3} + R_{F'} + R_{e2}} \tag{5.7}$$

$$Z_{Y2} = \frac{R_{e2} \cdot Z_{b3}}{Z_{b3} + R_{F'} + R_{e2}} \tag{5.8}$$

$$R_e = \frac{R_{F'} \cdot R_{e2}}{Z_{b3} + R_{F'} + R_{e2}} \tag{5.9}$$

Using the delta to star conversion the circuit appear as shown in figure 5.9. Having only one ground connection point *n*, forming reference for the voltage measuring. The ground connection in figure 5.9 may be seen as a virtual reference to the circuit, because it replaces the two ground connections in figure 5.7.

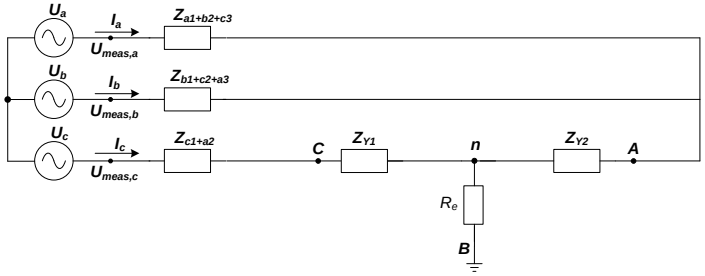

Figure 5.9: Principle sketch of one major section of the screen circuit, including ground fault in the second link box.

The virtual ground connection forms the voltage reference. Thereby the voltage reference is dependent on:

- Earthing resistance in the end of the major section and at the position of the fault
- The impedance of the screen element between the fault and the end of the major section.

Earthing resistance in the end of the major section

The influence of the earthing resistance in the end of the major section is studied by performing two simulations. The simulations show the deviation of the apparent screen impedances in respect to healthy state, as a function of fault resistance. For the first simulation the earthing resistance in the end of the major section is 0.1Ω and for the second simulation the earthing resistance is 5Ω.

The equations of the star connection are implemented in the remaining screen circuit, using the super position principle, as shown in Appendix B.

The fault resistance is increased from $0 - 50\Omega$ and the simulation results are shown in figure 5.10.

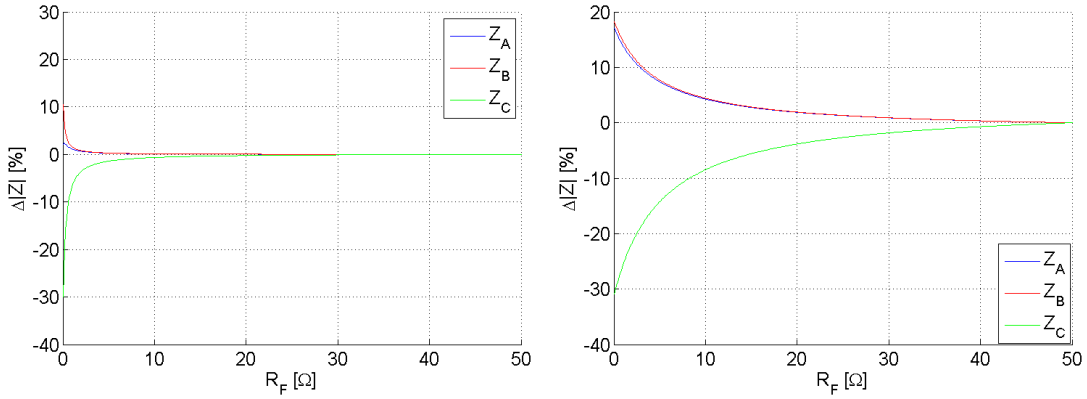

Figure 5.10: Magnitude of apparent screen impedances as a function of fault resistance. (a) Earthing resistance in the end of the major section of 0.1Ω. (b) Earthing resistance in the end of the major section of 5Ω.

From figure 5.10 it may be seen that for both earthing resistance the screen circuit approached healthy state, as the fault resistance increases.

If the earthing resistance in the end of the major section is increased, the apparent screen impedances differs significantly more from healthy state, than for the low earthing resistance in the end of the major section.

Screen circuit impedance

To study if an increase of the screen circuit impedance, influence the affect of a ground fault, there is performed another simulation. For this simulation the screen circuit impedances are calculated for an

applied frequency of 360Hz. This is compared to an applied measuring frequency of 50Hz. For both cases the earthing resistance in the end of the major section is 0.1Ω and the fault resistance is increased from $0 - 50\Omega$.

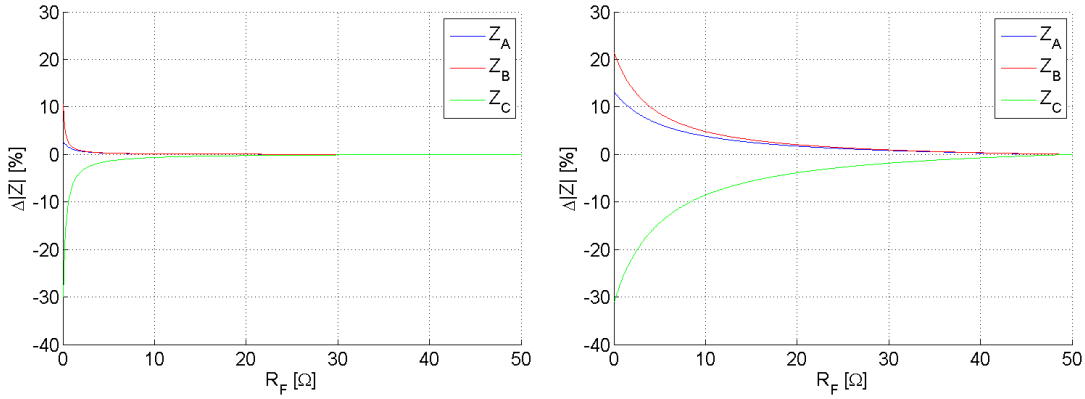

(a) (b)

Figure 5.11: Magnitude of apparent screen impedances, as a function of fault resistance, for earthing resistance in the end of the major section 0.1Ω. (a) 50Hz applied measuring frequency. (b) 360Hz applied measuring frequency.

From figure 5.11 it is seen that the relative deviations are equal when the fault resistance is bolted 0Ω for both frequencies. For an increasing fault resistances the apparent screen impedances approached healthy state for both frequencies, however the slope at which the apparent screen impedances approaches healthy state is significantly lower for 360Hz than for 50Hz. Thereby a larger ground fault resistance is detectable if the screen impedance is increased.

As for the Sc-Sc fault the Sc-Gr fault become more pronounced if the measuring frequency is increased. The frequency increase is as earlier explained limited by the resonance points, which is further explained in section 5.1.3 on the following page.

5.1.3 Consequences of increasing the measuring frequency

When increasing the frequency, the resonance points of the circuit may be considered. The resonance points may be estimated from the domination capacitances and inductance. The estimation will not provide the accurate frequency of the resonance points. This is shown by an example based on the cable line FRT-NOR.

The dominating inductance and capacitance of the FRT-NOR cable line are calculation to 5.12mH and 19.23µF accordingly. Based on the dominating components, the resonance frequency may be calculated to 507Hz using equation 5.10. The calculation is shown in Appendix H.

$$f_{resonance} = \frac{1}{2 \cdot \pi \sqrt{L \cdot C}} \quad [\text{Hz}] \quad (5.10)$$

Due to the distributed nature of the inductance and capacitance at a transmission line, the domination components may not provide the accurate frequency of the resonance point. This is illustrated in figure 5.12, where the resonance frequency, calculated by the dominating components, are compared to the same line, represented by 1, 3, and 10 π-sections. Also the exact π- model is shown. The exact π-model is often used as a reference in the frequency domain [16, p.22].

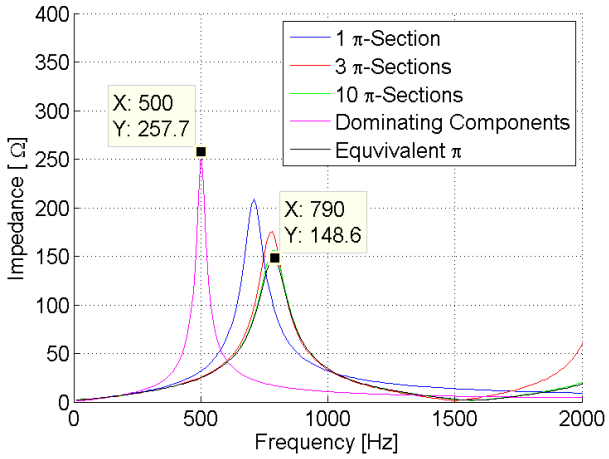

Figure 5.12: Frequency spectrum of one, three, ten, equivalent pi, and domination components model.

From figure 5.12 it may be seen that the three π-section representations, is close to the exact π. However 1π representation is approximately 100Hz below the others. The resonance frequency calculated by only the two dominating components is ≈ 30% lower that the exact π.
Thereby using the dominating components as the upper limit, there is a larger margin to the actual resonance point. The MATLAB script including the above calculations may be found on the attached CD in the folder: Matlab.

5.2 Measuring technique

The impedances method is based on the three phased apparent screen impedances, calculated by the voltages according to ground and the current at the measuring point. The problem analysis showed that the measuring voltage should be floating relative to ground.

5.2.1 Three phased measurement

The three impedances are calculated from the measured voltage and current, when a three phased flotation supply is applied to the screen circuit. This technique is used for FM1 in Appendix D, using a three phased auto transformer, which is not star point grounded. The measuring principle is illustrated by figure 5.13, where the voltages and currents are measured, using a three phased power analyzer.

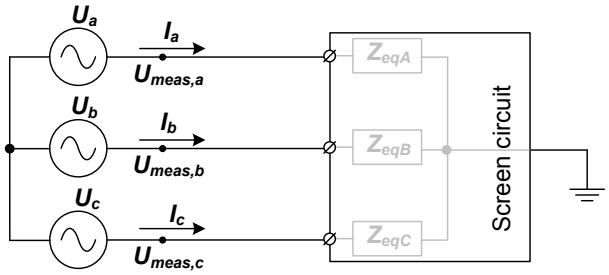

Figure 5.13: Three phased measuring principle.

5.2.2 Single phase measurement

For FM2 a single phase impedance measuring equipment is used. This is used in order to study the possibility of using line impedance measuring equipment for screen circuit condition determination. The line impedance measuring equipment provide the possibility of performing measurements with increased frequency, which is reasonable according to the previous section.

The line impedance measuring equipment, available from the cooperating company, is an Omicron CPC100 and a boosting unit CP CU1. The Omicron equipment apply a specified voltage or current and frequency within the limits given below:

- Voltage 0 – 500V
- Current 0 – 100A
- Frequency 15 – 400Hz

The Omicron CMC365 is used for performing measurements, because the line impedance equipment do not provide enough measuring inputs.

Procedure for super position measurement

The equivalent screen impedances are measured using the same procedure as for measuring line impedances. These are measured from three single phase measurements, using the coupling scheme shown in figure 5.14.

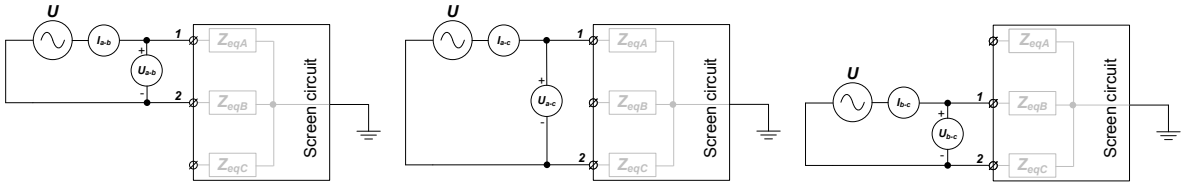

Figure 5.14: Measuring setup for screen impedance measurements.

Form the three measurements shown in figure 5.14 three impedances are measured: $Z_{A-B}, Z_{A-C}, Z_{B-C}$, these are the impedance of the three loops formed by the three screens.

From the loop impedances the equivalent screen impedances are calculated using, three equations with three unknowns, as shown by the equations below:

$$\begin{aligned} \mathbf{Z_{eqA}} &= \tfrac{1}{2} \cdot (\mathbf{Z_{A-B}} + \mathbf{Z_{A-C}} - \mathbf{Z_{B-C}}) \\ \mathbf{Z_{eqB}} &= \mathbf{Z_{A-B}} - \mathbf{Z_{eqA}} \\ \mathbf{Z_{eqC}} &= \mathbf{Z_{B-C}} - \mathbf{Z_{eqB}} \end{aligned} \qquad [\Omega] \quad (5.11)$$

The equivalent screen impedances in 5.11 are not equal to the apparent screen impedances, because the actual circuit according to ground is not considered. To include the influence of the grounding reference of the screen circuit three additional measurements are required. These are performed as shown in figure 5.15.

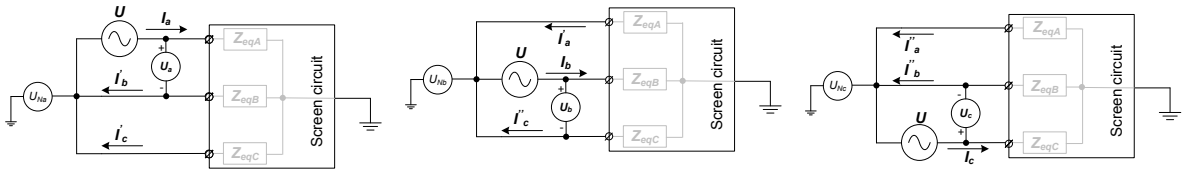

Figure 5.15: Measuring setup for three phased voltage respons, based on the super position method.

From each of the three measurements in figure 5.15 two voltage are needed. The Omicron line impedances measuring equipment are capable of measuring one voltage and one current, therefore additional measuring equipment is required.

The apparent screen impedances are then calculated based on the measured equivalent impedances. The

screen currents are calculated by the super position principle, using the equivalent impedances and the measured screen voltages from figure 5.15. The apparent impedances are then calculated from the vectorial sum of the phase and neutral voltage and the total phase current.

The currents are calculated based in the measurements shown in figure 5.15(a).

$$\begin{aligned} \mathbf{I_a} &= \frac{\mathbf{U_a}}{\mathbf{Z_{eqA}}+\left(\mathbf{Z_{eqB}}||\mathbf{Z_{eqC}}\right)} \\ \mathbf{I_b^{'}} &= \mathbf{I_a}\cdot\frac{\mathbf{Z_{eqC}}}{\mathbf{Z_{eqB}}+\mathbf{Z_{eqC}}} \\ \mathbf{I_c^{'}} &= \mathbf{I_a}\cdot\frac{\mathbf{Z_{eqB}}}{\mathbf{Z_{eqB}}+\mathbf{Z_{eqC}}} \end{aligned} \quad [\mathrm{A}] \quad (5.12)$$

The currents are calculated based in the measurements shown in figure 5.15(b).

$$\begin{aligned} \mathbf{I_b} &= \frac{\mathbf{U_b}}{\mathbf{Z_{eqB}}+\left(\mathbf{Z_{eqA}}||\mathbf{Z_{eqC}}\right)} \\ \mathbf{I_a^{'}} &= \mathbf{I_b}\cdot\frac{\mathbf{Z_{eqC}}}{\mathbf{Z_{eqA}}+\mathbf{Z_{eqC}}} \\ \mathbf{I_c^{''}} &= \mathbf{I_b}\cdot\frac{\mathbf{Z_{eqA}}}{\mathbf{Z_{eqA}}+\mathbf{Z_{eqC}}} \end{aligned} \quad [\mathrm{A}] \quad (5.13)$$

The currents are calculated based in the measurements shown in figure 5.15(c).

$$\begin{aligned} \mathbf{I_c} &= \frac{\mathbf{U_c}}{\mathbf{Z_{eqB}}+\left(\mathbf{Z_{eqA}}||\mathbf{Z_{eqB}}\right)} \\ \mathbf{I_a^{''}} &= \mathbf{I_c}\cdot\frac{\mathbf{Z_{eqB}}}{\mathbf{Z_{eqA}}+\mathbf{Z_{eqB}}} \\ \mathbf{I_b^{''}} &= \mathbf{I_c}\cdot\frac{\mathbf{Z_{eqA}}}{\mathbf{Z_{eqA}}+\mathbf{Z_{eqB}}} \end{aligned} \quad [\mathrm{A}] \quad (5.14)$$

Using the super position principle, the total screen current is calculated

$$\begin{aligned} \mathbf{I_{a,tot}} &= \mathbf{I_a}-\mathbf{I_a^{'}}-\mathbf{I_a^{''}} \\ \mathbf{I_{b,tot}} &= \mathbf{I_b}-\mathbf{I_b^{'}}-\mathbf{I_b^{''}} \\ \mathbf{I_{c,tot}} &= \mathbf{I_c}-\mathbf{I_c^{'}}-\mathbf{I_c^{''}} \end{aligned} \quad [\mathrm{A}] \quad (5.15)$$

Using the super position principle is the neutral voltage calculated. Based on the measurements shown in figure 5.15

$$\mathbf{U_N} = \mathbf{U_{NA}}+\mathbf{U_{NB}}+\mathbf{U_{NC}} \quad [\mathrm{V}] \quad (5.16)$$

The apparent impedances may now be calculated.

$$\begin{aligned} \mathbf{Z_A} &= \frac{\mathbf{U_N}+\mathbf{U_A}}{\mathbf{I_{a,tot}}} \\ \mathbf{Z_B} &= \frac{\mathbf{U_N}+\mathbf{U_B}}{\mathbf{I_{b,tot}}} \\ \mathbf{Z_C} &= \frac{\mathbf{U_N}+\mathbf{U_C}}{\mathbf{I_{c,tot}}} \end{aligned} \quad [\Omega] \quad (5.17)$$

A calculation example is shown in Appendix E.3 on page E-14.

A MATLAB script is made to handle the above equations. The script loads six measuring files and six scale files generated by the Omicron CMC 365. The script may be found on the attached CD, in the folder: *Matlab*.

5.2.3 Data processing of measured signals

As mentioned above the voltage and current curves are measured using the CMC365. From the measurements two thing should be determined:

- RMS value
- Phase angle

The CPC100 is provided with a selective filter so only the signals of interest, at the generated frequency are evaluated. Due to the lack of measuring inputs at the CPC100, it was chosen to use the CMC356 to record all data. It was decided to filter the recorded data by the means of a digital filter algorithm. Because the measured currents and voltages are used for impedance and voltage calculations later on, it is essential that the filter doesn't affect the magnitude and phase shift of the signal at the generated frequency. Therefore will the chosen filter be tested as followed.

A peak filter algorithm has been chosen. Figure 5.16 shows the frequency response of a peak filter tuned to 360Hz. The filter design have been done whit the MATLAB toolbox 'Filter Design'. At the tuned frequency the filter have unity gain and phase shift of 0°, as shown in the figure. The filter is designed to a sample rate of 9481$^{samples}/_{s}$ which corresponds to the chosen sample rate of the CMC 356.

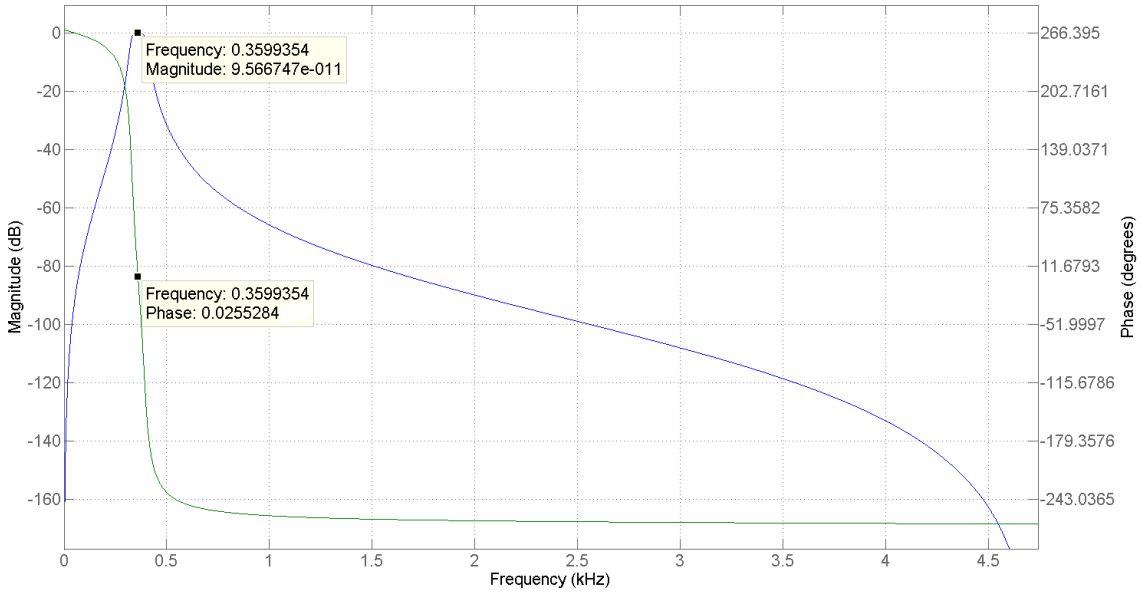

Figure 5.16: Frequency response of a peak-filter tuned to 360Hz

To test the filter a distorted signal with known frequency's, amplitude and phase shift is used. Figure 5.17 illustrate the principle.

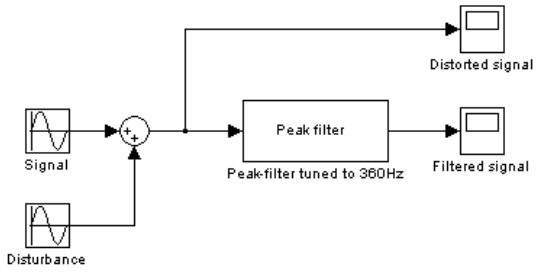

Figure 5.17: Testing the filter design with a know distorted signal.

Two distorted signals with the following frequencies have been generated:

Distorted signal 1

$$\begin{aligned} \text{Signal1} &= \sin(2\pi \cdot 360 \cdot n) \\ \text{Disturbance1} &= 0.2\sin(2\pi \cdot 900 \cdot n) \\ \text{Signal1}_{\text{Distorted}} &= \text{Signal1} + \text{Disturbance1} \end{aligned} \tag{5.18}$$

Distorted signal 2

$$\begin{aligned} \text{Signal2} &= \sin\left(2\pi \cdot 360 \cdot n - \tfrac{\pi}{3}\right) \\ \text{Disturbance2} &= 0.1\sin\left(2\pi \cdot 900 \cdot n + \tfrac{\pi}{3}\right) \\ \text{Signal2}_{\text{Distorted}} &= \text{Signal2} + \text{Disturbance2} \end{aligned} \tag{5.19}$$

Where n is a time column vector containing 100 periods at 360Hz with a time step equal to $1/9481$.

The distorted signals may be seen in figure 5.18(a)

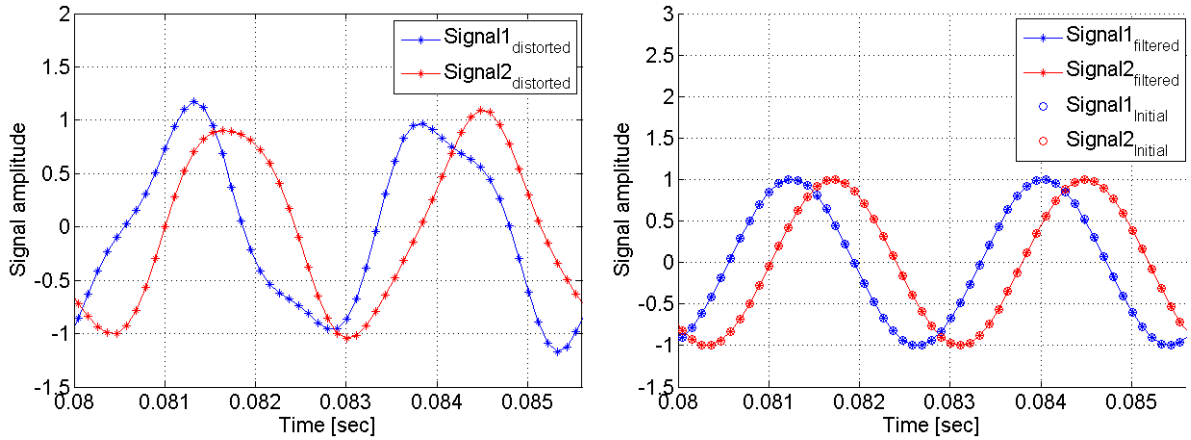

(a) (b)

Figure 5.18: (a) Distorted signals. (b) Filtered signals only consisting of the initial signal without the disturbance.

Figure 5.18(b) shows the filtered samples marked with * and the initial signal without the disturbance marked ∘. The RMS value of the filtered samples (100 periods) was calculated to 0.7071 which is equal to the RMS value of the initial signal since the amplitude is unity, hence $\frac{1}{\sqrt{2}} = 0.7071$.

The theoretical approach presented in [12] to calculate the average phase shift (ϕ) between two signals has been adapted here to calculate the phase shift between the two filtered column vectors.

The complex cross correlation coefficient is defined as equation 5.20.[12],[31, p. 124]:

$$\Gamma = \frac{< VI^* >}{\sqrt{< |V^2| >< |I^2| >}} \tag{5.20}$$

Where V(Signal1) and I(Signal2) are the complex representation of the amplitudes of the voltage and current, respectively. In this case are the amplitudes represented as real numbers only, and the conjugation between V and I, denote * in equation 5.20 has therefore no effect. Equation 5.20 holds true if and only if the mean values of the signals are 0 [31, p. 124].

The cross correlation factor gives a measure of dependence between two signals and is defined within the following interval; $-1 \leq \Gamma \geq 1$. In the special case where $< VI^* >= 0$ the signals are *orthogonal* [31, p. 124], hence $\Gamma = 0$. A correlation factor of $\Gamma = 1$ indicate that the correlation between V and I is good, hence when V increases in value I will do the same and vice versa, analogue to $\phi = 0$. A correlation factor of $\Gamma = -1$, indicates that V and I are inverted to each other, hence then V increases in value I will decrease, analogue to $\phi = \pi$.
Since the correlation factor in this case only consists of real numbers, it does not provide any information about I is leading or lagging V. To overcome this is the waveforms are analysed further, which will be done later.

The average values of the filtered signals are calculated using:[12]

$$< VI >= \frac{1}{N}\sum_{i=1}^{N} V_i I_i \tag{5.21}$$

$$< \left|V^2\right| >= \frac{1}{N}\sum_{i=1}^{N} |V_i|^2 \tag{5.22}$$

$$< \left|I^2\right| >= \frac{1}{N}\sum_{i=1}^{N} |I_i|^2 \tag{5.23}$$

[12] states that the average power factor between V and I is equal to the magnitude of Γ, hence $|\Gamma| = cos(\phi)$.

By using equation 5.21,5.22 and 5.23 the average values of the filtered samples shown in figure 5.18(b).

$$< VI >= 0.25$$

$$< |V^2| >= 0.5$$

$$< |I^2| >= 0.5$$

By using equation 5.20 Γ is calculated to 0.5, hence:

$$\Phi = \arccos(\Gamma) = 1.0472 = \frac{\pi}{3}$$

V is the reference and in order to evaluate if I is leading or lagging V the following steps are performed:

- Finding a sample (n_{peak}) there V have a positive peak
- Use n_{peak} and $n_{peak} + 1$ to check the slope (α) of I
- If α is positive I is lagging V
- If α is negative I is leading V

In this case α is negative, hence I lagging V this may also be seen in 5.19.

Below here is an extract of the MATLAB syntax used for the calculation of ϕ.

```
for i = 1:r
    VI(i) = V(i)*I(i);

    VV(i) = I(i)*I(i);

    II(i) = I(i)*I(i);
end

VImean = mean(VI)                              %average value of V*I
VVmean = mean(VV)                              %average value of V^2
IImean = mean(II)                              %average value of I^2

phi = acos(VImean/sqrt(VVFmean*IIFmean));      %calc phi by using the cross correlation factor

[peak sample] = max(V(1,1000:2000));              %Finding positiv peak @ V

if phi == 0                                       %If phase shift = 0 do nothing
    phi = phi;
elseif 0<(I(1,1000+sample+1)-I(1,1000+sample)) %check if I is leading or lagging xF
    phi = -phi;
end
```

5.2.4 Travelling Wave measurement

As mentioned in the problem formulation, travelling wave measurements could be carried out, if time allows. Travelling wave measurement was performed, and the test report may be found in Appendix F. The measuring data may be found in the attached CD in the folder: *Nors 25-01-2012*. As earlier mentioned it is decided, in cooperation with the supervisors, that the main focus of this study is the impedance method. For this reason the measurements are not further analyzed.

5.3 Chapter summary

The summary is divided according to the two main sections in this chapter.

Summary screen circuit analysis
It was found that by increasing the frequency of the measuring voltage and thereby the impedance of the circuit, the Sc-Sc will affect the apparent screen impedances for larger fault resistances. However the relative deviation for bolted Sc-Sc faults are not affected by the increased screen impedance.

The influence of the Sc-Gr fault to the apparent screen impedances are found to be dependent on the impedance of the screen circuit and the earthing resistance at the end of the major section.
If the impedance of the circuit is increased a larger fault resistance will have influence on circuit and therefore be detectable. The relative deviation, for bolted ground faults are not affected by the increased screen impedance.
The influence of the ground fault is more pronounced for larger earthing resistance at the end of the major section.

For the above mentioned reasons there is obtained higher sensitivity according to Sc-Sc and Sc-Gr fault when the measuring frequency is increased.

Summary Measuring techniques
It is described how the apparent screen impedance may be determined from a sequence of single phase measurements. This procedure making it possible to use general measuring equipment, and thereby the method easier to implement for the transmission companies.

There could possible be made an excel spreadsheet calculation of calculation of the apparent screen impedances, in the same way is for the line impedances, however an additional voltage measurement is required in order to obtain the reference according to ground.

The method require several calculations in order to determined the apparent screen impedance. These calculations may lead to increased inaccuracy, and thereby a increased margin is required in order not to risk an inaccurate measurement cause a wrong condition determination.

The chosen digital filter algorithm does not influence the amplitude of the original signal of interest. By filtering two signals the filter algorithm does not influence the phase shift (ϕ) between the signals. Furthermore is the approach presented in [12] to calculate ϕ found very useful.

Chapter 6

Validation of simulation model of FRT-NOR

In this chapter the DIgSILENT simulation model is compared and validated according to measurements performed during FM1 and FM2, on the cable line (FRT-NOR). The validation includes the cable line in both healthy and faulty state and at three different measuring frequencies.

6.1 Simulation model

The cable line between the substations Frøstrup(FRT) and Nors(NOR) has been modeled in DIgSILENT. The model is shown in figure 6.1. Appendix C provides a detailed description of the cable modeling. The DIgSILENT simulation model may be found on the attached CD in the folder '*DIgSILENT*'.

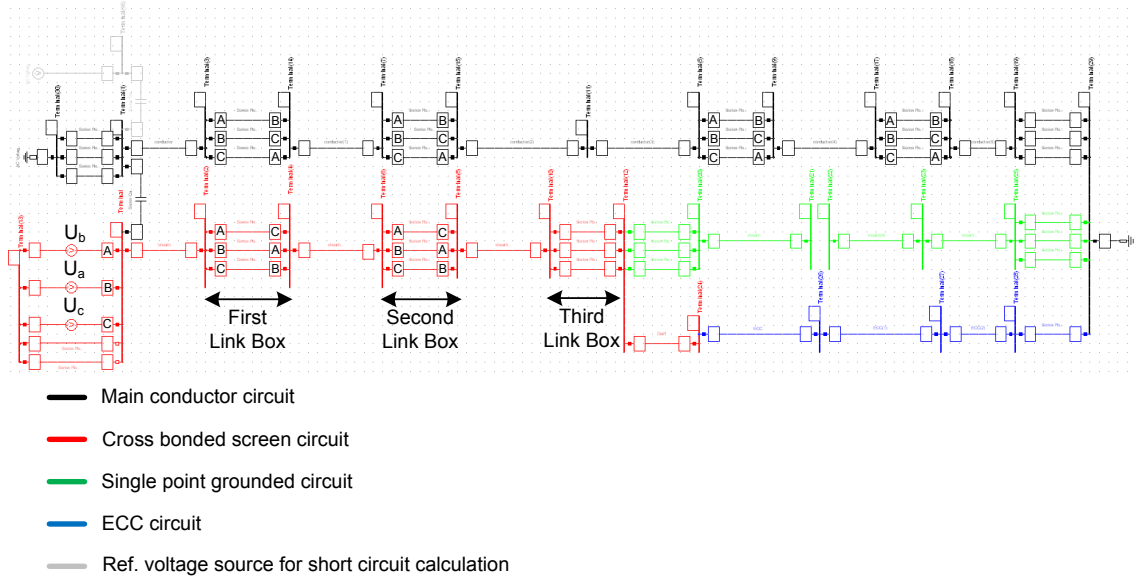

Figure 6.1: DIgSILENT model of the cable line FRT-NOR. Letters indicate the transposition.

Key parameters of the model are listed below:

- Earthing resistance in first link box: 0.2Ω.
- Earthing resistance in second link box: 7Ω.
- Earthing resistance in substations link box: 0.1Ω.
- Voltage source U_A: $1\angle 0$.
- Voltage source U_B: $1\angle -120$.
- Voltage source U_C: $1\angle 120$.

The letters in figure 6.1 illustrate the transposition of the core and screen conductors.

6.2 Model validation

In order to validate the simulation model, the simulated apparent impedances are compared to measured apparent impedances. The impedances are compared according to measurements performed during Field measurement 1(FM1) and Field measurement 2(FM2), described in Appendix D and E.

6.2.1 Model validation according to FM1

First the simulation model is validated according to FM1, for the screen circuit conditions given below:

- Healthy screen circuit.
- Screen to screen fault in first link box. (Sc-Sc FLB)
- Screen to ground fault in first link box. (Sc-Gr FLB)
- Screen to screen fault in second link box. (Sc-Sc SLB)
- Screen to ground fault in second link box. (Sc-Gr SLB)

A fault resistance of 2.6Ω is applied between Sc-Sc and Sc-Gr accordingly. There is selected a low resistor in order to obtain a clear effect on the circuit.

FM1 is a three phase measurement at power frequency (50Hz), performed in substation Nors. The measuring setup is shown in figure 6.2. The galvanic separation transformer provides floating measuring voltages. The autotransformer is used to decrease the applied voltage. The measurements are performed by using a three phased power analyzer. A detailed description is given by the test report in Appendix D.

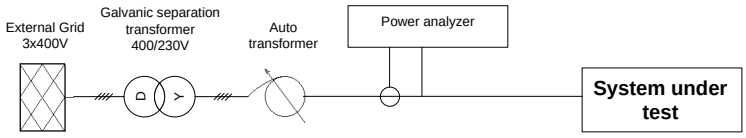

Figure 6.2: Sketch of measuring setup for impedance measurement, FM1.

The validation is divided into two parts:

1 In the first part the healthy screen circuit is considered. When the screen circuit is healthy, the circuit is symmetrical and no current flow through the ground. In this way, the validation is limited only to include the screen loop and not the ground loop. The deviations of apparent screen impedance are calculated using equation 6.1, and the relative deviations are calculated by equation 6.2.

$$\Delta Z = Z_{sim} - Z_{meas} \tag{6.1}$$

$$\Delta Z_{re-Healthy} = \frac{Z_{sim} - Z_{healthy}}{Z_{healthy}} \tag{6.2}$$

2 In order to study the behavior of the simulation model and the actual screen circuit during faults, there is performed a trend study. The trend study compares the deviation of screen impedance according the healthy state for the simulations and measurements. The deviations are calculated using equation 6.3.

$$\Delta Z_{re} = \frac{Z_{fault} - Z_{healthy}}{Z_{healthy}} \tag{6.3}$$

Healthy screen circuit at 50Hz

Simulations are compared to measurements for the healthy screen circuit in table 6.1. The deviations are calculated by equation 6.1 and the relative deviations by 6.2.

Screen	Measured $Z_{sim}[\Omega\angle^\circ]$	Simulated $Z_{meas}[\Omega\angle^\circ]$	Deviation $\Delta Z[\Omega\angle^\circ]$	Relative deviation $\Delta Z_{re}[\%\angle\%]$
A	$2.45\angle 45.45$	$2.25\angle 44.2$	$-0.20\angle -1.25$	$-8.15\angle -2.75$
B	$2.47\angle 46.19$	$2.25\angle 44.2$	$-0.22\angle -1.99$	$-8.92\angle -4.31$
C	$2.47\angle 45.58$	$2.25\angle 44.2$	$-0.22\angle -1.38$	$-8.91\angle -3.03$

Table 6.1: Comparison of simulated and measured impedances for the healthy screen circuit at 50Hz.

From table 6.1 it is seen that the apparent screen impedances deviate $8-9\%$ from measurements for all three screens during healthy state. The worst case measuring accuracy of the inductance for FM1 is $\pm 0.28\%$ calculated in Appendix D.

Trend Study according to FM1 - 50Hz

Because of the deviations during healthy state the trend study may not act as expected. The trend study is shown by table 6.2 to 6.5. The relative deviation of the individual screen impedances according to healthy state, is calculated by equation 6.3 and listed.

Sc-Sc FLB

Screen	Measured $\Delta Z_{re}[\%\angle\%]$	Simulated $\Delta Z_{re}[\%\angle\%]$
A	$0.37\angle 0.09$	$0\angle 0.05$
B	$-31.81\angle 2.55$	$-32.89\angle 1.92$
C	$-19.92\angle 45.06$	$-23.56\angle 43.21$

Table 6.2: Trend of simulations and measurements according to healthy screen circuit, for Sc-Sc fault in FLB at 50Hz.

Sc-Sc SLB

Screen	Measured $\Delta Z_{re}[\%\angle\%]$	Simulated $\Delta Z_{re}[\%\angle\%]$
A	$2.44\angle 14.76$	$0.89\angle 0.45$
B	$-15.70\angle 26.06$	$-6.67\angle 13.78$
C	$-17.43\angle 5.59$	$-11.11\angle 0.07$

Table 6.3: Trend of simulations and measurements according to healthy screen circuit, for Sc-Sc fault in SLB at 50Hz.

Sc-Gr FLB

Screen	Measured $\Delta Z_{re}[\%\angle\%]$	Simulated $\Delta Z_{re}[\%\angle\%]$
A	$4.07\angle 5.13$	$2.67\angle 0.05$
B	$3.65\angle 6.30$	$1.33\angle 7.24$
C	$-25.51\angle 11.25$	$-23.56\angle 11.52$

Table 6.4: Trend of simulations and measurements according to healthy screen circuit, for Sc-Gr fault in FLB at 50Hz.

Sc-Gr SLB

Screen	Simulated $\Delta Z_{re}[\%\angle\%]$	Measured $\Delta Z_{re}[\%\angle\%]$
A	$0.00\angle -0.20$	$-2.64\angle 13.55$
B	$0.40\angle 0.70$	$-7.80\angle 9.42$
C	$-2.20\angle 2.3$	$-12.88\angle 17.44$

Table 6.5: Trend of simulations and measurements according to healthy screen circuit, for Sc-Gr fault in SLB at 50Hz.

From table 6.2 to 6.5 it is seen that the simulation model behave in the same manner as the measurements of the actual circuit. The trend differs by $0-4\%$ for faults in FLB and $1-9\%$ for SLB. Based on these observations it is concluded that the measuring technique can be used.

Improving the accuracy of the simulation model

Table 6.1 showed that the simulated apparent screen impedances of the healthy circuit are $8-9\%$ lower than the measured. The measuring accuracy is calculated to 0.28% in Appendix D. The deviations are significantly larger than the measuring accuracy. For this reason are the deviations studied further. From table 6.1 it is seen that the deviations are very similar for the three screens. Therefore further analysis are focused on screen A. The measured and simulated screen A resistance and reactance are calculated and shown in table 6.6.

Screen	Resistance $[\Omega]$	Reactance $[\Omega]$
Measured Screen A impedance	1.72	1.75
Simulated Screen A impedance	1.61	1.57

Table 6.6: Measured and simulated screen A resistance and reactance.

Table 6.6 shows that the simulated resistance is $\approx 6.4\%$ lower than the measured. The resistance of the simulation model is based on the routine test report performed on the exact cable, and therefore considered highly accurate. The resistance deviation is therefore expected to be due to poor connections at the measuring setup, test cables, inaccurate temperature adjustment and inaccurate measuring equipment. This is studied further in the following section.

The reactance is $\approx 10.3\%$ lower than the measured. The deviation of reactance could be caused by the exact geometry of the cable line. It is considered not possible to keep an exact distance between the cables of 0.3m, for the entire cable line. Therefore the sensitivity of reactance according to the distance between the conductors are studied.

The distance between the cables are de- and increased as illustrated in figure 6.3 and the corresponding screen impedance and reactance are shown in table 6.7. The comparison is performed for screen

A at 50Hz. The distances between the cables are $0.25, 0.30, 0.35, 0.4$m accordingly. The deviation is calculated relative to a distance of 0.3m, which should be the distance between the cables.

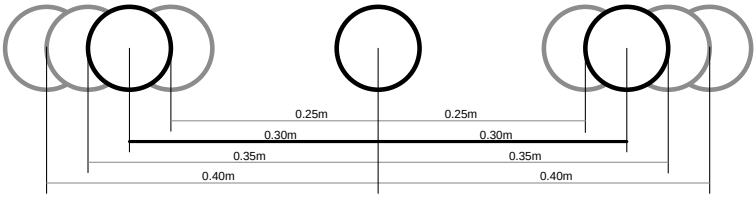

Figure 6.3: De- and increasing the distance between the cables, to study the deviation of reactance.

Distance	Simulated impedance $Z_{sim}[\Omega\angle^\circ]$	Simulated reactance $X_l[\Omega]$	Relative deviation $\Delta X_{l-re}[\%]$
0.25m	$2.15\angle 41.7$	1.43	-8.9
0.30m(reference)	$2.25\angle 44.2$	1.57	0
0.35m	$2.33\angle 46.2$	1.68	$+7.0$
0.40m	$2.40\angle 47.9$	1.78	$+13.4$

Table 6.7: Deviation of apparent screen reactance, relative to the distance between cables at 50Hz.

From table 6.7 it is seen that the reactance increases $\approx 7\%$ for an increase of 0.05m between the cables. The relative deviation of the reactance was calculated to 10.3%. Therefore the distance between the cables in the simulation model is increased to 0.35m.
The accuracy of FM1 measurements are in appendix D calculated to 0.28%, and the accuracy may therefore not cause the deviation. But it was found that the power analyzer has not been calibrated recently. It could therefore be reasonable to question if the high accuracy of the power analyzer is still obtained. It is decided to compare simulation results including the increased distance between the cables, to measurements from FM2.

6.2.2 Model validation according to FM2

FM2 is performed in substation Nors, at the same cable line as FM1. For FM2 the apparent impedances for different frequencies are calculated from a sequence of single phase measurements using the method described in chapter 5. The measuring setup is shown in figure 6.4, where the Omicron CPC100 and CP CU 10 is used as power supply and Omicron CMC356 is used to record measurements. Detailed description may be found in the test report in Appendix E.
The accuracy of the CMC365 is typical lower than 0.06% [5]. The apparent impedances are calculated based on 12 measurements. The worst case accuracy of the measurements are 1.02% including the accuracy of the current shunts. Even though a number of calculations are performed the total apparent impedance accuracy is expected lower than 2%.

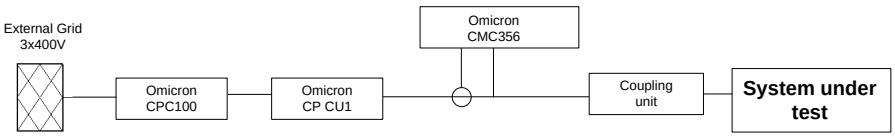

Figure 6.4: Sketch of measuring setup FM2.

The validation according to FM2 is divided into similar parts as for FM1. First the healthy state is considered, followed by a trend study for the same four fault conditions. All simulations are carried out for the increased distance between the cables at 0.35m.

Deviations between simulations and measurements are calculated by equation 6.1 and compared for 30Hz, 90Hz and for 360Hz in table 6.8, 6.9 and 6.10 accordingly.

Healthy 30 Hz Measured and simulated

Screen	Measured $Z_{meas}[\Omega\angle^\circ]$	Simulated $Z_{sim}[\Omega\angle^\circ]$	Relative deviation $\Delta Z[\%\angle\%]$
A	$1.92\angle 33.3$	$1.89\angle 32.1$	$1.6\angle 3.5$
B	$1.92\angle 33.5$	$1.89\angle 32.1$	$1.6\angle 4.2$
C	$1.92\angle 33.4$	$1.89\angle 32.1$	$1.1\angle 4.0$

Table 6.8: Comparison of simulations and measurements for healthy screen circuit at 30Hz.

Healthy 90 Hz Measured and simulated

Screen	Measured $Z_{meas}[\Omega\angle^\circ]$	Simulated $Z_{sim}[\Omega\angle^\circ]$	Relative deviation $\Delta Z[\%\angle\%]$
A	$3.59\angle 62.7$	$3.46\angle 61.8$	$3.8\angle 1.5$
B	$3.59\angle 62.8$	$3.46\angle 61.7$	$3.8\angle 1.8$
C	$3.58\angle 62.8$	$3.46\angle 61.8$	$3.5\angle 1.6$

Table 6.9: Comparison of simulations and measurements for healthy screen circuit at 90Hz.

Healthy 360 Hz Measured and simulated

Screen	Measured $Z_{meas}[\Omega\angle^\circ]$	Simulated $Z_{sim}[\Omega\angle^\circ]$	Relative deviation $\Delta Z[\%\angle\%]$
A	$15.1\angle 80.6$	$15.1\angle 80.3$	$0\angle 0.4$
B	$15.3\angle 79.9$	$15.3\angle 79.1$	$0\angle 0.9$
C	$15.2\angle 82.2$	$15.4\angle 82.2$	$-1.3\angle 0$

Table 6.10: Comparison of simulations and measurements for healthy screen circuit at 360Hz.

From the above tables it is seen that simulations and measurements are close to each other. The 30Hz simulation differ $1-4\%$ in respect to measurements, 90Hz simulations differ $1.5-3.8\%$ in respect to

measurements and 360Hz simulations differ $0-1.3\%$ in respect to measurements. A fault is more pronounced if the measuring frequency is increased as proposed in Section 5.1 on page 71. It is therefore reasonable that the model fits measurements best, for the highest frequency.

In the previous section where the simulations were compared with the measurements from FM1, there was found a deviation of the resistance which could not be explained due to the routine test. Therefore resistance and reactance are calculated for simulations and measurements during FM2, for 30Hz 90Hz and 360Hz. This is shown in table 6.11 and 6.12, where also the resistance and reactance from the previous section are shown.

Resistance

Screen	Measured $R_{meas}[\Omega]$	Simulated $R_{sim}[\Omega]$	Relative deviation $\Delta R_{re}[\%]$
50Hz	1.72	1.61	6.4
30Hz	1.60	1.60	0.0
90Hz	1.65	1.64	0.6
360Hz	2.47	2.54	2.8

Table 6.11: Comparison of resistance.

Reactance

Screen	Measured $X_{meas}[\Omega]$	Simulated $X_{sim}[\Omega]$	Relative deviation $\Delta X_{re}[\%]$
50Hz	1.75	1.68	4.0
30Hz	1.05	1.00	4.8
90Hz	3.19	3.05	1.4
360Hz	14.90	14.88	0.13

Table 6.12: Comparison of reactance.

Table 6.11 shows that the measured resistance of FM2 fits much better with simulations. This observation further supports the questioning of the accuracy of the power analyzer. All of the deviations, with the exception of one, are below the accuracy of 3.0%. A trend study of 30 and 360Hz is carried out in the following section.

6.2.3 Trend study

The trend studies compare the trends of the simulations and measurements results, for the four fault conditions. The relative deviation of the screens impedances are calculated according to healthy screen circuit for 30Hz and 360Hz.

Trend study 30Hz

The trend of simulations and measurements for applied 30Hz measuring voltages, are calculated by equation 6.3 on page 91 and compared in table 6.13 to 6.16.

Sc-Sc FLB - 30 Hz

Screen	Measured $\Delta Z_{re}[\%\angle\%]$	Simulated $\Delta Z_{re}[\%\angle\%]$
A	$-21.8\angle-50.8$	$-23.3\angle-52.8$
B	$-29.7\angle11.4$	$-30.7\angle3.3$
C	$1.0\angle-0.5$	$1.6\angle-0.8$

Table 6.13: Trend of simulations and measurements according to healthy screen circuit, for Sc-Sc fault in FLB at 30Hz.

Sc-Sc SLB - 30 Hz

Screen	Measured $\Delta Z_{re}[\%\angle\%]$	Simulated $\Delta Z_{re}[\%\angle\%]$
A	$-15.1\angle8.6$	$-10.6\angle0.2$
B	$1.0\angle3.4$	$0\angle0.3$
C	$-5.2\angle-15.9$	$-5.8\angle-16.8$

Table 6.14: Trend of simulations and measurements according to healthy screen circuit, for Sc-Sc fault in SLB at 30Hz.

From table 6.13 and 6.14 it may be seen that the relative deviations of the apparent screen impedances are very similar for the measurements and the simulations. The largest deviation between measurements and simulations are $\approx 4.5\%$ for a Sc-Sc fault in SLB. It may also be seen that deviation from healthy state is $\approx 15\%$ more pronounced for Sc-Sc fault in FLB than in SLB.

Sc-Gr FLB - 30 Hz

Screen	Measured $\Delta Z_{re}[\%\angle\%]$	Simulated $\Delta Z_{re}[\%\angle\%]$
A	$5.7\angle1.8$	$2.1\angle7.4$
B	$-23.4\angle-10.4$	$-23.8\angle-10.9$
C	$2.1\angle-7.0$	$4.2\angle-5.8$

Table 6.15: Trend of simulations and measurements according to healthy screen circuit, for Sc-Gr fault in FLB at 30Hz.

Sc-Gr SLB - 30 Hz

Screen	Measured $\Delta Z_{re}[\%\angle\%]$	Simulated $\Delta Z_{re}[\%\angle\%]$
A	$-4.7\angle-0.3$	$-2.1\angle-1.9$
B	$0\angle0.4$	$0.5\angle-0.4$
C	$1.0\angle1.6$	$1.1\angle0.7$

Table 6.16: Trend of simulations and measurements according to healthy screen circuit, for Sc-Gr fault in SLB at 30Hz.

From table 6.15 and 6.16 it can be seen that the trend of the simulation is very similar to the trend of the measurements for the ground fault at 30Hz. The largest deviation is screen A for Sc-Gr fault in FLB for which the trend differs by $\approx 3.6\%$. By comparing the deviations of FLB and SLB, it is seen that a Sc-Gr fault is $\approx 20\%$ more pronounced for when it is applied in FLB than in SLB.

Trend study 360 Hz

The trend of simulations and measurements for applied 360Hz measuring voltages, are calculated by equation 6.3 and compared in table 6.17 to 6.20.

Sc-sc FLB - 360 Hz

Screen	Measured $\Delta Z_{re}[\%\angle\%]$	Simulated $\Delta Z_{re}[\%\angle\%]$
A	$-62.6\angle-56.8$	$-68.9\angle-55.7$
B	$-69.3\angle2.2$	$-71.9\angle-0.8$
C	$4.7\angle-2.5$	$4.8\angle-4.5$

Table 6.17: Trend of simulations and measurements according to healthy screen circuit, for sc-sc fault in FLB at 360Hz.

Sc-sc SLB - 360 Hz

Screen	Measured $\Delta Z_{re}[\%\angle\%]$	Simulated $\Delta Z_{re}[\%\angle\%]$
A	$-36.8\angle5.7$	$-40.7\angle2.4$
B	$-1.1\angle-1.3$	$1.0\angle-1.3$
C	$-27.1\angle-26.6$	$-32.9\angle-27.1$

Table 6.18: Trend of simulations and measurements according to healthy screen circuit, for sc-sc fault in SLB at 360Hz.

From table 6.17 and 6.18 it may be seen that for sc-sc fault the trend of the simulations are very equal to the trend of the measurements, for an applied measuring voltage at 360Hz. The largest trend deviation is $\approx 6\%$ for screen A for fault in FLB.
It is also observed that the deviation according to healthy state is $\approx 26\%$ larger for fault in FLB that for faults in SLB.

Sc-gr FLB - 360 Hz

Screen	Measured $\Delta Z_{re}[\%\angle\%]$	Simulated $\Delta Z_{re}[\%\angle\%]$
A	$10.7\angle4.8$	$13.7\angle5.5$
B	$-42.4\angle0.3$	$-36.9\angle1.9$
C	$6.3\angle-10.7$	$6.1\angle-11.5$

Table 6.19: Trend of simulations and measurements according to healthy screen circuit, for sc-gr fault in FLB at 360Hz.

Sc-gr SLB - 360 Hz

Screen	Measured $\Delta Z_{re}[\%\angle\%]$	Simulated $\Delta Z_{re}[\%\angle\%]$
A	$-13.4\angle-0.4$	$-12.0\angle0.2$
B	$1.6\angle-4.8$	$3.2\angle-4.9$
C	$5.5\angle1.6$	$4.8\angle2.4$

Table 6.20: Trend of simulations and measurements according to healthy screen circuit, for sc-gr fault in SLB at 360Hz.

From table 6.19 and 6.20 it can be seen that the deviation of the simulation results are very similar to the deviations of the measurements. The largest disagreement between the trend of the simulations and measurements are 3% for screen A in FLB.
It is also observed that the largest deviation from healthy state is $\approx 40\%$ for FLB and 13% for SLB.

6.3 Chapter summary

Due to the significantly better agreement between simulations and measurements performed during FM2 than for FM1, it might be reasonable to question the accuracy of the power analyzer. Furthermore the last calibration of the power analyzer was 15 years ago, hence the accuracy may no longer apply.

Simulations are compared to measurements for healthy screen circuit and it was found that by increasing the distance between the cables from 0.3m to 0.35m the simulation model fits the measuring results within 1.6% at 30Hz, within 3.6% at 90Hz and within 1% at 360Hz.

The trend study showed that the trend of the simulations according to Sc-Sc and Sc-Gr faults in FLB and SLB are equal to the trend of the measurements within a margin of 6%.

From the above assumptions it has been confirmed that a sequence of single phase measurements can be used to determine the apparent screen impedances.

It is observed that a Sc-Sc fault of 2.6Ω affects the apparent screen impedances by $\approx 15\%$ more when it is applied in FLB than in SLB at 30Hz. For 360Hz the deviation is $\approx 30\%$ larger for fault in FLB than for fault in SLB.

The Sc-Gr fault of 2.6Ω affect the apparent screen impedances $\approx 20\%$ more when it is applied in FLB than in SLB for an applied measuring voltage at 30Hz and $\approx 30\%$ for 360Hz.

The largest deviations of the simulations according to measurements are 6%, therefore the simulation model is considered sufficient to be used for performing study cases, in the following chapter.

Chapter 7

Study cases performed at the cable line FRT-NOR

This chapter presents four study cases performed at the cable line FRO-NOR. The study cases are analyzed using the DIgSILENT cable model validated in chapter 6. The detectable fault resistance will be determined. The result of a link box test is compared with simulation results in order to determine if a water filled link box is detectable. Fault localization on the FRO-NOR cable line is discussed. Finally, a sensitivity analysis of selected parameters are carried out.

The following study cases are chosen in cooperation with N1.

- **Screen to screen fault.** The screen to screen fault represents a short circuit between the two conductors in the bonding cable connecting the link box to the cable joint.
- **Single screen to ground fault.** The single screen to ground fault is representing a short circuited SVL.
- **Disconnected screen conductor.** Disconnected screen conductor in a link box
- **3-screen to ground fault.** The 3-screen to ground fault represent a link box filled with water.

The following study cases are all performed with faults in the second link box, unless other is stated. The study cases are simulated using the DIgSILENT model, described in appendix C. The simulation model may be found on the attached CD in the folder: *DIgSILENT*

In order to determine if a fault is detectable or not an evaluation scheme has been made. The deviation of the apparent impedance magnitude between healthy and faulty state is divided into two categories.
If a screen impedance differs more than 5% from the corresponding healthy screen impedance, is it determined that the given screen impedance have an abnormal value and the screen circuit have a detectable faulty link box. If the screen impedance differs less than 5% is it determined that the screen circuit is healthy. The 5% deviation is attributed to the accuracy of the measurement equipment and the simulation model's deviation from the physical system.

The fault categories mentioned above are each indicated with a color. A screen conductor that differs more than 5% is marked with **green** indicating a detectable fault. **Red** indicate that the faulty screen

conductor differs less than 5%, meaning that the fault is undetectable. Figure 7.1 illustrate the division of the categories. The screen impedance deviation is calculated using equation 7.1.

$$\Delta|Z|(R_f) = \left(\frac{|Z|_{sim}(R_f)}{|Z|_{healthy}} \right) - 1 \quad [\%] \quad (7.1)$$

Where $|Z|_{healthy}$ may be found in table 7.1.

The healthy screen magnitudes are used as reference in the following study cases.

Screen	At 30Hz $\|Z\|[\Omega]$	At 360Hz $\|Z\|[\Omega]$
A	1.89	15.1
B	1.89	15.3
C	1.89	15.4

Table 7.1: Healthy screen impedances at different frequencies.

An example of the fault categories are shown in figure 7.1.

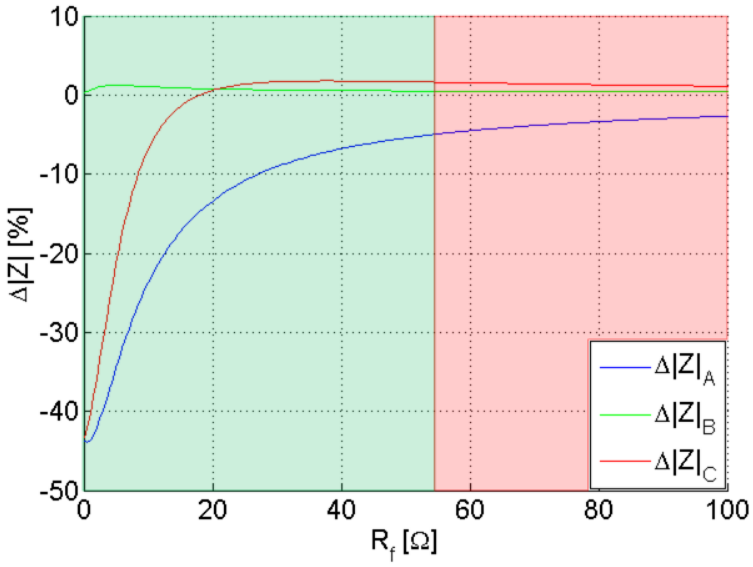

Figure 7.1: Illustrates the detectable fault resistance.

The two categories illustrated in the above figure may now be used to determine the detectable fault resistance.

- Detectable fault resistance $R_f < 55\Omega$
- Undetectable fault resistance $R_f > 55\Omega$

7.1 Screen to screen fault

A short circuited bonding cable will affect the screen circuit as a Sc-Sc fault, such a fault is shown in figure 7.2. The bonding cable is the connection between the joint and the link box.

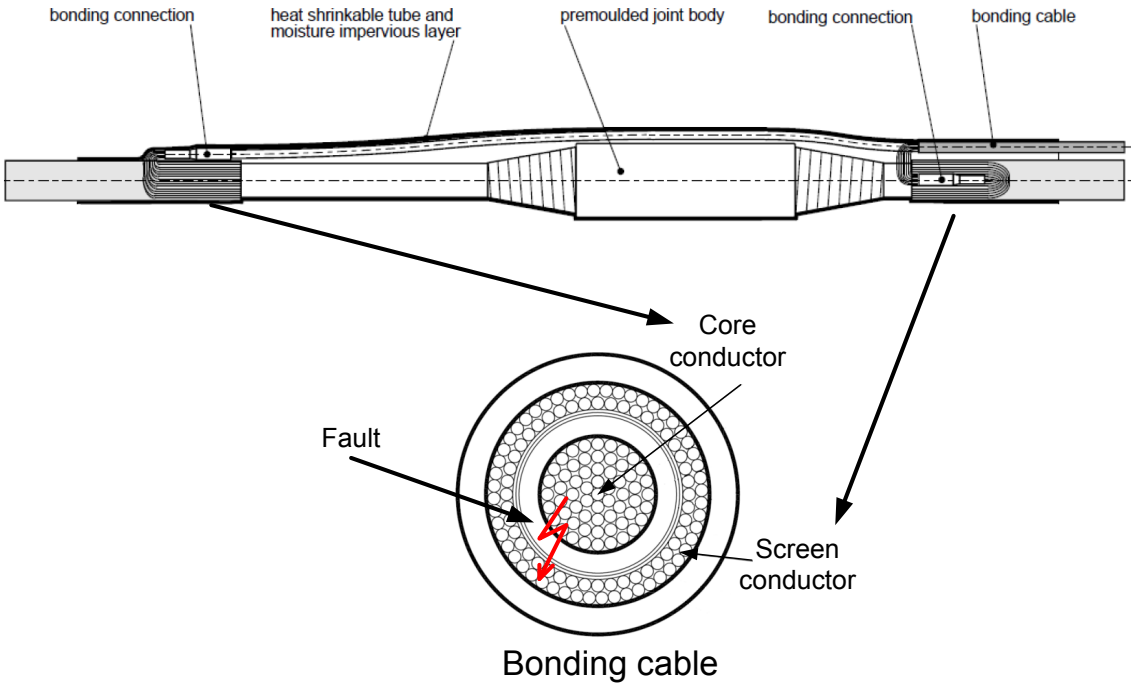

Figure 7.2: Illustration of the connections between the cable joint and bonding cable. The fault indicates a short circuit between screen and core conductor in the bonding cable.

A representation of a Sc-Sc fault in DIgSILENT is shown in figure 7.3.

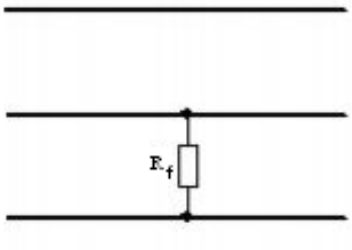

Figure 7.3: Definition of screen to screen fault.

Simulation results are shown in figure 7.4. Simulations are performed at a measuring frequency of 30Hz and 360Hz.

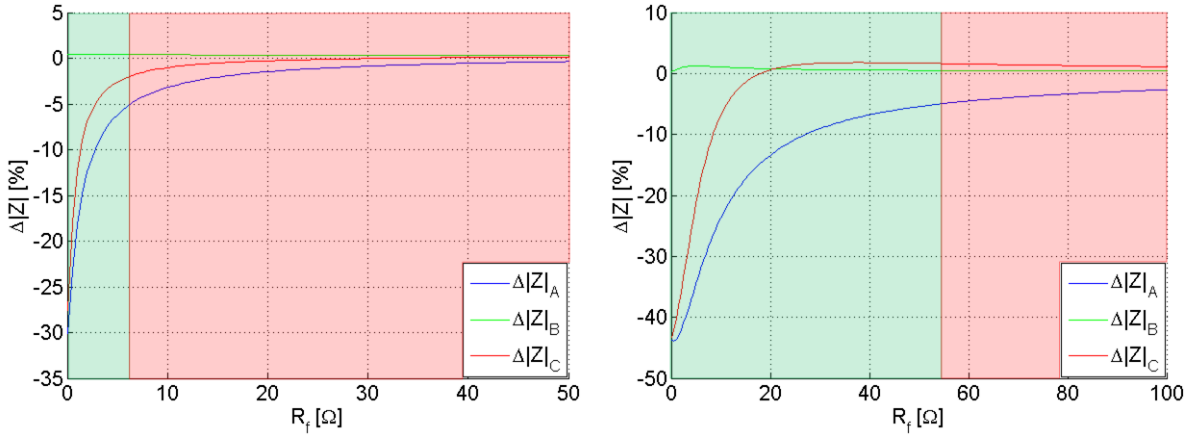

(a) (b)

Figure 7.4: Simulation results of a screen to screen fault applied in the SLB at (a) 30Hz and (b) 360Hz

At 30Hz.

- Detectable fault resistance $R_f < 6\Omega$
- Undetectable fault resistance $R_f > 6\Omega$

At 360Hz.

- Detectable fault resistance $R_f < 55\Omega$
- Undetectable fault resistance $R_f > 55\Omega$

By increasing the measuring frequency the detectable fault resistance increases up to 55Ω.

7.2 Screen to ground fault

A SVL may become faulty due to ageing, degradation of the metal oxide material or moisture penetration [33][44]. A faulty SVL may become a short circuit and thereby be represented as shown in figure 7.5.

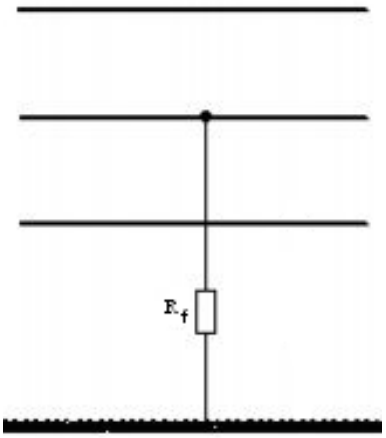

Figure 7.5: Definition of screen to ground fault.

A shorted SVL is simulated and the results are shown in figure 7.6. The fault is applied in SLB. Simulations are performed with a measuring frequency at 30Hz and 360Hz.

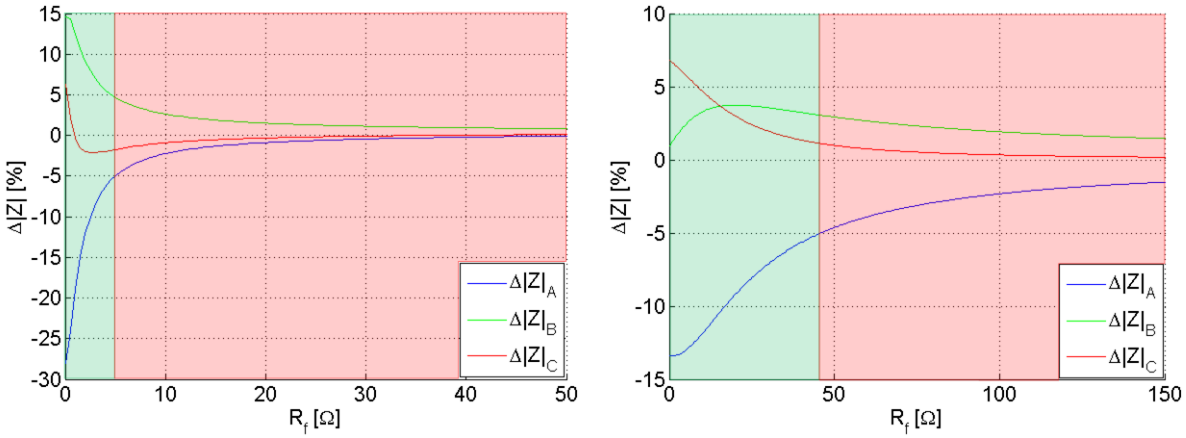

Figure 7.6: Simulation results of a screen to ground fault applied in the SLB at (a) 30Hz and (b) 360Hz

At 30Hz:

- Detectable fault resistance $R_f < 5\Omega$
- Undetectable fault resistance $R_f > 5\Omega$

At 360Hz:

- Detectable fault resistance $R_f < 46\Omega$
- Undetectable fault resistance $R_f > 46\Omega$

Since the earthing resistance at the SLB is 7Ω, a Sc-Gr fault is not detectable at 30Hz. If the measuring frequency is increased to 360Hz a faulty SVL with an internal resistance of up to 39Ω becomes detectable, hence the earthing resistance is 7Ω.

7.3 Disconnected screen conductor

In case a screen conductor is total disconnected, hence the screen is open ended. The screen resistance is infinity large at a DC measurement. Applying AC to the open ended screen will cause a capacitive charging current to flow. The charging current will return through the shunt capacitances of the two healthy screens, hence the applied voltage source is floating.
The open ended screen may be represented as shown in figure 7.7(a). The voltage drop across R_{cable} and Xl_{cable} is relatively small since the charging current represent only a minor portion of the total current in healthy state, hence $U_s \approx U_r$. Based on this assumption is the screen circuit simplified to the total shunt capacitance of the disconnected screen conductor, as shown in figure 7.7(b).

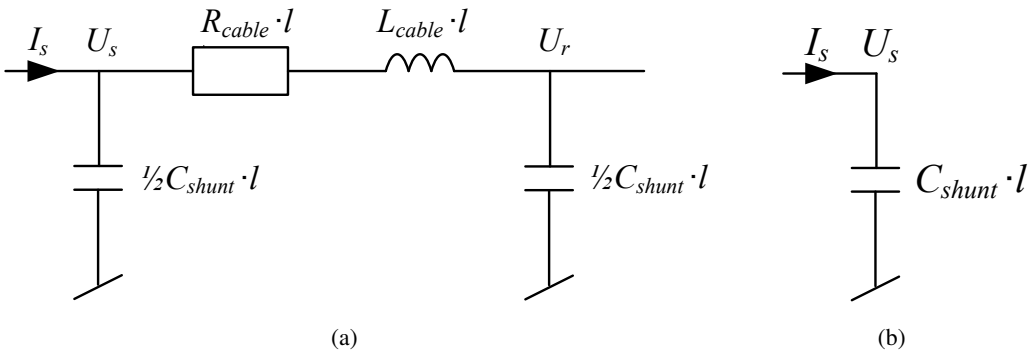

Figure 7.7: (a) Equivalent circuit of a disconnected screen conductor represented as a pi section. (b) Simplified equivalent circuit representing a disconnected screen conductor

The shunt capacitance of the total cable length is calculated in appendix H, to 19.23µF. Due to the length dependency of the shunt capacitance may a disconnected screen conductor in FLB, SLB or TLB be calculated as a fraction of the total shunt capacitance.
A disconnected screen in TLB at 50Hz:

$$X_c = \frac{1}{2\pi \cdot 50 \cdot 19.23 \cdot 10^{-6}} = 165.5\Omega \tag{7.2}$$

A disconnected screen in SLB at 50Hz:

$$X_c = \frac{1}{2\pi \cdot 50 \cdot \frac{2}{3} \cdot 19.23 \cdot 10^{-6}} = 248.3\Omega \tag{7.3}$$

A disconnected screen in FLB at 50Hz:

$$X_c = \frac{1}{2\pi \cdot 50 \cdot \frac{1}{3} \cdot 19.23 \cdot 10^{-6}} = 496.3\Omega \tag{7.4}$$

Simulation results where the screen is disconnected in FLB, SLB and TLB respectively are shown in table 7.2

Screen	Disconnection FLB [$\Omega\angle^\circ$]	Disconnection SLB [$\Omega\angle^\circ$]	Disconnection TLB[$\Omega\angle^\circ$]
A	$2.2\angle 44.2$	$2.2\angle 44.2$	$2.2\angle 44.2$
B	$477.3\angle -89.4$	$239.7\angle -89.7$	$159\angle -89.7$
C	$2.2\angle 44.2$	$2.2\angle 44.2$	$2.2\angle 44.2$

Table 7.2: Simulation results for disconnected screen conductor in FLB, SLB and TLB respectively.

The simulation results in table 7.2 shows that a disconnected screen will represent a difference of more than 5% compared to the healthy screen impedance, hence this type of fault is detectable. It is also observed that the fault impedance is highly capacitive, due to the charging current. Furthermore is it possible to locate at which link box the disconnection is since the shunt capacitance dependents on the length of the screen conductor.

7.4 3-screen to ground fault

A 3sc-gr fault may appear if a link box is leaking and is filled with water. This study case will fist considerer the detectable fault resistance based on simulation results. This is followed by a laboratory test where a link box, similar to the ones used at the FRT-NOR cable line, is filled with water. The test results are compared with the simulation results.

7.4.1 Simulation results

The 3-screen to ground fault is represented as shown in figure 7.8.

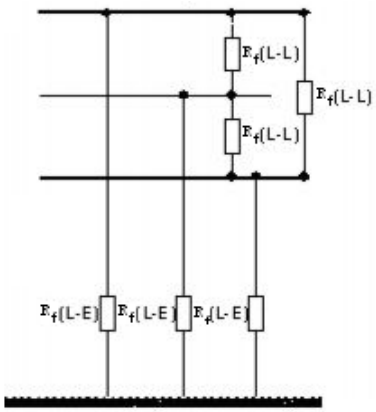

Figure 7.8: Definition of 3-screen to ground fault.

Where: $R_f(L-E) = R_f(L-L) + 7\Omega$, while the earthing resistance at the SLB is 7Ω.

$R_f(L-L)$ is represented at the x-axis, in figure 7.9, . The fault is applied in SLB. Simulations are performed with measuring frequencies of 30Hz and 360Hz.

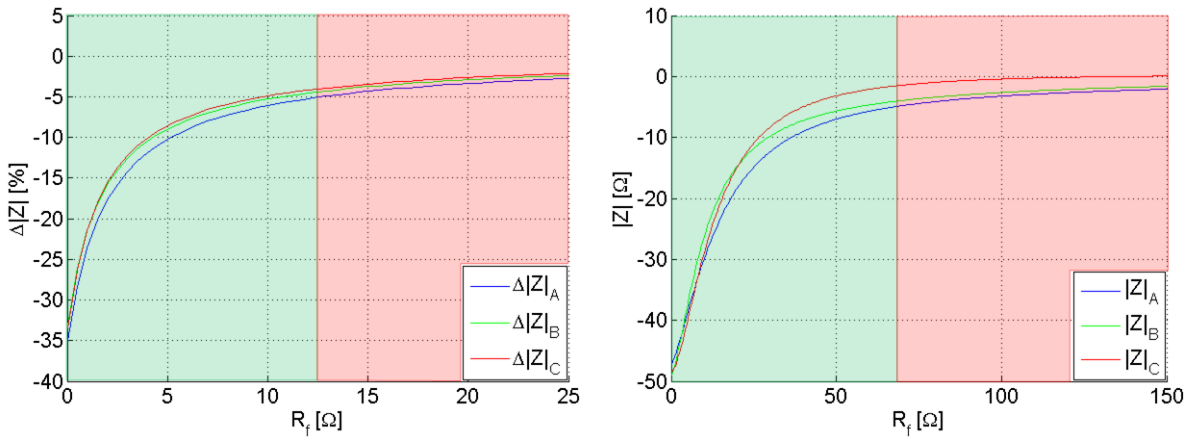

(a) (b)

Figure 7.9: Simulation results of a 3-screen to ground fault applied in the SLB at (a) 30Hz and (b) 360Hz

At 30Hz, figure 7.9(a).

- Detectable fault resistance $R_f < 13\Omega$
- Undetectable fault resistance $R_f > 13\Omega$

At 360Hz, figure 7.9(b).

- Detectable fault resistance $R_f < 68\Omega$
- Undetectable fault resistance $R_f > 68\Omega$

By increasing the measuring frequency the magnitude of the detectable fault resistance was increased from $13 - 68\Omega$.

7.4.2 Link box test

The project group has performed a number of tests where a link box has been filled with water. This was done in order to determine the expected fault resistance of a water filled link box. The complete test report may be found in appendix G.

The test showed that the water conductivity is depending on the location at which it is collected.

Link boxes at cross country cable lines will most likely be installed in farmer's field. A water sample from the field, shown in figure 7.10, had the following conductivity: $636 \mu S/cm$.

Figure 7.10: The red arrow indicates the place at which water sample has been collected.

A water sample was collected from a water hole placed near by the university, see figure 7.11. The conductivity was measured to $853 \mu S/cm$.

Figure 7.11: Water hole near AAU, where the second water sample was collected.

A third water sample was collected form a lake at the university. The location at which the sample is taken may be seen in figure 7.12. The conductivity of the sample is measured to $1040 \mu S/cm$.

Figure 7.12: Small Lake near AAU, where third water sample was collected.

A mixture of the samples in figure 7.11 and 7.12 were used for the test. The conductivity of the mixture was measured to 892$\mu S/cm$. Figure 7.13(a) shows the water filled link box and the measuring points. Measuring results are shown in figure 7.13(b).

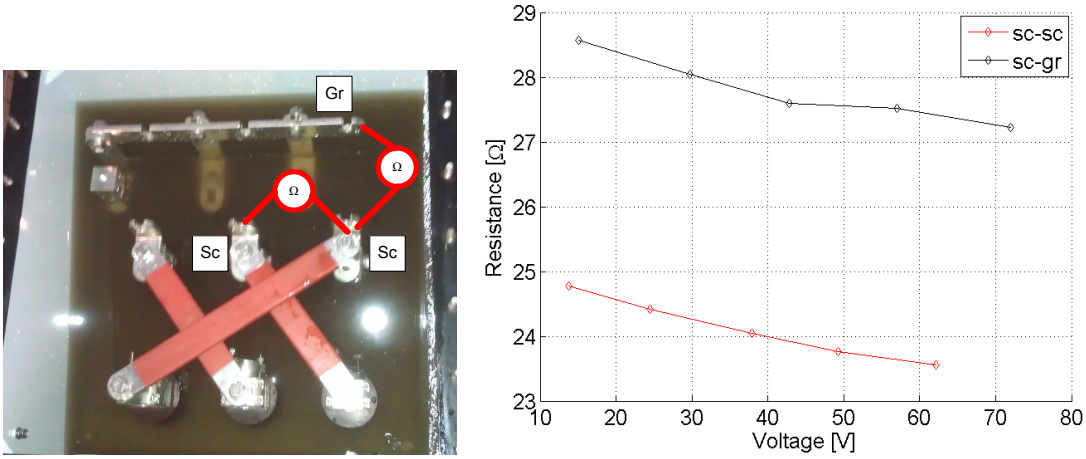

(a) (b)

Figure 7.13: (a) Water filled link box and measuring points. (b) Measured resistances as a function of applied voltage.

With an applied voltage of 50V the Sc-Sc resistance was measured to $\approx 24\Omega$ and Sc-Gr $\approx 27.5\Omega$.

The Sc-Sc (Sc-Gr) resistance dependents on the conductivity of the water this is further explained in appendix G. A resistance interval which corresponds to the conductivities of the collected water samples are calculated in above mentioned appendix. The interval is shown in figure 7.14.

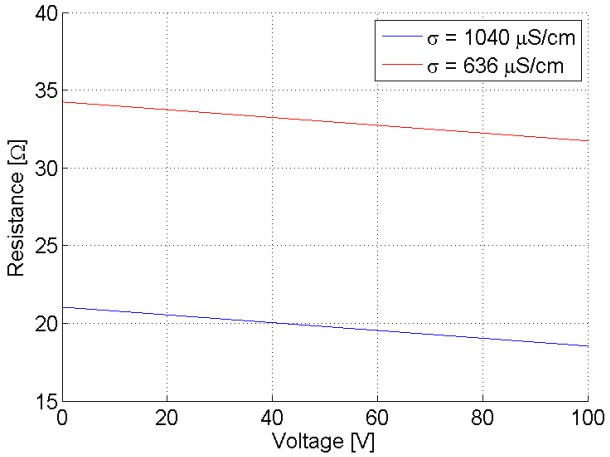

Figure 7.14: Resistance between Sc-Sc in a water filled link box. The water conductivity is 636 and 1040$\mu S/cm$ respectively.

Test results showed that resistance interval corresponding to the conductivities of the water samples, was $20-35\Omega$ as shown in figure 7.14. The simulation results at a measuring frequency of 360Hz showed that a fault resistance of up to 68Ω was detectable, hence a water filled link box is detectable.

7.5 Fault localization

Fault localization is difficult at the FRT-NOR cable line due to the inaccessible third link box. Figure 7.15 illustrates the deviation of a faulty screen conductor in case of a fault (Sc-Sc, Sc-Gr and 3Sc-Gr). The faults are applied in the FLB and the SLB respectively. Only if a screen impedance differs more than 50% the fault may be localized to the FLB. If the faulty screen impedance differs less, it is impossible to localize the fault to an exact link box.

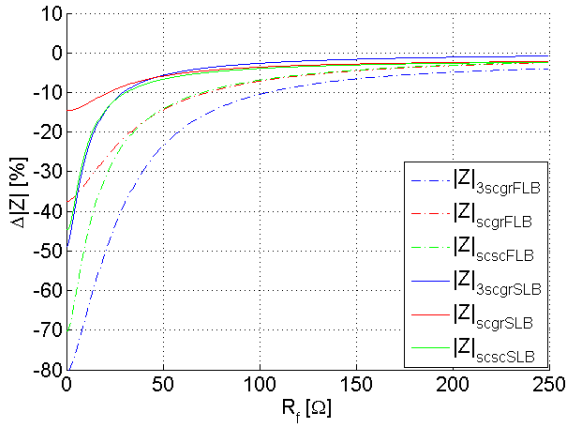

Figure 7.15: The three fault types (3Sc-Gr, Sc-Gr and Sc-Sc) applied in the FLB and SLB.

If the TLB was accessible fault localization would have been possible, since the major section then could be measured at both ends. In case of a Sc-Sc fault with $R_f = 25\Omega$. Measurements would indicate that one of the faulty screens would differ $\approx 10\%$ at one end and $\approx 25\%$ at the other, hence the second measurement indicates that the faulty link box is localized closest to the second measuring site. This statement is true if the screen conductors are star point connected at the end opposite to the measuring point of the major section.

7.6 Sensitivity analysis of selected parameters

Table 7.3 shows the impact of increasing a parameter at the FRT-NOR cable line in respect to the maximum detectable fault resistance at 3Sc-Gr, Sc-Sc and Sc-Gr faults. The arrows in the table indicate whereas the detectable fault resistance increases (↑) or decreases (↓).

	3Sc-Gr	Sc-Sc	Sc-Gr
FRT-NOR(max R_f) [Ω]	68	55	46
Increased parameter values			
Screen cross section area	-	-	-
Minor section length	↑	↑	↑
Flat formation width	↑	↑	↑
Tight triangular formation	↓	↓	↓
Grounding resistance at fault location	-	-	↓
Grounding resistance at TLB	-	-	↑

Table 7.3: Increased cable system parameters values and there effect on fault detection at a measuring frequency of 360Hz.

- Increasing the cross section area of the screen to $240mm^2$ did not have significant influence at the detectable fault resistance due to the fact that the screen circuit at 360Hz is mainly inductive.

- By increasing the length of the minor sections the detectable fault resistances for all three cases increases, since the screen circuit impedance is increased.

- The screen circuit impedance is increased if the distance between the cables are increased (hence larger current loop causes larger inductance) and the detectable fault resistance is increased at all cases.

- If the cable system is laid in tight triangular formation the screen circuit impedance is decreased (current loops between the cables are decreased), hence the detectable fault resistance is decreased.

- Increasing the grounding resistance at the faulty link box causes a decrease for the detectable fault resistance in case of Sc-Gr faults. Because the measurable fault resistance remains the same namely 46Ω, hence a larger portion of the resistance is the earthing resistance.

- 3Sc-Gr and Sc-Sc faults are not influenced by increased earthing resistance at the faulty link box or in the third link box(TLB). By increasing the earthing resistance at TLB is the detectable fault resistance at Sc-Gr faults increased as earlier mentioned in chapter 5.

7.7 Chapter summary

Four study cases have been analyzed for the cable line FRT-NOR and it is concluded that it is possible to detected all four fault types.

By increasing the measuring frequency to 360Hz is it possible to detect higher fault resistances compared to a measuring frequency of 30Hz. This is valid for the study cases listed in table 7.4.

Study case	R_f [Ω]	Comment
3Sc-Gr	68	-
Sc-Gr	39	$R_{earth} = 7\Omega$
Sc-Sc	55	-

Table 7.4: Detectable fault resistance @ 360Hz.

In order to detect a disconnected screen conductor in one of the link boxes the measuring frequency should be low, in this case 50Hz. By doing so the reactance of the screen shunt capacitance is high, hence the return path for the current is relative high-impedance. At this fault type it is possible to detect and localize the faulty link box furthermore is the fault impedance characterized by being capacitive.

Fault localization is only possible if the impedance differ more than 50%, since measurements only can be performed at substation Nors.

Laboratory tests indicated that a link box filled with water would represent a 3-screen to ground fault of $\approx 35\Omega$, hence with a measuring frequency of 360Hz this would be detectable.

Sc-Gr faults are sensitive to the earthing resistances at the link boxes. An increased earthing resistance at the TLB increases the detectable fault resistance. 3Sc-Gr, Sc-Sc and Sc-Gr are all sensitive to the spacing between the three phases and the length of the sections. A larger spacing between the phases and/or a longer section length will increase the detectable fault resistance.

Chapter 8

Cable systems with several major sections

This chapter provides suggestions on how the impedance method may be applied to cable systems consisting of more than one major section. In general this requires access to some of the link boxes. The minimum of accessible link boxes are considered and it is studied how to make a strategic choice of which boxes to be accessed.

8.1 Introduction to cable system consisting of more than one major section

The problem analysis showed that the limitation of the impedance method is the major section next to the measuring point, due to the star connection of the cable screens. Cross bonded cable lines may consist of several major sections, depending on the length of the line.
If the entire cable line consist of two major sections, each major section may be measured by performing one measurement from each end of the cable line as shown in figure 8.1. Hence no link boxes should be accessed.

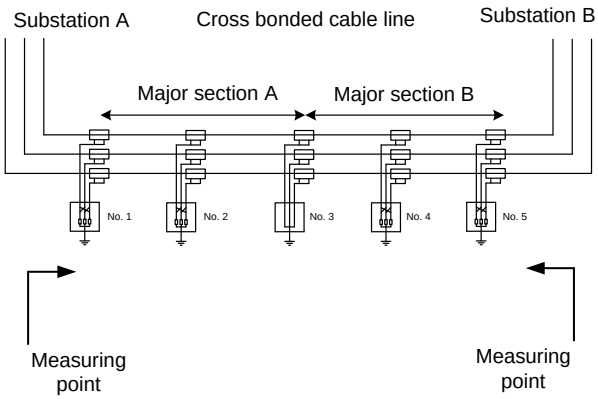

Figure 8.1: Measuring points for a cable system with two major sections.

For cable lines consisting of three major sections, the two outer major sections A and C, may be measured from each end, as shown in figure 8.2. Section B is star point connected in both ends and cannot be measured. Therefore access to link box 3 or 6 is required in order to measure the entire screen circuit.

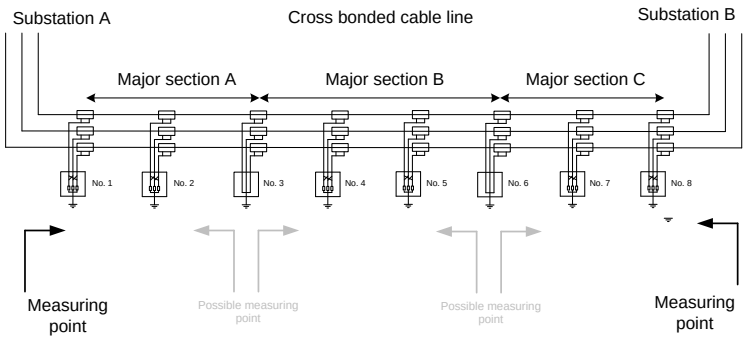

Figure 8.2: Measuring points for a cable system with three major sections.

The placing and thereby the accessibility of the link boxes differs from line to line. For some lines, as the measured FRT-NOR all link boxes are buried in the ground. For other lines, as the Horns Rev 2 cable, every third link box is brought to the surface [29]. This study distinguish between:

- Cable lines where all the link boxes are difficult to access. Meaning that all link boxes are buried in the ground, and can only be accessed by digging.
- Cable lines where every third link box is easily accessed. The link boxes separating the major sections are placed where they can be accessed without digging.

The two types of systems are considered in the following two sections.

8.2 Cable systems with difficult accessible link boxes

A cable system with difficult accessible link boxes are characterized by having all link box buried into the ground. The only way to access the link boxes are by digging down to them. In order to use the impedance method on a cable system consisting of more than two major sections a number of link boxes should be accessed each time the condition of the link boxes should be evaluated. Figure 8.3 illustrate a cable system consisting of four major sections. In this case the minimum number of link boxes there should be accessed in order to evaluate the condition the entire line is one - link box number 6.

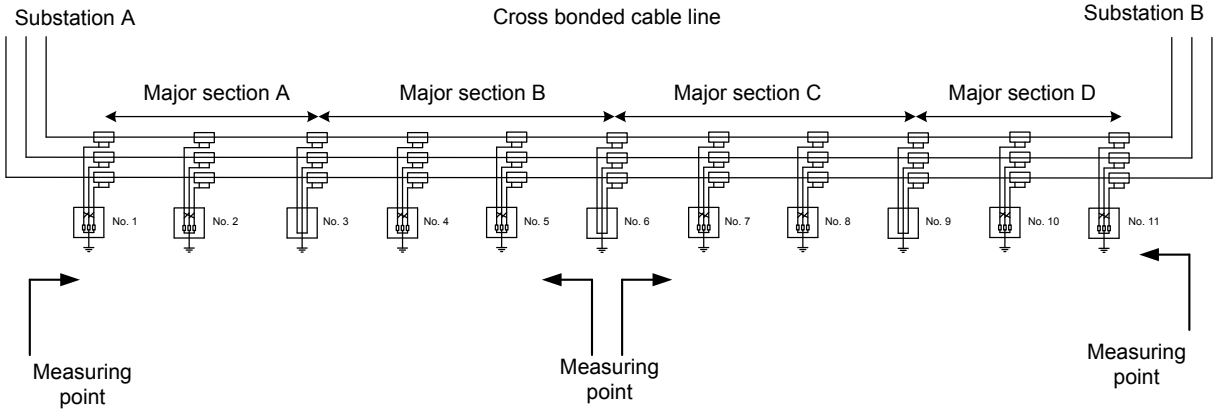

Figure 8.3: Measuring points for a cable system with four major sections.

Table 8.1 shows how many and which link boxes there should be accessed, in order to measure all link boxes of cable lines, consisting of 1-8 major sections.

No. of major sections	Quantity. of accessible link boxes	Link box No.
1-2	0	-
3-4	1	3 - 6
5-6	2	6 and 9 - 6 and 12
7-8	3	6, 12 and 15 - 6, 12 and 18

Table 8.1: The quantity of accessible link boxes and the link box number, counted from one substation.

The minimum of link boxes there needs to be accesses are a consequence of the fact that the impedance method is limited by the star point connection of the screens. Therefore in order to use the impedance method there should be measured directly in each section.

N1 has estimated that gaining access to a buried link box would cost approximately 40,000 Dkk and 4 days of work including restoration.
It is expected that the cable line has a lifespan of 40 years. The cable manufacturer prescribes that the link boxes should be inspected every two years.

The cumulative cost of accessing the number of link boxes stated in table 8.1 is shown in figure 8.4. The lifetime of the cable system is expected to be 40 years and the link boxes are accessed every two year.

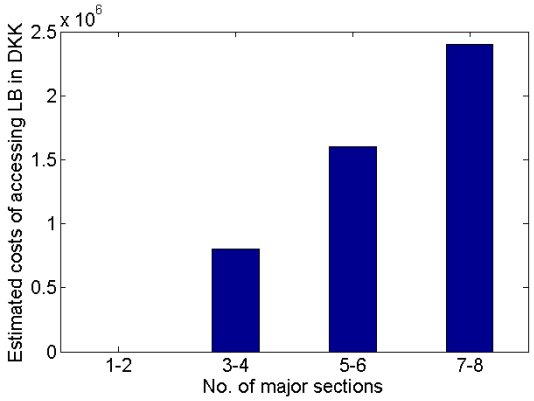

Figure 8.4: Estimated costs of accessing the number of link box stated in table 8.1. Expected lifetime of the cable system is 40 years.

The cost of this maintenance can be reduced significantly by placing the selected link boxes easily accessible.

8.3 Cable systems with easily accessible link boxes

A link box is easily accessible if it is placed in a well or the box is brought to the surface. This could either be done to the number of link boxes mentioned in table 8.1 or every third link box.

If every third link box is easily accessible the task of condition determination is significantly different, and a number of different measuring techniques may be used. In this section only the use of the impedance method is considered.

In case every third link box is easily accessible and the impedance method is used to determine the condition of the link boxes the following procedure could be used.
Figure 8.5 illustrates a cable line consisting of three major sections. The three sections are connected in series as proposed in the problem analysis 3.4.3 on page 63. The screens are star point connected, but ungrounded at the end opposite to which the measurements are performed.

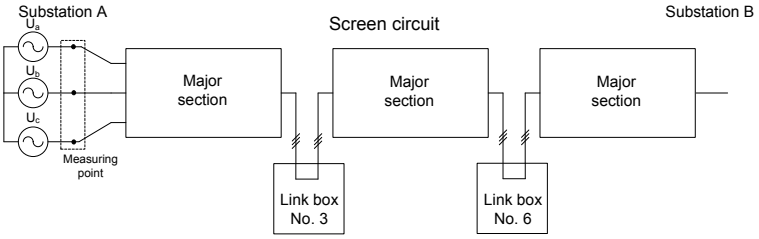

Figure 8.5: Three major sections connected in series.

Impedance measurements may be performed either one or from both ends.

- If the measurements are only performed from one end, the most difficult link box to determine the condition of, is the one closest to the star point. The detectable fault resistance depends on the screen impedance between the faulty link box and the star point connection.

- If the measurements are performed from both ends of the line, the most faraway link box from the measuring sites, is the most difficult one to determine the condition of. This is because for this setup the link box with the smallest screen circuit behind position of the fault. Since it is possible to measure from both ends of the screen circuit the entire system can be evaluated through two measurements. For the system above the most faraway link box would be #4, counted from the substation where the measurement is performed.

If the measurements are performed from both ends of the most difficult link boxes to determine the condition of, is the boxes in the middle of the line. These boxes are furthest from both measuring point.

8.3.1 Analysis of series connected sections

Resonance frequency

The screen circuit analysis in section 5.1 and the sensitivity analysis in section 7 showed that the largest detectable Sc-Sc and 3Sc-Gr fault resistance is increased if the measuring frequency is increased. When the screen circuit is increased to include several major sections, both the series inductance and shunt capacitance are increased due to the proportionality to the cable length. The resonance frequency decreases with increasing cable length. This should be considered when selection measuring frequency. Calculation of the resonance frequency is shown in Appendix H.

Shunt capacitance

The screen circuit analysis in section 5.1 and the sensitivity analysis in section 7 showed that the largest detectable ground fault resistance is increased, if the earthing resistance at the end of the major section is increased. The sensitivity analysis also showed that the detectability of Sc-Sc and 3Sc-Gr fault is not affected by the resistance in the end of the section.

When every third link box is easily accessible the grounding in the end of the section could possibly be removed. If the grounding is removed the potentials of the screen circuit, according to ground, is determined by the shunt capacitances.
This may be seen in figure 8.6 where the three screen conductors are represented as π-sections.

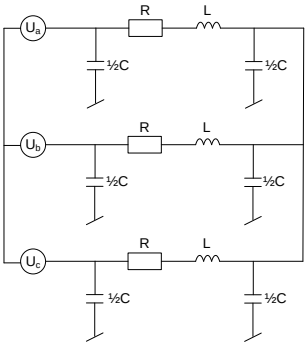

Figure 8.6: Ungrounded screen circuit.

Applying a ground fault may be seen as a fault resistance parallel to the shunt capacitance, as shown in figure 8.7. The shunt impedance depends on the impedance of the fault and the shunt capacitance. The impedance of the shunt capacitor increases for decreasing frequency. It may for this reason be reasonable use low measuring frequency, when detection for ground faults.

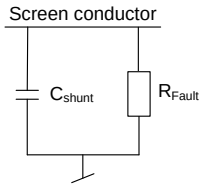

Figure 8.7: Parallel connection of shunt capacitance and ground fault.

Example of three major sections connected in series

An example of three series connected major sections, will now be shown. The example consider measurements performed from one and both ends. The largest detectable fault resistances are determined, for the fault cases listed below. The screen circuit:

- Sc-Sc
- Sc-Gr
- 3Sc-Gr

The parameters of the major sections in figure 8.5 are identical to the major section at the FRT-NOR cable line. By series connection the three major sections the total cable line length become 34.56km long. The DIgSILENT simulation model may be found on the attached CD in the folder '*DIgSILENT*'.

According to section 8.3.1 a high simulation frequency should be selected for Sc-Sc and 3Sc-Gr fault detection. The resonance frequency of the circuit is calculated to 260Hz using the DIgSILENT model. Therefore is the simulation frequency chosen to 150Hz for 3Sc-Gr and Sc-Sc fault detection.

For ground fault detection a frequency of 20Hz is chosen, in order to increase the impedance of the shunt capacitance, as explained in section 8.3.1.

Measuring from one end.

For faults at the 8th link box, the screen circuit will appear as shown in figure 8.8. Using the 5% detectability limit the detectable fault resistances are given in table 8.2.

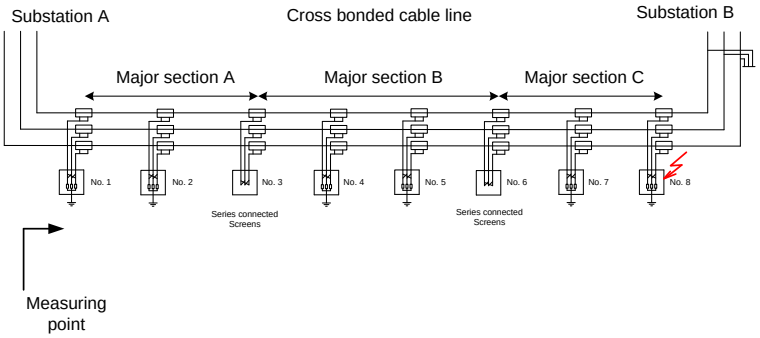

Figure 8.8: Three major sections connected in series.

Fault type	Resistance
Sc-Sc	5Ω
Sc-Gr	115Ω
3Sc-Gr	15Ω

Table 8.2: Largest detectable fault resistances, at 8th link box for three major sections in series.

Form table 8.2 it may be seen that the largest detectable fault resistances are quite low. For this setup it would not possible to detect the water filled link box. The sc-gr fault is the most prominent and thereby easiest to detect.

Measuring from both ends.

Faults in the 4th link box are simulated and the results are shown in figure 8.10. The screens are star point connected but ungrounded at the opposite end to which the simulations are performed, as for the previous case.

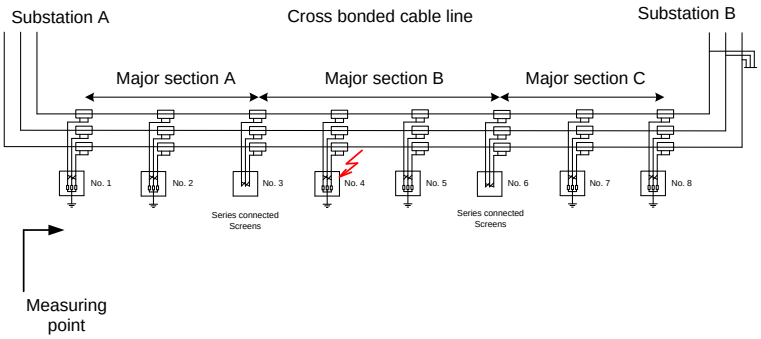

Figure 8.9: Three major sections connected in series.

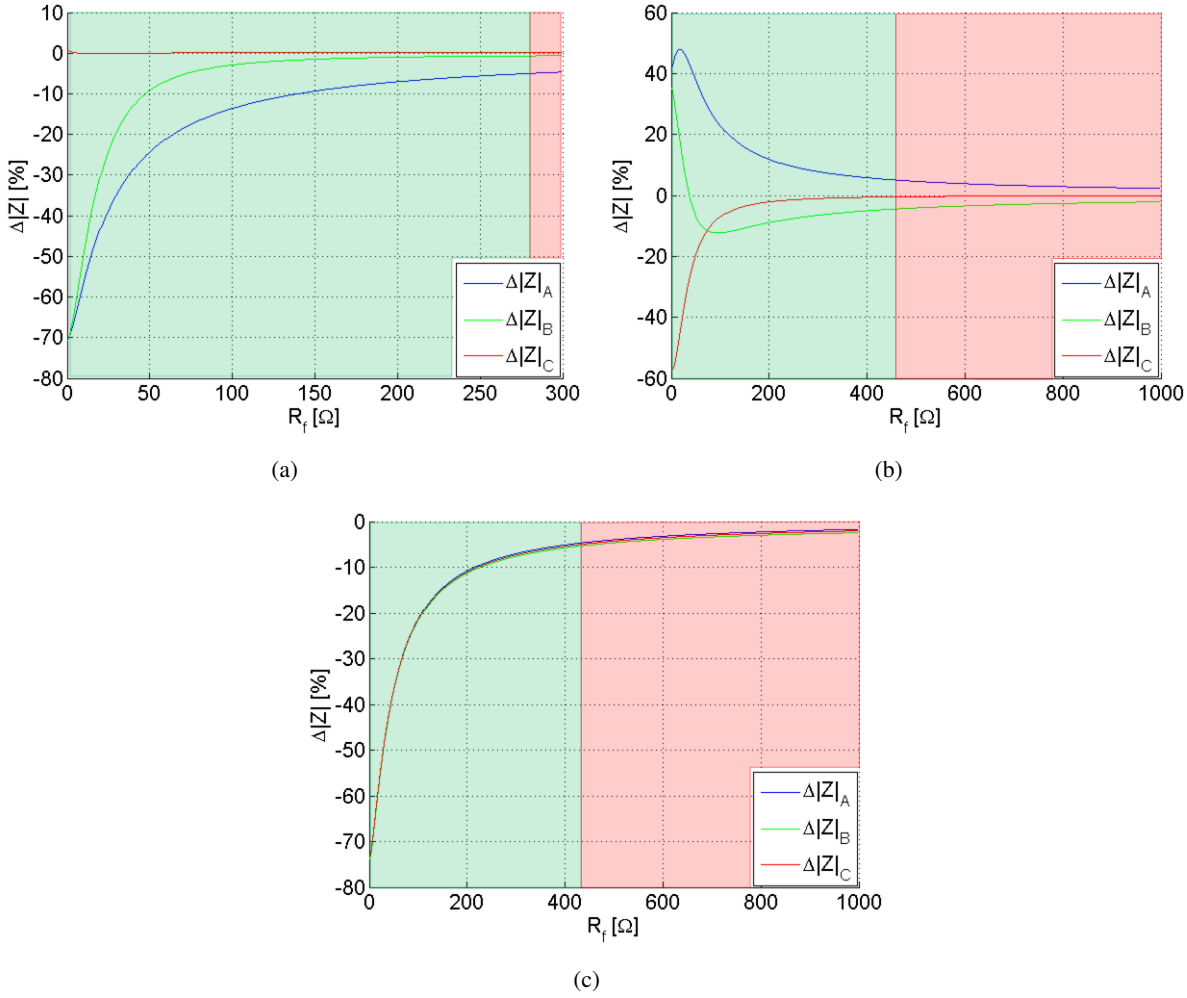

Figure 8.10: Largest detectable fault resistance for the three fault types: (a) Sc-sc fault measuring frequency 150Hz. (b) Sc-gr fault measuring frequency 20Hz. (c) 3sc-gr fault measuring frequency 150Hz.

The detectable fault resistances, illustrated by the colors, in figure 8.10 are listed in table 8.3.

Fault type	Resistance
Sc-Sc	279Ω
Sc-Gr	462Ω
3Sc-Gr	432Ω

Table 8.3: Largest detectable fault resistances, for the three series connected major sections.

It is seen that the largest detectable fault resistances are significantly larger than the detectable fault resistances when the measurements are only performed from one end. The detectable fault resistances are also much higher than, the detectable fault resistance from the study cases in chapter 7, where faults are simulated in SLB for only one major section.

Localization of a fault.

The previous section showed that the largest detectable fault resistance was 460Ω, at a cable system consisting of three major sections. The fault could be detected by series connecting the screen circuit of the sections, and performing measurements from both ends.
In case a measurement indicates a faulty screen circuit, the fault may be located using the following procedure. The procedure is divided into three steps.

1 Location faulty half.

2 Location faulty major section

3 Location faulty box

The steps are explained below and may also be seen in the block diagram shown in figure 8.16.

The screen circuit of three major sections, connected in series are shown in figure 8.11. In order to establish the series connection link box (LB) No. 3 and 6 are accessed, and can thereby be visual inspected.

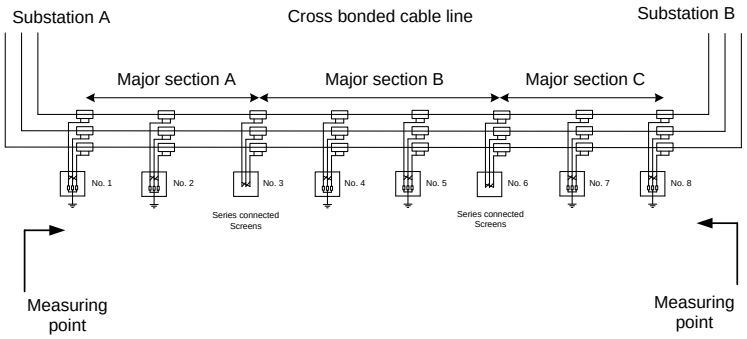

Figure 8.11: Three major sections connected in series.

1 The first step is to measure the apparent screen impedances in both ends of the cable line, substation A and substation B. For each of the measurements the three screens should be star point connected, but not grounded at the opposite end.

The lowest measured apparent screen impedance indicate at which half of the line, the fault is located. If the lowest screen impedance is measured in substation A, the fault is located in link box 1, 2 or 4, due to the visual inspection of LB. No. 3. Hence if the lowest apparent screen impedance is measured in substation B, the fault is located in link box 5, 7 or 8.

For this example the lowest apparent screen impedance is measured in substation A, and the fault is therefore located in link box 1, 2 or 4, see figure 8.12.

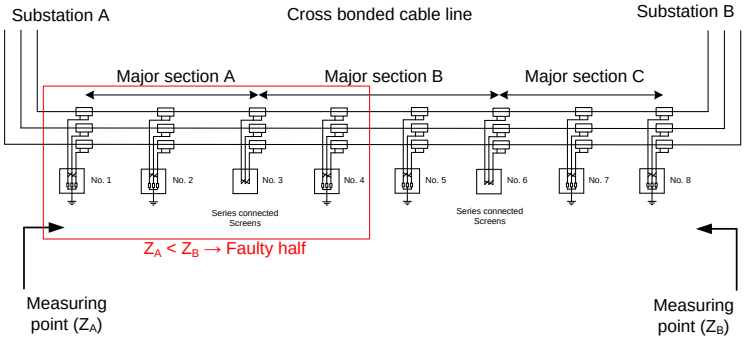

Figure 8.12: Three major sections connected in series.

2 The second step is to remove the connections in LB No. 3. When the connections are removed the apparent screen impedances should be measured in LB. 3, towards substation B (Z_{3-B}) as shown in figure 8.13. For this measurement the screens should be star point connected, but not grounded in substation B.

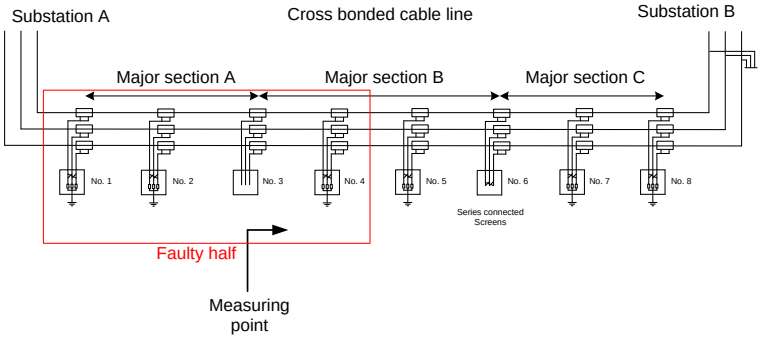

Figure 8.13: Three major sections connected in series.

The only possibly faulty link box in this direction is LB. No. 4. This measurement will now tell if link box No. 4 is faulty or not.
For this example no faults are measured, and LB. No. 4 is considered healthy. The faulty LB. may now be No. 1 or 2, as shown in figure 8.14.

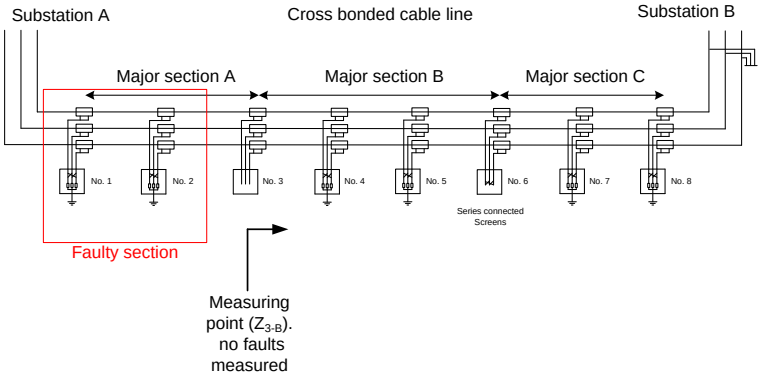

Figure 8.14: Three major sections connected in series.

3 The third step includes two measurements. One from LB. No. 3 and another from substation A,

as shown in figure 8.15. For each of the measurements the three screens should be star point connected, but not grounded at the opposite end.

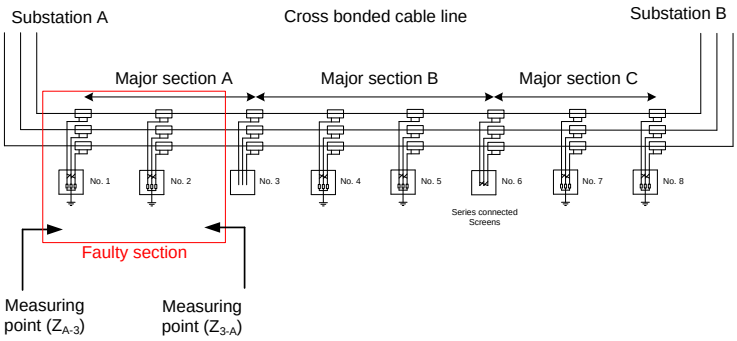

Figure 8.15: Three major sections connected in series.

As described above the three screens should be star point connected at the opposite end. For this reason these measurements only cover one major section. When only one major section is measured the largest detectable fault resistance is lower as for the series connection, due to the lower healthy screen circuit impedance. This is a disadvantage of this fault location procedure.

The largest detectable fault resistances of the two measurements in step three, are shown in table 8.4. Therefore if a fault is located in LB. No. 1 or 2. The fault may be detected from the initial measurement, but can not be located, if the fault resistance is larger than the values given in table 8.4.

Fault type	Resistance
Sc-Sc	190Ω
Sc-Gr	1300Ω
3Sc-Gr	260Ω

Table 8.4: Detectable fault resistances, for faults in the FLB.

It is also seen that for the Sc-Gr fault, a larger fault resistance is detectable, when the circuit is reduced to one major section. Hence this type of fault may be localized using this method.

The fault localization is illustrated in figure 8.16.

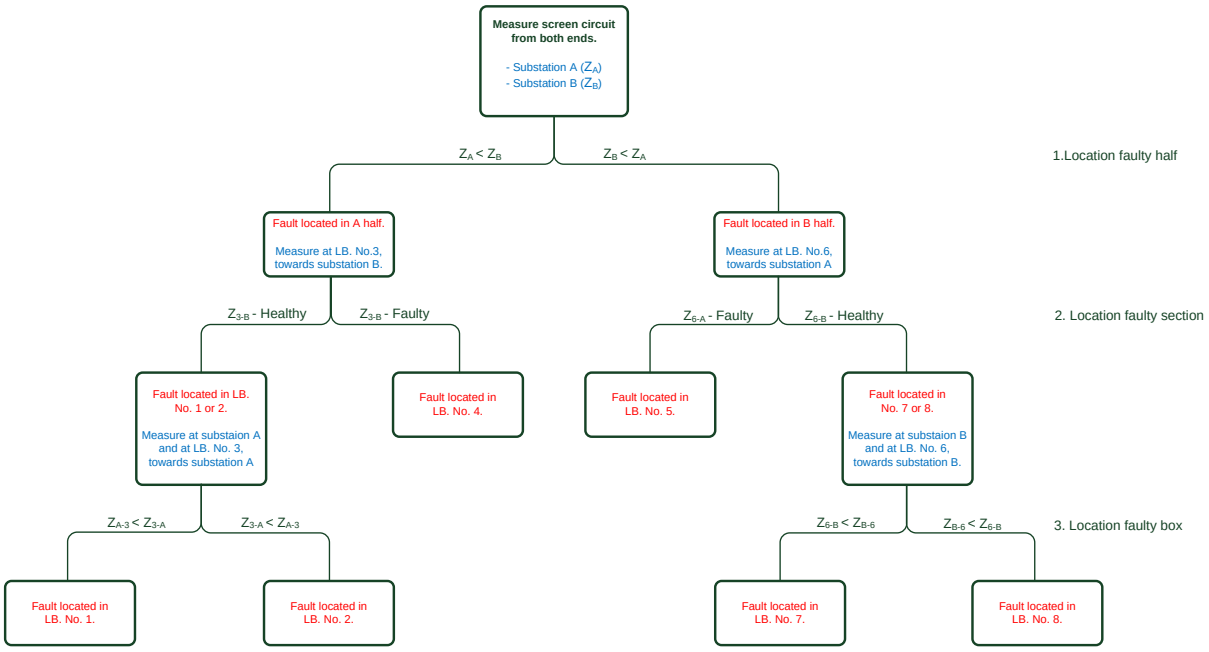

Figure 8.16: Procedure for fault location at three major sections.

8.4 Practical considerations

This chapter showed that accessing one or more link boxes are necessary, when a screen circuit consists of more than two major sections and the impedance method is used to determine the screen circuit condition. It is therefore highly recommendable to make selected link boxes easy accessible, when new cable lines are established. The maintenance of a cable system is limited only to a few components (substation equipment and link boxes) compared to a OHL. The maintenance of an OHL is much more comprehensive, as the following listing indicates:

- Inspection of insulators
- Inspection of phase conductors
- Inspection of ground wire connections to tower
- Inspection of the tower galvanization
- Strength test of conductors
- Inspection of mounting and tower bolts
- Inspection of concrete foundation
- Inspection of tower grounding
- Pruning of trees near OHL (trimming)
- Removing bird nests at towers
- Inspection of vibration dampers... ect.

It is important to recognize that transmission lines do not become maintenance free when established as cables. In order to do the cable line maintenance less complicated, both time and money is saved. The cumulative cost of accessing a underground link box was earlier estimated to 800,000 Dkk, if the lifetime of the cable line is 40 years [7] and the link box is accessed every two years, as prescribed by the cable manufacturer [37]. Considering a cable line consisting of 8 major sections with 23 link boxes would cost approximately 18 million Dkk only to get access to the link boxes.
The main argument for cable down the Danish transmission grid is the visual pollution OHL's are responsible for. Figure 8.17 illustrate the visual difference by an OHL and cable line as seen from ground level. If every link box was brought to the surface would this be much less visible and the number of visible boxes would also be less than the towers at the OHL system.

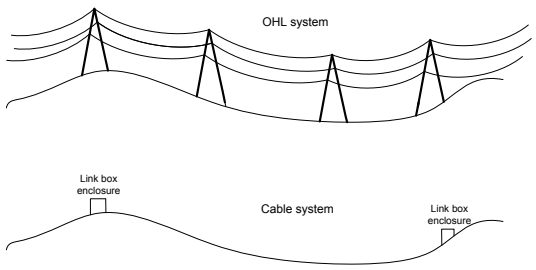

Figure 8.17: Visual impact of OHL vs. cable lines, with accessible link boxes.

From a practical point of view would the maintenance of the cable system be much more time and cost effective, if some or all link boxes are placed on the surface. The technology that may be used for placing the link boxes on surface is known and tested. The main part of the 10kV grid in Denmark is under grounded and many 10kV/0.4kV transformers are placed in a housing that might be suitable as an enclosure for the link boxes, as figure 8.17 illustrates.

8.5 Chapter summary

- Using the impedance method for condition determination, access is required to at least one end of each major section. Therefore at lines consisting of more than two major sections, access to at least one link box is required. In order to access each major section minimum every sixth link box should be accessed. The minimum number of link boxes there should be accessed is given in table 8.1.
- Alternatively if every third link box is accessible, the screens could be series connected. If the screens are series connected the entire screen circuit could be measured from one or both ends. An example of three major sections connected in series are shown The detectable fault resistances from one and both ends measuring are shown in table

Fault type	Measuring in one end Resistance	Measuring in both ends Resistance
Sc-Sc	5Ω	279Ω
Sc-Gr	115Ω	462Ω
3Sc-Gr	15Ω	432Ω

Table 8.5: Detectable fault resistances, for measurements in one and both ends accordingly.

From table 8.5 it is seen that it is possible to detect significantly larger fault resistances by performing measurements from both ends.

However the fault resistances in table do not consider the location of the fault, but only the evaluation of whether the screen circuit is healthy or fault.

There is given a procedure and limitations that could be used for localization of faults.

Since the major sections needs to be series connected, every third link box must be accessed, hence a visual inspection of these link boxes may be carried out and the condition can be evaluated.

When several sections are connected in series the resonance frequency of the circuit is decreased. This should be considered when selection the frequency of the measuring voltage.

Chapter 9

Conclusion of link box condition monitoring

Cross country transmission cable lines have in many cases some or all of the link boxes placed underground. This makes the maintenance of these time consuming and costly. It is therefore of great interest to determine the condition of the link boxes without accessing them.

A state of the art analysis showed that the research within the specific area is very limited. Therefore no recommendations and no suggestions exist, besides the cable manufacture who prescribes visual inspection every two years [37]. N1 have estimated the cost of digging down to one link box, to approximately 40,000 Dkk. Cable lines have an expected life time of up to 40 years, hence accessing one single link would cost 0.8 million Dkk, if this was done every two years.

Therefore the purpose of this project is to develop a diagnostic tool, which may be used to determine the condition of the link boxes without digging down to the boxes.

Due to the lack of experience within the area, this project is based on how already used measuring techniques can be converted and used for link box condition determination. The main focus of the project is analysis of how an impedance measuring may be used for condition determination. The advantage of using known measuring techniques are that measuring equipment is available both for the project and for further use by the transmission companies.

A main part of the project is considerations of, to what extent, an impedance measurement reflects the condition of the link boxes. The measuring techniques are improved in order to detect the largest fault resistance. The measuring techniques are tested in respect to field measurements.

The results of the project are divided into three main parts:

1. Screen circuit analysis and performance of measurements.

   The screen circuit is analyzed with respect to a Sc-Sc and a Sc-Gr fault. The analysis showed that the Sc-Gr becomes significantly more pronounced, using un-grounded measuring voltage, due to the reference displacement. The analysis also showed that both fault become more pronounced

and thereby more detectable, if the measuring frequency is increased. By increasing the frequency, the resonance frequencies of the circuit should be considered in order to measure below the resonance points. The analysis also showed that the detectability of the Sc-Gr fault is dependent on the earthing resistance at TLB. For larger resistance at TLB a Sc-Gr fault is more pronounced and a larger fault resistance is detectable.

Performance of measurements are considered regarding the use of line impedance measuring equipment. It is shown that a single phase line impedance measuring equipment can be used to determined the apparent screen impedances, defined in section 3.4.2 on page 46, from a sequence of single phase measurements. The technique is based on two sets of measurements. The first set is used to calculate the equivalent screen impedances also defined in section 3.4.2 on page 46 and the last set is used to obtain the three phased response of the screen circuit. The measurements are calculated based on the super position principle.

The advantage of the measuring technique is that the apparent screen impedances can be obtained using single phase line impedances measuring equipment. The disadvantage is that the apparent impedances are calculated from several measurements and therefore measuring inaccuracy may be accumulated.

2. Study cases
   A simulation model of the cable line FRT-NOR was made in the simulation software DIgSILENT. The model was validated through two field measurements performed at the cable line in January 2012. The first field test was based on three phased power supply and a power analyzer was used to measure the impedance of the screen circuit. The second field test was used to test a measuring technique where six single phase measurements was used to calculate a three phased impedance representation of the screen circuit. By using the super position technique this was possible. Furthermore was the power supply adjustable in frequency and the measurements was carried out in a frequency span of $30-360$Hz. The power supply was an Omicron CPC100 and CP CU1. All data was recorded with an Omicron CMC356, all the measuring equipment is owned by N1. It was an important issue that the measuring devices were known/ owned by the transmission company so that the work from this report can be used afterwards. The second field test showed that measuring technique worked very well and the results were used to validate the simulation model. The largest deviation between the simulation model and the measurements was 6% but in most cases was the deviation less than 3%.
   Four study cases were chosen in cooperation with N1:

   - Sc-Gr fault
   - Sc-Sc fault
   - 3sc-Gr fault
   - Disconnected screen

   Based on the measurement accuracy of the Omicron 356 and the simulation model it was decided that the largest detectable fault, for this project is defined as a fault condition there the deviation between healthy and faulty screen impedance is 5%.

   Simulation results showed that for a simulation frequency of 360Hz, is the largest detectable fault resistance as follows:

- Sc-Gr fault 46Ω
- Sc-Sc fault 55Ω
- 3sc-Gr fault 68Ω

Laboratory tests indicated that a water filed link box could be modeled as a 3sc-Gr fault in the simulation model. The fault resistances between the screens and from screen to ground were measured to $\approx 35\Omega$. Hence water filed link boxes at the FRT-NOR cable line, would be detectable with the impedance method.

At the above listed study cases fault localization is very difficult. Only in case of a very low fault resistance at screen to screen fault and 3sc-Gr fault localization to the first link box was possible. If third link box had been accessible fault location would have been possible. Since this would give the possibility to measure the major section from both ends. The study case were a screen conductor was disconnected showed that the simulated fault resistance is equal to the shunt capacitance of the faulty screen. Hence localization of the fault is possible since the shunt capacitance is proportional to the length of the line. The simulation frequency should be low in respect to the other study cases, due to increase of the capacitive shunt reactance, in the case the frequency was chosen to 50Hz.

3. Cable systems with several major sections
   The final part of this report is dealing with cable systems with several major sections. At least one link box at the end of a major section should be accessible in order to use the impedance method presented in this work. These link boxes should be made easy accessible either by mounting the box on the ground surface or in a well, this will spare time and money when the condition of the screen circuit is evaluated. In case every third link box is made easy accessible a method was presented where all major sections at the line was series connected. In this case a cable line with three major sections were considered. By performing two measurements one in each substation which the line connects, all the link boxes in the cable line can be evaluated. The largest detectable fault resistances for the following study cases were:

   - Sc-Gr fault 462Ω
   - Sc-Sc fault 279Ω
   - 3sc-Gr fault 432Ω

   The detectable fault resistance becomes up to 9 times larger in respect to cable system only consisting of one major section.

   If a fault is detected within the values above, fault localization is possible if the fault resistance, for the different study cases, is less than:

   - Sc-Gr fault 462Ω
   - Sc-Sc fault 190Ω
   - 3sc-Gr fault 260Ω

   It should be note that:

   - Sc-Sc faults with a fault resistance $190\Omega < R_f < 279\Omega$ is only detectable.

- 3sc-Gr faults with a fault resistance $260\Omega < R_f < 432\Omega$ is only detectable.

The conclusion of the initial problem is that the condition of the link boxes in a cross bonded transmission cable system **can** be determined without having physical access to them using the impedance method. Studies of the cable line FRO-NOR, showed that it is possible to detect a water-filled link box.

Based on the work presented in this report it is recommended that minimum one link box at the end of each major section of any given cable line, is easy (permanent) accessible so that the condition of the screen circuit (link boxes) can be determined using the impedance method.

Chapter 10

Future work

As mentioned in the state of the art analysis, the subject of this study has until now, not been given much attention. Therefore this project may be seen as the preliminary work, within the area. Many subjects are therefore still to be considered and some are listed here:

- As mentioned in Measuring Technique, section 5, an excel spread sheet could be used to handle the measuring data. The spread sheet could be programmed to perform the calculation of the apparent impedances directly from the recorded data file, from the measuring equipment. This could largely simplify the data processing and reduce the risk of calculation errors.

- Alternatively the Omicron line impedance measuring equipment could be extended with additional measuring inputs. The coupling between the different screen conductors could be made automatic. Thereby could the recorded data be stored in one exportable file and used in above mentioned excel spread sheet.

- Sc-Gr faults may be studied further in order to determine if the impedance method can detect a shot circuited SVL.

- Sc-Sc fault may be studied further in order to determine if the impedance method can detect a bonding cable fault.

- The DC measuring technique could be further studied in case of cable systems where every third link box is accessible. The star point connection could then be removed and an insulation test could be performed on the cable screens.

- The Travelling wave method could be further analyzed based on the Field test #3 in appendix F and the corresponding measurement results.

- Combining the travelling wave method and the impedance method could be studied in order to improve fault localization. Fault detection by impedance measurements and fault localization by travelling wave measurements.

- As an alternative measuring technique, a surveillance of the charging currents at the cable termination could be studied. A change in the cross bonded screen circuit may lead to changes of

the charging currents. If this measurement could be could be useful, the screen circuit could be measured, while the line is in service.

Bibliography

[1] C.L. Bak C. F. Jensen, U.S. Gudmundsdottir. State of the art analysis of online fault location on ac cables in underground transmission systems. In *Proceedings of the 22nd Nordic Insulation Symposium 2011, NORD-IS'11*, nov. 2011.

[2] Cigré. Special bonding of high voltage power cables, 2005. Working Group B1.18.

[3] I. Daut, S. Hasan, S. Taib, R. Chan, and M. Irwanto. Harmonic content as the indicator of transformer core saturation. In *Power Engineering and Optimization Conference (PEOCO), 2010 4th International*, pages 382 –385, june 2010.

[4] J Lewis Blackburn Thomas J Domin. *Protective Relaying Principles and Applications*. CRC Press Taylor and Francis Group, 3rd edition, 2007.

[5] Omicron electronics GmbH. Cmc 356 reference manual. Provided with the Omicron software. ().

[6] Elektricitetsrådet. *Stærkstrøms bekendtgørelsen for elektriske installationer*. Sikkerhedsstyrelsen, 1st edition, 2001.

[7] Energinet.dk.

[8] Energinet.dk. Kabelhandlingsplan 132-150kV, 2009. (in Danish).

[9] A.L.O. Fernandez and N.K.I. Ghonaim. A novel approach using a firann for fault detection and direction estimation for high-voltage transmission lines. *Power Delivery, IEEE Transactions on*, 17(4):894 – 900, oct 2002.

[10] Gasiorowich Fishbane and Thornton. *Physics for scientists and engineers with modern Physics*. Pearson Prentice Hall, 3rd edition, 2005.

[11] Fluke. Principles, testing methods and applications. `www.newarkinone.thinkhost.com/brands/promos/Earth_Ground_Resistance.pdf`. (Seen on 20-10-2011).

[12] D. Despan J.-P. Rudant A. Bedidi P. Borderies G. Nesti, D. Tarchi and E. Bachelier. Phase shift and decorrelation of radar signal related to soil moisture changes. In *2nd Int. Workshop on Retrieval of Bioand Geo-Physical Parameters from SAR Data for Land Applications*, pages 423 –430, oct. 1998.

[13] DIGSILENT GmbH Germany. Digsilent technical documentation, model description cable modelling, 2005.

[14] K.V. Gouramanis, C.G. Kaloudas, T.A. Papadopoulos, G.K. Papagiannis, and K. Stasinos. Sheath voltage calculations in long medium voltage power cables. In *PowerTech, 2011 IEEE Trondheim*, pages 1 –7, june 2011.

[15] Allan Greenwood. *Electrical transients in power systems*. Wiley, 2st edition, 1991.

[16] Unnur Stella Guðmundsdóttir. *Modelling of long High Voltage AC cables in Transmission Systems*. PhD thesis, Aalborg University, Department of Energy Technology, 2010.

[17] B. Gustavsen. Panel session on data for modeling system transients insulated cables. In *Power Engineering Society Winter Meeting, 2001. IEEE*, volume 2, pages 718 –723 vol.2, 2001.

[18] Peter R. Hansen, 2011. E-mail correspondence with external supervisor from N1.

[19] Erik Hüche. *Digital signal behandling*. Nyt teknisk forlag, 1st edition, 2006.

[20] IEC. 60229 - tests on cable oversheaths which have a special protective function and are applied by extrusion, 1982.

[21] IEC. 60287-1-1 electric cables calculation of the current rating, 1995.

[22] IEC. 60099-4 - metal-oxide surge arresters without gaps for a.c. systems, 2004.

[23] IEEE. Ieee - guide for the application of sheat-bounding methods for single-conductor cables and the calculation of induced voltages and currents an cable sheaths., 1986.

[24] IEEE. Ieee guide for the design and installation of cable systems in substations, 1993.

[25] IEEE. Ieee guide for safety in ac substation grounding, 2000.

[26] IEEE. Ieee guide for determining fault location on ac transmission and distribution lines, 2005.

[27] IEEE. Ieee guide for fault locating techniques on shielded power cable systems, 2007.

[28] Thomas J. Overbye J. Duncan Glover, Mulukutla S. Sarma. *Power system Analysis and design*. Thomson, 4th edition, 2008.

[29] Faria da Silva F. Bak C. L. Jensen, C. F. and W. Wiechowski. Switching studies for the horns rev 2 wind farm main cable. In *Proceedings of the International Conference on Power Systems Transients, IPST 2011*, volume 1, June 2011.

[30] JR. John J. Grainger, William D. Stevenson. *Power system Analysis*. McGraw-Hill, 1th edition, 1994.

[31] A. M. Breipohl K. Sam Shanmugan. *Random Signals Detaction, Estimation and Data Analysis*. John Wiley and Sons, Inc., 1st edition, 1988.

[32] Erwin Kreyszig. *Advanced Engineering mathematics*. Wiley, 9th edition, 2006.

[33] K. Lahti, K. Kannus, and K. Nousiainen. Diagnostic methods in revealing internal moisture in polymer housed metal oxide surge arresters. *Power Delivery, IEEE Transactions on*, 17(4):951 – 956, oct 2002.

[34] Minghua Li, Bingyin Xu, and Zhang Yan. A novel sheath fault location method for high voltage power cable. In *Properties and Applications of Dielectric Materials, 2003. Proceedings of the 7th International Conference on*, volume 1, pages 195 – 198 vol.1, june 2003.

[35] N1. Mødereferat 163, elteknikermøde d. 3. og 4. marts, 2010. (in Danish).

[36] Syed A. Nasar. *Electric power systems*. Mc Graw Hill, 1st edition, 1990.

[37] Nexans. Final documentation report, sysem a, substation nors to substation frøstrup, 2012.

[38] P. Nichols, D. Woodhouse, and J. Yarnold. The effects of earth potential rise on surge arrester specification in specially bonded cable systems. In *Power Engineering Conference, 2008. AUPEC '08. Australasian Universities*, pages 1 –6, dec. 2008.

[39] P. Nichols and J. Yarnold. The effect of an underground to overhead transition point on the specification of sheath voltage limiters in underground networks. In *Power Engineering Conference, 2009. AUPEC 2009. Australasian Universities*, pages 1 –6, sept. 2009.

[40] P. Nichols and J. Yarnold. A sensitivity analysis of cable parameters and their influence on design choices for minimum sheath voltage limiter specification in underground cable systems. In *Power Engineering Conference, 2009. AUPEC 2009. Australasian Universities*, pages 1 –6, sept. 2009.

[41] Haiqing Niu, Xin Zhou, Zhang Yao, Xiaobing Wang, Yinxia Shi, and Yuxiang Xu. Parameter analysis and research on sheath lightning overvoltage of single-core cable. In *Power and Energy Engineering Conference, 2009. APPEEC 2009. Asia-Pacific*, pages 1 –4, march 2009.

[42] Daníel Leó Ólason, Bjarni Helgi Thorsteinsson, Kenneth Rønsig Kanstrup, Kasper Schultz Pedersen, Morten Thule Hansen, and Thomas Ebdrub. *Overvoltages when de energizing 150kV combined cable/overheadline with connected shunt reactor*. Aalborg University, Department of Energy Technology, 2010.

[43] PACAD. Applications of pscad / emtdc, 2008. Manitoba HVDC Research Centre Inc. 244 Cree Crescent, Winnipeg, Manitoba R3J 3W1 Canada.

[44] B. Parmigiani, D. Quaggia, E. Elli, and S. Franchina. Zinc oxide sheath voltage limiter for hv and ehv power cable: Field experience and laboratory tests. *Power Delivery, IEEE Transactions on*, 1(1):164 –170, jan. 1986.

[45] E. F. Peschke and R. von Olshausen. *Cable systems for High and extra-high voltage*. Publicis MCD Verlag, Erlangen and Munich, 3rd*skal tjekkes* edition, 1999.

[46] Alexander Sadiku. *Fundamentals of electric circuits*. McGraw Hill, 3rd edition, 2007.

[47] Wang Shaowu, Liang Xidong, and Huang Lengceng. Experimental study on the pollution flashover mechanism of polymer insulators. In *Power Engineering Society Winter Meeting, 2000. IEEE*, volume 4, pages 2830 –2833 vol.4, 2000.

[48] Tektronix. Data sheet. `http://www.tek.com/datasheet/mixed-signal-oscilloscopes-9`. (Seen on 16-05-2012).

[49] Tektronix. Data sheet. `http://www.tek.com/datasheet/mixed-signal-oscilloscopes-11`. (Seen on 16-05-2012).

[50] William A. Thue. *Electrical Power cable engineering*. Marcel Dekker Inc, 2nd edition, 2003.

[51] C. Bak U. Gudmundsdottir, B. Gustavsen and W. Wiechowski. Field test and simulation of a 400 kv crossbonded cable system. In *IEEE Transactions on Power Delivery*, pages 1 –8, 2010.

[52] Voltech. Pm3000ace universal power analyser. VPN 86-264/3. ().

[53] S. Vørts. *Elektriske fordelingsanlæg*. Polyteknisk forlag, 3rd edition, 1990.

[54] Gerhard Ziegler. *Numerical Distance Protection*. Publicis Corporate Publishing, Erlanger, 3rd edition, 2008.

Appendix

Appendix A

Impedance calculation of screen to screen fault

This appendix show how the apparent screen impedance Z_a, Z_b and Z_c, from the three phase screen circuit in section 3.4.2, are calculated.

In figure A.1 vectors are denoted with boldfaced letters. Subscript letters denotes screen *a*, *b* or *c*. The subscript number $1-3$ denotes the section. Where first section is between the measuring point and first link box, second section is between first and second link box and the third section is between the second and third link box.

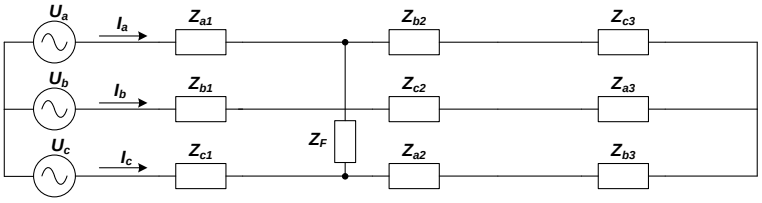

Figure A.1: Equivalent screen circuit of a major section.

The used section impedances are from the DIgSILENT simulation results shown in tabular 3.3. For this calculation the impedances for each section are considered equal to $1/3$ of screen a:

$$\mathbf{Z_{a1-3}} = \mathbf{Z_{b1-3}} = \mathbf{Z_{c1-3}} = \frac{1}{3}\left(|\mathbf{Z_a}|\angle\phi_a\right) = 0.265\angle 44.23\Omega \tag{A.1}$$

The phase voltages have the following magnitudes and angles:

$$\begin{array}{rcrcl} \mathbf{U_a} & = & |\mathbf{U_a}|\angle\phi_a & = & 1\angle 0 \\ \mathbf{U_b} & = & |\mathbf{U_b}|\angle\phi_b & = & 1\angle -120 \\ \mathbf{U_c} & = & |\mathbf{U_c}|\angle\phi_c & = & 1\angle 120 \end{array} \quad [\mathrm{V}] \tag{A.2}$$

The screen circuit in figure A.1 is simplified to the screen circuit shown in figure A.2.

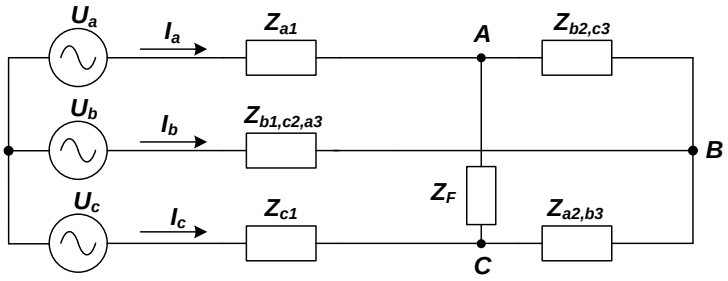

Figure A.2: Simplified equivalent screen circuit of a major section.

Where:

$$\begin{aligned} \mathbf{Z_{b2,c3}} &= \mathbf{Z_{b2}} + \mathbf{Z_{c3}} &&= 0.531\angle 44.23 \\ \mathbf{Z_{a2,b3}} &= \mathbf{Z_{a2}} + \mathbf{Z_{b3}} &&= 0.531\angle 44.23 \\ \mathbf{Z_{b1,c2,a3}} &= \mathbf{Z_{b1}} + \mathbf{Z_{c2}} + \mathbf{Z_{a3}} &&= 0.796\angle 44.23 \end{aligned} \quad [\Omega] \quad \text{(A.3)}$$

The delta connection between point A,B and C in figure A.2 is transformed to a star connection as shown in figure A.3, using equation A.5 [46, p. 392].

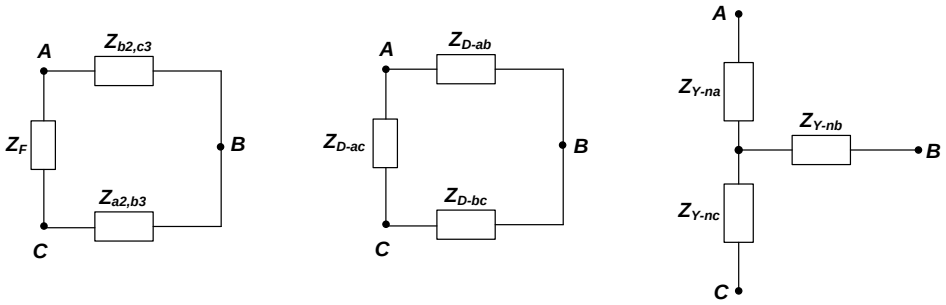

Figure A.3: Delta to star transformation.

Where:

$$\begin{aligned} \mathbf{Z_{b2,c3}} &= \mathbf{Z_{D-ab}} \\ \mathbf{Z_{a2,b3}} &= \mathbf{Z_{D-bc}} \\ \mathbf{Z_F} &= \mathbf{Z_{D-ac}} \end{aligned} \quad [\Omega] \quad \text{(A.4)}$$

$$\begin{aligned} \mathbf{Z_{Y-an}} &= \frac{\mathbf{Z_{D-ac}} \cdot \mathbf{Z_{D-ab}}}{\mathbf{Z_{D-ac}} + \mathbf{Z_{D-ab}} + \mathbf{Z_{D-bc}}} &&= 0.415\angle 33.12 \\ \mathbf{Z_{Y-cn}} &= \frac{\mathbf{Z_{D-ac}} \cdot \mathbf{Z_{D-bc}}}{\mathbf{Z_{D-ac}} + \mathbf{Z_{D-ab}} + \mathbf{Z_{D-bc}}} &&= 0.415\angle 33.12 \\ \mathbf{Z_{Y-bn}} &= \frac{\mathbf{Z_{D-ab}} \cdot \mathbf{Z_{D-bc}}}{\mathbf{Z_{D-ac}} + \mathbf{Z_{D-ab}} + \mathbf{Z_{D-bc}}} &&= 0.074\angle 77.35 \end{aligned} \quad [\Omega] \quad \text{(A.5)}$$

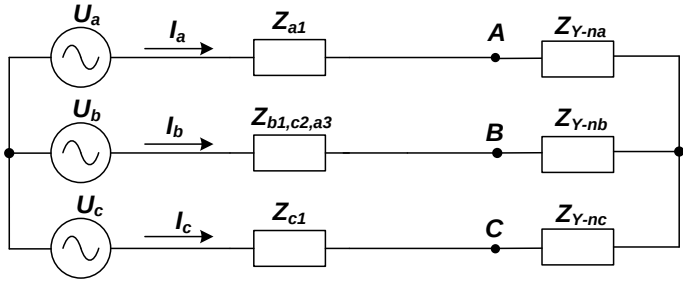

Figure A.4: Equivalent screen circuit with star transformed impedances.

The circuit in figure A.4 is simplified. The new circuit is shown in figure A.5.

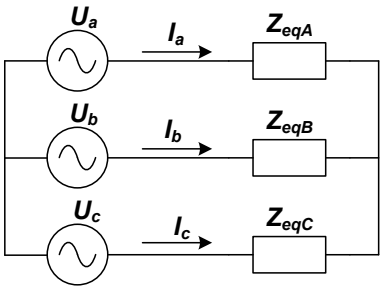

Figure A.5: Screen circuit with equivalent screen impedances.

Where the equivalent screen impedances:

$$\begin{array}{rcrcl} \mathbf{Z_{eqA}} & = & \mathbf{Z_{a1}} + \mathbf{Z_{Y-na}} & = & 0.678\angle 37.41 \\ \mathbf{Z_{eqB}} & = & \mathbf{Z_{b1,c2,a3}} + \mathbf{Z_{Y-nb}} & = & 0.859\angle 46.93 \\ \mathbf{Z_{eqC}} & = & \mathbf{Z_{c1}} + \mathbf{Z_{Y-nc}} & = & 0.678\angle 37.41 \end{array} \quad [\Omega] \quad \text{(A.6)}$$

The three unbalanced screen current $\mathbf{I_a}$,$\mathbf{I_b}$ and $\mathbf{I_c}$ are calculated using the superposition Theorem [46, p. 421]. Superposition Theorem is to short circuit two of the three voltage sources and calculate all currents in the circuits, this procedure is repeated for each screen as shown in figure E.20(a)-E.20(c).

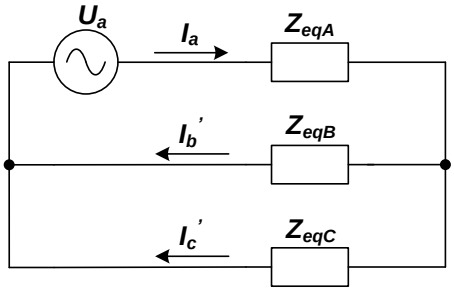

Figure A.6: screen voltage b and c is short circuited.

Where:

$$\begin{aligned} \mathbf{I_a} &= \frac{\mathbf{U_a}}{\mathbf{Z_{eqA}}+\left(\mathbf{Z_{eqB}}||\mathbf{Z_{eqC}}\right)} = 0.946\angle -38.96 \\ \mathbf{I_b'} &= \mathbf{I_a}\cdot\frac{\mathbf{Z_{eqC}}}{\mathbf{Z_{eqB}}+\mathbf{Z_{eqC}}} = 0.419\angle -44.23 \\ \mathbf{I_c'} &= \mathbf{I_a}\cdot\frac{\mathbf{Z_{eqB}}}{\mathbf{Z_{eqB}}+\mathbf{Z_{eqC}}} = 0.531\angle -34.43 \end{aligned} \quad [\mathrm{A}] \quad (A.7)$$

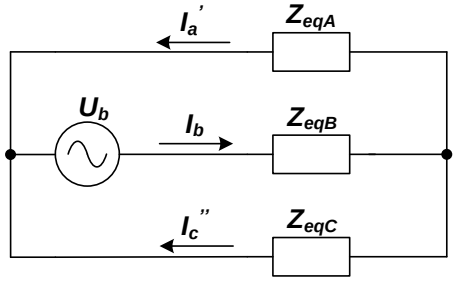

Figure A.7: screen voltage a and c is short circuited.

Where:

$$\begin{aligned} \mathbf{I_b} &= \frac{\mathbf{U_b}}{\mathbf{Z_{eqB}}+\left(\mathbf{Z_{eqA}}||\mathbf{Z_{eqC}}\right)} = 0.838\angle -164.27 \\ \mathbf{I_a'} &= \mathbf{I_b}\cdot\frac{\mathbf{Z_{eqC}}}{\mathbf{Z_{eqA}}+\mathbf{Z_{eqC}}} = 0.419\angle -164.27 \\ \mathbf{I_c''} &= \mathbf{I_b}\cdot\frac{\mathbf{Z_{eqA}}}{\mathbf{Z_{eqA}}+\mathbf{Z_{eqC}}} = 0.4188\angle -164.27 \end{aligned} \quad [\mathrm{A}] \quad (A.8)$$

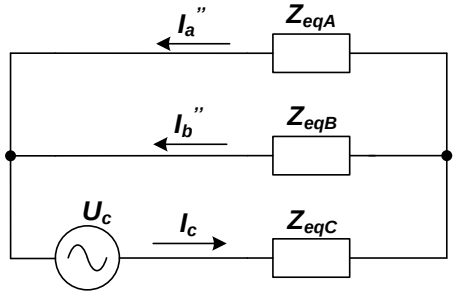

Figure A.8: screen voltage a and b is short circuited.

Where:

$$\begin{aligned} \mathbf{I_c} &= \frac{\mathbf{U_c}}{\mathbf{Z_{eqB}}+\left(\mathbf{Z_{eqA}}||\mathbf{Z_{eqB}}\right)} = 0.946\angle 81.07 \\ \mathbf{I_a''} &= \mathbf{I_c}\cdot\frac{\mathbf{Z_{eqB}}}{\mathbf{Z_{eqA}}+\mathbf{Z_{eqB}}} = 0.531\angle 85.26 \\ \mathbf{I_b''} &= \mathbf{I_c}\cdot\frac{\mathbf{Z_{eqA}}}{\mathbf{Z_{eqA}}+\mathbf{Z_{eqB}}} = 0.419\angle 75.75 \end{aligned} \quad [\mathrm{A}] \quad (A.9)$$

The total screen current is then calculated by adding the three screen current, from the superposition calculation. As seen the in equation A.10 the screen currents are unbalanced whereas the screen voltages are balanced.

$$\begin{array}{rcl} \mathbf{I_{a,tot}} & = & \mathbf{I_a} - \mathbf{I_a^{'}} - \mathbf{I_a^{''}} \quad = \quad 1.490\angle -42.69 \\ \mathbf{I_{b,tot}} & = & \mathbf{I_b} - \mathbf{I_b^{'}} - \mathbf{I_b^{''}} \quad = \quad 1.256\angle -164.27 \\ \mathbf{I_{c,tot}} & = & \mathbf{I_c} - \mathbf{I_c^{'}} - \mathbf{I_c^{''}} \quad = \quad 1.356\angle 85.12 \end{array} \quad [\mathrm{A}] \quad \text{(A.10)}$$

The three apparent screen impedances Z_A,Z_B and Z_C can now be calculated.

$$\begin{array}{rcl} \mathbf{Z_A} & = & \frac{\mathbf{U_a}}{\mathbf{I_{a,tot}}} \quad = \quad 0.672\angle 42.69 \\ \mathbf{Z_B} & = & \frac{\mathbf{U_b}}{\mathbf{I_{b,tot}}} \quad = \quad 0.796\angle 44.23 \\ \mathbf{Z_C} & = & \frac{\mathbf{U_c}}{\mathbf{I_{c,tot}}} \quad = \quad 0.738\angle 34.84 \end{array} \quad [\Omega] \quad \text{(A.11)}$$

Using the apparent screen impedances the circuit appear as in figure A.9.

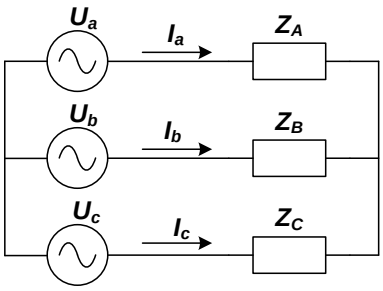

Figure A.9: Screen circuit, expressed with apparent screen impedances.

The impedances are further used in section 3.4.2.

Appendix B

Impedance calculation of screen to ground fault

This appendix show how the apparent screen impedance Z_a, Z_b and Z_c, from the three phase circuit in section 3.4.2, are calculated. The circuit is shown in figure B.1.
In the figure vectors are denoted with boldfaced letters. Subscript letters denotes screen a, b or c. The subscript number $1-3$ denotes the section. Where first section is between the measuring point and first link box, second section is between first and second link box and the third section is between the second and third link box.

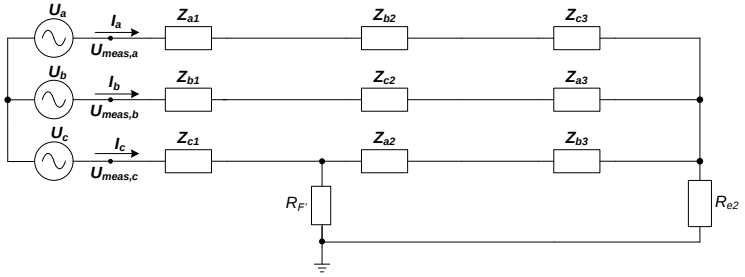

Figure B.1: Screen circuit one major section. Ground fault in the first link box, earth impedance neglected.

The used section impedances are from the DIgSILENT simulation results shown in tabular 3.3. For this calculation the impedances for each section are considered equal to $1/3$ of screen a:

$$\mathbf{Z_{a1-3}} = \mathbf{Z_{b1-3}} = \mathbf{Z_{c1-3}} = \frac{1}{3}\left(|\mathbf{Z_a}|\angle\phi_a\right) = 0.265\angle 44.23\Omega \tag{B.1}$$

The screen voltages have the following magnitudes and angles:

$$\begin{array}{rcrcr} \mathbf{U_a} & = & |\mathbf{U_a}|\angle\phi_a & = & 1\angle 0 \\ \mathbf{U_b} & = & |\mathbf{U_b}|\angle\phi_b & = & 1\angle -120 \\ \mathbf{U_c} & = & |\mathbf{U_c}|\angle\phi_c & = & 1\angle 120 \end{array} \quad [\mathrm{V}] \tag{B.2}$$

The aim of this calculation is to determine the apparent screen impedances, which is defined as the voltage at the measuring points $U_{meas,a}$, $U_{meas,b}$ and $U_{meas,c}$ in relation to ground, divided by the current at the same point I_a, I_b and I_c.

The screen circuit in figure 3.54 is simplified by adding series connected impedances and shown again in figure B.2.

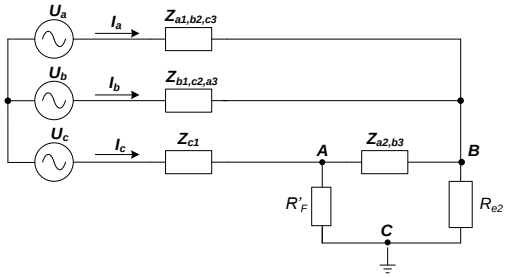

Figure B.2: Simplified screen circuit of one major section.

From figure B.2 it can be seen that the two resistances $R_{F'}$ and R_{e2} together with the impedance $Z_{a2,b3}$ forms a delta connection between the points A, B and C. The delta connection is transformed to a star connection in figure B.3, using equation B.4 [46, p.392].

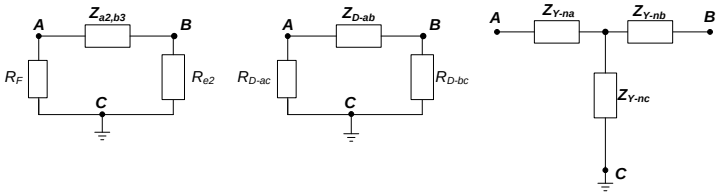

Figure B.3: Delta to star transformation.

Where:

$$\begin{aligned} \mathbf{Z_{a2,b3}} &= \mathbf{Z_{D-ab}} \\ \mathbf{R_F} &= \mathbf{Z_{D-ac}} \\ \mathbf{R_{e2}} &= \mathbf{Z_{D-bc}} \end{aligned} \quad [\Omega] \quad \text{(B.3)}$$

$$\begin{aligned} \mathbf{Z_{Y-an}} &= \frac{\mathbf{Z_{D-ac}} \cdot \mathbf{Z_{D-ab}}}{\mathbf{Z_{D-ac}} + \mathbf{Z_{D-ab}} + \mathbf{Z_{D-bc}}} = 0.260\angle 43.20 \\ \mathbf{Z_{Y-bn}} &= \frac{\mathbf{Z_{D-ab}} \cdot \mathbf{Z_{D-bc}}}{\mathbf{Z_{D-ac}} + \mathbf{Z_{D-ab}} + \mathbf{Z_{D-bc}}} = 0.260\angle 43.20 \\ \mathbf{Z_{Y-cn}} &= \frac{\mathbf{Z_{D-ac}} \cdot \mathbf{Z_{D-bc}}}{\mathbf{Z_{D-ac}} + \mathbf{Z_{D-ab}} + \mathbf{Z_{D-bc}}} = 4.906\angle -1.03 \end{aligned} \quad [\Omega] \quad \text{(B.4)}$$

After the delta to star transformation the circuit appear as shown in figure B.4.

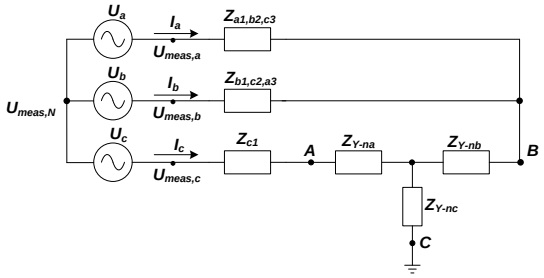

Figure B.4: Equivalent screen circuit, after transformation from delta to star connection.

Now the equivalent screen impedances Z_{eqA}, Z_{eqB} and Z_{eqC} can be determined by addition, using equation B.5.

$$\begin{array}{lcccl} \mathbf{Z_{eqA}} & = & \mathbf{Z_{a1,b2,c3}} & = & 0.796\angle 44.23 \\ \mathbf{Z_{eqB}} & = & \mathbf{Z_{b1,c2,a3}} & = & 0.796\angle 44.23 \\ \mathbf{Z_{eqC}} & = & \mathbf{Z_{c1}+Z_{Y-na}+Z_{Y-nb}} & = & 0.786\angle 43.54 \end{array} \quad [\Omega] \quad \text{(B.5)}$$

Using the equivalent screen impedances, the circuit may look like figure B.5.

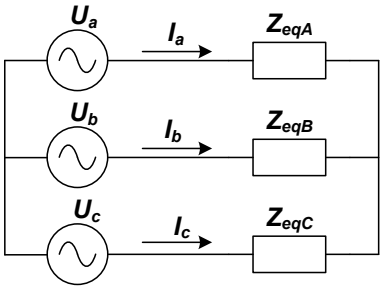

Figure B.5: Screen circuit with equivalent screen impedances.

The next step is to determine the screen currents $\mathbf{I_a}$,$\mathbf{I_b}$ and $\mathbf{I_c}$, this is done using superposition [46, p. 421]. The voltages source are short circuited one by one, and each screen current determined. By addition the resulting screen currents are determined. The three circuits used for super position in shown in figure B.6-B.8.

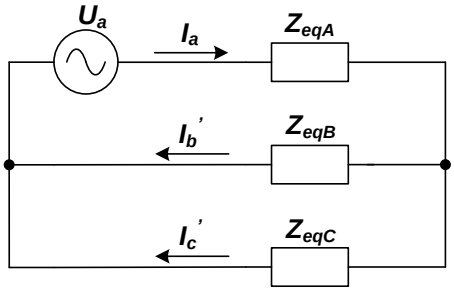

Figure B.6: screen voltage b and c is short circuited.

Where:

$$\begin{aligned} \mathbf{I_a} &= \frac{\mathbf{U_a}}{\mathbf{Z_{eqA}}+\left(\mathbf{Z_{eqB}}||\mathbf{Z_{eqC}}\right)} &= 0.839\angle -44.12 \\ \mathbf{I_b'} &= \mathbf{I_a}\cdot\frac{\mathbf{Z_{eqC}}}{\mathbf{Z_{eqB}}+\mathbf{Z_{eqC}}} &= 0.417\angle -44.46 \\ \mathbf{I_c'} &= \mathbf{I_a}\cdot\frac{\mathbf{Z_{eqB}}}{\mathbf{Z_{eqB}}+\mathbf{Z_{eqC}}} &= 0.422\angle -43.77 \end{aligned} \quad [\mathrm{A}] \quad \text{(B.6)}$$

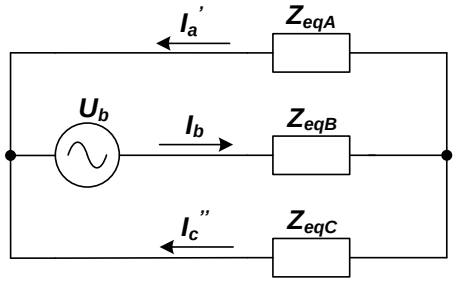

Figure B.7: screen voltage a and c is short circuited.

Where:

$$\begin{aligned} \mathbf{I_b} &= \frac{\mathbf{U_b}}{\mathbf{Z_{eqB}}+\left(\mathbf{Z_{eqA}}||\mathbf{Z_{eqC}}\right)} &= 0.417\angle -164.50 \\ \mathbf{I_a'} &= \mathbf{I_b}\cdot\frac{\mathbf{Z_{eqC}}}{\mathbf{Z_{eqA}}+\mathbf{Z_{eqC}}} &= 0.839\angle -164.15 \\ \mathbf{I_c''} &= \mathbf{I_b}\cdot\frac{\mathbf{Z_{eqA}}}{\mathbf{Z_{eqA}}+\mathbf{Z_{eqC}}} &= 0.422\angle -163.81 \end{aligned} \quad [\mathrm{A}] \quad \text{(B.7)}$$

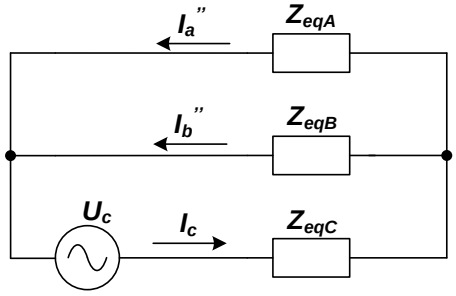

Figure B.8: screen voltage a and b is short circuited.

Where:

$$\begin{aligned} \mathbf{I_c} &= \frac{\mathbf{U_c}}{\mathbf{Z_{eqB}}+\left(\mathbf{Z_{eqA}}||\mathbf{Z_{eqB}}\right)} &= 0.8446\angle 76.20 \\ \mathbf{I_a''} &= \mathbf{I_c}\cdot\frac{\mathbf{Z_{eqB}}}{\mathbf{Z_{eqA}}+\mathbf{Z_{eqB}}} &= 0.422\angle 76.20 \\ \mathbf{I_b''} &= \mathbf{I_c}\cdot\frac{\mathbf{Z_{eqA}}}{\mathbf{Z_{eqA}}+\mathbf{Z_{eqB}}} &= 0.422\angle 76.20 \end{aligned} \quad [\mathrm{A}] \quad \text{(B.8)}$$

The total screen current is then calculated by adding the three screen current, from the superposition calculation.

$$\begin{array}{rcl} \mathbf{I_{a,tot}} = \mathbf{I_a} - \mathbf{I_a'} - \mathbf{I_a''} = 1.2633\angle -44.35 \\ \mathbf{I_{b,tot}} = \mathbf{I_b} - \mathbf{I_b'} - \mathbf{I_b''} = 1.255\angle -163.92 \\ \mathbf{I_{c,tot}} = \mathbf{I_c} - \mathbf{I_c'} - \mathbf{I_c''} = 1.267\angle 76.20 \end{array} \quad [\text{A}] \quad \text{(B.9)}$$

The next step is to determine the voltage at the star point, where the three voltage sources are connected. It is assumed that no current flow through Z_{Y-nc}, and the voltage is equal on both sides. From these considerations the voltage at the star point may be determined by equation B.10.

$$\mathbf{U_{meas,N}} = \mathbf{I_c}(\mathbf{Z_{Y-na}} + \mathbf{Z_{c1}}) - \mathbf{U_c} = 0.334\angle -59.87 \quad [\text{V}] \quad \text{(B.10)}$$

Now the voltages at the measuring points can be determined. This is done by adding the voltage source to the voltage at point $\mathbf{U_{meas,N}}$:

$$\begin{array}{rcl} \mathbf{U_{meas,A}} = \mathbf{U_{meas,N}} + \mathbf{U_A} = 1.203\angle -13.92 \\ \mathbf{U_{meas,B}} = \mathbf{U_{meas,N}} + \mathbf{U_B} = 1.202\angle -106.05 \\ \mathbf{U_{meas,C}} = \mathbf{U_{meas,N}} + \mathbf{U_C} = 0.666\angle 119.92 \end{array} \quad [\text{V}] \quad \text{(B.11)}$$

The three apparent screen impedances Z_A, Z_B and Z_C can now be calculated.

$$\begin{array}{rcl} \mathbf{Z_A} = \frac{\mathbf{U_{meas,A}}}{\mathbf{I_{a,tot}}} = 0.952\angle 30.42 \\ \mathbf{Z_B} = \frac{\mathbf{U_{meas,B}}}{\mathbf{I_{b,tot}}} = 0.958\angle 57.35 \\ \mathbf{Z_C} = \frac{\mathbf{U_{meas,C}}}{\mathbf{I_{c,tot}}} = 0.526\angle 43.72 \end{array} \quad [\Omega] \quad \text{(B.12)}$$

Using the apparent screen impedances the circuit appear as in figure B.9.

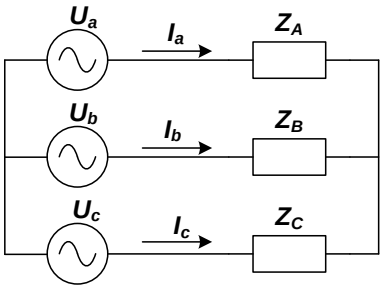

Figure B.9: Screen circuit, expressed with apparent screen impedances.

The impedances are further used in section 3.4.2.

Appendix C

DIgSILENT simulation model

This appendix include information about the DIgSILENT model of the FRT-NOR cable line and a cable model used in the problem analysis.

C.1 Model of the FRT-NOR cable line

Modelling of the FRT-NOR cable line is based on the parameters given in the system description.

C.1.1 Parameter determination

The following parameters are required in order to set up the cable model in DIgSILENT:

1 Conductor resistivity, DC resistance and thickness(radius)
2 Inner semi conductive layer relative permittivity and thickness
3 Insulation relative permittivity and thickness
4 Outer semi conductive layer relative permittivity and thickness
5 Sheath resistivity, DC resistance and thickness
6 Outer insulation relative permittivity and thickness.

Beside the above listed parameters the model also require the geometry of the cable system. Figure C.1 shown a cross section view of the actual cable and the layers that is modelled in DIgSILENT.

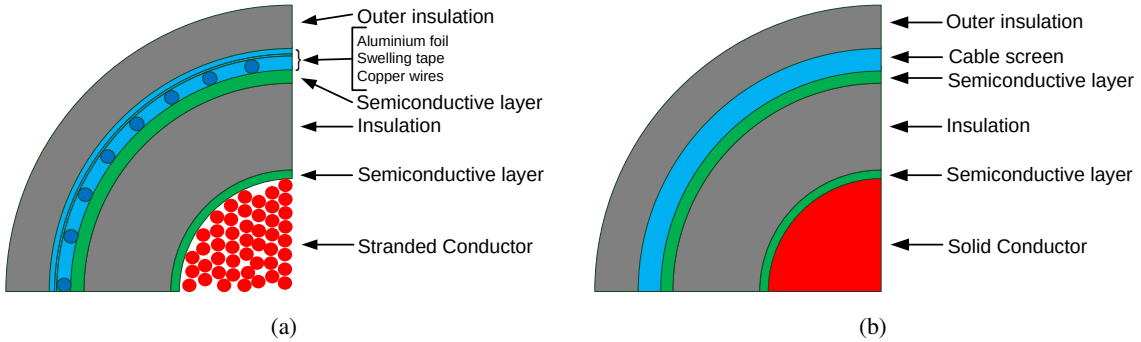

Figure C.1: Cross section view of the coaxial cable. (a) Shows the actual cable. (b) Shows the layers which are modelled in DIgSILENT.

From figure C.1 it may be seen that the model differs from the actual cable by the number of layers and the structure of several layers. The differences are taken into consideration by adjusting the model parameters. The determination of the model parameters are explained in the following.

1 The conductor of the actual cable is made of stranded aluminium wires as describes in section 2. For the DIgSILENT model the conductor may be modelled as a solid or hollow conductor and not stranded. For this thesis it is chosen to model the conductor as a solid conductor see C.2.

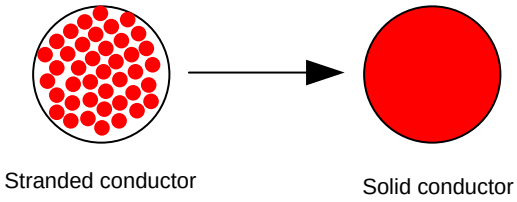

Figure C.2: The actual stranded conductor is modelled as a solid conductor, with corresponding DC resistance.

For DIgSILENT modelling there are two ways to model a stranded conductor as a solid conductor, by using a filling factor or DC resistance of the conductor. For this thesis the last method is used and the DC resistance R_{DC} is calculated.
First the resistance R_0 is calculated for a cable length l of 1000m from the resistivity and the cross section by equation C.1. The resistance R_0 is then adjusted according to the temperature of the cable system. The temperature corrected resistance R_{DC} is calculated using equation C.2.

$$R_0 = \frac{\rho_{Al} \cdot l}{A} = \frac{2.826 \cdot 10^{-8} \cdot 1000}{1200 \cdot 10^{-6}} = 23.55^{\mathrm{m\Omega}/\mathrm{km}} \tag{C.1}$$

Where:
ρ_{Al} is the resistivity of Aluminium $2.826 \cdot 10^{-8}\Omega$m [21, p.61]
A is the effective cross section of the conductor.

The resistance R_0 is adjusted to a ground temperature of $5°C$ according to the system description. R_{DC} is calculated by equation C.2. In case has line has been in service before the measurements are performed, the resistance should be corrected for operating temperature. Measurements made for this project are made before the line is taken into service for the first time and thereby the cables are at ground temperature.

$$R_{DC} = R_0 \cdot (1 + \alpha_{Al-20}(\theta - 20)) \quad [\Omega] \tag{C.2}$$

$$R_{DC} = 0.02355 \cdot (1 + 4.03 \cdot 10^{-3}(5 - 20)) = 22.13^{\mathrm{m\Omega}/\mathrm{km}} \tag{C.3}$$

Where:
α_{Al-20} is the temperature coefficient for Aluminium $4.03 \cdot 10^{-3}\Omega$m [21, p.61]
θ is the actual temperature of the cable, ($5^{\circ}C$) as described in the system description.

2 In DIgSILENT it is possible to model the semi conductive layers as independent layer. Therefore these should not be included in the isolation layer, as were common practice for the previous versions of the simulation software [51]. According to the data sheet the inner semi conductive layer is 1mm thick. The conductivity of the semi conductive layers are much lower than both the conductor and the screen [16, p.35]. Therefore the resistivity is set to 10^6 which is $\approx 3.5 \cdot 10^5$ times larger than the resistivity of the conductor and also the default value for the simulation model.
The semi conductors may not be neglected according to the isolation property, this is due to the relative permeability (ε_{r-semi}) which is in the order of 1000 due to a high carbon content. Hence the relative permittivity of 1000 is much higher then that of the insulation $\varepsilon_{r-XLPE} = 2.5$ [17] [21].

3 The insulation is made of XLPE as described in section 2. The thickness of the insulation is 16mm from table 2.1. The permeability of XLPE for this voltage rate is 2.5 [21, p.65]. The di-electric loss angle of the insulation is 0.001 according to [21, p.65].

4 The outer semi conductive layer has identical electrical properties as the inner semi conductive layer. Therefore the relative permittivity ε_{r-semi} is modelled as 1000 according to [17]. The resistivity is, as the inner semi conductive layer set to 10^6. The thickness are 2.1mm according to table 2.1 in the system description.

5 As explained in the system description in section 2 and shown in figure C.3(a) the cable is provided with both a copper wired screen and a aluminium foil separated with a thin layer of semi conductive swelling tape. The copper wired screen and the aluminium foil are directly connected together both at each junction and cable ends and are therefore normally considered as a single equivalent conducting layer for cable modelling [16, p.36]. The screen layers of the actual cable and the modelled screen layers are shown in figure C.3.

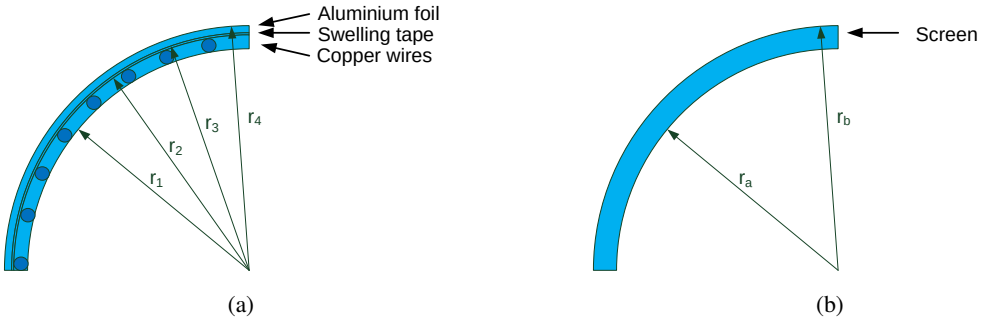

Figure C.3: Cross section view of the screen of the coaxial cable. (a) Shows the layers of the actual cable screen. (b) Shows the layers which may be modelled in the DIgSILENT.

For determination of the screen resistance, the copper wires and the aluminium foil are considered individual. The copper wires may be considered in several ways. For EMT-based software it is common practice to model the screen as a tubular layer with a thickness equal to the diameter of the copper wires and the resistivity is set to twice the resistivity of copper, to compensate for the gab between the wires[16],[17].

Another approach proposed by the author of [29] is based on the same technique as used for the stranded conductor. Using this technique the copper wires are modelled as a tubular layer with a

thickness equal to the diameter of the copper wires. The resistivity of the tubular layer is reduced to have electrical properties as the actual copper screen.

The cable screen is modelled according to the same method as for the conductor. Therefore the DC resistance of the screen is determined. This is done by considering the copper wires and the aluminium foil individual. The copper screen consist of 95mm^2 copper, which resistance for a length l of 1000m is determined by equation C.4.

$$R_{0-sc.Cu} = \frac{\rho_{Cu} \cdot l}{A} = \frac{1.7241 \cdot 10^{-8} \cdot 1000}{95 \cdot 10^{-6}} = 181.5^{\mathrm{m\Omega}/\mathrm{km}} \tag{C.4}$$

The resistivity of copper ρ_{Cu} is $1.7241 \cdot 10^{-8}$ [21, p.61]. The DC resistance $R_{0-sc.Cu}$ is adjusted for a temperature of $5°C$ using equation C.5, where the temperature coefficient for copper α_{Cu-20} is $3.93 \cdot 10^{-3}$ according to [21, p.61].

$$R_{DC-sc.Cu} = R_{0-sc.Al} \cdot (1 + \alpha_{Cu-20}(\theta - 20)) \quad [\Omega] \tag{C.5}$$

$$R_{DC-sc.Cu} = 0.1815 \cdot (1 + 3.93 \cdot 10^{-3}(5 - 20)) = 170.8^{\mathrm{m\Omega}/\mathrm{km}} \tag{C.6}$$

After the resistivity of the copper screen is determined the aluminium foil is considered.

The resistance of the aluminium foil is calculated from the cross section area and the resistivity of the material. The cross section area is calculated from the inner and outer radius of the aluminium foil $A_{Al} = (r_4^2 - r_3^2)\pi = (41.69^2 - 41.49^2)\pi = 52.26\mathrm{mm}^2$ see figure C.3. The resistivity of aluminium is $2.826 \cdot 10^{-8}\Omega$m [21, p.61]. The resistance of the aluminium foil $R_{0-sc.Al}$ is also determined for a length l of 1000m by equation C.7.

$$R_{0-sc.Al} = \frac{\rho_{Al} \cdot l}{A} = \frac{2.826 \cdot 10^{-8} \cdot 1000}{52.26 \cdot 10^{-6}} = 540.8^{\mathrm{m\Omega}/\mathrm{km}} \tag{C.7}$$

The DC resistance of the aluminium foil is adjusted for a temperature of $5°C$, according to the system description, using equation C.8.

$$R_{DC-sc.Al} = R_{0-sc.Al} \cdot (1 + \alpha_{Al-20}(\theta - 20)) \quad [\Omega] \tag{C.8}$$

$$R_{DC-sc.Al} = 0.5408 \cdot (1 + 4.03 \cdot 10^{-3}(5 - 20)) = 508.1^{\mathrm{m\Omega}/\mathrm{km}} \tag{C.9}$$

The total screen DC resistance is determined as a parallel connection of the copper and the aluminium resistance by equation C.10.

$$R_{DC-screen} = \frac{R_{DC-sc.Cu} \cdot R_{DC-sc.Al}}{R_{DC-sc.Cu} + R_{DC-sc.Al}} = \frac{0.1708 \cdot 0.5081}{0.1708 + 0.5081} = 127.8^{\mathrm{m\Omega}}/_{\mathrm{km}} \quad \text{(C.10)}$$

Beside the DC resistance the model also require the thickness of the screen. This is determined as the diameter of the copper wires summed with the thickness if the aluminium foil see equation C.11.

$$Th_{screen} = d_{Cu} + Th_{Al} = 1.39 + 0.2 = 1.59\mathrm{mm} \quad \text{(C.11)}$$

Where:
Th_{screen} is the total modelled screen thickness
d_{Cu} is the diameter of the copper wires
Th_{Al} is the thickness of the aluminium foil.

6 The outer most layer is the outer covering. This is made of PE which has a relative permittivity ε_{r-Oins} of 2.3 and a di electric loss angle of 0.001 according to [21, p.65] and a thickness of 3.8mm according to the system description in section 2.

Input parameters for the DIgSILENT model may be found in table C.1.

Layer	Parameter	Value
Conductor	Thickness	21mm
	DC resistance at $5°C$	$22.13^{\mathrm{m\Omega}}/_{\mathrm{km}}$
Inner semi conductive layer	Thickness	1.0mm
	Relative permittivity(ε_{r-semi})	1000
Insulation	Thickness	16.0mm
	Relative permittivity(ε_{r-ins})	2.5
Outer semi conductive layer	Thickness	2.1mm
	Relative permittivity(ε_{r-semi})	1000
Screen	Thickness	1.59mm
	DC resistance at $5°C$	$127.8^{\mathrm{m\Omega}}/_{\mathrm{km}}$
Outer covering	Thickness	3.8mm
	Relative permittivity(ε_{O-ins})	2.3

Table C.1: Input parameters for the DIgSILENT model.

Later in the project the routine test of the exact cable became available. From this the measured screen resistance is provided. The routine test stated the value: $0.145^{\Omega}/_{\mathrm{km}}$ at $20°C$. The resistance is corrected for a cable temperature of $5°C$ by equation C.12.

$$R_{DC} = R_0 \cdot (1 + \alpha(\theta - 20)) \quad [\Omega] \quad \text{(C.12)}$$

The screen consist of both copper and aluminium for which the temperature correction coefficients are different. By using both it was found that the DC resistance only differs by $\approx 0.2 ^{\mathrm{m}\Omega}/_{\mathrm{km}}$. It is therefore chosen to use the coefficient of copper, because copper is dominating by cross section area.

The resistance $0.136 ^{\Omega}/_{\mathrm{km}}$ is implemented in the simulation model.

The above calculated screen resistance is together with the rest of the cable parameters in table C.1 used for cable modelling in the following section.

C.1.2 Cable modelling in DIgSILENT

The cable parameters determinated in the previous section are implemented in DIgSIELNT according to the description in [13]. For modelling a cable system in the simulation software three elements may be used. The single-core cable type (TypCab), the cable system type (Typ-Cabsys), and the cable system coupling element (ElmCabsys)[13].

Single core cable type

The single core cable type(TypCab) is used to model a single core coaxial cable, consisting of a defined number of layers. Figure C.4 shown the input window at which the cable parameters may be typed in.

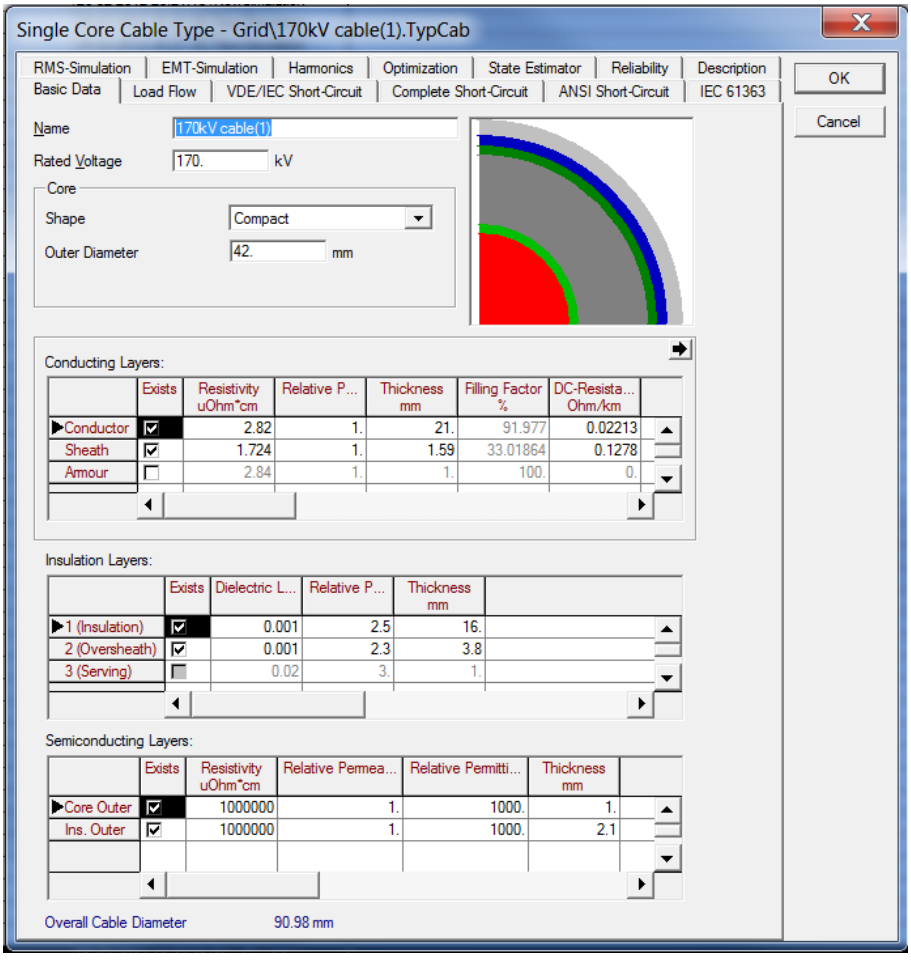

Figure C.4: Modelling of coaxial cable in DIgSILENT.

From figure C.4 it can be seen that the cable is modelled using six layers. Two conductive layers conductor and screen, two semi conductive layers inner and outer semi conductive layer accordingly and two layers of insulation, the insulation and the outer covering.

Cable system type

The cable system type(Typ-Cabsys) provide information of the formation of the cables placing in the ground see figure C.5. The distance between the cables and the depth of the cables are defined in this window, as horizontal and vertical coordinates x and y accordingly.

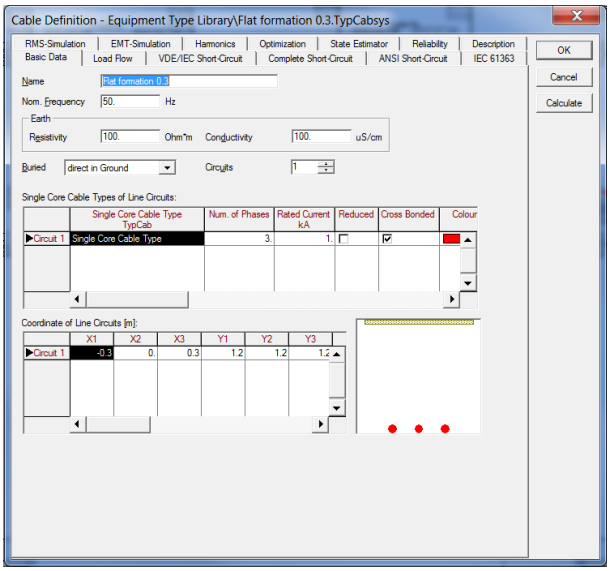

Figure C.5: Cable layout in DIgSILENT.

Figure C.5 shows that the cable line are modelled as a flat formation with a horizontal distance of 0.3m between the cables according to the system description in section 2.

In order to connect the cable type to the system type the coupling elements(ElmCabsys) is used. The coupling element is shown in figure C.6. Figure C.6 also shows a capacitor connected between the conductor and the screen circuit, this has no electrical purpose but is included for making the making the software consider the overall model as one system and not two insulated areas.

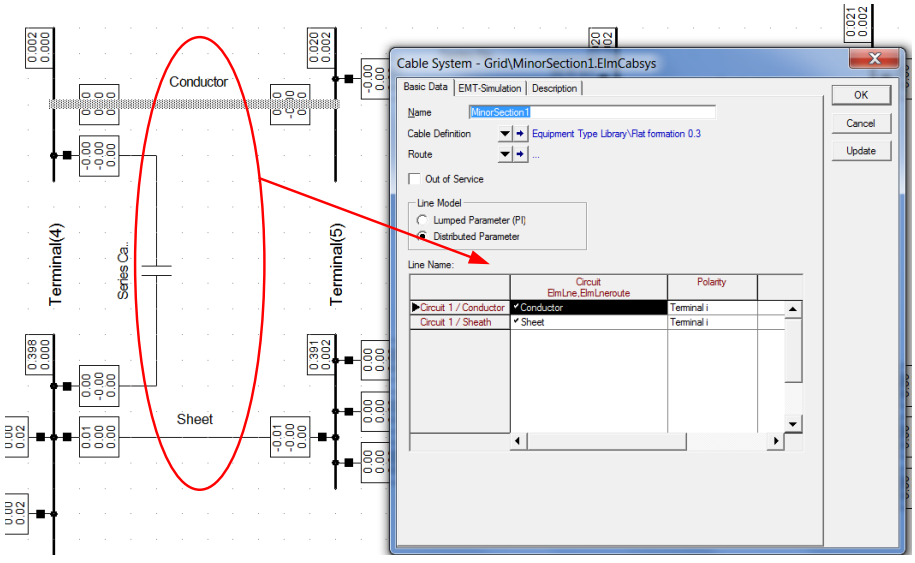

Figure C.6: Cable layout in DIgSILENT.

Cross bonding points

The cross bonding points are performed with three single phase reactors. Using single phase reactors it is possible to determine the phases on the bus bar at which the reactor should be connected as shown in figure C.7.

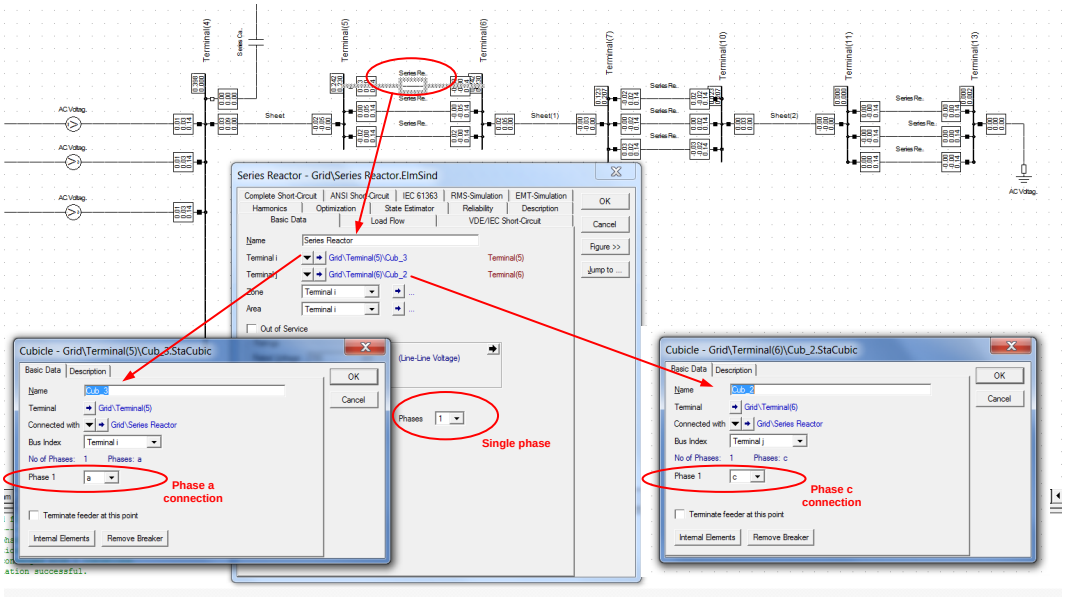

Figure C.7: DIgSILENT modelling of cross bonding, using three single phase reactors.

Grounding point

At the end of the major section the cable screens are ground connected. The grounding point is performed using a voltage source which voltage are set equal to zero. The connection from the three cable screens are performed using three single phase reactors at the cross bonding points. The reactors connect each of the cable screens to a single phase bus bar. The voltage source used for grounding is connected to this single phase bus bar as shown in figure C.8.

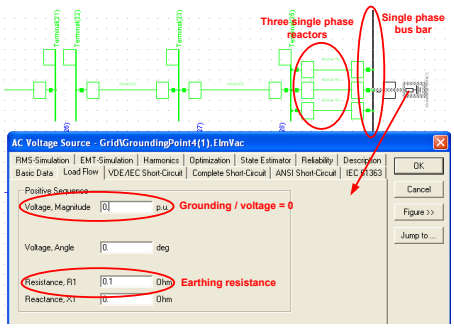

Figure C.8: DIgSILENT modelling of the screen grounding point at the end of the cable line.

The earthing resistance is set equal to 0.1Ω at the grounding point in figure C.8.

Line Element

The line element is used for both the core and the screen. For this the length of the section is applied corresponding the system description 3.84km. The line element is shown in figure C.9.

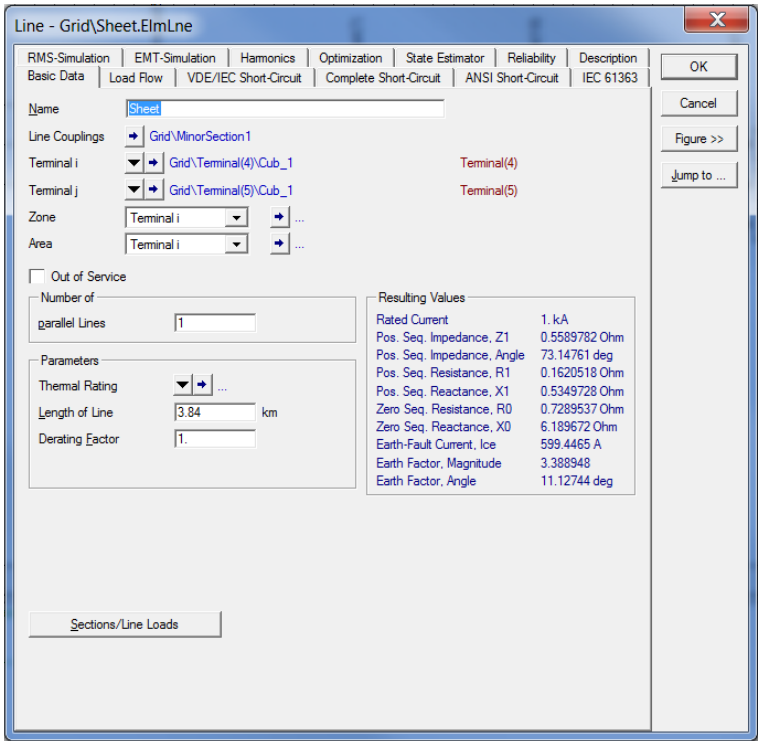

Figure C.9: Line element in DIgSILENT at which the section length is specified.

ECC

The ECC is modelled based on the same Principe used for the conductor. The diameter and the DC-resistance is found in the ABB XLPE land cable systems, users guide, table 20 to 11.2mm and $0.192^{\Omega}/_{\text{km}}$.

The DC-resistance is adjusted to a ground temperature of $5°C$ according to the system description using equation C.13.

$$R_{DC-ecc} = R_0 \cdot (1 + \alpha_{Cu-20}(\theta - 20)) \quad [\Omega] \quad \text{(C.13)}$$

$$R_{DC-ecc} = 0.193 \cdot (1 + 3.93 \cdot 10^{-3}(5 - 20)) = 0.182^{\text{m}\Omega}/_{\text{km}} \quad \text{(C.14)}$$

.

Where:
α_{Cu-20} is the temperature coefficient for Copper $3.93 \cdot 10^{-3}\Omega$m [21, p.61].
θ is the actual temperature of the cable, $(5°C)$ as described in the system description.

Implementation of the ECC is done using a single core cable type shown in figure C.10.

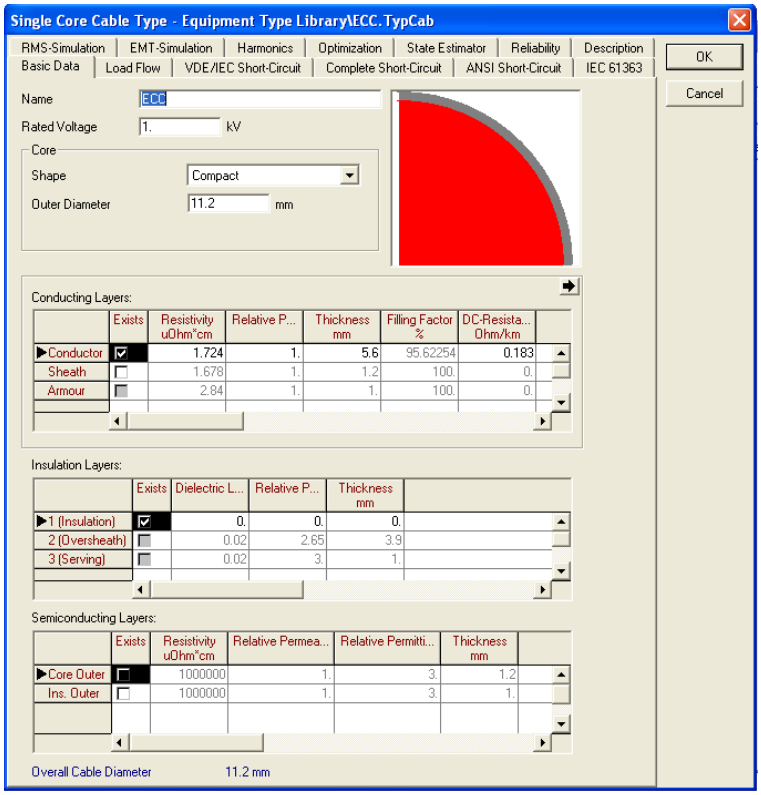

Figure C.10: DIgSIELENT modelling of the ECC.

Cable system with ECC

The cable systems for the sections with the ECC, is modelled as shown in figure C.11.

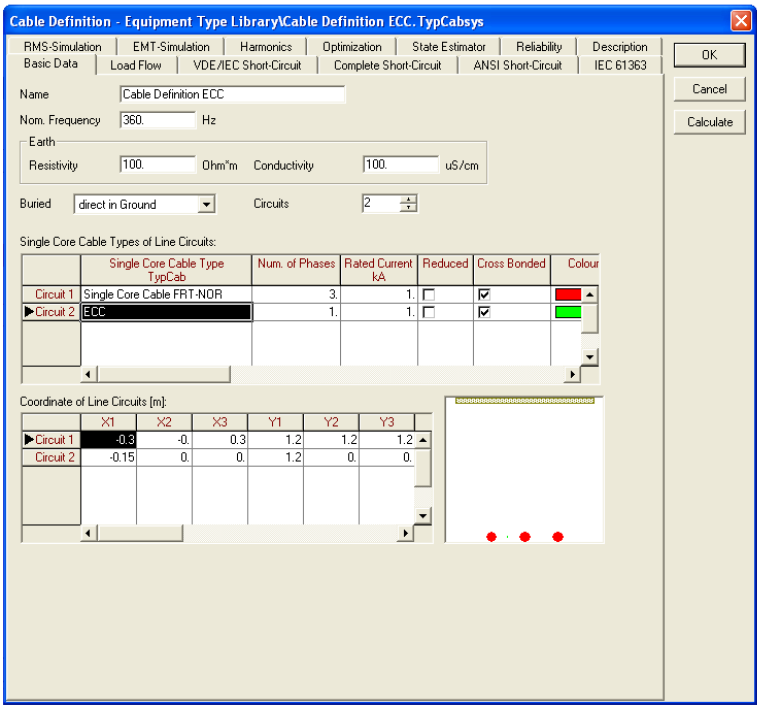

Figure C.11: Cable system for sections equipt with ECC.

For the sections with the ECC the coupling element is expanded also to include the ECC as shown in figure C.12.

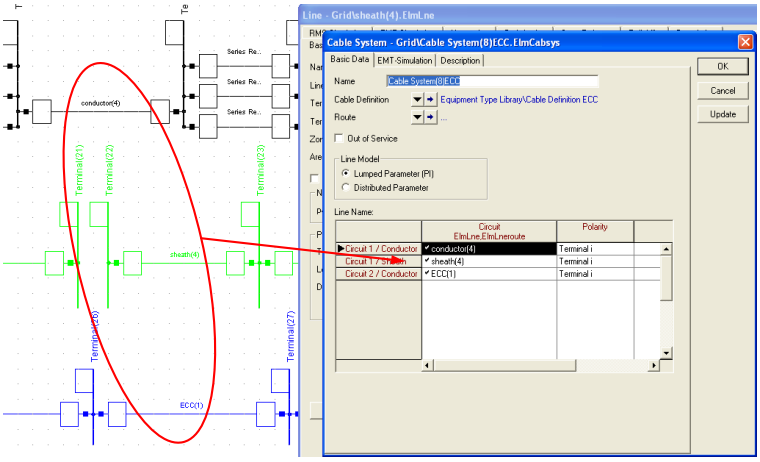

Figure C.12: Coupling element for sections with ECC.

Overall diagram

The overall diagram of the DIgSILENT model is shown in figure C.13.

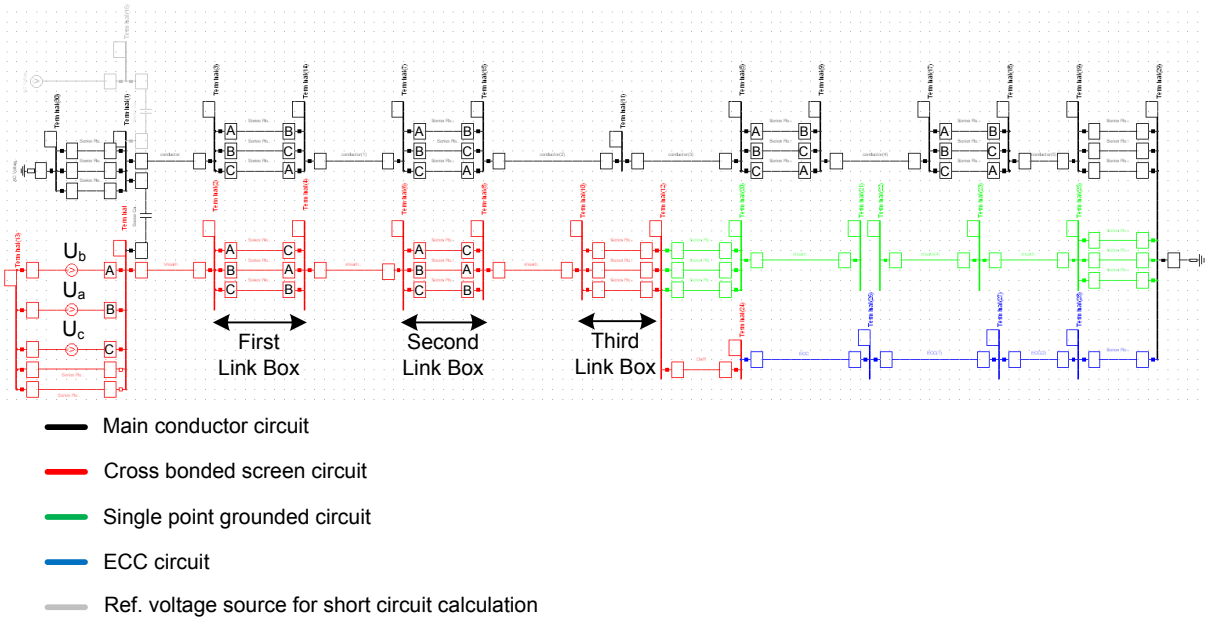

Figure C.13: Overall DIgSILENT model, showing the entire system.

C.2 Cable model used in the problem analysis

For evaluation of the impedance method in the problem analysis is uses the DIgSILENT model shown in figure C.14.

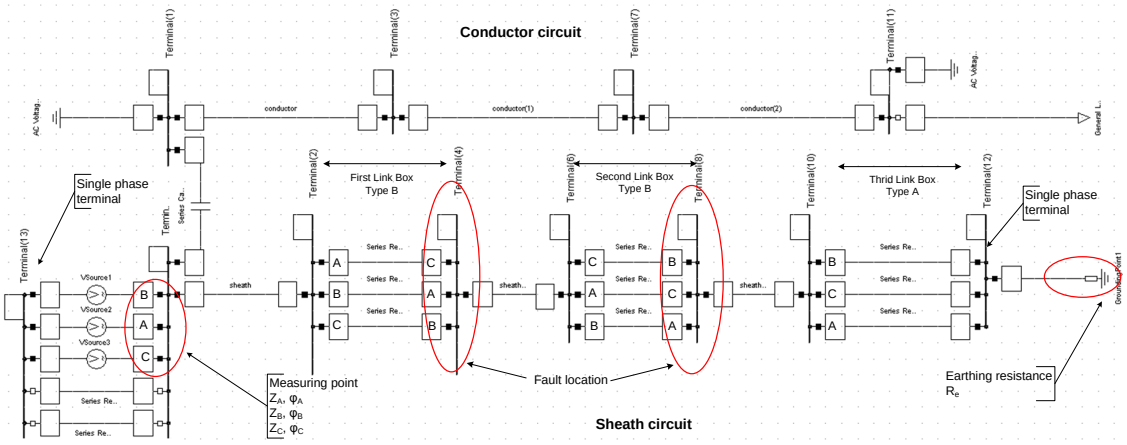

Figure C.14: Overall DIgSILENT model, used in problem analysis.

Figure C.15 shows the data input for the cable model above. The data input is provided by [42]. Each minor section is 1km long, hence the entire cable line have a length of 3km. The earthing resistance at the third link box is set to 10Ω.

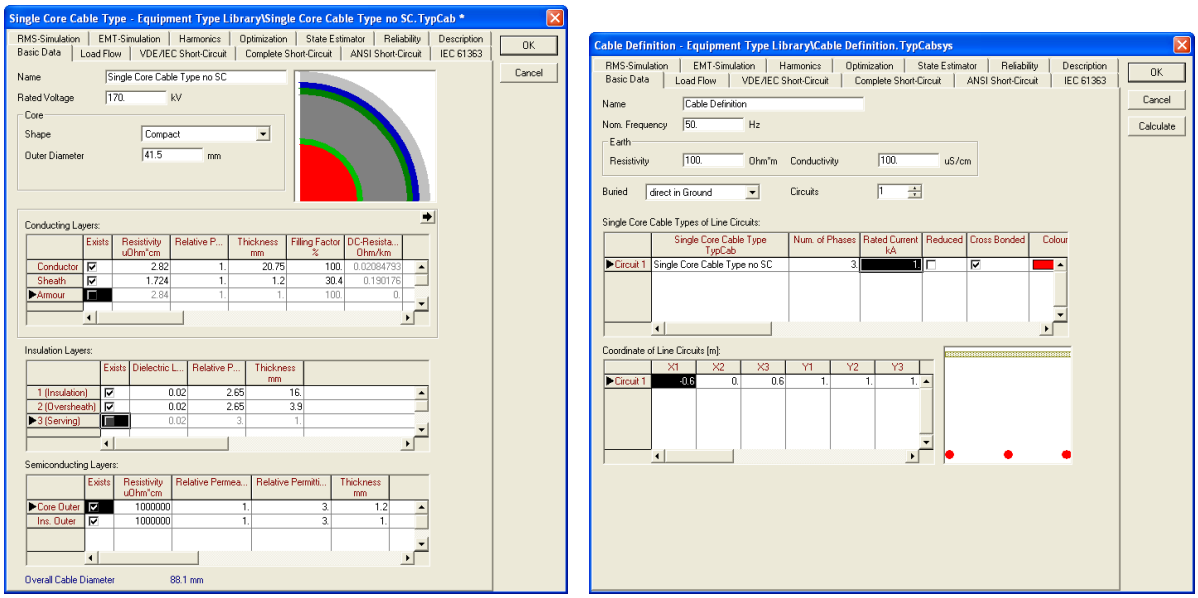

(a) (b)

Figure C.15: Input data for the cable model used in the problem analysis.

Appendix D

Field measurement #1 of the 150kV line between Frøstrup and Nors

The 150kV transmission line at which the measurement will be performed is a 15.1km long, new established cable line which replaces an excising OHL between Frøstrup and Nors. Frøstrup and Nors(FRT-NOR) is located in the north western part of Jutland as shown in figure D.1.

Figure D.1: Geographical placing of the 150kV line between Frøstrup and Nors.

The purpose of the measurement is to obtain measuring data on the screen circuit of a cross bonded cable system. The data will be used for validation of a measuring technique for link box condition determination.

The cable line consists of three single core coaxial cables. The coaxial cables are placed in flat formation 1.2m below the ground surface with a horizontal distance of 0.3m between the cables as shown in figure D.2.

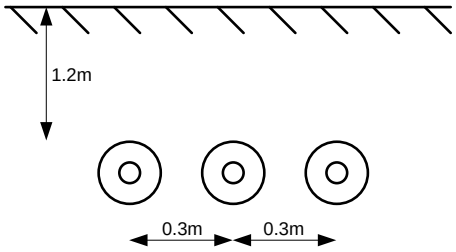

Figure D.2: Cross section layout of the cable line between Frøstrup and Nors. The three coaxial cables are placed in flat formation with 0.3m between the cables and 1.2m below the ground surface.

All cables are insulated by XLPE and with a cross section area of 1200mm^2. The line represents one major cross bonded section, followed by two minor sections using single point bounding. The three minor sections of the cross bonded section is 3840m each. The two sections using single point grounding are 1280m and 2300m accordingly. The line is both transposed and cross bonded. A sketch of the line is shown in figure D.3. Detailed description of the cable system is given in system description in chapter 2.

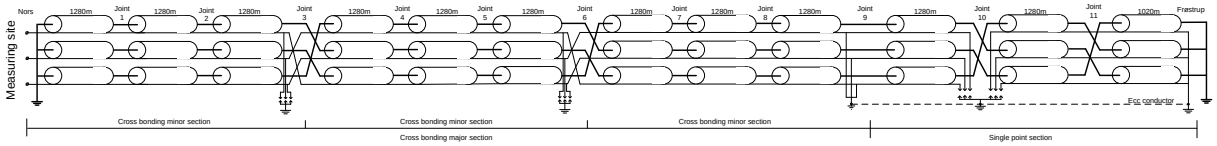

Figure D.3: Bonding schematic for the 150kV transmission line connection Frøstrup and Nors in the northern part of Jutland.

The measurements are performed at HV substation Nors at the termination of the cable line. From figure D.3 it may be seen that the screen circuit is star connected at grounded at joint 9. Because of the star connection at joint 9, the measuring circuit will be the cable line from Nors to the cross bonding point at joint 9 as shown in figure D.4.

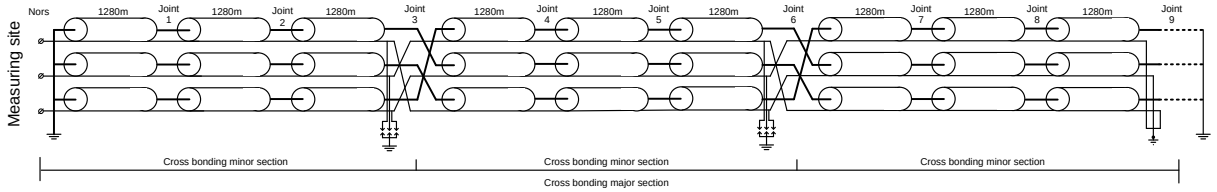

Figure D.4: Measured part of the cable line FRT-NOR.

For this measurement only the circuit formed to the cable screens are of interest, therefore figure D.4 may be reduced only to include the cable screens. The impedances of the three cable parts of each minor section may also be lumped together. The reduced circuit is shown in figure D.5. Figure D.5 shown the physical placing of the screen circuit and the lumped impedances are marked Z_{xy} where x represents the screen conductor and y represents the minor section.

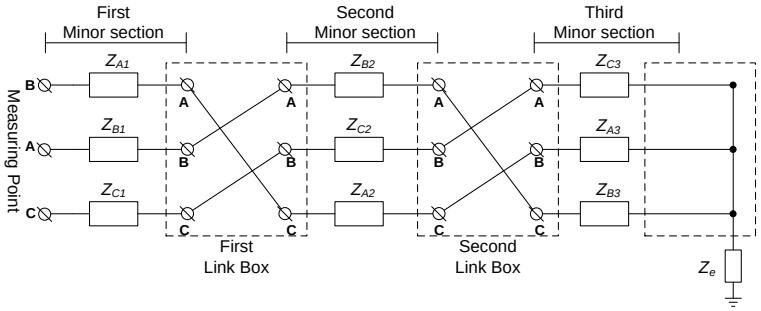

Figure D.5: Measured part of the cable line FRT-NOR.

D.1 Planning field measurements FRT-NOR

It is planned to do three sets of measurement. The different sets are done to obtain measuring for different fault conditions. All faults are implemented by insertion a resistance in the link boxes. The three sets are listed below in the order at which they are planned to be performed:

SET 1:

- Healthy screen circuit

SET 2 - Faults in the FLB:

- Sc-Sc fault in the FLB. (2.6Ω)
- Sc-Gr fault in the FLB. (2.6Ω)

SET 3 - Faults in the SLB:

- Sc-Sc fault in the SLB. (2.6Ω)
- Sc-Gr fault in the SLB. (2.6Ω)

The electric equivalent screen circuits for the four fault conditions are shown in figure D.6. These are based on figure D.5. Figure D.6 shows the screen circuit, not taking care of the physical placing of the elements of the screen circuit due to cross-bonding. The link box faults are marked by a fault resistance of 2.6Ω.

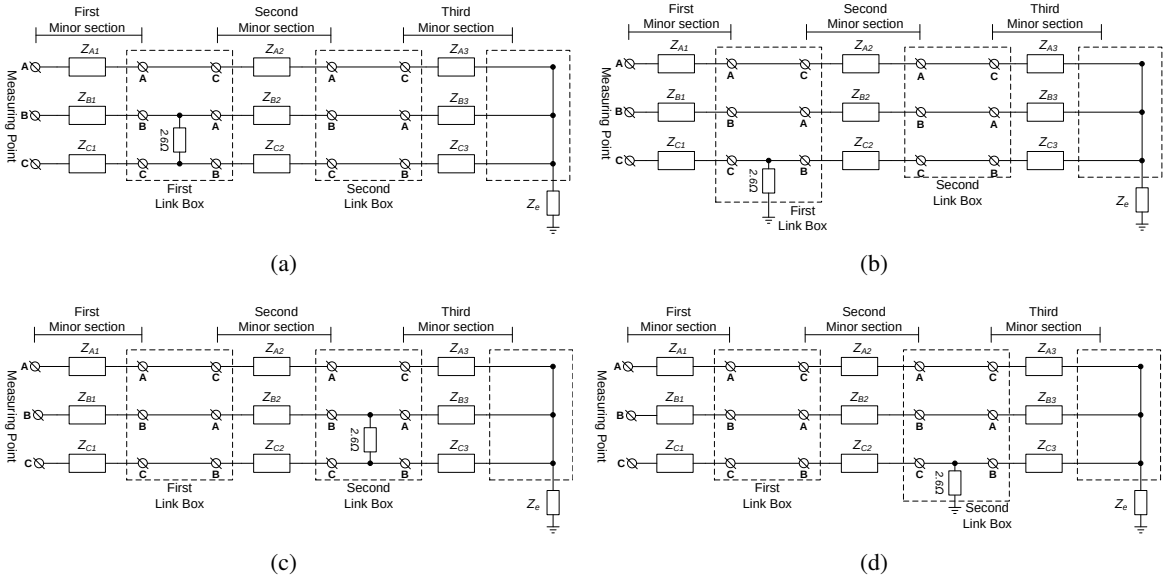

Figure D.6: Electrical equivalent screen circuit of the measuring circuit shown in figure D.4. (a) shows screen B to screen C fault in the first link box. (b) shows screen C to ground fault in the first link box. (c) shows screen A to screen B fault in the second link box. (c) shows screen C to ground fault in the second link box.

D.1.1 Simulation model

A simulation model similar to the line FRT-NOR is set up, in the simulation software DIgSILENT. A detailed describtion of the model may be found in Appendix C An overview of the simulation model is shown in figure D.7.

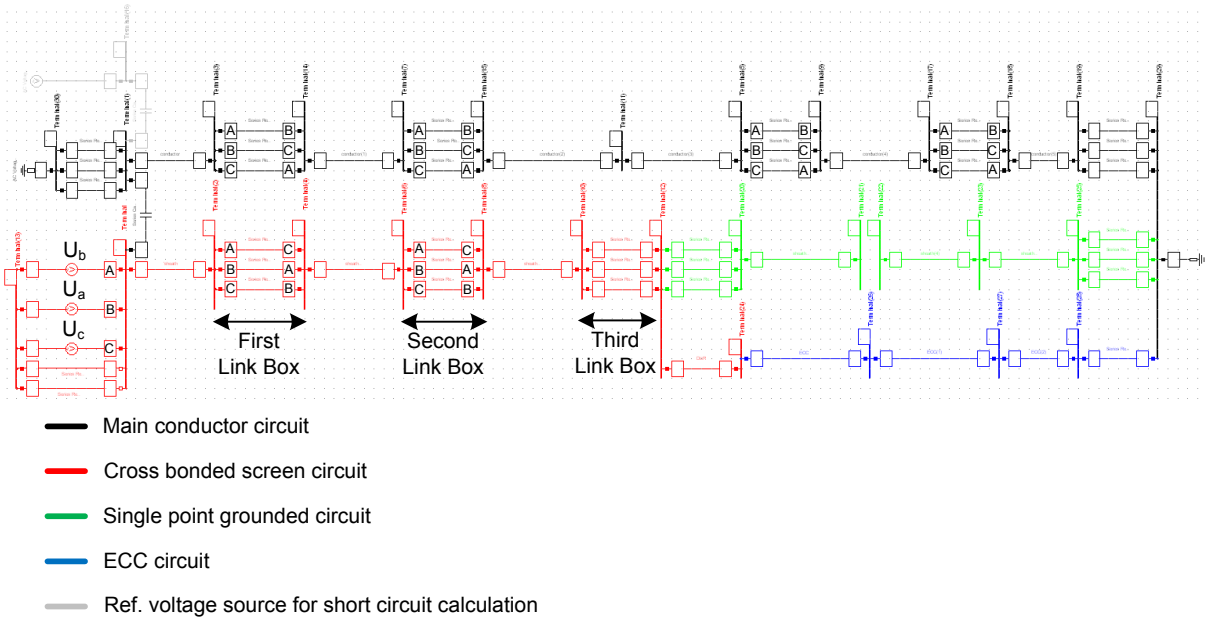

Figure D.7: DIgSILENT model of the 150kV cable line between Frøstrup and Nors, used for AC fault simulations.

For the simulation the core conductor of the three cables are grounded in both ends which will also be the case for the actual circuit during measurement.
During the simulation the screen circuit is supplied by three star connected voltage sources. The values of these are listed below:

Vsource1 = $1\text{V}\angle 0°$ (Magnitude in RMS)
Vsource2 = $1\text{V}\angle -120°$ (Magnitude in RMS)
Vsource3 = $1\text{V}\angle 120°$ (Magnitude in RMS)

The grounding resistance in FLB is 0.2Ω, in SLB 7Ω and in substations 0.1Ω. The apparent screen impedances are calculated based on the voltage and current at sources U_A, U_B and U_C in figure D.7.

D.1.2 Simulations results of FRT-NOR FM1

Before the measurements are carried out there are made simulations to see what to expect of the measurements. Simulations are also used to study what variations of the fault resistance, means to the measured apparent screen impedances.

Simulation sets

For the simulation three phases are applied to the three screen conductors. The simulation provide apparent impedances at the measuring point. There are made simulations for five different fault conditions. One simulation where the screen circuit is intact, and four different fault conditions. The five simulations are listed below:

SET 1:

- Healthy screen circuit

SET 2 - Faults in the FLB:

- Sc-Sc fault in the FLB. (2.6Ω)
- Sc-Gr fault in the FLB. (2.6Ω)

SET 3 - Faults in the SLB:

- Sc-Sc fault in the SLB. (2.6Ω)
- Sc-Gr fault in the SLB. (2.6Ω)

The fault conditions are simulated as a short circuit either between two screen conductors or between one screen and the grounded enclosure in the first or the second link box. The short circuit resistance for the measurement is chosen to 2.6Ω because this value is possible to apply in the link boxes. For the measurement the added fault resistance is 2.6Ω but this value is expected to within a precision of a few hundred milli-ohms due to mechanical connections and temperature changes. To take the possible variations of the fault resistance into consideration, simulations are made with fault resistance from $2-3\Omega$ and the apparent impedances are shown as graphs. From the graphs it can be seen what influence, variations of fault impedances have to the apparent phase impedances.
The apparent phase impedances of the screen circuit for the five different conditions are listed in table D.2. These are calculated based on a fault resistance of exactly 2.6Ω.

SET1 - Healthy screen circuit
For the Healthy screen circuit three phases are applied and the apparent impedances are simulated. The results are presented in table D.1.

Screen	$\lvert Z\rvert[\Omega]$	$\phi[^\circ]$
Z_A	2.25	44.20
Z_B	2.25	44.20
Z_C	2.25	44.20

Table D.1: Simulated apparent impedances for the healthy screen circuit.

SET2 - Sc-Sc fault in the FLB (B-C, 1.LB)

For this simulation there is applied a screen to screen fault between screen A and C in the first link box. The fault resistance is changed from $2-3\Omega$. The magnitude and angle of the apparent impedance at the measuring point are simulated and shown in figure D.8(a) and D.8(b).

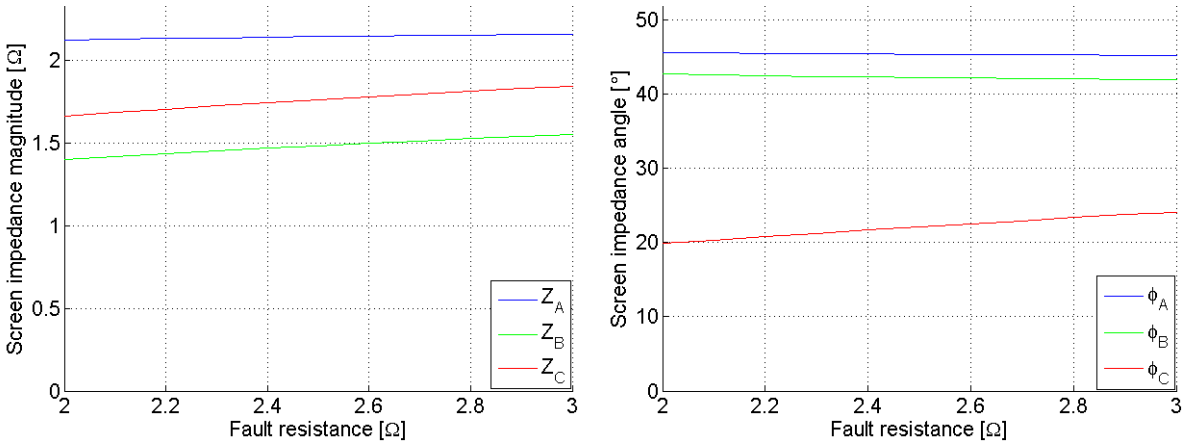

(a) (b)

Figure D.8: Simulated apparent impedances with fault resistance between two phases in first link box changed from $2-3\Omega$.

From figure D.8(a) and D.8(b) it can be seen that the apparent impedance of the two screens between which the fault is applied are approximately 0.7Ω lower than the non faulty screen. The apparent impedance of the non faulty screen is unaffected by the fault.

SET2 - Sc-Gr fault in the FLB (C-Gr, 1.LB)

For this simulation there is applied a Sc-Gr fault from screen C in the FLB. The fault resistance is changed from $2-3\Omega$. The magnitude and angle of the apparent impedance at the measuring point are simulated and shown in figure D.9(a) and D.9(b). It may be seen from the figures that the fault resistance is changed from $12-13\Omega$, this is because there is included a grounding resistance of 10Ω.

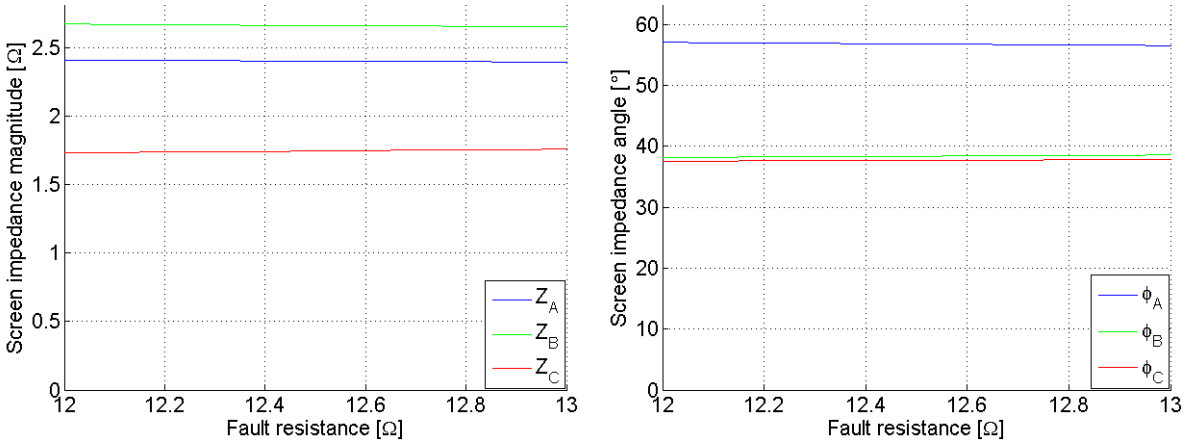

(a) (b)

Figure D.9: Simulated apparent impedances with fault resistance between one screen and ground in first link box changed from $2-3\Omega$.

From figure D.9(a) and D.9(b) it can be seen that the screen from which the fault is applied has dropped to approximately 0.9Ω compared to healthy screen circuit. The apparent impedances of the non faulty screens has increased approximately 1Ω from healthy screen circuit.

SET3 - Sc-Sc fault in the SLB (B-C, 2.LB)

For this simulation there is applied a Sc-Sc fault in the SLB. The fault resistance is changed from $2-3\Omega$. The magnitude and angle of the apparent impedance at the measuring point are simulated and shown in figure D.10(a) and D.10(b).

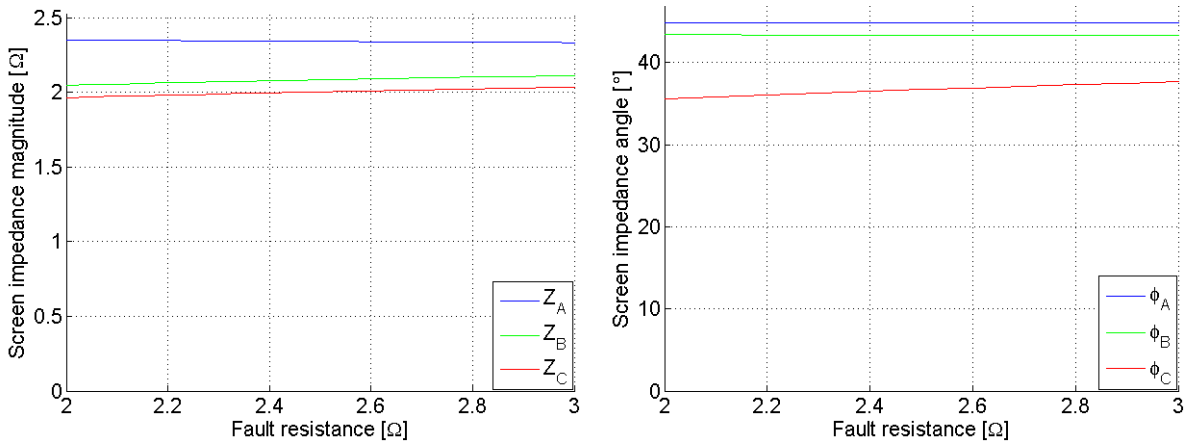

(a) (b)

Figure D.10: Simulated apparent impedances with fault resistance between two phases in second link box changed from $2-3\Omega$.

SET3 - Sc-Gr fault in the SLB (C-Gr, 2.LB)

For this simulation there is applied a Sc-Gr fault in the SLB. The fault resistance is changed from $2-3\Omega$. The magnitude and angle of the apparent impedance at the measuring point are simulated and shown in figure D.11(a) and D.11(b). It may be seen from the figures that the fault resistance is changed from $12-13\Omega$, this is because there is included a grounding resistance of 10Ω.

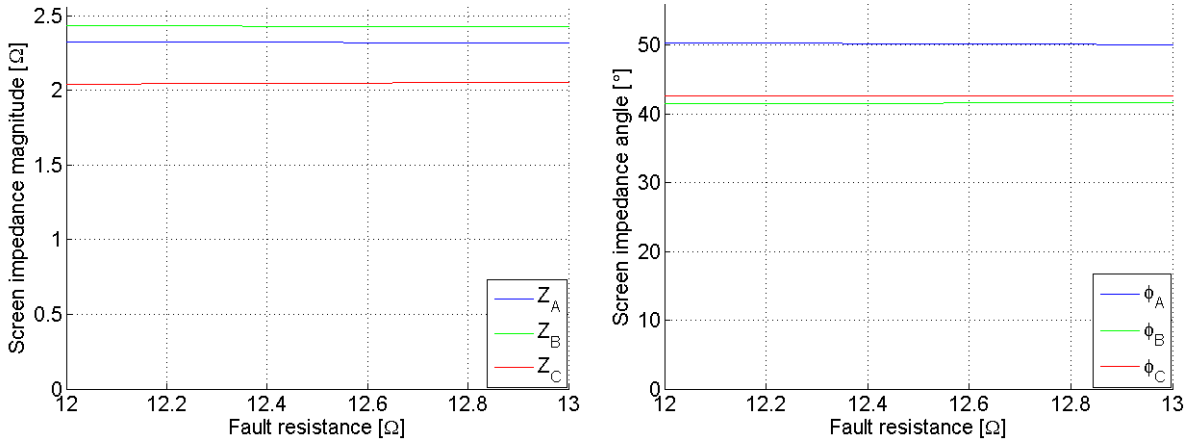

(a) (b)

Figure D.11: Simulated apparent impedances with fault resistance between one phase and ground in second link box changed from $2-3\Omega$.

D.1.3 SET 1-3 Summary

The simulation results in figure D.8(a) to D.11 shown the effect of the variances of the fault resistance between $2-3\Omega$. From the figures it is concluded that the measured apparent impedances are influenced by maximum 100mΩ when the fault resistance is changed from $2-3\Omega$. The condition which is most sensitive to variations of the fault resistance is when a Sc-Sc fault is applied in the FLB. The phase of the apparent impedance is maximum influenced by 3° when the fault resistance is changed from $2-3\Omega$. Also according to the phase, the Sc to Sc fault in the FLB is the most sensitive.

As explained in the beginning of this section simulated impedance for a fault resistance of 2.6Ω is summed up in table D.2.

Simulation	Apparent impedance[$\Omega\angle^\circ$]		
	Z_A	Z_B	Z_C
healthy screen circuit	2.25$\angle$44.20	2.25$\angle$44.20	2.25$\angle$44.20
B-C, FLB	2.25$\angle$44.22	1.51$\angle$45.05	1.72$\angle$63.30
C-Gr, FLB	2.31$\angle$44.42	2.28$\angle$47.40	1.72$\angle$49.29
B-C, SLB	2.27$\angle$44.40	2.10$\angle$50.29	2.00$\angle$44.20
C-Gr, SLB	2.25$\angle$44.10	2.24$\angle$44.50	2.20$\angle$43.20

Table D.2: Apparent impedances for the five simulations. For all of the cases the fault resistance is 2.6Ω.

Table D.2 provide target values for measurement. The earlier presented grapes may be used to foresee the influence of the deviation of the fault resistance on the apparent impedances.

D.2 Performing measurement

Date: 11.1.2012.
Location: 150kV HV station Nors, Buskkærvej 13, 7700 Thisted.
Participants: Morten Thule Hansen(AAU), Kasper Schultz Pedersen(AAU), Peter Rønne-Hansen (N1), Lars Brix (N1).

The measurements will be performed at the 150kV HV station Nors, on the 150kV cable line FRT-NOR.

D.2.1 Measuring process

The cable line which is subject to measurement is just established and not taking into operation at the time. The cable line is intended to replace an excising OHL. During the test the OHL will be taking out of service for safety reasons. By disconnecting the existing OHL line the surrounding noise may also be reduced.

To achieve high safety when working at HV systems there is set up a process for the events and the order in which whey should be performed during the test.

The following list presents the order of events, which will be performed during the test:

1 The OHL is disconnected and de-energized by N1
2 The OHL is grounded and locked in both ends by N1
3 Measuring equipment are brought into the measuring site and the tent is set up
4 The ground connections at the cable termination in Nors is disconnected see figure D.15
5 Possible induced screen voltages are measured according to ground, for safety reasons
6 DC resistance measurement is performed, between screen and to ground
7 Measuring SET 1 is performed
8 Measuring SET 2 is performed
9 Measuring SET 3 is performed
10 Ground connection at the cable terminations are re-established
11 The OHL grounding is removed by N1
12 The OHL is put into service by N1

D.2.2 Dimensioning test setup

In order to dimension the equipment for the measuring setup it is studied how much power the system can handle without being subject to any damage and how much power may possible be delivered by available testing equipment.

During the measurement voltage will be applied to the screens of the three cables. The screen of the cables are insulated for DC 25kV [20]. The cable screen represents a cross section area of 95mm^2 and is for this reason capable of carrying more than 100A [6, p.185]. From these assumptions it is concluded that the test voltage and current are limited by the testing equipment.

The system will be supplied by three phases which voltages are floating according to ground potential. This can be done using a galvanic separation transformer and a three phased auto transformer. The university owns galvanic separation transformers and three phased auto transformers with a rated power of 5kVA and 6.24kVA respectively. These are with a physical size and mass which make it possible to be transported to the measuring site Nors. The auto transformer beside the power capability also has a maximum current capability of 8A at the secondary side.

From simulation the relation between applied voltage, current and dissipated power for the actual circuit can be studied. The condition which represents the lowest impedance is when a fault is applied between two phases in the first link box. For this condition the current will increase fastest according to applied voltage. A simulation is performed using a fault resistance of 0Ω between phase *a* and *c* in the first link box. Simulation results are shown in figure D.12(a) and D.12(b).

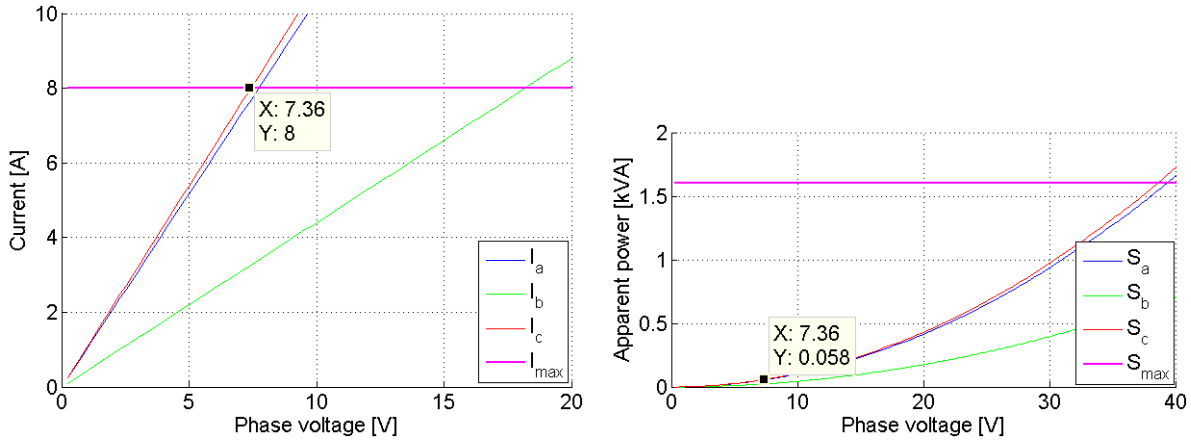

(a) (b)

Figure D.12: (a)Current in the three phases as a function of applied phase voltage. (b) Dissipated apparent power per phase as a function of applied phase voltage.

The current limitation of the auto transformer is marked on figure D.12(a) as a pink line and the date cursor indicate the corresponding voltage for phase *c*. From the figure it can be seen that the current is at the maximum when the circuit is supplied by 7.36V. From figure D.12(b) the dissipated apparent power corresponding to a voltage of 7.4V can be seen, also marked by a data cursor. It can be seen that this point is much lower than the horizontal pink line in figure D.12(b) indication the maximum apparent power of the galvanic separation transformer.

From the study it is concluded that the measuring equipment are suitable for the test. It is decidable to choose the applied voltage and current so that coupling of surrounding noise into the circuit may be reduced but still keeping a sufficient margin from the limits of the equipment. In order to fulfill the mentioned criteria it is decided to increase the voltage until the three currents are approximately 5A. By increasing the voltage the three phase current may differ from each other according to the given fault situation. It is important be aware that the highest current not become close the current limitation of the auto transformer.

If the current become close the current limitation of the auto transformer, the core of the transformer may saturate. If the core of the transformer become close to saturation, the characteristic become non-linear. A non-linear characteristic lead to generation of harmonic currents [3]. Simulations and calculations are carried out for 50Hz only therefore only this frequency should be evaluated during the measurement. In

order to consider the possible content of harmonic during the measurement it may be preferred to record the waveforms to be able to analyze the frequency content of the signal.

D.2.3 Measuring setup

The measuring setup for the field measurement #1 is shown in figure D.13.

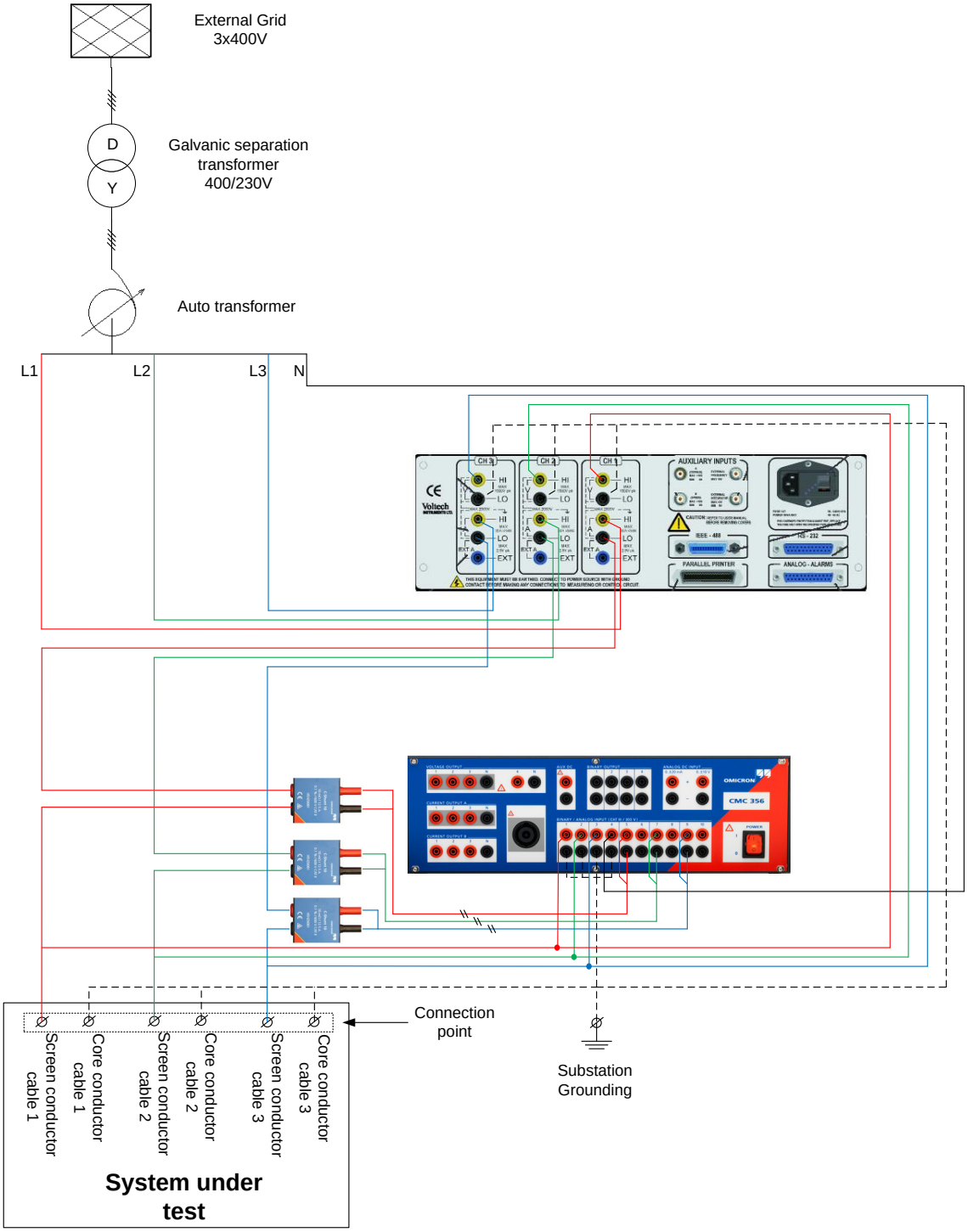

Figure D.13: Measurement setup for field tests. Three phased supply is provided by the cooperation company N1.

Three phases are applied to the screen circuit. The three phases are supplied by the auto transformer in

order to make the voltage adjustable. The three phase voltages and three phase currents are recorded. Also the voltage at the star point of the voltages sources are measured. All voltages are measured according to ground potential. The measurement is performed using both Omicron CMC356 and Voltech PM3000A. The procedure is repeated for the four different fault conditions.

The complete measuring setup is placed in the HV substation Nors where all measurements are performed.

I order to keep the measuring equipment dry a tent is installed at the measuring site in Nors. The tent is non-magnetic to prevent coupling from the surroundings. The site is shown on figure D.14

Figure D.14: Test setup next to cable termination in HV substation Nors.

The grounding of the cable screen is removed as shown in figure D.15. The connection between cable screen and the Omicron connection box is done by grounding cables as shown in figure D.15.

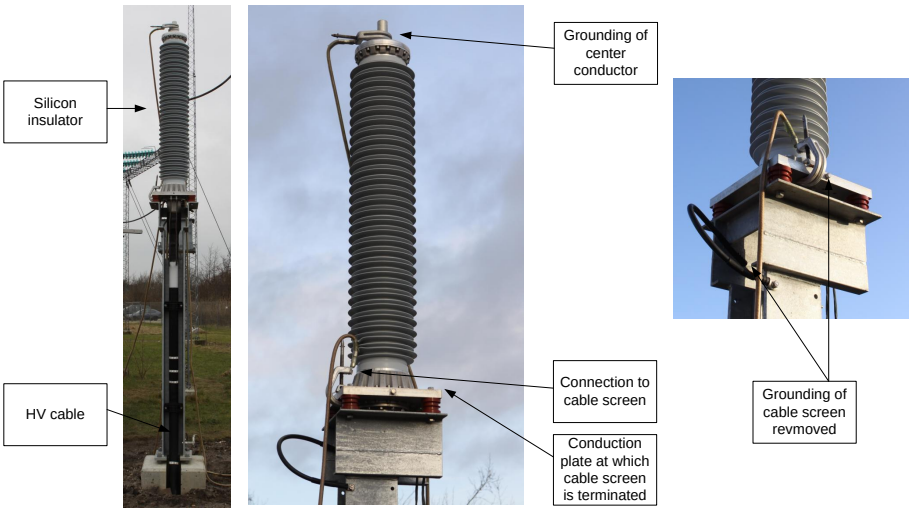

Figure D.15: Cable termination in the HV substation Nors.

Connection of fault simulation resistance in link box is shown in figure D.16 . The resistance is connected between two screen connections or between one screen and ground.

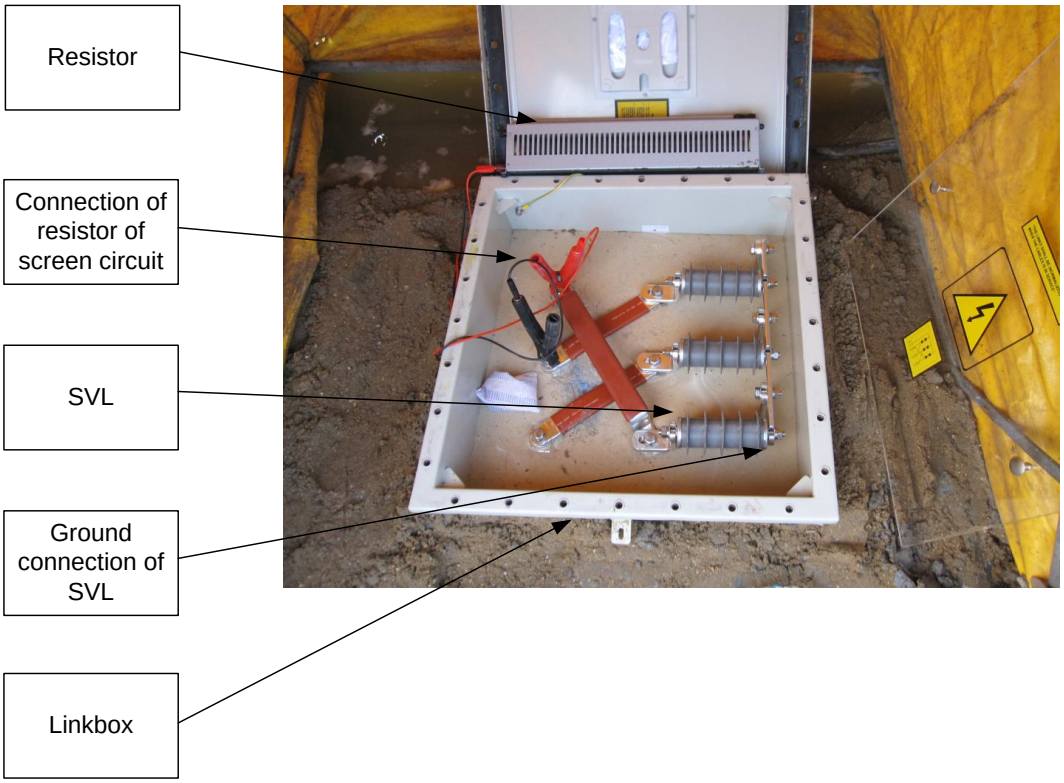

Figure D.16: Linkbox with fault simulation resistor placed between two cable screens.

As ground potential the substation grounding is used. The substation ground is accessed, by connection to the copper wires used for equipment grounding inside the substation as shown in figure D.17.

Figure D.17: Connection to substation ground.

D.2.4 Measuring equipment

Table D.3 includes the instruments, which will be used for field measurement #1. As earlier explained the screen circuit is supplied by three phases though a galvanic separation transformer and an autotransformer shown in figure D.13.

Type	Producer	Model	AAU number
Galvanic separation transformer	Noratel	6-010-718711	93629
Auto transformer	Metrel	MTH 450/B	89101
Universal relay test set	Omicron	CMC 365	owned by N1
Grounding box	Omicron	CP GB1	owned by N1
Universal power analyzer	Voltech	PM3000A	29388
C-Shunt Precision shunts	Omicron	C-Shunt 10	owned by N1
Variable effect resistance 2.5Ω	Danotherm	2.5Ω slider	-

Table D.3: Instruments used for field measurement 1.

The Omicron universal relay test set (CMC356) is connected to a PC which is equipped with omicron test universe software.

Figure D.18: Omicron CMC356 Universal relay test set.

The CP GB1 grounding box including overvoltage protection which conducts to ground in case of overvoltages. The grounding box is used as **connection point** between the measuring equipment and the cable system as shown in figure D.13.

Figure D.19: Omicron CP GB1 Grounding box.

The Omicron C-Shunt10 current shunts have a measuring range of $0 - 12.5$A. The shunt resistance is 10mΩ.

Figure D.20: Omicron C-shunt 10 current shunt.

The universal power analyzer measures voltages and currents. The power analyzer is equipped with a filter which makes it possible only to measure the fundamental frequency.

Figure D.21: Voltech PM3000A power analyzer.

During the test, the voltage is increased slowly using the auto transformer in figure D.22. While increasing the current is observed on the display of the power analyzer. It is decided to increase the voltage until the current is approximately 5A in order not to overload the auto transformer.

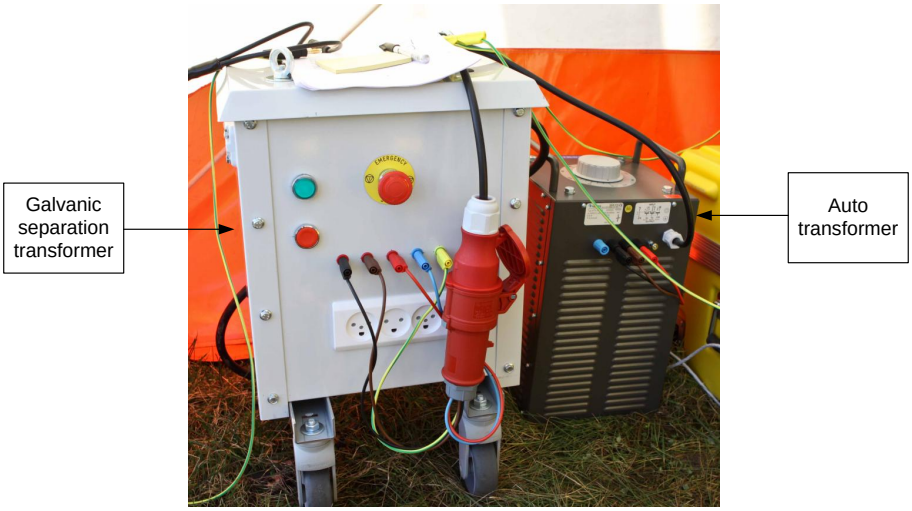

Figure D.22: Galvanic separation transformer and autotransformer.

Connection between the measuring equipment and the cable system is shown in figure D.23. Test cables with banana plugs and crocodile clamps are used for connection of the measuring equipment. Connection from the grounding box to the system is performed using grounding cables as shown in figure D.23.

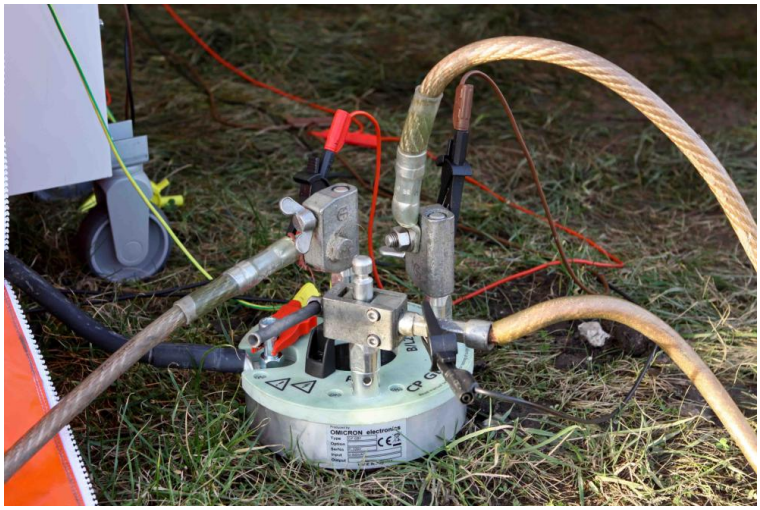

Figure D.23: Omicron CP GB1 grounding box including over voltage protection. Used as connection point to the system.

Measurement performed using both power analyzer and Omicron relay testing set shown in figure D.24. Recording with Omicron is manually triggered and measurements are logged at a 9.48kHz sampling rate with a time span of 15 sec. Recording from power analyzer is done manually, by reading the values from the display for each fault conditions.
The measuring range on the power analyzer is automatically set to 20V and 10A. The power analyzer is set to measure only to fundamental frequency.

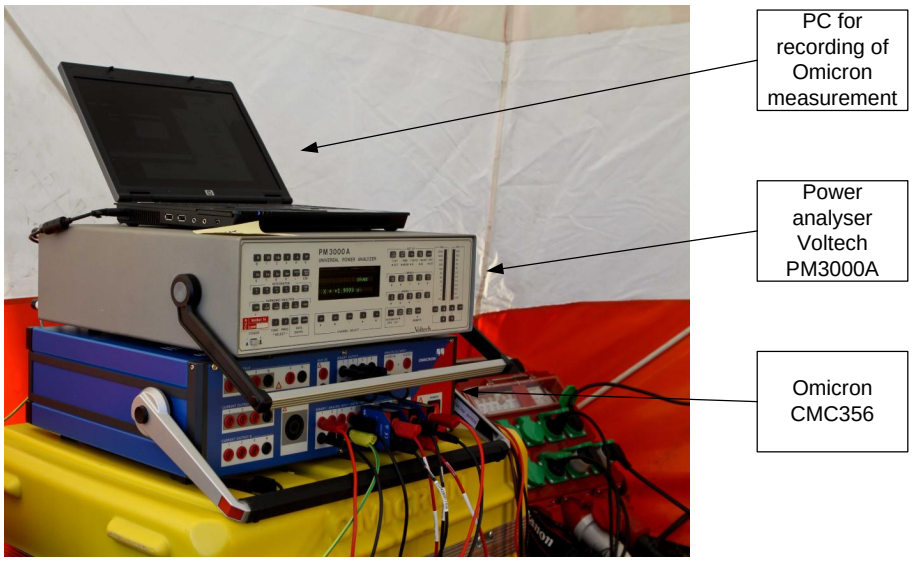

Figure D.24: Measuring equipment for measuring set 1. Power analyzer and Omicron CMC356, with recording PC.

D.2.5 Measuring accuracy

The purpose of the measurement is validation of screen condition determination. The analyses showed that a condition change may only affect the system impedance by a small value, relative to healthy circuit, therefore measurement accuracy is important. The measuring is influence by accuracy of the measuring equipment and the temperature at the measuring site.

Equipment accuracy

Measurements are performed using both Power analyzer and Omicron CMC356 as shown in figure D.13. Both measuring instruments are connected at the same time. Figure D.13 shows that the current measurements of the two instruments are connected in series and the voltage measurements are performed at the point of connection. Using this connection setup the current measurement for both instruments will account for both the current obtained by the circuit and for the current absorbed by the voltage measurement see figure D.25. The input impedance for the instruments are 500kΩ and 1MΩ accordingly. The voltage applied for the measurement is in the range of 10V which generate a current of 30μA see equation D.1 and D.2. It is concluded that this current is so small that it will not affect the measurement.

$$I_v = \frac{U}{R_{voltech}} = \frac{10}{1M} = 10\mu A \qquad \text{(D.1)}$$

$$I_o = \frac{U}{R_{omicron}} = \frac{10}{500k} = 20\mu A \qquad \text{(D.2)}$$

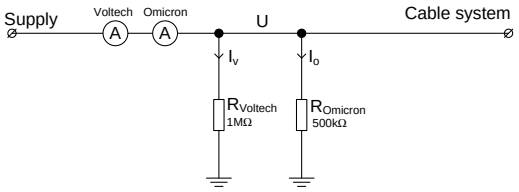

Figure D.25: Setup scheme of voltage and current measurement.

Accuracy of Power analyzer - Voltech PM3000A
The power analyzer is directly connected from the voltage supply(autotransformer) meaning no probes are used as shown in figure D.13.

From the datasheet [52] it is found that the power analyzer measures voltage and current with an accuracy of:

$$\pm 0.05\%rdg \pm 0.05\%mg \qquad \text{(D.3)}$$

Where:
- *rdg* means reading
- *mg* means measuring range.

This means that the accuracy is dependent of the size of the readings and the measuring range. The reading differ according to measurement but the voltage range is 20V and the current range is 10A for all measurement.

Measurement	Power analyzer Range	Power analyzer accuracy
Voltage phase A	20V	$\pm 0.05\%rdg \pm 10$mV
Voltage phase B	20V	$\pm 0.05\%rdg \pm 10$mV
Voltage phase C	20V	$\pm 0.05\%rdg \pm 10$mV
Current phase A	10A	$\pm 0.05\%rdg \pm 5$mA
Current phase B	10A	$\pm 0.05\%rdg \pm 5$mA
Current phase C	10A	$\pm 0.05\%rdg \pm 5$mA

Table D.4: Accuracy of the power analyzer measurement.

To relate the accuracies from table D.4 direct to voltage and current, there will be calculated an example. The example is carried out with basis of the values measured for phase A on the healthy screen circuit from table D.8.

$$U_A = \pm 0.0005 \cdot 13.035 \pm 10\text{mV} = \pm 16.5\text{mV} \tag{D.4}$$

Accuracy of the measured current is calculated using equation D.5.

$$I_A = \pm 0.0005 \cdot 5.309 \pm 5\text{mA} = \pm 7.7\text{mA} \tag{D.5}$$

Accuracy of Omicron CMC356

The Omicron CMC356 is able to measure voltages in the range of $0-600$V [5]. This means that the voltage can be measured directly without using any probes from the connection point in figure D.13. The voltage measurement is therefore only influenced by the accuracy of the voltage inputs. The typical accuracy of the omicron is by the reference manual [5] found to:

$$\pm 0.06\%rdg \tag{D.6}$$

Where:
- *rdg* means reading.

The current is measured using current shunts shown in figure D.20. The used current shunts has a maximum ability of 12.5A which is converted to 125mV. The current measurement is influenced by both the accuracy of the current shunt and the accuracy of the voltage input of the omicron. The two accuracies shall be added in order to determine the resulting accuracy.
The accuracy of the current shunts are $\pm 0.1\%$ and the accuracy of the voltage input is $\pm 0.06\%rdg$. The total worst case accuracy is therefore determined to $\pm 0.16\%$ using the min/max method.

Measurement	Probe division	Probe accuracy	Omicron CMC356
Voltage phase A	no probe	-	$\pm 0.06\%rdg$
Voltage phase B	no probe	-	$\pm 0.06\%rdg$
Voltage phase C	no probe	-	$\pm 0.06\%rdg$
Current phase A	12.5A/125mV	$\pm 0.1\%$	$\pm 0.16\%rdg$
Current phase B	12.5A/125mV	$\pm 0.1\%$	$\pm 0.16\%rdg$
Current phase C	12.5A/125mV	$\pm 0.1\%$	$\pm 0.16\%rdg$

Table D.5: Accuracy of the Omicron CMC356.

As for the power analyzer, there will for the Omicron, be made an accuracy calculation example. The accuracy for voltage and current given in table D.5 is used. This example is carried out based of the same measurement as the previous example, measured for phase A on the healthy screen circuit. The measured values are given in figure D.8. Accuracy of the measured voltage is calculated using equation D.7.

$$U_A = \pm 0.0006 \cdot 13.035 = \pm 7.8\text{mV} \tag{D.7}$$

Accuracy of the measured current is calculated using equation D.8.

$$I_A = \pm 0.0016 \cdot 5.309 = \pm 8.5\text{mA} \tag{D.8}$$

In case the impedance was calculated based on the Omicron recorded data the accuracy of the impedance would be the sum of the accuracies: $\pm 0.22\%$.

Impedance Accuracy

For this thesis the impedance is the parameter of most interest. The impedance of the measurement is calculated using ohms law using equation D.9.

$$Z = \frac{U}{I} \quad [\Omega] \tag{D.9}$$

The previous section describes that there are some accuracies influencing the voltage and current measurement. The impedance is the quotient of two accuracies. Therefore the worst case accuracy of the impedance becomes the sum, of the two accuracies.

The accuracy of the impedance measured by the power analyzer may be calculated from the accuracy of the voltage and current. Based on the previous example the voltage accuracy is $\pm 0.13\%$ from equation D.4 and the current $\pm 0.15\%$ from equation D.5. The worst case accuracy of the impedance becomes the sum of the voltage and current accuracy: $\pm 0.28\%$. It is seen that both accuracies are lower than 0.5%. It is chosen to use the measurements from the power analyzer further, because from the power analyser the

voltages and currents can be obtained directly. The recorded voltages and currents from the CMC356, should be analyzed by data processing to obtain the apparent screen impedances.

D.3 Measuring results

The resistor, used as fault resistor is shown in figure D.16. The resistance of the fault resistor is measured at the site with the temperature of the surroundings. The value is presented in table D.6.

Parameter	R[Ω]
R_{fault}	2.6

Table D.6: Measured fault resistor is the site.

The DC resistance of the screen circuit is measured using a fluke 179 with AAU number 70388. The resistances are presented in table D.7.

Parameter	R[Ω]
R: L1-L2	3.2
R: L1-L3	3.3
R: L2-L3	3.2

Table D.7: Measured loop resistances using fluke 179.

D.3.1 Power analyser

Healthy screen circuit

The values given in table D.8 are measuring results of the healthy screen circuit. The values are measured by the power analyzer, while the screen circuit is supplied by galvanic separation transformer and auto transformer. The measuring setup may be seen in figure D.13.

	Voltage[V]	Current[A]	PF	R[Ω]	X[Ω]
Screen *A*	13.035	5.309	0.701(ind)	1.7218	1.7494
Screen *B*	12.443	5.046	0.692(ind)	1.7072	1.7794
Screen *C*	12.681	5.133	0.700(ind)	1.7288	1.7639

Table D.8: Measuring results for the healthy screen circuit.

From the measured resistance and reactance the corresponding measured impedances may be calculates using equation D.10 and D.11 this is referred to as the measured impedance.

$$|Z| = \sqrt{R^2 + X^2} \qquad \text{(D.10)} \qquad\qquad \angle Z = cos^{-1}(PF) \qquad \text{(D.11)}$$

The measured impedances are compared to the simulated and the deviations are calculated using equation D.12 and shown in table D.9. The sign indicated if the simulated value is higher or lower than the measured. $+$ indicates a higher simulated value, and $-$ indicates that the simulated value is lower than the measured. The relative deviations are calculated from equation D.13 these are also shown in table D.9.

$$\Delta Z = Z_{meas} - Z_{sim} \qquad \text{(D.12)} \qquad\qquad \Delta Z_{re} = \frac{\Delta Z}{Z_{meas}} \qquad \text{(D.13)}$$

	Simulated $Z_{sim}[\Omega\angle^\circ]$	Measured $Z_{meas}[\Omega\angle^\circ]$	Deviation $\Delta Z[\Omega\angle^\circ]$	Relative deviation $\Delta Z_{re}[\%\angle\%]$
Screen *A*	$2.25\angle 44.2$	$2.4546\angle 45.45$	$-0.20\angle -1.25$	$-8.15\angle 2.75$
Screen *B*	$2.25\angle 44.2$	$2.4659\angle 46.19$	$-0.22\angle -1.99$	$-8.92\angle 4.31$
Screen *C*	$2.25\angle 44.2$	$2.4698\angle 45.58$	$-0.22\angle -1.38$	$-8.91\angle 3.03$

Table D.9: Comparison of simulated and measured impedances for the healthy screen circuit.

From the simulated and measured values it is observed that the system close to symmetrical, when no faults are applied. It is also observed that the measured impedances are $8-9\%$ larger in amplitude and $1-3\%$ larger in phase than values.

Sc-Sc fault in FLB (B-C, 1st LB)

The values given in table D.10 are measuring results of the screen circuit with a Sc-Sc fault present in the FLB. The values are measured by the power analyzer, while the screen circuit is supplied by galvanic separation transformer and auto transformer. The measuring setup may be seen in figure D.13

	Voltage[V]	Current[A]	PF	R[Ω]	X[Ω]
Screen *A*	11.623	4.754	0.701(ind)	1.7162	1.7420
Screen *B*	11.026	6.558	0.707(ind)	1.1901	1.1879
Screen *C*	11.052	5.589	0.906(ind)	1.7919	0.8368

Table D.10: Measuring results with a Sc-Sc fault at 2.6Ω in the FLB.

Simulated and measured apparent screen impedances are shown in table D.11.

	Simulated $Z_{sim}[\Omega\angle^\circ]$	Measured $Z_{meas}[\Omega\angle^\circ]$
Screen *A*	2.25∠44.22	2.4454∠45.49
Screen *B*	1.51∠45.05	1.6815∠45.01
Screen *C*	1.72∠63.30	1.9777∠25.04

Table D.11: comparison of simulated and measured impedances for Sc-Sc fault at 2.6Ω in the FLB.

Form table D.11, it is seen than in general there are measured larger impedances than there are simulated. The measurements are further used for model validation in Chapter 6.

Sc-Gr fault in FLB (C-Gr, 1st LB)

The values given in table D.12 are measuring results of the screen circuit with a Sc-Gr fault present in the FLB. The values are measured by the power analyzer, while the screen circuit is supplied by galvanic separation transformer and auto transformer. The measuring setup may be seen in figure D.13

	Voltage[V]	Current[A]	PF	R[Ω]	X[Ω]
Screen *A*	13.165	5.160	0.672(ind)	1.7148	1.8887
Screen *B*	13.353	5.220	0.728(ind)	1.8622	1.7552
Screen *C*	10.462	5.672	0.761(ind)	1.4046	1.1959

Table D.12: Measuring results with a Sc-Gr fault at 2.6Ω in the FLB.

Simulated and measured apparent screen impedances are shown in table D.13.

	Simulated $Z_{sim}[\Omega\angle^\circ]$	Measured $Z_{meas}[\Omega\angle^\circ]$
Screen *A*	2.31∠42.22	2.5510∠47.78
Screen *B*	2.28∠47.40	2.5590∠43.28
Screen *C*	1.72∠49.29	1.8447∠40.45

Table D.13: Comparison of simulated and measured impedances for Sc-Gr fault of 2.6Ω in the FLB.

Form table D.13, it is seen than in general there are measured larger impedances than there are simulated. The measurements are further used for model validation in Chapter 6.

Sc-Sc fault in SLB (B-C, 2nd LB)

The values given in table D.14 are measuring results of the screen circuit with a Sc-Sc fault present in the SLB. The values are measured by the power analyzer, while the screen circuit is supplied by galvanic separation transformer and auto transformer. The measuring setup may be seen in figure D.13

	Voltage[V]	Current[A]	PF	R[Ω]	X[Ω]
Screen *A*	11.606	4.844	0.780(ind)	1.8709	1.4974
Screen *B*	11.097	5.447	0.724(ind)	1.4762	1.4032
Screen *C*	11.119	5.339	0.832(ind)	1.7343	1.1527

Table D.14: Measuring results with a Sc-Sc fault at 2.6Ω in the SLB.

Simulated and measured apparent screen impedances are shown in table D.15.

	Simulated $Z_{sim}[\Omega\angle^\circ]$	Measured $Z_{meas}[\Omega\angle^\circ]$
Screen *A*	2.27∠44.40	2.3964∠38.74
Screen *B*	2.10∠50.29	2.0367∠43.61
Screen *C*	2.00∠44.20	2.0824∠33.70

Table D.15: Comparison of simulated and measured impedances for Sc-Sc fault of 2.6Ω in the SLB.

The Measurements are further used for model validation in Chapter 6.

Sc-Gr fault in SLB (C-Gr, 2nd LB)

The values given i table D.16 are measuring results of the screen circuit with a Sc-Gr fault present in the SLB. The values are measured by the power analyzer, while the screen circuit is supplied by galvanic separation transformer and auto transformer. The measuring setup may be seen in figure D.13

	Voltage[V]	Current[A]	PF	R[Ω]	X[Ω]
Screen *A*	12.473	5.200	0.774(ind)	1.8506	1.5120
Screen *B*	12.127	5.330	0.745(ind)	1.6965	1.5162
Screen *C*	11.751	5.459	0.792(ind)	1.7059	1.3113

Table D.16: Measuring results with a Sc-Gr fault at 2.6Ω in the SLB.

Simulated and measured apparent screen impedances are shown in table D.17.

	Simulated $Z_{sim}[\Omega\angle^\circ]$	Measured $Z_{meas}[\Omega\angle^\circ]$
Screen *A*	2.25∠44.10	2.3897∠39.29
Screen *B*	2.24∠44.50	2.2753∠41.84
Screen *C*	2.20∠43.20	2.1517∠37.63

Table D.17: Comparison of simulated and measured impedances for Sc-Gr fault of 2.6Ω in the SLB.

The measurements are further used for model validation in Chapter 6.

D.3.2 Omicron CMC356

The measuring results shown in the figures below are measured with Omicron CMC356. The measuring setup may be seen in figure D.13. Measuring results may be found at the CD in folder *Nors 11-01-2012*. The recorded waveforms are used to analyze the harmonic content of the measured voltage and currents. It is believed that possible harmonic currents / voltages caused by the non-linear magnetization curve of the auto transformer.

Intact screen circuit

By looking at the voltage and current waveforms shown in figure D.26(a) and D.26(b) it is not expected that the harmonic content of other than the fundamental frequency of 50Hz is present. However the voltage waveform is bit flattened at the positive peaks.

In order to determine the harmonic contents of the signals a discrete Fourier transform (DFT) is used. An efficient algorithm to compute this is a fast Fourier transform (FFT).

The fundamental frequency is 50Hz and the window for the FFT is therefore the number of samples recorded over a time period of 20ms.

The sampling rate is 28.4kHz number of samples are therefore

$$N_{sample} = 28400 \cdot 0.02 = 568 \tag{D.14}$$

The N_{sample} samples of the voltage and current waveforms are computed with the FFT algorithm which return the DFT as shown in figure D.26(c) and D.26(d).

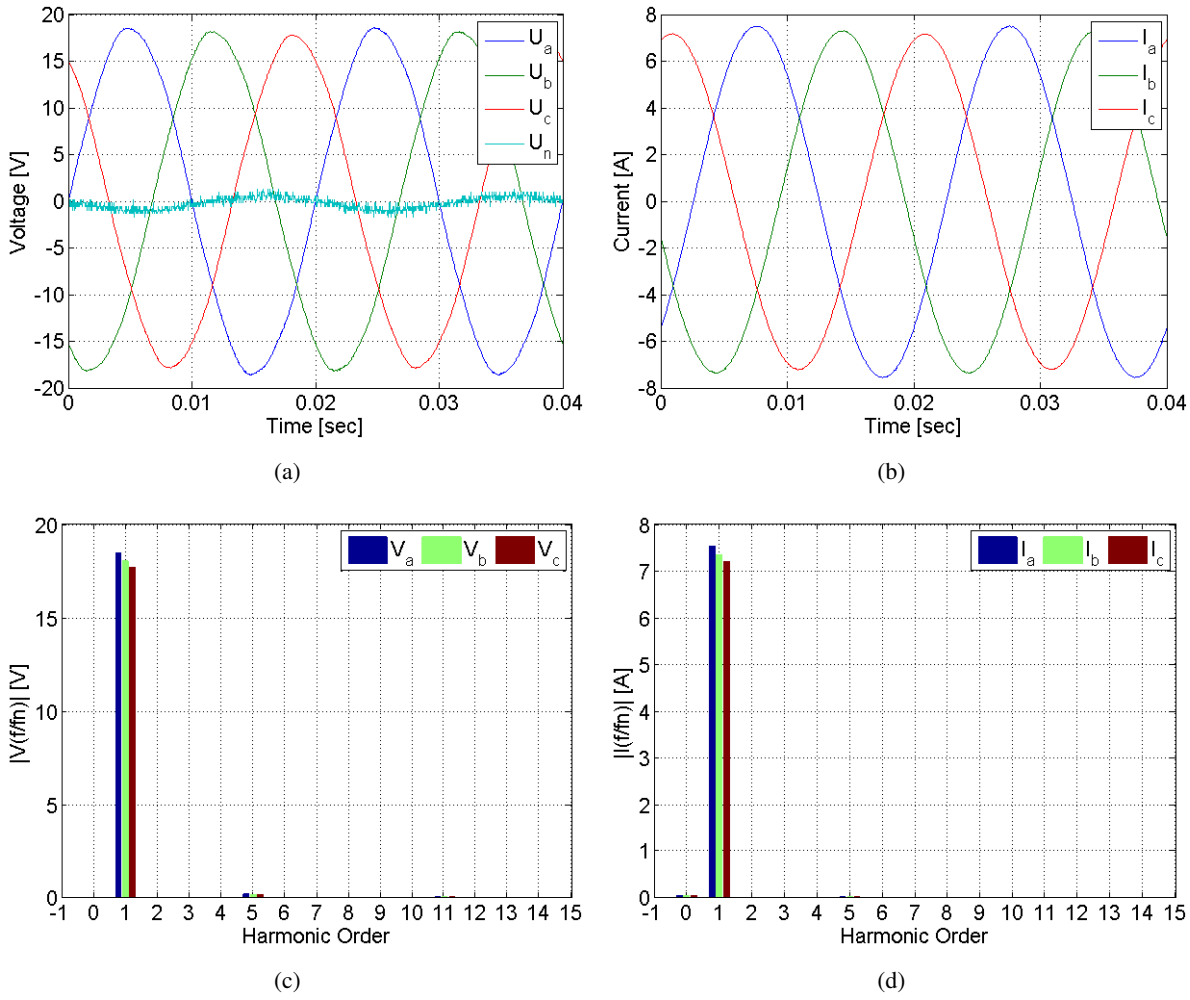

Figure D.26: Measured voltages and currents waveforms are shown in (a) and (b) corresponding frequency spectra are shown in (c) and (d), for the intact screen circuit.

From the DFT in figure D.26 it is seen that the fundamental frequency of 50Hz is domination the fifth and 11^{th} are negligible. Therefore it is concluded that the non-linearity of the auto transformer do not influence the results.

Sc-Sc fault in FLB (B-C, 1st link box)

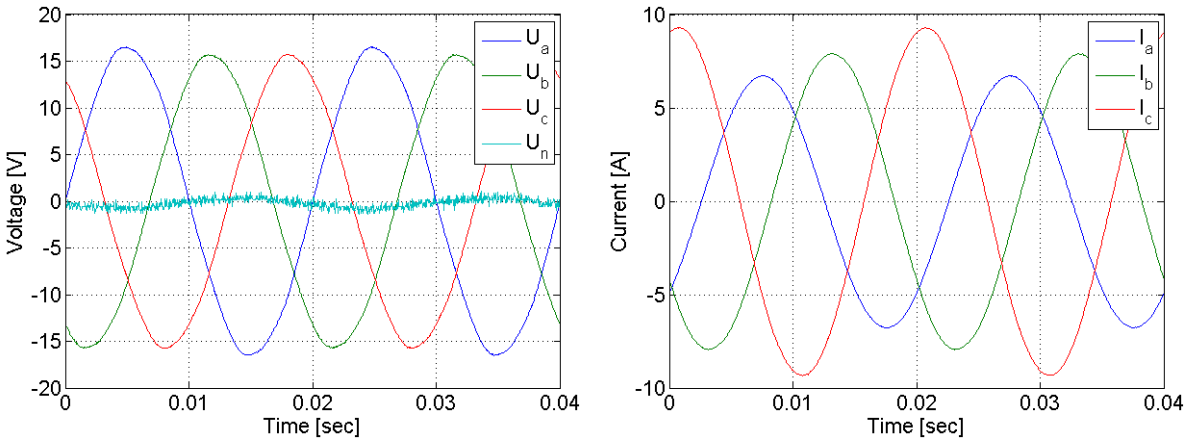

(a) (b)

Figure D.27: Measured voltage and current waveforms with a Sc-Sc fault at 2.6Ω in the FLB.

Figure D.27 shows that the screen voltages are balanced whereas the currents are unbalanced indicating that a two screen fault is present in a link box, according to the analysis in appendix A.

Sc-Gr fault in FLB (C-Gr, 1st link box)

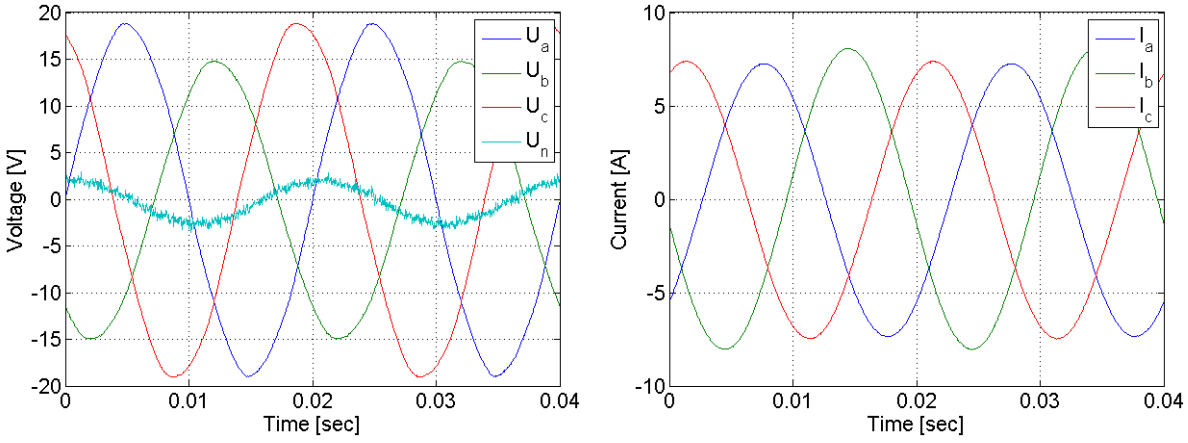

(a) (b)

Figure D.28: Measured voltage and current waveforms with a screen-ground fault at 2.6Ω in the first link box.

Figure D.28 shows that the phase currents are balanced and the voltages are unbalanced indicating that a single Sc-Gr fault is present in one of the link boxes, according to the analysis in appendix B. It should also be noted that the neutral voltage at the star connected sources also as increased indicating that a ground fault is present.

Sc-Sc fault in SLB (B-C, 2nd link box)

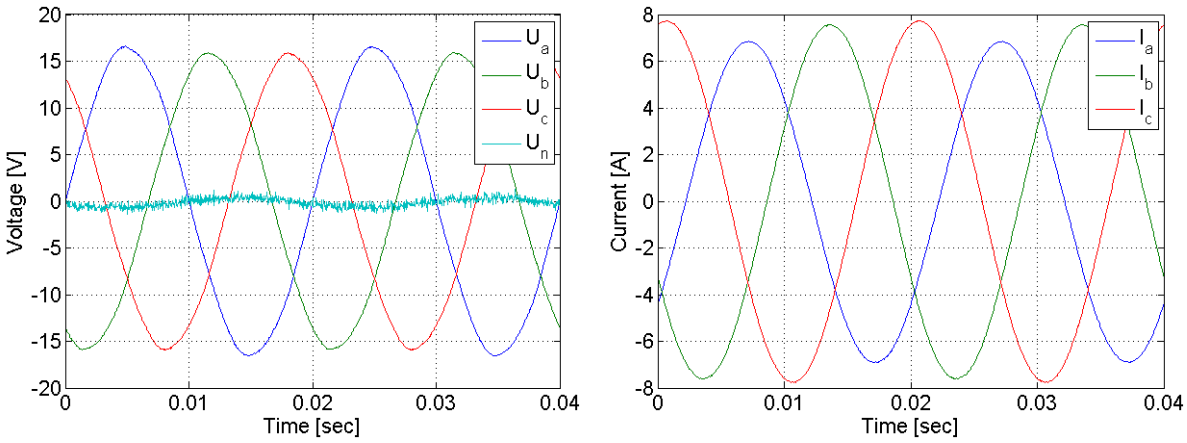

(a) (b)

Figure D.29: Measured voltages and currents waveforms with a Sc-Sc fault at 2.6Ω in the SLB.

Figure D.29 shows that the screen voltages are balanced whereas the currents are unbalanced indicating that a two screen fault is present in a link box, according to the analysis in appendix A.

Sc-Gr fault in SLB (C-Gr, 2nd link box)

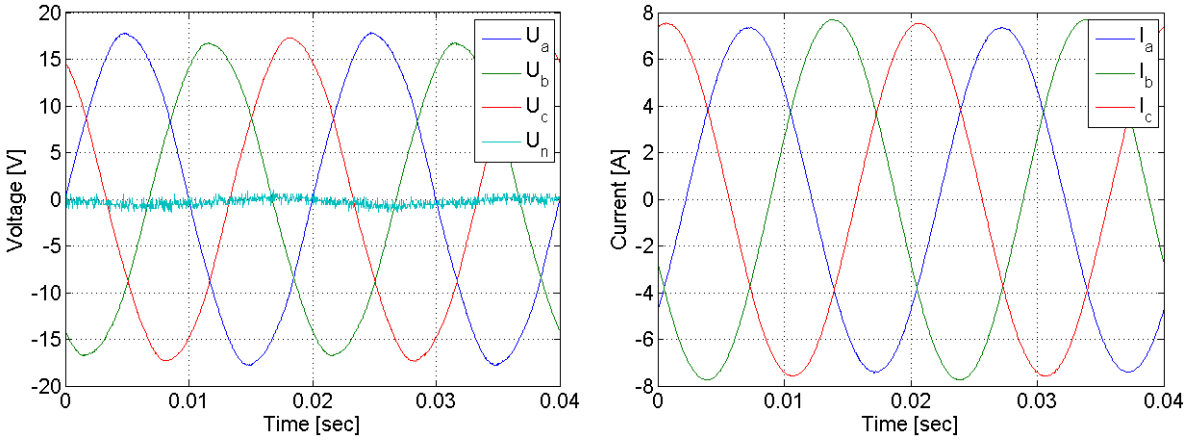

(a) (b)

Figure D.30: Measured voltages and currents waveforms with a Sc-Gr fault at 2.6Ω in the SLB.

Figure D.30 both the screen voltages and currents are balanced making it difficult to determine if the screen circuit is faulty or not. Because of the balanced screen voltages the neutral voltage at the star connected sources hasn't increased.

D.4 Field measurement #1 summary

From the waveforms recorded by the omicron it is observed that the harmonic content is so little that it will not influence the measurement.

From the measuring results from both the power analyzer and the omicron it can be seen that the screen circuit is close to symmetrical when no faults are applied.

When there is applied a Sc-Sc fault in the FLB it can be seen from table D.10 and the figures D.27(a) and D.27(b), that the currents become unsymmetrical but the voltages are symmetrical.

If there is applied a Sc-Gr fault in the FLB it can be seen from table D.16 and the figures D.28(a) and D.28(b), that the voltages become unsymmetrical and the currents are symmetrical.

For the SLB the Sc-Sc fault may be identified by the same characteristic in figure D.29(a) and D.29(b). Ground fault in the SLB is difficult to identify, for this case there it is observed, from figure D.30(a) and D.30(b), that both voltages and currents are close to symmetrical.

Appendix E

Field measurement #2 of the 150kV line between Frøstrup and Nors

Field measurement #2 is performed at the same, 150kV cable line as field measurement #1. A sketch of the cable line is shown in figure E.1, detailed description of the specific line may be found in the system description.

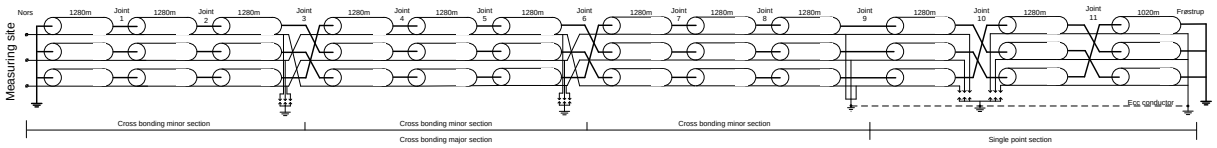

Figure E.1: Bonding schematic for the 150kV transmission line connection Frøstrup and Nors in the northern part of Jutland.

Field measurement #2 have three main purposes:

1 To study the three phase respons of the screen circuit from a sequence of single phase measurements
2 To study the influence for different fault resistances
3 To study the frequency respons of the screen circuit for a higher frequency then the fundamental 50Hz for this measurement 360Hz is applied.

The single phase measurements are performed in order to study the possibility of obtaining the three phase response of the screen circuit, from a sequence of single phase measurements. This is of interest because a three phased voltage source with changeable frequency was not available. A single phase measuring supply is available from the co-operation company, which have the option to change the frequency.

The increased frequency measurement is carried out in order to increase the healthy impedance of the screen circuit.

E.1 Planning field measurements #2 FRT-NOR

The measurements performed during field measurement #2 are divided into three sets. For all of the three sets the screen circuit is applied by AC voltage where the frequency is increased in steps from $30 - 360$Hz.

Both studies are performed for nine different screen conditions which are listed below.
SET 1:

- Healthy screen circuit

SET 2 - Faults in the first link box(FLB):

- (Sc-Sc) fault in the (FLB). (2.6Ω)
- (Sc-Gr) fault in the (FLB). (2.6Ω)
- (Sc-Sc) fault in the (FLB). (108Ω)
- (Sc-Gr) fault in the (FLB). (108Ω)

SET 3 - Faults in the second link box(SLB):

- (Sc-Sc) fault in the (SLB). (2.6Ω)
- (Sc-Gr) fault in the (SLB). (2.6Ω)
- (Sc-Sc) fault in the (SLB). (108Ω)
- (Sc-Gr) fault in the (SLB). (108Ω)

Each screen condition include six measurements, three used for determination of equivalent phase impedances and three used to obtain the three phased voltage response of the circuit.

For all five conditions and a sequence of seven frequencies are applied and recorded. The frequencies are $30, 70, 90, 210, 260, 310, 360$Hz. The frequencies are chosen not to be multiplies of the operation frequency 50Hz, in order to avoid disturbances from the fundamental and harmonics of this.

E.1.1 Simulation model

Sc-Sc and Sc-Gr faults are simulated in both first and second link box as indicated in figure E.2. The faults are simulated with a fault resistance of 2.6Ω and 108Ω. The earthing resistance in first link box is 0.2Ω and in the second link box 7Ω as stated in the system description.

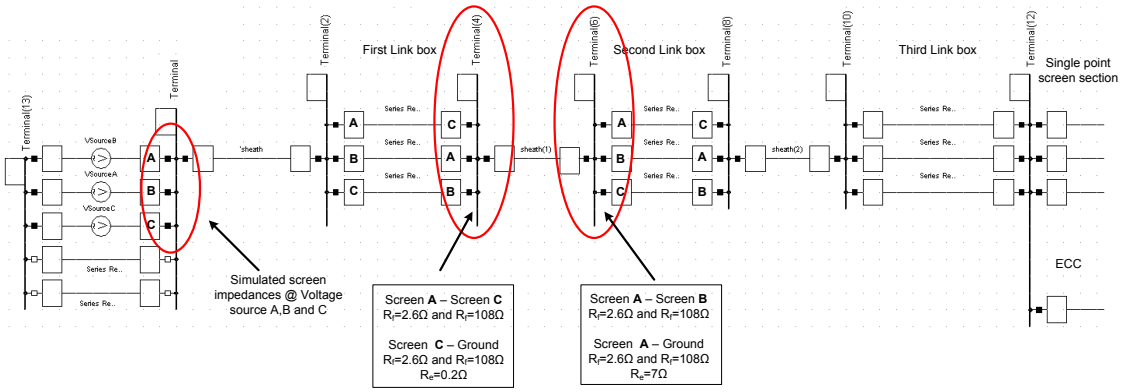

Figure E.2: Detail of figure C.13 in appendix C, showing the screen circuit and what terminals the faults are applied.

The voltage sources are set to following values.

$$\begin{aligned} V_{sourceA} &= 1\angle 0 \\ V_{sourceB} &= 1\angle -120 \\ V_{sourceC} &= 1\angle 120 \end{aligned} \quad [\text{kV}] \quad \text{(E.1)}$$

In the following the screen impedances are notated screen A, B and C. This corresponds to the screen impedance at voltage source A, B and C.

- (Sc-Sc) fault in FLB (terminal 4) is applied between screen **A** and **C**
- (Sc-Gr) fault in FLB (terminal 4) is applied to screen **C**, the fault resistance is respectively 2.8Ω and 108.2Ω
- (Sc-Sc) fault in SLB (terminal 6) is applied between screen **A** and **B**
- (Sc-Gr) fault in SLB (terminal 6) is applied to screen **A**, the fault resistance is respectively 9.6Ω and 115Ω

E.1.2 Simulation results

The following tables shows the simulated results at a fundamental frequency of 360Hz.

Healthy screen circuit

Healthy impedance	$\|Z\|$ [Ω]	ϕ [°]
Screen A	13.8	80.1
Screen B	14.0	78.3
Screen C	14.2	81.6

Table E.1: Simulated apparent impedances at 360Hz, healthy screen circuit.

Faults in FLB

Sc-Sc 2.6Ω FLB	$\|Z\|$ [Ω]	ϕ [°]
Screen A	4.5	35.1
Screen B	4.1	77.0
Screen C	15.0	77.5
Sc-Sc 108Ω FLB		
Screen A	14.2	73.8
Screen B	13.0	74.2
Screen C	14.3	81.6
Sc-Gr 2.8Ω FLB		
Screen A	15.1	82.3
Screen B	11.7	80.5
Screen C	14.3	75.9
Sc-Gr 108.2Ω FLB		
Screen A	13.9	81.2
Screen B	13.6	77.0
Screen C	14.4	80.9

Table E.2: Simulated results for fault cases in FLB, fundamental frequency is 360Hz.

Faults in SLB

Sc-Sc 2.6Ω SLB	$\|Z\|$ [Ω]	ϕ [°]
Screen A	8.3	81.6
Screen B	14.1	77.4
Screen C	9.8	59.5
Sc-Sc 108Ω SLB		
Screen A	13.5	78.8
Screen B	14.0	78.3
Screen C	14.4	79.8
Sc-Gr 9.6Ω SLB		
Screen A	12.3	81.4
Screen B	14.2	73.9
Screen C	15.1	83.0
Sc-Gr 115Ω SLB		
Screen A	13.5	79.4
Screen B	14.2	77.7
Screen C	14.3	82.4

Table E.3: Simulated results for fault cases in SLB, fundamental frequency is 360Hz.

E.2 Performing measurement #2

Date: 18.1.2012.
Location: 150kV HV station Nors, Buskkærvej 13, 7700 Thisted.
Participants: Morten Thule Hansen(AAU), Kasper Schultz Pedersen(AAU), Peter Rønne-Hansen (N1), Lars Brix (N1).

The measurements will be performed at the 150kV HV substation Nors, on the 150kV cable line FRT-NOR.

E.2.1 Measuring process

The cable line which is subject to measurement is just established and not taking into operation at the time. The cable line is intended to replace an excising OHL. During the test the OHL will be taking out of service for safety reasons. By disconnecting the existing OHL line the surrounding noise may also be reduced.

To achieve high safety when working at HV systems there is set up a process for the events and the order in which whey should be performed during the test.

The following list presents the order of events, which will be performed during the test:

1 The OHL is disconnected and de-energized by N1
2 The OHL is grounded and locked in both ends by N1
3 Measuring equipment are brought into the measuring site
4 The ground connections at the cable termination in Nors is disconnected se figure D.15
5 Possible induced screen voltages are measured according to ground, for safety reasons
6 Measuring SET 1 is performed
7 Measuring SET 2 is performed
8 Measuring SET 3 is performed
9 Ground connections at the cable terminations are re-established
10 The OHL grounding is removed by N1
11 The OHL is put into service by N1

E.2.2 Measuring setup

Field measurements #2 only includes single phase measurements. All measurements are supplied by the Omicron CPC100 and CP CU10 see figure E.11 and E.12. The CPC100 and CP CU10 setup, are only capable of supplying single phase, and may be controlled to apply a given voltage or a given current. For this test it is decided not to do measurements using the CPC100 but only perform measurements by the Omicron CMC365 see figure E.10. The CPC100 and CP CU10 are used only for power supply.

For each circuit condition there is performed six single phase measurements divided between two different measuring setup. The two measuring setup are referred to as measuring setup one and measuring setup two and shown in figure E.5 and E.7.

1 Measuring setup one is used for calculation of equivalent screen impedances see figure E.3. Three measuring combinations are performed to obtain all combinations of the screen circuit.

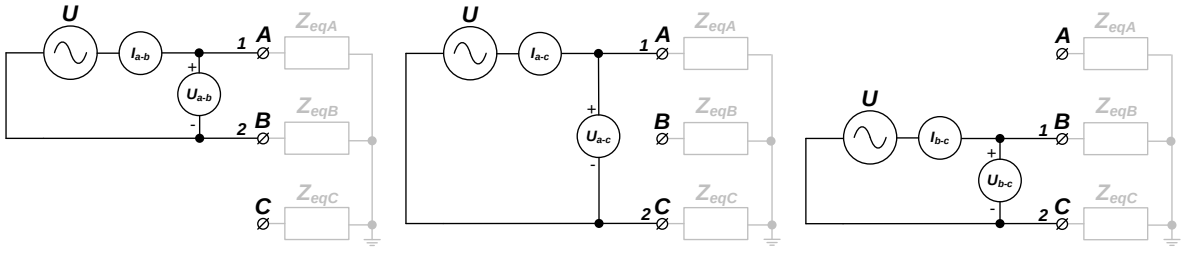

Figure E.3: Measuring setup for screen impedance measurements.

2 Measuring setup two is used for calculation of the three phase voltage response of the circuit, based on the super position method see figure E.4. The star point voltage is determined using equation E.2. Also the applied voltage is measured.

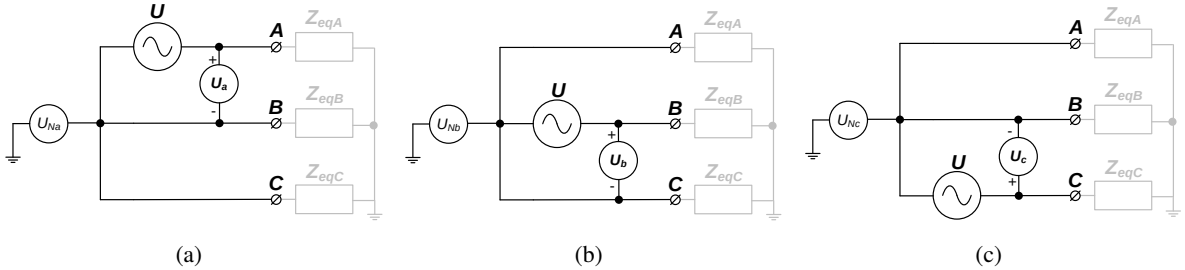

Figure E.4: Measuring setup for three phased voltage response, based on the super position method.

$$U_{star} = U_{Na} + U_{Nb} + U_{Nc} \tag{E.2}$$

Measuring setup one

Measuring setup one is shown in figure E.5. For this measuring setup the applied voltage and current are measured and recorded by the Omicron CMC356. The supply and measuring equipment are connected to the screen circuit in three different combinations: A-B, A-C or B-C. The connections are performed using the grounding box shown in figure E.13, the three different combinations are illustrated in figure E.6.

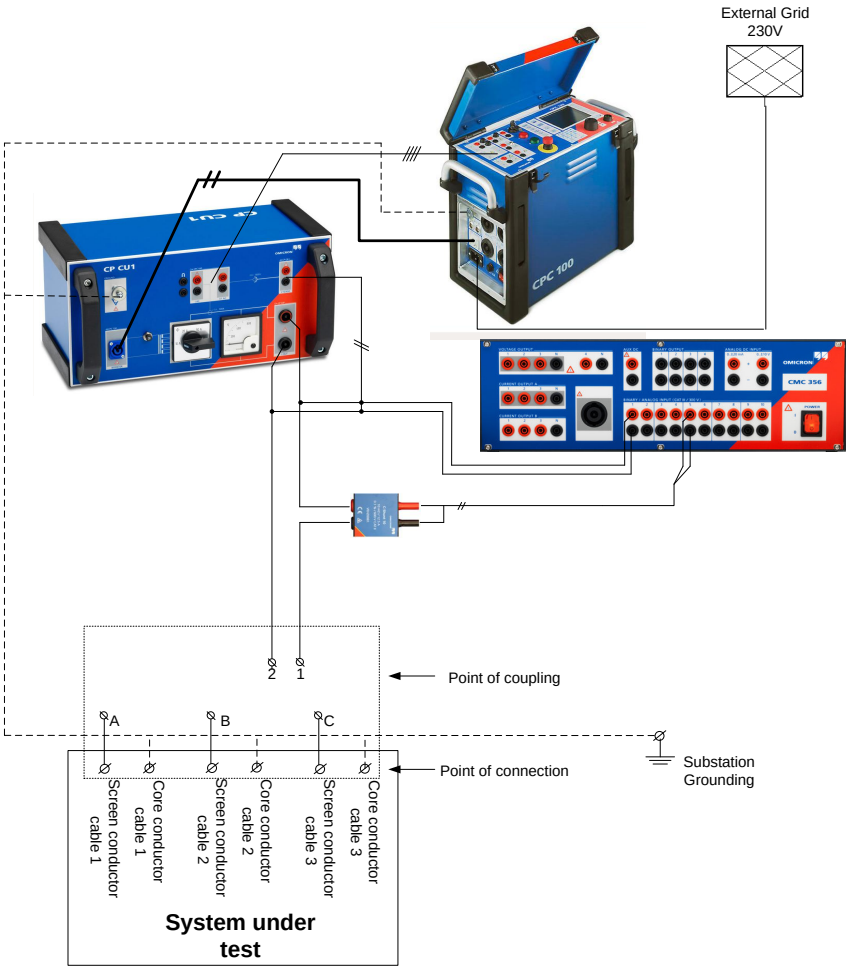

Figure E.5: Measurement setup one for field measurement #2 tests.

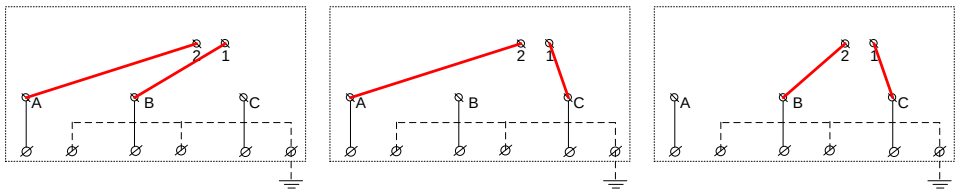

(a) (b) (c)

Figure E.6: The three combinations performed using measuring setup one. (a) Shows measuring of loop A-B. (b) Shows measuring of loop A-C. (c) Shows measuring of loop B-C.

Measuring setup two

Measuring setup two is the super position method see figure E.7. For this setup two voltages are measured and recorded by the Omicron CMC356 shown in figure E.10. The two voltages are: The applied voltage and the star point voltage according to ground as shown in figure E.7. The overall diagram of the measuring setup may be seen in figure E.7. The three connections are shown in figure E.8.

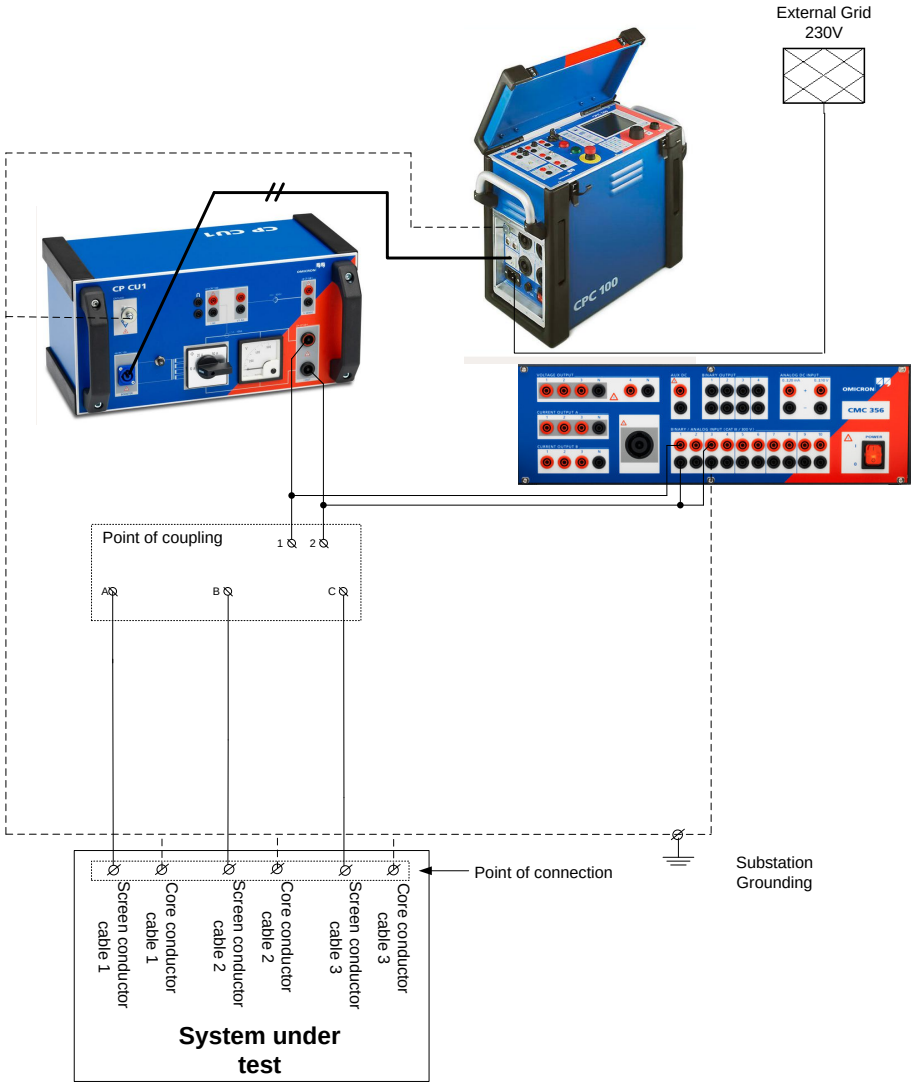

Figure E.7: Measurement setup two, for field measurement #2 tests.

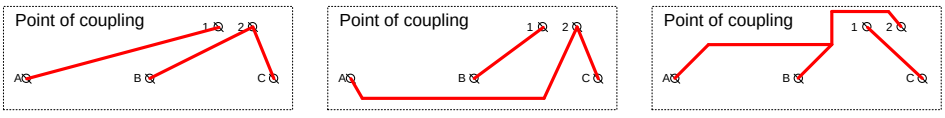

(a) (b) (c)

Figure E.8: The three connections performed using measuring setup two. (a) Shows measuring super position for source one. (b) Shows measuring super position for source two. (c) Shows measuring super position for source three.

As earlier explained the measuring setup is placed in substation Nors next to the cable termination as shown in figure E.9. The same non-magnetic tent that were used for field measurements #1 is again used for protection of the equipment from unlikely weather.

Figure E.9: Test setup in substation Nors, placed next to the cable termination.

The connections from the measuring equipment to the screen circuit are performed almost in the same way as were used for field measurements #1. The center conductors are grounded during the test, the grounding of the screen conductors are removed and connected to the grounding box using earthing cables.

Further illustrations of the connections to the cable screens, implementation of screen faults in the link boxes and grounding connections for the measuring connections may be found in field measurements #1, in Appendix D.

E.2.3 Measuring equipment

Table E.4 includes the instruments, which will be used for field measurement #2. Measuring setup one and two uses the same equipment.

Type	Producer	Model	AAU number
Universal relay test set	Omicron	CMC 365	owned by N1
Universal testing device	Omicron	CPC 100	owned by N1
Multifunctional coupling unit	Omicron	CP CU 1	owned by N1
Grounding box	Omicron	CP GB1	owned by N1
C-Shunt Precision shunts	Omicron	C-Shunt 10	owned by N1
Variable effect resistance 2.5Ω	Danotherm	2.5Ω slider	-
Variable effect resistance 100Ω	Danotherm	100Ω slider	-

Table E.4: Instruments used for FM 2.

The Omicron universal relay test set (CMC356) is connected to a PC which is equipped with Omicron test universe software.

Figure E.10: Omicron CMC356 Universal relay test set.

The Omicron universal testing device is programmed from the associated software to perform a scequence of measurements with defined frequency and voltage or current.

Figure E.11: Omicron CPC 100 Universal testing device.

The Omicron multifunctional coupling unit, generating the power supply for measurement. The unit is controlled from the Omicron CPC 100.

Figure E.12: Omicron CP CU 1 multifunctional coupling unit.

The CP GB1 grounding box including overvoltage protection which conducts to ground in case of overvoltages. The grounding box is used as **connection point** between the measuring equipment and the cable system as shown in figure E.5 and E.7.

Figure E.13: Omicron CP GB1 Grounding box.

The Omicron C-Shunt10 current shunts have a measuring range of $0-12.5$A. The shunt resistance is 10mΩ.

Figure E.14: Omicron C-shunt 10 current shunt.

E.2.4 Measuring accuracy

The purpose of the measurement is validation of screen condition determination. The analyses showed that a condition change may only affect the system impedance by a small value, relative to healthy circuit, therefore measurement accuracy is important. The measuring is influence by accuracy of the measuring equipment and the temperature at the measuring site.

Equipment accuracy

Measurements are performed using Omicron CMC356 as shown on figure E.5 and E.7 therefore the accuracy of the CMC356 is considered. Both current and voltage measurement are performed at the point of connection.

Accuracy of Omicron CMC356

The Omicron CMC356 is capable for measuring voltages in the range of $0-600$V [5]. This means that the voltage can be measured directly without using any probes from the connection point in figure E.5 and E.7. The voltage measurement is therefore only influenced by the accuracy of the voltage inputs. The typical accuracy of the omicron is by the reference manual [5] found to:

$$\pm 0.06\%rdg \tag{E.3}$$

Where:
- rdg means reading.

The current is measured using current shunts shown in figure E.14. The used current shunts has a maximum ability of 12.5A which is converted to 125mV. The current measurement is influenced by both the accuracy of the current shunt and the accuracy of the voltage input of the Omicron. The two accuracies shall be added in order to determine the worst case accuracy.
The accuracy of the current shunts are $\pm 0.1\%$ and the accuracy of the voltage input is $\pm 0.06\%rdg$. The total accuracy is therefore determined to $\pm 0.16\%$ using the min/max method.

Measurement	Probe division	Probe accuracy	Omicron CMC356
Voltage phase A	no probe	-	$\pm 0.06\%rdg$
Voltage phase B	no probe	-	$\pm 0.06\%rdg$
Voltage phase C	no probe	-	$\pm 0.06\%rdg$
Current phase A	12.5A/125mV	$\pm 0.1\%$	$\pm 0.16\%rdg$
Current phase B	12.5A/125mV	$\pm 0.1\%$	$\pm 0.16\%rdg$
Current phase C	12.5A/125mV	$\pm 0.1\%$	$\pm 0.16\%rdg$

Table E.5: Accuracy of the Omicron CMC356.

In order to relate the relative accuracies in table E.5 to real quantities there are made a calculation example. For the example the accuracies for voltage and current given in table E.5 are used. The example is based in the measurements performed on the healthy screen circuit.

Accuracy of the measured voltage is calculated using equation E.4.

$$U_A = \pm 0.0006 \cdot 156.2 = \pm 93.7\text{mV} \tag{E.4}$$

Accuracy of the measured current is calculated using equation E.5.

$$I_A = \pm 0.0016 \cdot 5.1 = \pm 8.16\text{mA} \tag{E.5}$$

For this thesis the impedance is the parameter of most interest. The impedance is calculated based on the measured voltage and current. In the case where the impedance calculation is based on one voltage and one current measurement the resulting worst case accuracy is the sum of the accuracies for the voltage and current respectively.
For this test the accuracy of the impedance would be $\pm 0.22\%$.

When the impedance calculation is based on the sum of several voltage and current measurements, the total accuracy is the sum of the accuracy of each single measurement. An example could be the star point voltage calculated by equation E.2. For this parameter three values are measured to obtain one voltage, for this voltage the resulting accuracy is the sum of the accuracies of each measurement.

$$A_{U_{star}} = A_{U_{Na}} + A_{U_{Nb}} + A_{U_{Nc}} \tag{E.6}$$

Where:
A_x is the accuracy of the subscript x.

For the star point voltage the accuracy may be calculated by equation E.6 to: $0.06 + 0.06 + 0.06 = \pm 0.18\%$.

The apparent impedances are calculated based on 12 measurements. The worst case accuracy of the measurements are 1.02% including the accuracy of the current shunts. Even though a number of calculations are performed the total apparent impedance accuracy is expected lower than 2%.

E.3 Measurement results

As described earlier each measuring case consists of two different test setup and the total number of measurements are six. The measurements are subdivided onto three measurements which includes the source-voltage and current, as shown in figure E.5 and three measurement witch include the source-voltage and star point to ground voltage, as shown in figure E.7. Measuring results may be found at the CD in folder *Nors 18-01-2012*.

Valid for all six measurements are that they are recorded for a period of 14 seconds. Each record consists of seven different fundamental frequencies. The fundamental frequency is changed every two seconds. The fundamental frequencies are:

Time [Sec]	Fundamental frequency [Hz]
0 – 2	30
2 – 4	70
4 – 6	90
6 – 8	210
8 – 10	260
10 – 12	310
12 – 14	360

Table E.6: Fundamental frequencies for each recording.

The CPC 100 is delivering 10A at the first five fundamental frequencies and 5A at the two highest fundamental frequencies.

In figure E.15 is the waveforms of the voltage and the current shown. The measured waveforms are recorded with CMC 356 as shown in the test setup in figure E.5. The recorded voltage is measured between screen ***A*** and ***B*** and the recorded current is measured in screen ***A***, as shown in figure E.3(a). No fault is present in the screen circuit.

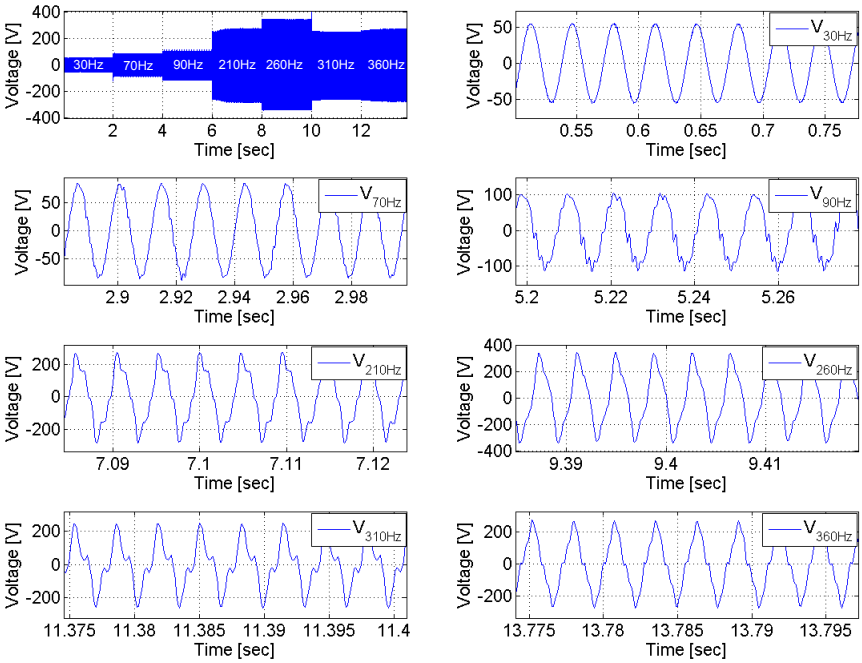

(a)

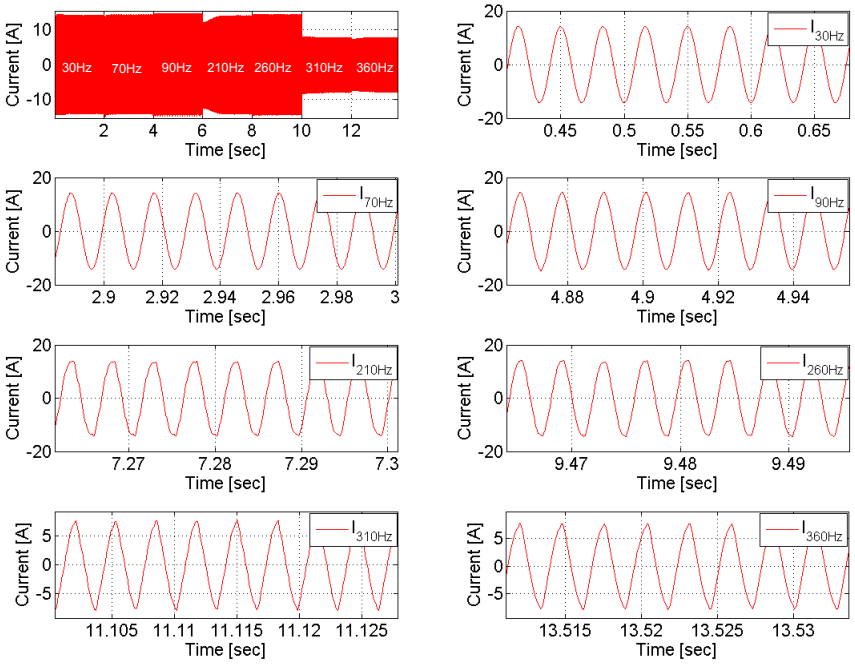

(b)

Figure E.15: (a) Measured voltage between screen ***A*** and ***B***. (b) Measured current when screen ***A*** and ***B*** are connected. No fault is present in the screen circuit.

As the above figures illustrates the current and especially the voltage waveforms consists not only of the fundamental frequency but also harmonics of higher order.

In order to determine the harmonic contents of the signals a discrete Fourier transform (DFT) is used. An efficient algorithm to compute the frequency content is a fast Fourier transform (FFT) [32, p.526].

The time window of the FFT is one period of the fundamental frequency, hence 30Hz will have a window of 33.3ms and 360Hz a window of 2.78ms.
The sampling rate of the recorded waveforms are 9.5kHz.
In order to reconstruct a continuous signal more than two samples per period is need [19, p.208]. The highest order of harmonic that can be reconstructed for the 360Hz measurements are therefore.

$$\text{Max harmonic order} = \frac{\text{samplings rate} \cdot \text{period time}}{2} = \frac{9500 \cdot 0.00278}{2} = 13.2 \Rightarrow 13 \tag{E.7}$$

The result of the FFT analysis is shown in figure E.16. The figure illustrate the frequency content of the seven fundamental frequencies listed in table E.6. The figures illustrate the harmonic content up to the order of 13.

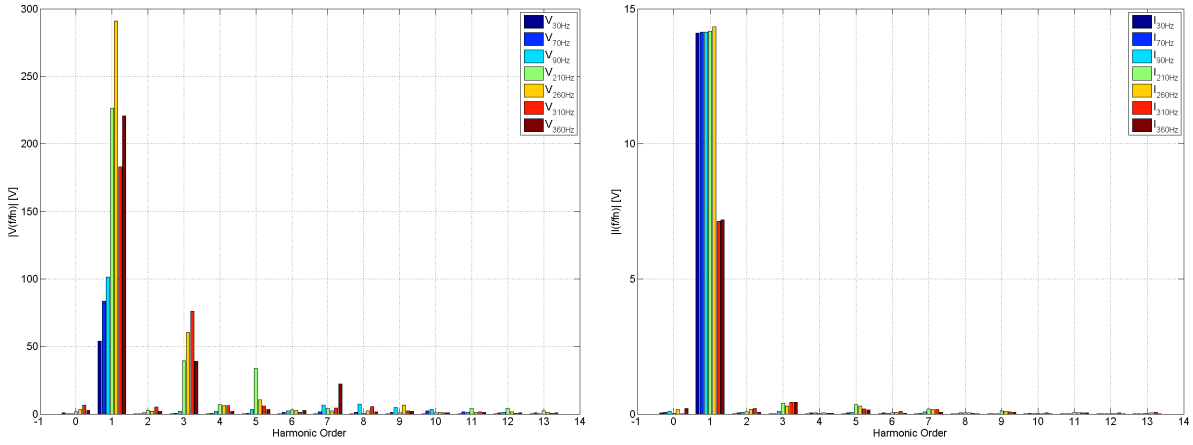

(a) (b)

Figure E.16: Frequency content of the measured voltage and current for the healthy screen circuit.

Harmonics of orders 3, 5 and 7 is the most dominating harmonics.

In order to use the measurement results for the further processing these need to be filtered so that only the fundamental frequency is left. In order to do so the recorded data will be filtered with peak filters, which is inverted notch filters. Seven filters are made each tuned to one fundamental frequency 30, 70, 90, 210, 260, 310 and 360Hz respectively.

The filters are made in MATLAB by using the toolbox ' Filter Design '. A screenshot of the design for the peak filter tuned at 360Hz and the filter response is shown in figure E.17.

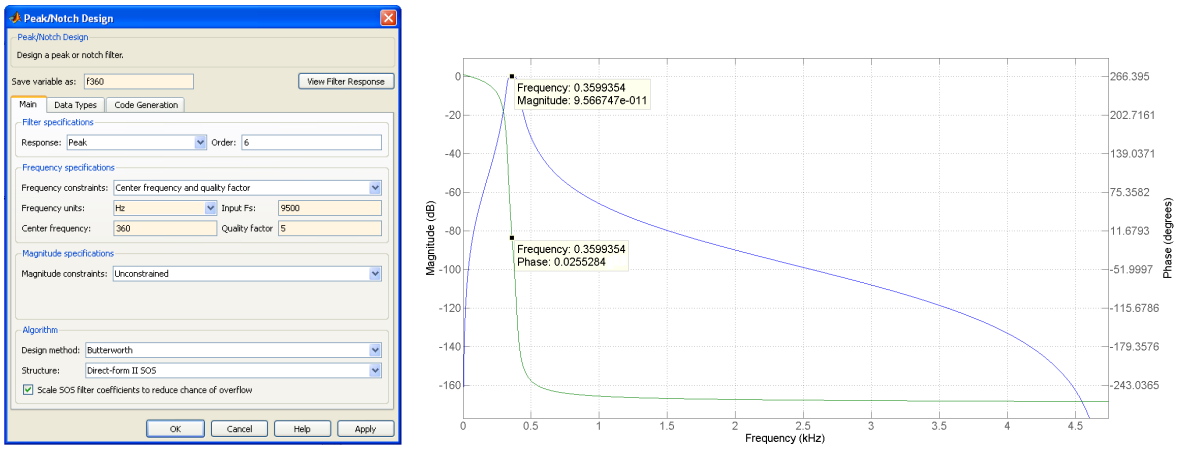

(a) (b)

Figure E.17: (a) Screenshot of the filter builder tool in MATLAB. (b) Filter response of a peak filter tuned at 360Hz.

The recorded data from figure E.15 has been filtered and the result is shown in figure E.18.

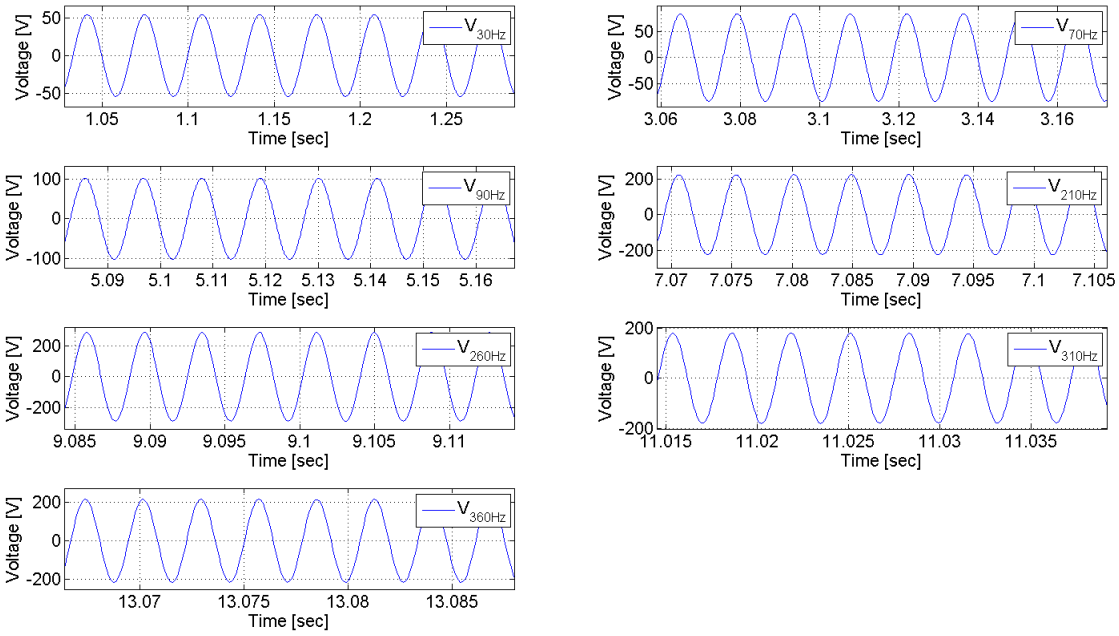

(a)

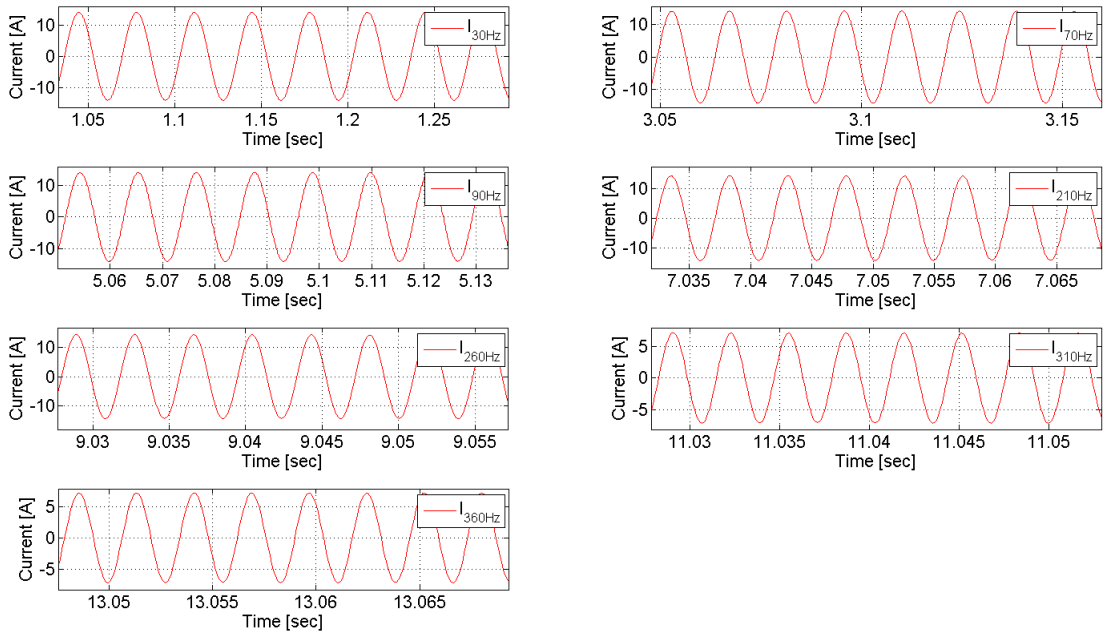

(b)

Figure E.18: (a) Measured voltage between screen ***A*** and ***B*** after filtering. (b) Corresponding current in screen ***A*** and ***B*** after filtering. No fault is present in the screen circuit.

A record of 500ms for each of the seven frequency samples have been filtered. The filtered data is used to calculate the effective values (RMS value) of the respective voltage and currents and the phase shift between these. The following figure shows a section of the syntax that calculates the above mentioned RMS-values and phase shift.

```
for i = 1:7
Vfrms(i) = sqrt(mean(Vaa(:,N,i).^2));                    %Calc RMS voltage 7 freq.
Ifrms(i) = sqrt(mean(Iaa(:,N,i).^2));                    %Calc RMS current 7 freq.

V(:,i) = Vaa(:,N,i);                                     %Converting matrix :x3 => :x2
I(:,i) = Iaa(:,N,i);                                     %Converting matrix :x3 => :x2

for j = 1:max(size(V))
   VI(j,i) = V(i)*I(i);
end

for j = 1:1:max(size(V))
   VV(j,i) = V(i)*V(i);
end

for j = 1:1:max(size(V))
   II(j,i) = I(i)*I(i);
end

VImean(i) = mean(VI(:,i))                                %average value of V*I
VVmean(i) = mean(VV(:,i))                                %average value of V^2
IImean(i) = mean(II(:,i))                                %average value of I^2

cosT(i) = VImean(i)/sqrt(VVmean(i)*IImean(i));        %calc cos(phi) by using the cross correlation factor
end

angleRad = acos(cosT);                                   %Calc phi [rad]

for i = 1:7
[peak sample] = max(V(1000:2000,i));                %Finding positiv peak @V
if angleRad(i) == 0                                      %If phase shift = 0 do nothing
    angleRad(i) = angleRad(i);
elseif 0<(I(1000+sample+1,i)-I(1000+sample,i))  %check if I is leading or lagging V
    angleRad(i) = -angleRad(i);
end
end
```

The theoretical approach presented in [12] to calculate the average phase shift (Φ) between two signals has been adapted here to calculate the phase shift between the two filtered column vectors.

The complex cross correlation coefficient is defined as [12],[31, p. 124]:

$$\Gamma = \frac{< VI^* >}{\sqrt{< |V^2| >< |I^2| >}} \tag{E.8}$$

Where V and I are the complex representation of the amplitudes of the voltage and current, respectively. In this case are the amplitudes represented as real numbers only and the conjugation between V and I, denote * in E.8 has therefore no effect. E.8 holds true if and only if the mean values of the signals are 0 [31, p. 124].

The cross correlation factor gives a measure of dependence between two signals. $-1 \leq \Gamma \geq 1$ in case $< VI^* >= 0$ the signals are *orthogonal* [31, p. 124], hence $\Gamma = 0$. If the correlation factor for V and I is unity then is the correlation between the signals good, meaning that if V increases in value I will do the same and vice versa analogue to $\Phi = 0$. On the other hand if $\Gamma = -1$, means that V and I is inverted. Then V increases in value I will decrease, hence $\Phi = \pi$.
Since the correlation factor in this case only consists og real numbers it does not provide any information about I is leading or lagging V. To overcome this the waveforms are analyzed, which will be done later.

The average values of the filtered signals are calculated using:[12]

$$< VI >= \frac{1}{N}\sum_{i=1}^{N} V_i I_i \tag{E.9}$$

$$< \left|V^2\right| >= \frac{1}{N}\sum_{i=1}^{N} |V_i|^2 \tag{E.10}$$

$$< \left|I^2\right| >= \frac{1}{N}\sum_{i=1}^{N} |I_i|^2 \tag{E.11}$$

[12] states that the average power factor between V and I is equal to the magnitude of Γ, hence $|\Gamma| = cos(\Phi)$.

It is now checked if I is leading or lagging V the following steps are performed:

- Finding a sample (n_{peak}) there V have a peak
- Use n_{peak} and $n_{peak} + 1$ to check the slope (α) of I
- If α is positive I is lagging V
- If α is negative I is leading V

As earlier mentioned six measurements are needed in order to calculate the apparent impedances of the phases. In the table below is shown the RMS values, from the measurements with a fundamental frequency of 360Hz

Measurement	U [V]	U_N [V]	I [A]	ϕ [°] (ref. U)
Screen A-B	156.2	-	5.1	-80.7
Screen B-C	153.8	-	5.1	-80.8
Screen A-C	155.4	-	5.1	-80.7
Screen A	116.9	40.0	-	-179.4
Screen B	115.7	38.0	-	-179.5
Screen C	115.6	38.4	-	-179.9

Table E.7: Measurement results of the 360Hz measurements

E.3.1 Analysis of field measurements

Using the six single phase measurement results in table E.7, it is possible to calculate the apparent impedances of the screen circuit and compare this, to the simulation results performed in section E.1.2. The procedure for calculation the apparent impedances are shown and explained in the following.

Screen impedances are calculated from the measurements shown in figure E.19.

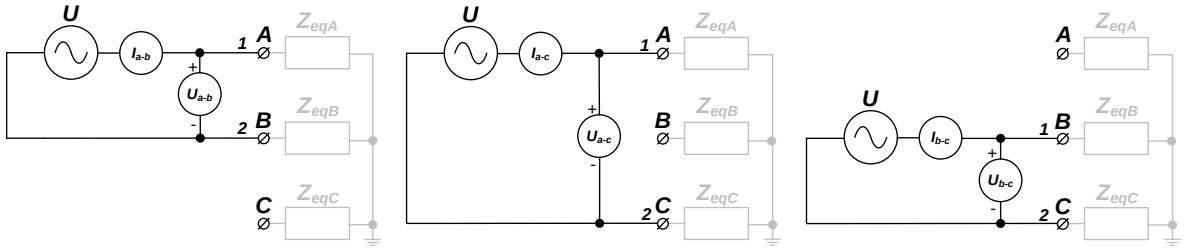

(a) (b) (c)

Figure E.19: Measuring setup for screen impedance measurements.

Screen **A-B** impedance:

$$\mathbf{Z_{A-B}} = \frac{U\angle 0}{I\angle\phi} = \frac{156.2\angle 0}{5.1\angle -80.7} = 30.6\angle 80.7 \quad [\Omega] \quad \text{(E.12)}$$

Screen **B-C** impedance:

$$\mathbf{Z_{B-C}} = \frac{U\angle 0}{I\angle\phi} = \frac{153.8\angle 0}{5.1\angle -80.8} = 30.2\angle 80.8 \quad [\Omega] \quad \text{(E.13)}$$

Screen **A-C** impedance:

$$\mathbf{Z_{A-C}} = \frac{U\angle 0}{I\angle\phi} = \frac{155.4\angle 0}{5.1\angle -80.7} = 30.5\angle 80.7 \quad [\Omega] \quad \text{(E.14)}$$

Calculation of the equivalent phase impedances will now be done.

The three impedances in the above equations are the sum of two equivalent screen impedances, as shown in equation E.15.

$$\begin{aligned} \mathbf{Z_{A-B}} &= \mathbf{Z_{eqA}} + \mathbf{Z_{eqB}} \\ \mathbf{Z_{A-C}} &= \mathbf{Z_{eqA}} + \mathbf{Z_{eqC}} \\ \mathbf{Z_{B-C}} &= \mathbf{Z_{eqB}} + \mathbf{Z_{eqC}} \end{aligned} \quad [\Omega] \quad \text{(E.15)}$$

Solving the three equations with three unknowns the equivalent screen impedances may be determined.

By isolation and rearranging of the equations in E.15, $\mathbf{Z_{eqA}}$, $\mathbf{Z_{eqB}}$ and $\mathbf{Z_{eqC}}$ are determined.

$$\begin{array}{rcl} \mathbf{Z_{eqA}} & = & \frac{1}{2}\cdot(\mathbf{Z_{A-B}}+\mathbf{Z_{A-C}}-\mathbf{Z_{B-C}}) \\ \mathbf{Z_{eqB}} & = & \mathbf{Z_{A-B}}-\mathbf{Z_A} \\ \mathbf{Z_{eqC}} & = & \mathbf{Z_{B-C}}-\mathbf{Z_B} \end{array} \quad [\Omega] \quad \text{(E.16)}$$

$$\begin{array}{rcl} \mathbf{Z_{eqA}} & = & 15.4\angle 80.6 \\ \mathbf{Z_{eqB}} & = & 15.1\angle 80.8 \\ \mathbf{Z_{eqC}} & = & 15.0\angle 80.8 \end{array} \quad [\Omega] \quad \text{(E.17)}$$

Equation E.17 are the equivalent impedances of the circuit.

The super position principle is used to determine the currents based on the above calculated impedances. For this calculation it is essential which voltage there is applied. The applied voltages are the last three voltages U in table E.7. The voltages are phase shifted so that they represent a three phased voltage source, as shown in equation E.18.

$$\begin{array}{rcl} \mathbf{U_a} & = & 116.9\angle 0 \\ \mathbf{U_b} & = & 115.7\angle -120 \\ \mathbf{U_c} & = & 115.6\angle 120 \end{array} \quad [\mathrm{V}] \quad \text{(E.18)}$$

Using the applied voltages, the super position principle is applied. The three currents corresponding to each voltage source are determined as shown in figure E.20.

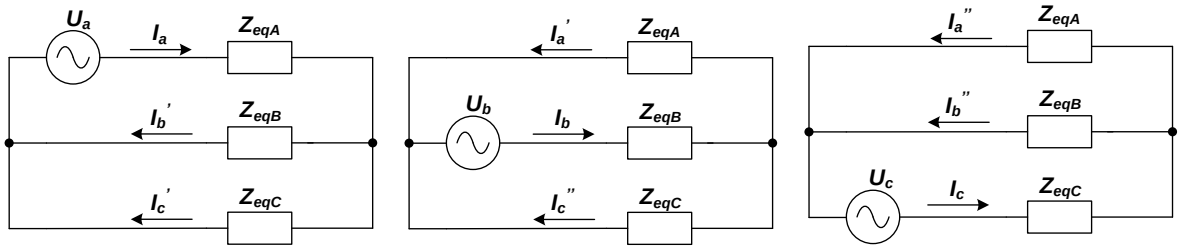

(a) (b) (c)

Figure E.20: Screen circuits used for current calculations.

Voltage applied to screen **A** whereas screen **B** and **C** are short circuited.

$$\begin{array}{rcl} \mathbf{I_a} & = & \frac{\mathbf{U_a}}{\mathbf{Z_{eqA}}+\left(\mathbf{Z_{eqB}}||\mathbf{Z_{eqC}}\right)} = 5.1\angle -80.7 \\ \mathbf{I_b'} & = & \mathbf{I_a}\cdot\frac{\mathbf{Z_{eqC}}}{\mathbf{Z_{eqB}}+\mathbf{Z_{eqC}}} = 2.5\angle -80.7 \\ \mathbf{I_c'} & = & \mathbf{I_a}\cdot\frac{\mathbf{Z_{eqB}}}{\mathbf{Z_{eqB}}+\mathbf{Z_{eqC}}} = 2.5\angle -80.7 \end{array} \quad [\mathrm{A}] \quad \text{(E.19)}$$

Voltage applied to screen **B** whereas screen **A** and **C** are short circuited.

$$\begin{array}{rcl} \mathbf{I_b} & = & \frac{\mathbf{U_b}}{\mathbf{Z_{eqB}}+\left(\mathbf{Z_{eqA}}||\mathbf{Z_{eqC}}\right)} = 5.1\angle 159.2 \\ \mathbf{I_a^{'}} & = & \mathbf{I_b}\cdot\frac{\mathbf{Z_{eqC}}}{\mathbf{Z_{eqA}}+\mathbf{Z_{eqC}}} = 2.5\angle 159.3 \\ \mathbf{I_c^{''}} & = & \mathbf{I_b}\cdot\frac{\mathbf{Z_{eqA}}}{\mathbf{Z_{eqA}}+\mathbf{Z_{eqC}}} = 2.6\angle 159.1 \end{array} \quad [\mathrm{A}] \quad \text{(E.20)}$$

Voltage applied to screen **C** whereas screen **B** and **C** are short circuited.

$$\begin{array}{rcl} \mathbf{I_c} & = & \frac{\mathbf{U_c}}{\mathbf{Z_{eqB}}+\left(\mathbf{Z_{eqA}}||\mathbf{Z_{eqB}}\right)} = 5.1\angle 39.2 \\ \mathbf{I_a^{''}} & = & \mathbf{I_c}\cdot\frac{\mathbf{Z_{eqB}}}{\mathbf{Z_{eqA}}+\mathbf{Z_{eqB}}} = 2.5\angle 39.3 \\ \mathbf{I_b^{''}} & = & \mathbf{I_c}\cdot\frac{\mathbf{Z_{eqA}}}{\mathbf{Z_{eqA}}+\mathbf{Z_{eqB}}} = 2.6\angle 39.1 \end{array} \quad [\mathrm{A}] \quad \text{(E.21)}$$

The three phased representation is the sum of the above calculated screen currents.

$$\begin{array}{rcl} \mathbf{I_{a,tot}} & = & \mathbf{I_a}-\mathbf{I_a^{'}}-\mathbf{I_a^{''}} = 7.6\angle -80.9 \\ \mathbf{I_{b,tot}} & = & \mathbf{I_b}-\mathbf{I_b^{'}}-\mathbf{I_b^{''}} = 7.6\angle 159.4 \\ \mathbf{I_{c,tot}} & = & \mathbf{I_c}-\mathbf{I_c^{'}}-\mathbf{I_c^{''}} = 7.7\angle 39.1 \end{array} \quad [\mathrm{A}] \quad \text{(E.22)}$$

Finally the neutral voltage at the voltage sources start point is calculated.

$$\begin{array}{c} \mathbf{U_N} = \mathbf{U_{NA}}+\mathbf{U_{NB}}+\mathbf{U_{NC}} = 2.1\angle -164.4 \\ \mathbf{U_N} = 40\angle -179.4+38\angle(-179.5-120)+38.4\angle(-179.9+120) = 2.1\angle -164.4 \end{array} \quad [\mathrm{V}] \quad \text{(E.23)}$$

The apparent impedances with no fault at the screen circuit may now be determined. This is done by adding the star point voltage to the three source voltages. The resulting voltages are divided by the total current.

$$\begin{array}{rcccl} \mathbf{Z_A} & = & \frac{\mathbf{U_N}+\mathbf{U_A}}{\mathbf{I_{a,tot}}} & = & 15.1\angle 80.6 \\ \mathbf{Z_B} & = & \frac{\mathbf{U_N}+\mathbf{U_B}}{\mathbf{I_{b,tot}}} & = & 15.3\angle 79.9 \\ \mathbf{Z_C} & = & \frac{\mathbf{U_N}+\mathbf{U_C}}{\mathbf{I_{c,tot}}} & = & 15.2\angle 82.0 \end{array} \quad [\Omega] \quad \text{(E.24)}$$

E.3.2 Calculation of measuring results

In the following tables are the measuring results with a fundamental frequency of 360Hz presented. All the shown impedances are processed in the same way as the calculated impedances showed in subsection E.3.1.

Healthy screen circuit

Apparent impedance	$\|Z\|$ [Ω]	ϕ [°]
Screen A	15.1	80.6
Screen B	15.3	79.9
Screen C	15.2	82.0

Table E.8: Measured screen impedances at 360Hz, healthy screen circuit.

Fault cases in FLB

Sc-Sc 2.6Ω FLB	$\|Z\|$ [Ω]	ϕ [°]
Screen A	8.3	81.6
Screen B	14.1	77.4
Screen C	9.8	59.5
Sc-Sc 108Ω FLB		
Screen A	13.5	78.8
Screen B	14.0	78.3
Screen C	14.4	79.8
Sc-Gr 2.6Ω FLB		
Screen A	12.3	81.4
Screen B	14.2	73.9
Screen C	15.1	83.0
Sc-Gr 108Ω FLB		
Screen A	13.5	79.4
Screen B	14.2	77.7
Screen C	14.3	82.4

Table E.9: Measuring results for fault cases in FLB, fundamental frequency is 360Hz.

Fault cases in SLB

Sc-Sc 2.6Ω SLB	$\|Z\|$ [Ω]	ϕ [°]
Screen A	9.5	85.2
Screen B	15.1	78.8
Screen C	11.1	60.2
Sc-Sc 108Ω SLB		
Screen A	14.7	79.1
Screen B	15.3	79.8
Screen C	15.3	79.9
Sc-Gr 2.6Ω SLB		
Screen A	13.1	80.2
Screen B	15.5	76.0
Screen C	16.0	83.3
Sc-Gr 108Ω SLB		
Screen A	14.9	80.2
Screen B	15.2	79.6
Screen C	15.3	81.8

Table E.10: Measuring results for fault cases in SLB, fundamental frequency is 360Hz.

E.3.3 Calculation of deviations

This section deals with the deviations between the healthy screen circuit and the faulty screen circuit at a fundamental frequency of 360Hz.
Also the deviations between the measured and simulated results at healthy state are evaluated. The comparison is used to determine if the simulation model is useful or not.

$$\begin{aligned} |Z|_{deviation} &= \frac{|Z|_{measured} - |Z|_{simulated}}{|Z|_{simulated}} \cdot 100 \\ \phi_{deviation} &= \frac{\phi_{measured} - \phi_{simulated}}{\phi_{simulated}} \cdot 100 \end{aligned} \quad [\%] \quad \text{(E.25)}$$

Above equations are used for calculating the deviation between the measured and simulated results for the healthy screen circuit, deviation may be seen in table E.11.

Screen	$\lvert Z\rvert$ [%]	ϕ [%]
A	9.4	0.6
B	9.3	2.0
C	7.0	0.5

Table E.11: Deviation between the measured and simulated results for the healthy screen circuit. Fundamental frequency is 360Hz

In the following tables are the deviation between the healthy and faulty screen circuit calculated using equation E.26.

$$\begin{aligned} |Z|_{deviation,measured} &= \frac{|Z|_{meas.app.imp.} - |Z|_{healthy-meas}}{|Z|_{healthy-meas}} \cdot 100 \\ \phi_{deviation,measured} &= \frac{\phi_{meas.app.imp.} - \phi_{healthy-meas}}{\phi_{healthy-meas}} \cdot 100 \\ |Z|_{deviation,simulated} &= \frac{|Z|_{sim.app.imp.} - |Z|_{healthy-sim}}{|Z|_{healthy-sim}} \cdot 100 \\ \phi_{deviation,simulated} &= \frac{\phi_{sim.app.imp.} - \phi_{healthy-sim}}{\phi_{healthy-sim}} \cdot 100 \end{aligned} \quad [\%] \quad \text{(E.26)}$$

Deviation for fault cases in FLB.

Sc-Sc 2.6Ω FLB	Deviation measured $\|Z\|$ [%]	Deviation measured ϕ [%]	Deviation simulated $\|Z\|$[%]	Deviation simulated ϕ[%]
A	-53.0	1.2	-67.4	-56.2
B	-61.4	-3.1	-70.7	-1.7
C	1.3	-27.4	5.6	-5.0
Sc-Sc 108Ω FLB				
A	2.0	-2.2	2.9	-7.9
B	-8.5	-2.0	-7.1	-5.2
C	0	-2.7	0.7	0
Sc-Gr 2.6Ω/2.8Ω FLB				
A	10.6	1	9.4	2.7
B	-42.5	-7.5	-16.4	2.8
C	6.6	1.2	0.7	-7.0
Sc-Gr 108Ω/108.2Ω FLB				
A	1.3	-1.5	0.7	1.4
B	-5.2	-2.8	-2.9	-1.7
C	0	0.5	1.4	-0.9

Table E.12: Deviation of measured and simulated fault cases in FLB, fundamental frequency is 360Hz.The deviation is calculated by using equation E.26.

Deviation for fault cases in SLB.

Sc-Sc 2.6Ω SLB	Deviation measured $\|Z\|$ [%]	Deviation measured ϕ [%]	Deviation simulated $\|Z\|$[%]	Deviation simulated ϕ[%]
A	-37.1	5.7	-39.9	1.9
B	-1.3	-1.4	0.7	-1.1
C	-27.0	-26.6	-31.0	-27.1
Sc-Sc 108Ω SLB				
A	-2.6	-1.9	-2.2	-1.6
B	0	-0.1	0	0
C	0	-2.6	1.4	-2.2
Sc-Gr 2.6Ω/9.6Ω SLB				
A	-13.2	-0.5	-10.9	1.6
B	1.3	-4.9	1.4	-5.6
C	5.3	1.6	6.3	1.7
Sc-Gr 108Ω/115Ω SLB				
A	-1.3	-0.5	-2.2	-0.9
B	0.7	-0.4	1.4	-0.8
C	0.7	-0.2	0.7	1.0

Table E.13: Deviation of measured and simulated fault cases in SLB, fundamental frequency is 360Hz.The deviation is calculated by using equation E.26.

Fault cases in FLB

Graphical illustration of table E.12. Apparent impedance deviation for fault cases in FLB.

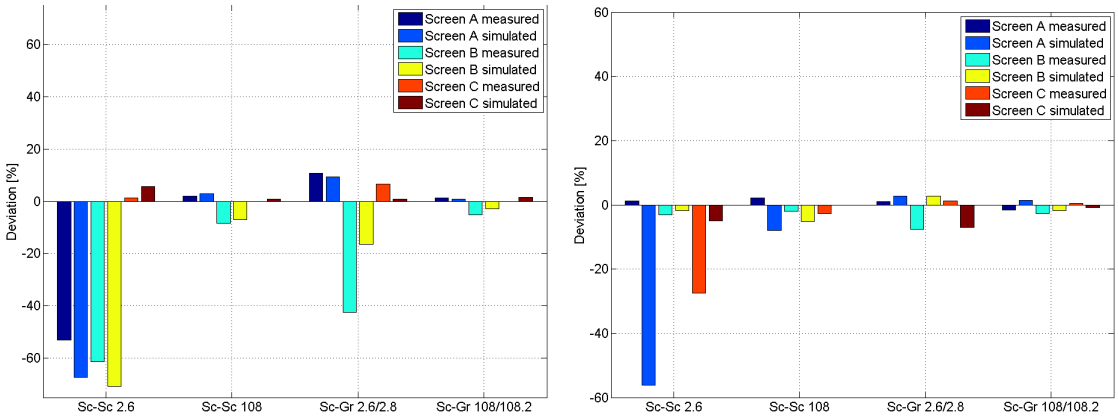

(a) (b)

Figure E.21: Apparent impedance deviation for fault cases in FLB. (a) Magnitude deviation. (b) Angle deviation.

Fault cases in SLB

Graphical illustration of table E.13. Apparent impedance deviation for fault cases in SLB.

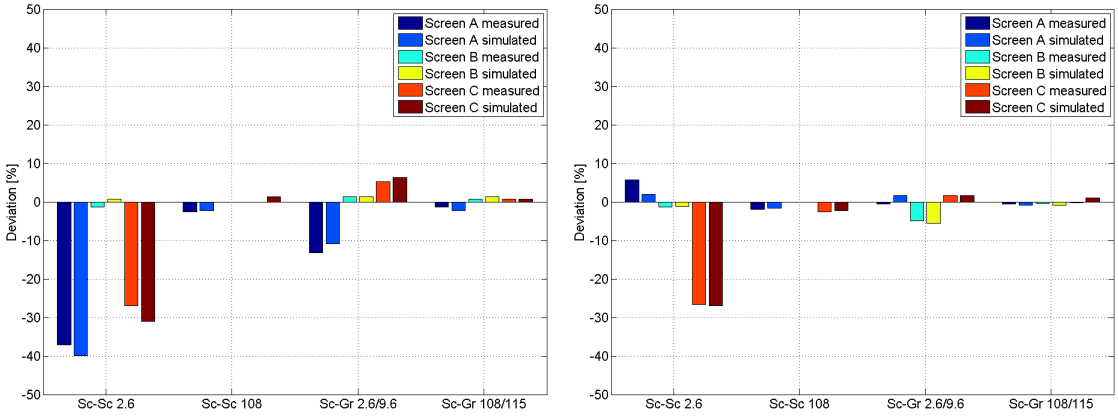

(a) (b)

Figure E.22: Apparent impedance deviation for fault cases in SLB. (a) Magnitude deviation. (b) Angle deviation.

As figure E.21 and E.22 illustrate that the trend is the same for simulated and measured results. Fault cases with a low resistance fault of 2.6Ω are detectable whereas fault cases with a high fault resistance of 108Ω are less detectable. Since the trend is the same this measuring technique is believed to be valid to use for the determination of the condition of the screen circuit.

E.4 Field measurement #2 summary

From the analysis of measuring results, it is seen that some data processing may be used to determine the apparent screen impedances from the sequence of single phase measurements.

From figure E.21 and E.22 it may be seen that there are significant deviations between simulations and measurements. The deviations are analyzed further when the simulation model is validated in chapter 6.

Appendix F

Field measurement #3 of the 150kV line between Frøstrup and Nors

The third field measurement (FM3) is an impulse test. This test was carried out as an additional measuring method to the impedance method. Together with the supervisors and N1 it was decided only to include a detailed study of the impedance method in this report.

This measuring report is included as an appendix which may be used for further studies. Measuring results may be found at the CD in folder *Nors 25-01-2012*.

FM3 is performed at the same 150kV cable line as FM1 and FM2. Line data may be found in the system description in chapter 2 on page 5.

F.1 Planning field measurements #3 FRT-NOR

The measurements performed during FM3 are divided into two sets. Healthy screen circuit and faults applied in the second link box (SLB). It was not possible to apply faults to first link box (FLB) because the drainage equipment which should keep the hole free of water was broken, and the hole was flooded. All measurements are performed in HV substation Nors. The fault conditions screen to screen (Sc-Sc) and screen to ground (Sc-Gr) are further explained in section 3.3 on page 26.

SET 1:

- Healthy screen circuit

SET 2 - Faults in SLB:

- (Sc-Sc) fault in SLB. (2.5Ω)
- (Sc-Gr) fault in SLB. (2.5Ω)
- (Sc-Sc) fault in SLB. (100Ω)
- (Sc-Gr) fault in SLB. (100Ω)
- Dismounted SVL.

For set 1 and set 2 there are applied a 2kV standard lightning impulse ($1.2/50\mu s$) to each screen and core conductor. Current and voltages are measured at all screens and core conductors. Furthermore each impulse is repeated and measured three times.

F.1.1 Simulation model

A PSCAD simulation model was made as a part of the planning. The parameters used for the cable modeling are calculated using the approach presented in [51]. The input parameters are listed in table F.1. The PSCAD model may be found at the attached CD in the folder *PSCAD*.

Layer	Parameter	Value
Conductor	Radius	0.021m
	Resistivity	$3.23 \cdot 10^{-8}\Omega$m
	Permeability	1
Insulation	Thickness	0.0191m
	Permittivity	2.96
	Permeability	1
Screen	Thickness	0.00159m
	Resistivity	$3.45 \cdot 10^{-8}\Omega$m
	Permeability	1
Outer insulation	Thickness	0.0038m
	Permittivity	2.3
	Permeability	1

Table F.1: Input parameters for the PSCAD model.

The PSCAD simulation model is shown in figure F.1.

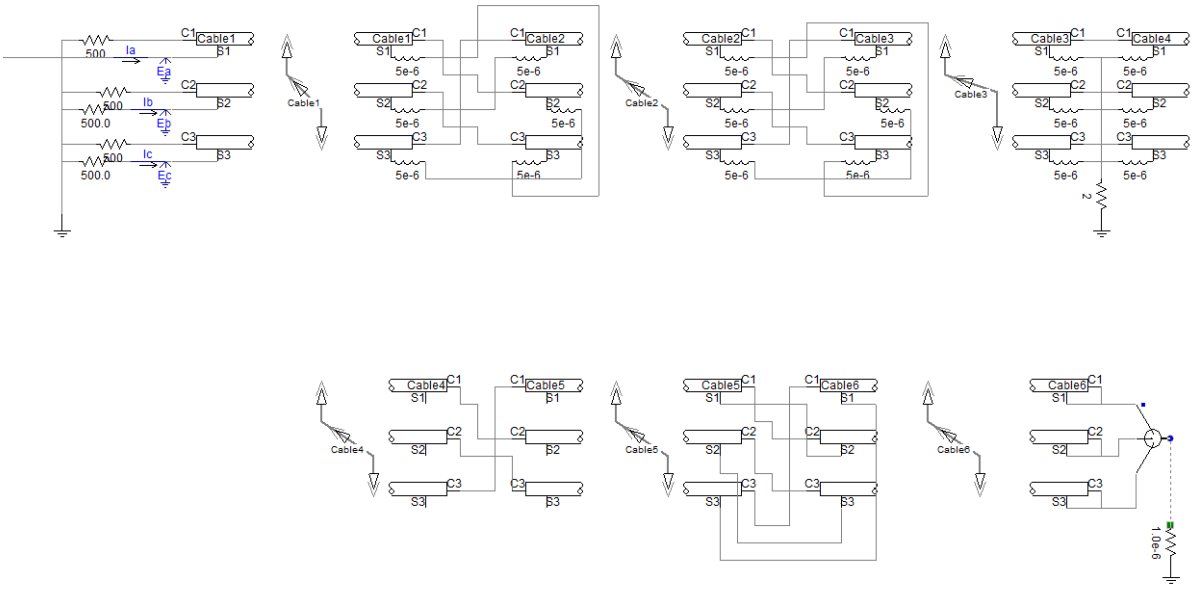

Figure F.1: PSCAD model used for field measurement preparation.

Placing of the cables in the PSCAD simulation model is shown in figure F.2.

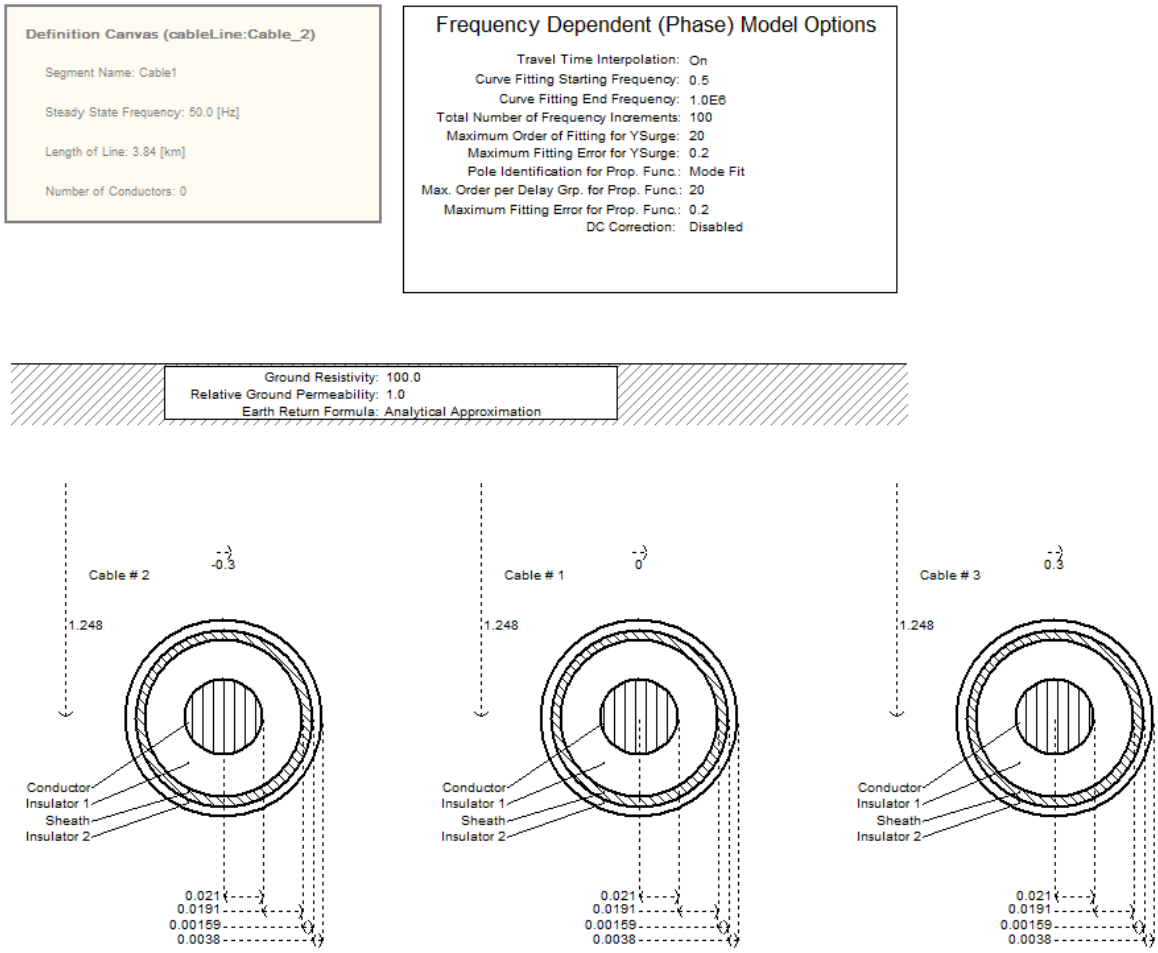

Figure F.2: Cable layout in the PSCAD model.

The impulse generator is modeled as shown in figure F.3, according to the PSCAD modeling guide [43]. The 5µH is the inductance of the cable, connecting the impulse generator to the cable termination [16, p.92].

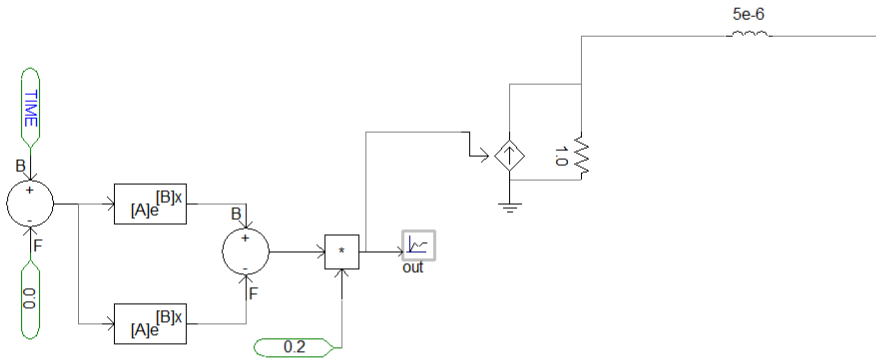

Figure F.3: PSCAD modeling of lightning impulse.

F.1.2 Simulation results

The cable line is simulated where no faults are applied and an impulse is applied to screen three. Simulation results are shown in figure F.4 to F.7.

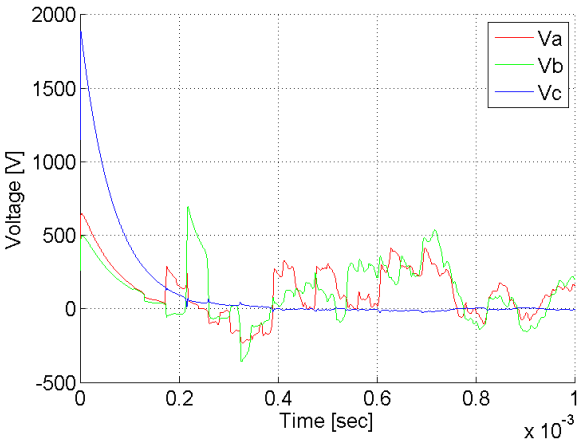

Figure F.4: Screen voltages, impulse applied to screen three.

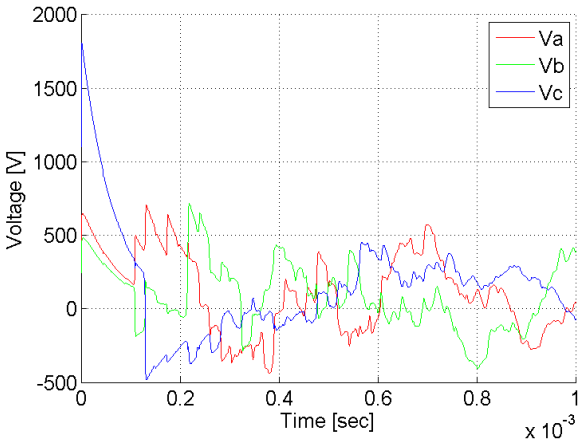

Figure F.5: Core voltages, impulse applied to screen three.

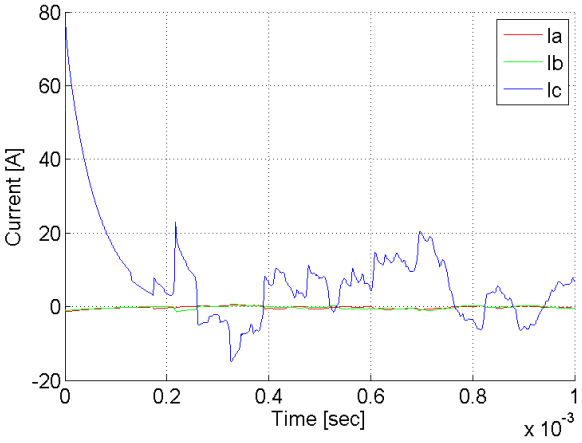

Figure F.6: Screen currents, impulse applied to screen three.

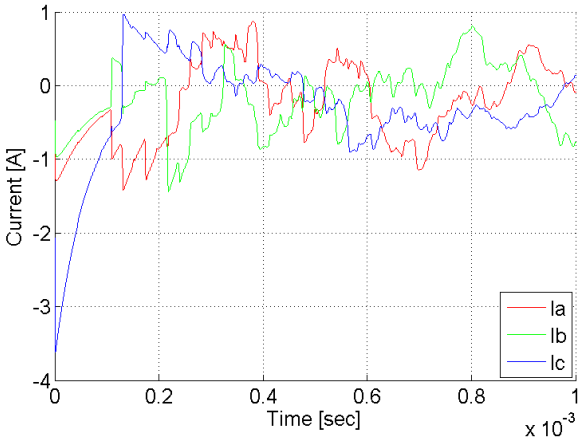

Figure F.7: Core currents, impulse applied to screen three.

F.2 Performing measurement #3

Date: 25.1.2012.
Location: 150kV HV station Nors, Buskkærvej 13, 7700 Thisted.
Participants: Morten Thule Hansen(AAU), Kasper Schultz Pedersen(AAU), Peter Rønne-Hansen (N1), Lars Brix (N1).

The measurements are performed in substation Nors, at the 150kV cable line FRT-NOR.

F.2.1 Measuring process

The cable line which is subject to measurement is just established and not taking into service at the time. The cable line is intended to replace an excising OHL. During the test the OHL will be taking out of service for safety reasons.

To achieve high safety when working at HV systems there is set up a process for the events and the order in which they should be performed during the test.

The following list presents the order of events, which will be performed during the test:

1 The OHL is disconnected and de-energized by N1
2 The OHL is grounded and locked in both ends by N1
3 Measuring equipment is brought into the measuring site
4 The ground connections at the cable termination in Nors are disconnected se figure D.15
5 Possible induced screen voltages are measured according to ground, for safety reasons
6 Measuring SET 1 is performed
7 Measuring SET 2 is performed
9 Ground connections at the cable terminations are re-established
10 The OHL grounding is removed by N1
11 The OHL is taken into service by N1

F.2.2 Measuring setup

An impulse generator is used to generate a standard lightning impulse, with 2kV chest voltage. Four scopes are used to measure three screen voltages, three screen currents, three core voltages and three core currents.

Measurements are performed in one end of the cable line in substation Nors. The impulse is applied to each screen and core conductor one at a time. The measuring setup is shown in figure F.8 and F.9.

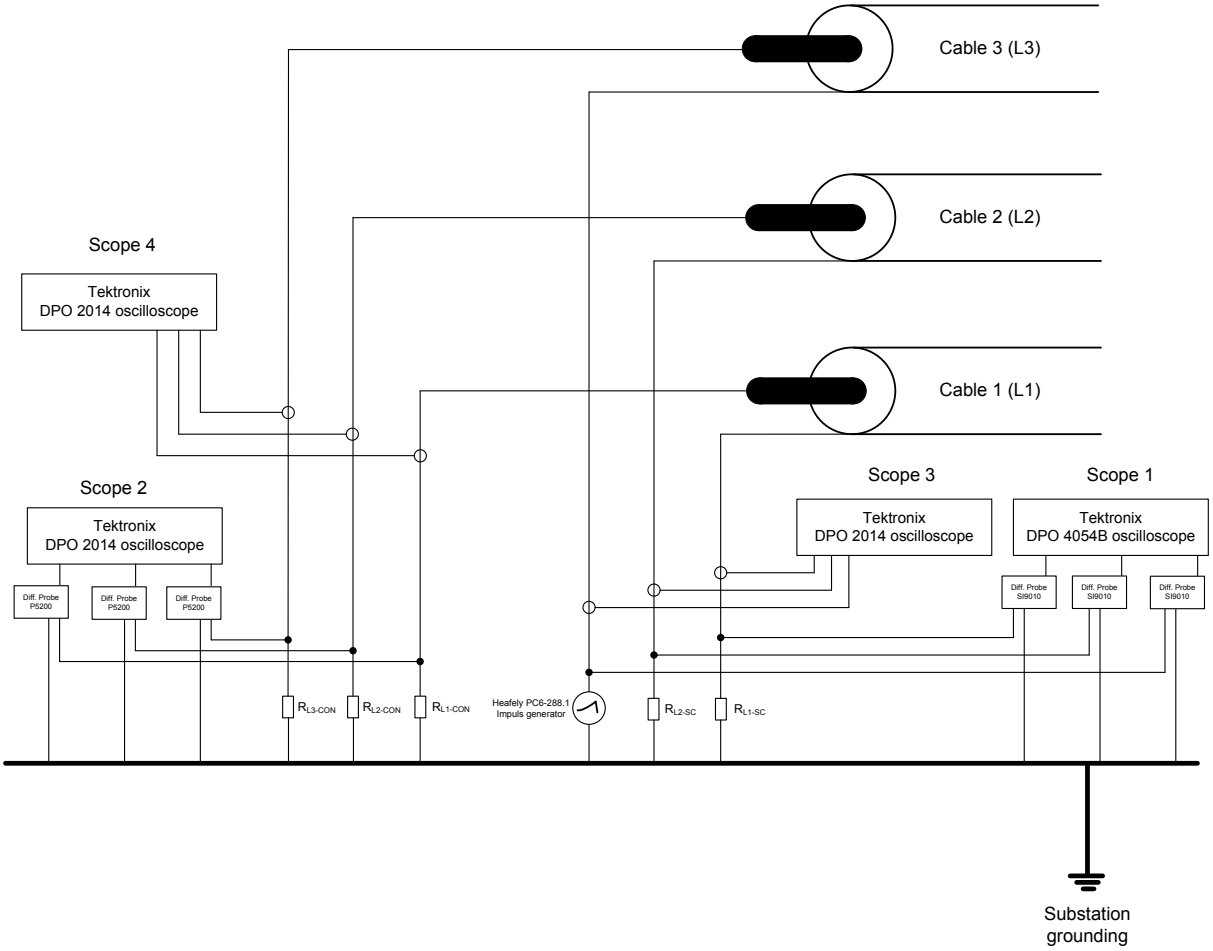

Figure F.8: Measurement setup for impulse applied to one of the screen conductors. Measuring resistances are shown in table F.5.

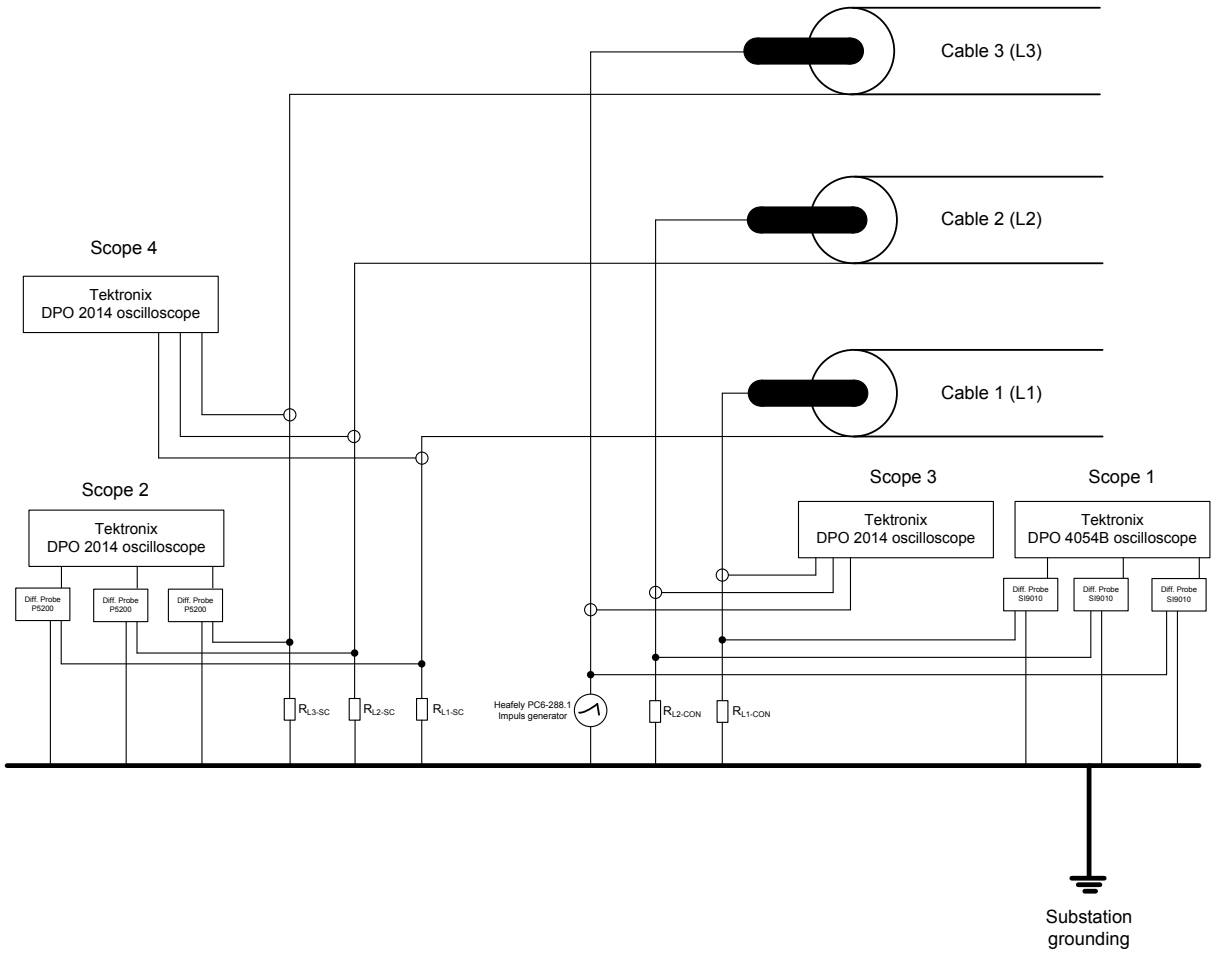

Figure F.9: Measurement setup for impulse applied to one of the core conductors. Measuring resistances are shown in table F.5.

As earlier explained the measuring setup is placed in substation Nors next to the cable termination as shown in figure F.10. The same non-magnetic tent that was used for FM1 and FM2 is used again to protect the equipment from bad weather.

Figure F.10: Test setup in substation Nors, placed next to the cable termination.

The connections from the measuring equipment to the cables are performed using grounding cables. The grounding cables connect the cable termination to the coupling board shown in figure F.16. At the coupling board the probes are easily changes between the between conductors and screens according to where the impulse is applied.

The grounding of the screen conductors are removed and grounding cables are used to connect screen and core conductors to the coupling board.

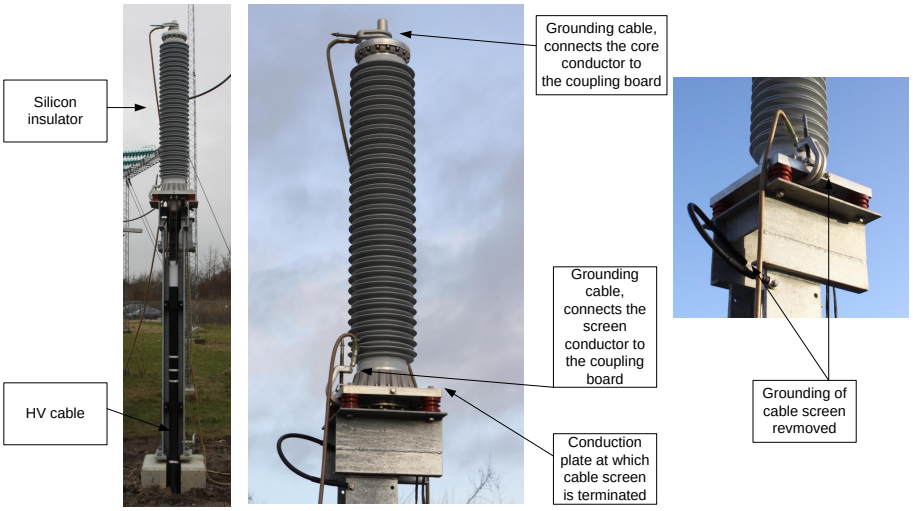

Figure F.11: Cable termination in substation Nors. Grounding of screens are removed and connected to grounding cables.

F.2.3 Measuring equipment

Table F.2 includes the instruments, which will be used for FM #3.

Type	Producer	Model	AAU number
Impulse generator	Haefely	PC6-288.1	-
Digital oscilloscope	Tektronix	DPO 4054B	92345
Digital oscilloscope	Tektronix	DPO 2014	92314
Digital oscilloscope	Tektronix	DPO 2014	-
Digital oscilloscope	Tektronix	DPO 2014	-
HV Differential probe	Sapphire Instruments	SI-9010	77694
HV Differential probe	Sapphire Instruments	SI-9010	77695
HV Differential probe	Sapphire Instruments	SI-9010	89235
HV Differential probe	Tektronix	P5200	88440
HV Differential probe	Tektronix	P5200	88443
HV Differential probe	Tektronix	P5200	88444
Current probe	Tektronix	TCPO150	79022
Current probe	Tektronix	TCP0030	79027
Current probe	Tektronix	TCP0030	92340
Current probe	Tektronix	TCP0030	92341
Current probe	Tektronix	TCP0030	83328
Current probe	Tektronix	TCP0030	83329
Couplings board incl. resistors	ESPH3-1031	V1.0	-
Variable effect resistance 2.5Ω	Danotherm	2.5Ω slider	-
Variable effect resistance 100Ω	Danotherm	100Ω slider	-

Table F.2: Instruments used for FM 3.

The surge tester used for impulse test is a Haefely PC6-288.1 surge tester shown in figure F.12. The impulse generator generates a 2.00kV $1.2/50\mu$sec impulse.

Figure F.12: Haefely PC6-288.1 surge tester.

Two types of scopes are used. One type is used for generating a trigger signal for the other three scopes.

The Tektronix DPO4054B oscilloscope is used for measuring and recording voltages and to generate trigger signal for the other three scopes.

Figure F.13: Tektronix DPO4054B digital oscilloscope.

One Tektronix DPO2014 oscilloscope is used for measuring and recording voltages and two of the same type is used for measuring and record currents. These are all triggered by the Tektronix DPO4054B.

Figure F.14: Tektronix DPO2014 digital oscilloscope.

F.2.4 Bandwidth of oscilloscopes

In order to gain acceptable resolution on the measurements there should be at least 10 samples during the front time of 1.2µs [16, p.53]. Therefore the sample time should be no larger than 120ns see equation F.1.

$$SampleTime \leq \frac{1.2 \cdot 10^{-6}}{10} = 120\text{ns} \tag{F.1}$$

The largest sample time require a sampling frequency of on less than 8.33MHz, see equation F.2.

$$SampleFrq \geq \frac{1}{120 \cdot 10^{-9}} = 8.33\text{MHz} \tag{F.2}$$

The bandwidth of the oscilloscopes are 100MHz and 500MHz accordingly [48] [49]. The bandwidths of the oscilloscopes are more than 10 times larger than the requirement and may therefore be used.

In order to record the applied impulse and the reflections the scopes are used in single trigger mode. In single trigger mode the waveforms shown on the oscilloscopes screen are stored, therefore the horizontal scale should be considered. Also the amount of stored points are decided on the scopes individual. Unfortunately it was not possible to choose the same amount of stored points for the two different oscilloscopes.

The horizontal scale and amount of stored points are given in table F.3.

Type	Horizontal scale	Stored points
DPO4054B	$200^{\mu s}/_{div}$	100k
DPO2014	$200^{\mu s}/_{div}$	125k

Table F.3: Record settings for scopes.

From the settings in table F.3 the sampling frequency of the recorded signals can be calculated for the two scope modes accordingly, see equation F.3 and F.4. The oscilloscope screens are horizontal divided into 10 divisions.

$$\text{SampleFrq}_{4054B} = \frac{100k}{200^{\mu s}/_{div} \cdot 10} = 50\text{MHz} \quad . \text{(F.3)}$$

$$\text{SampleFrq}_{2014} = \frac{125k}{200^{\mu s}/_{div} \cdot 10} = 62.5\text{MHz} \quad . \text{(F.4)}$$

It is seen that the sampling frequency of the stored signals meets the requirement in equation F.2.

F.2.5 Amplitude of measured voltages

Simulations performed during the planning are used to predict the voltages and currents that should be measured.

Impulse on screen
When the 2.0kV impulse is applied to one of the screen conductors, the voltages at the other screens should not exceed 0.7kV. The voltages at the core conductors are all below 2.0kV

The current at the energized screen has a peak value of 77A, the currents at the other screens are below 2A. The currents in the core conductors do not exceed 4A.

Impulse on core conductor
When the 2.0kV impulse is applied to one of the core conductors, the voltages at the other core conductors should not exceed 0.7kV. The voltages at the screen conductors are all below 1.1kV

The current at the energized core conductor has a peak value of 40A, the currents at the other cores are below 2A. The currents in the screens conductors do not exceed 3A.

Two types of differential probes are used. The probes the ratio setting of the probes are set as shown in table F.4.

Type	Ratio
Sapphire	1/1000
Tektronix	1/500

Table F.4: Ratio of the differential probes.

The three Sapphire probes are used to measure the three screen voltages and the three Tektronix are used to measure the three core voltages. The differential probes are shown in figure F.15.

Figure F.15: Six differential probes used for voltage measurement.

F.2.6 Current measurement

For the current measurement two types of current probes are used. One type for measuring the current at the applied impulse and the other type is used for measuring the current of the five other conductors.

The current probe used for the applied impulse is a Tektronix TCPO150, which is apple of measuring current up to 150A. The other current probes are Tektronix TCP0030 which are able to measure up to 30A. The current probes may be seen at the couplings board in figure F.16.

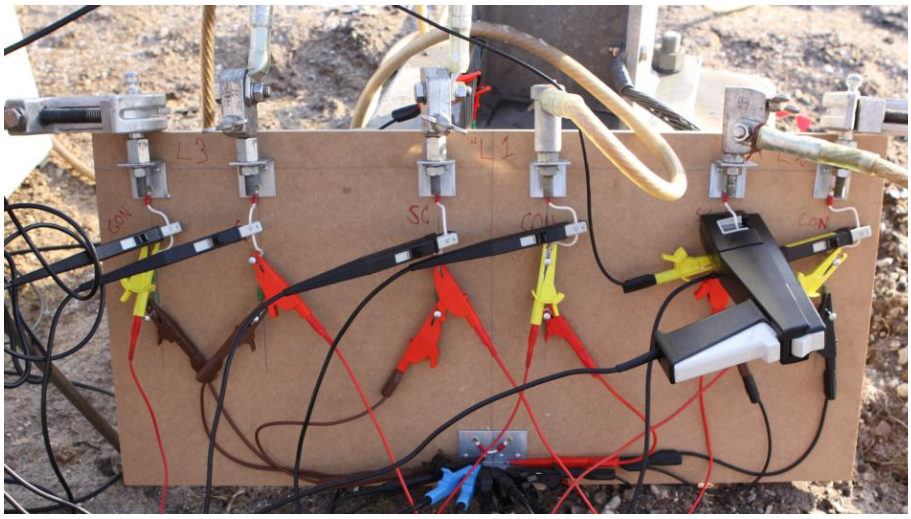

Figure F.16: Coupling board. The current probes are connected to the white wires.

F.3 Measurement results

Measuring and fault resistances were measured after the test was performed, by a Fluke F179 multimeter, AAU number 72503C02 and is given in table F.5. R_1 and R_2 are the applied fault resistances.

Resistor	Value
L1-CON	532.7Ω
L1-SC	533.7Ω
L2-CON	539.0Ω
L2-SC	538.8Ω
L3-CON	540.0Ω
L3-SC	533.7Ω
R1	2.3Ω
R2	99.7Ω

Table F.5: Measured resistances.

For impulse applied to screen conductors(Sc1, Sc2, Sc3), the following screen circuit conditions are measured:

- Healthy screen circuit.
- Sc-Sc fault in SLB (R1).
- Sc-Sc fault in SLB (R2).
- Sc-Gr fault in SLB (R1).
- Sc-Gr fault in SLB (R2).
- SVL dismounted.

For impulse applied to center conductors(L1, L2, L3), the following screen circuit conditions are measured:

- Healthy screen circuit.
- Sc-sc fault in SLB (R1).
- Sc-gr fault in SLB (R1).

The screen circuit conditions listed below is selected to be shown in the following pages. The rest of the measurements may be found on the attached CD.

- Healthy screen circuit, impulse on screen 3.
- Sc-Sc fault in SLB(R1), impulse on screen 3.
- Sc-Gr fault in SLB(R1), impulse on screen 3.
- Dismounted SVL in SLB, impulse on screen 3.
- Healthy screen circuit, impulse on core conductor 3.

Healthy screen circuit.

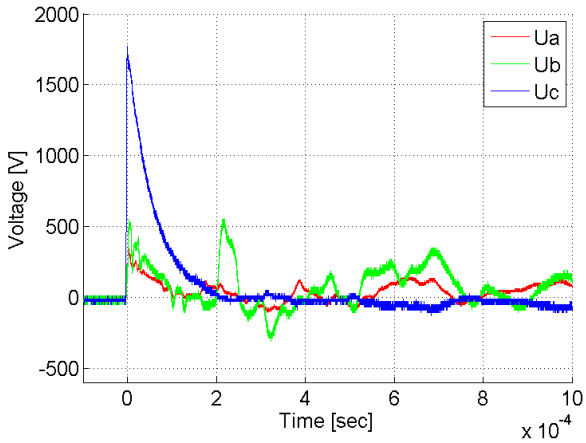

Figure F.17: Screen voltages, when an impulse is applied to screen 3.

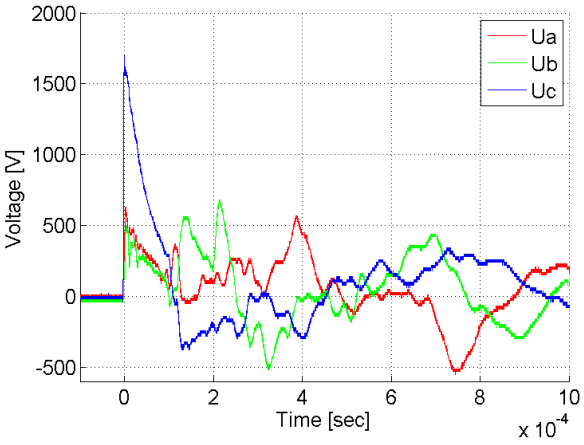

Figure F.18: Core conductor voltages, when an impulse is applied to screen 3.

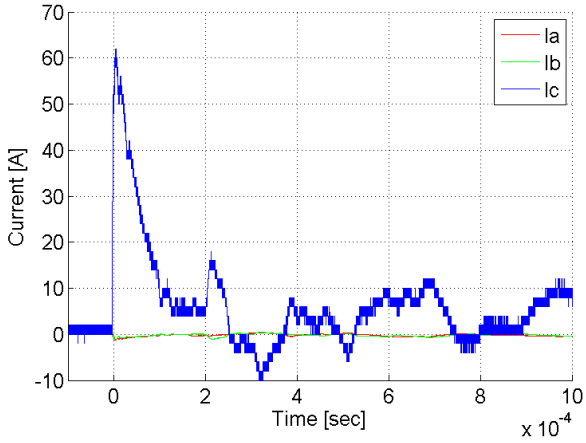

Figure F.19: Screen currents, when an impulse is applied to screen 3.

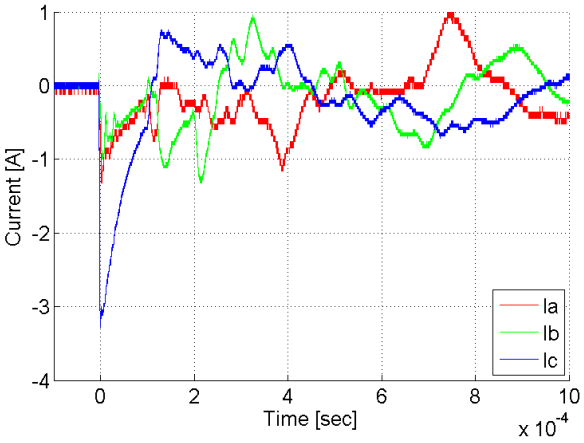

Figure F.20: Core conductor currents, when an impulse is applied to screen 3.

Sc-Sc SLB.

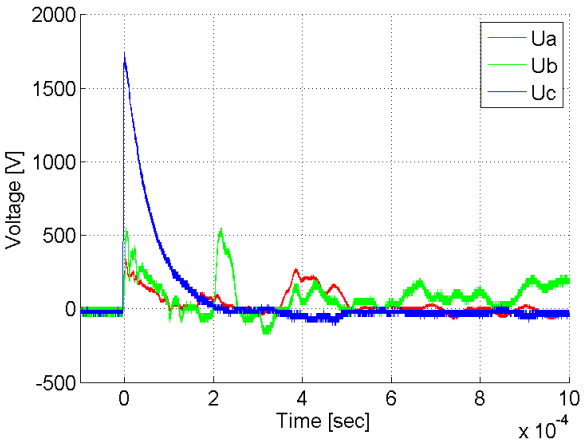

Figure F.21: Screen voltages, impulse on screen 3, Sc-Sc SLB (R1).

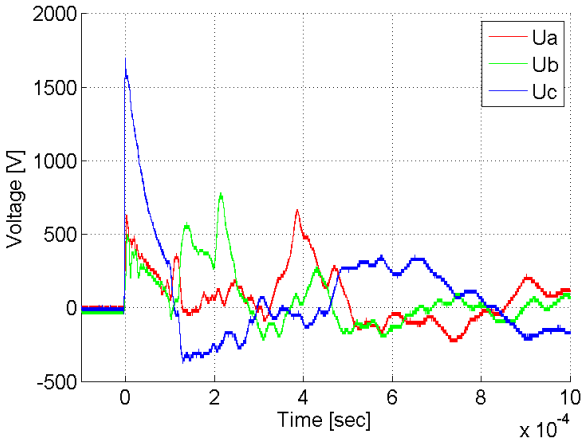

Figure F.22: Core conductor voltages, impulse on Screen 3, Sc-Sc SLB (R1).

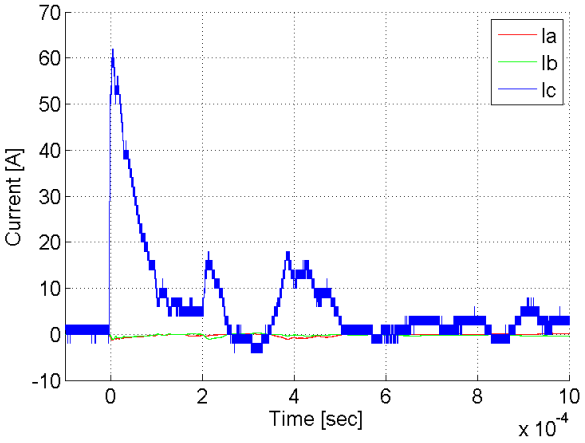

Figure F.23: Screen currents, impulse on screen 3, Sc-Sc SLB (R1).

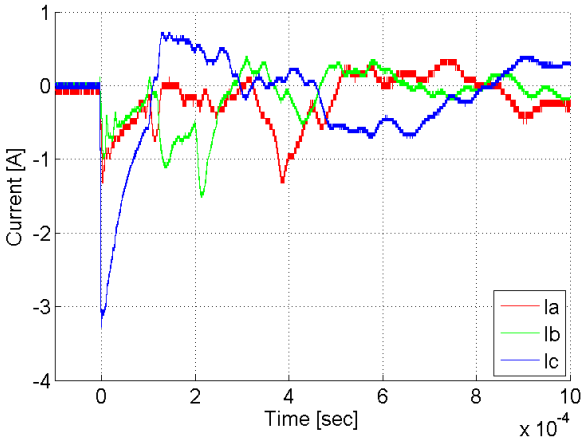

Figure F.24: Core conductor currents, impulse on Screen 3, Sc-Sc SLB (R1).

Sc-Gr SLB

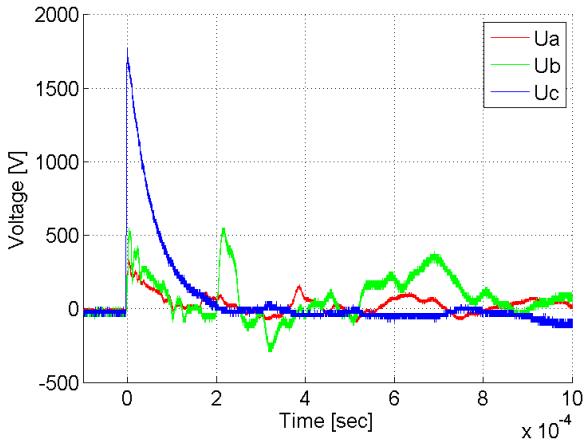

Figure F.25: Screen voltages, impulse on screen 3, Sc-Gr SLB (R1).

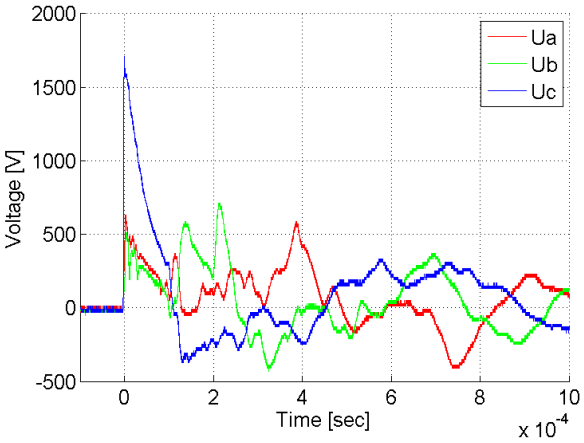

Figure F.26: Core conductor voltages, impulse on Screen 3, Sc-Gr SLB (R1).

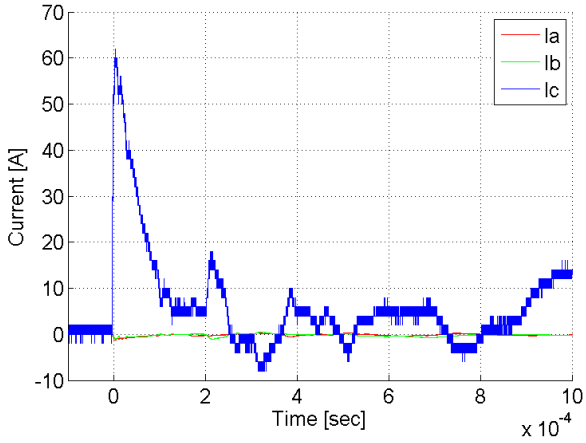

Figure F.27: Screen currents, impulse on screen 3, Sc-Gr SLB (R1).

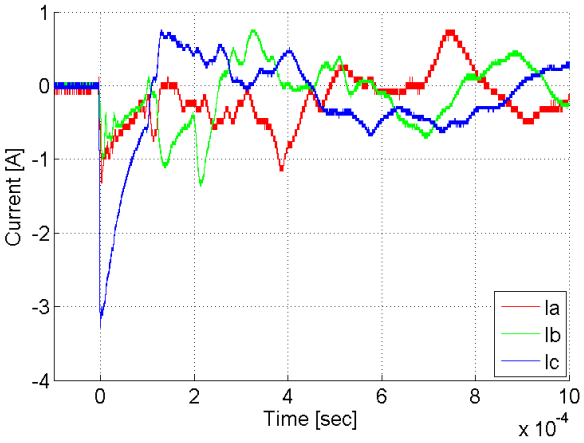

Figure F.28: Core conductor currents, impulse on Screen 3, Sc-Gr SLB (R1).

Dismounted SVL in SLB

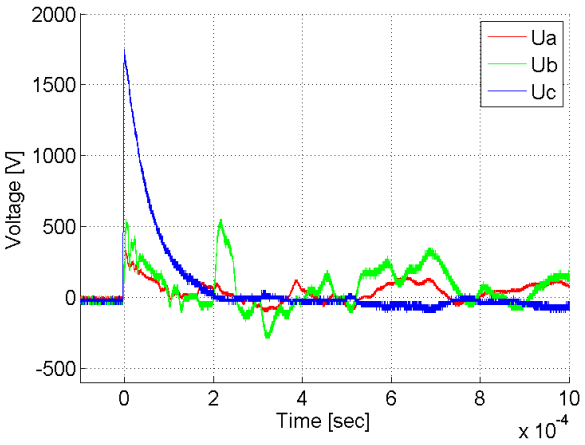

Figure F.29: Screen voltages, impulse on screen 3, dismounted SVL in SLB.

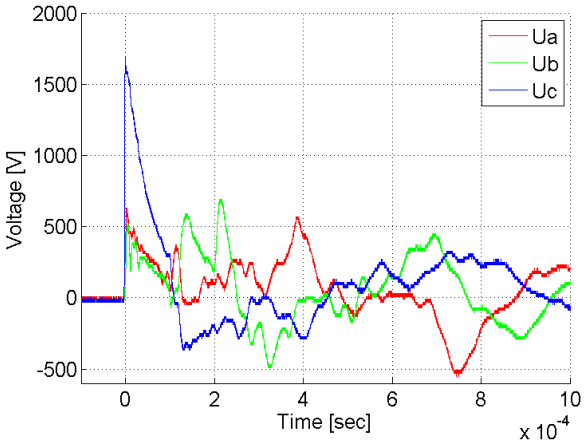

Figure F.30: Core conductor voltages, impulse on screen 3, dismounted SVL in SLB.

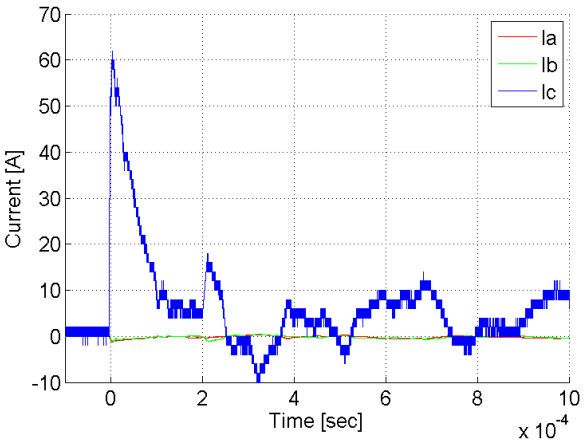

Figure F.31: Screen currents, impulse on screen 3, dismounted SVL in SLB.

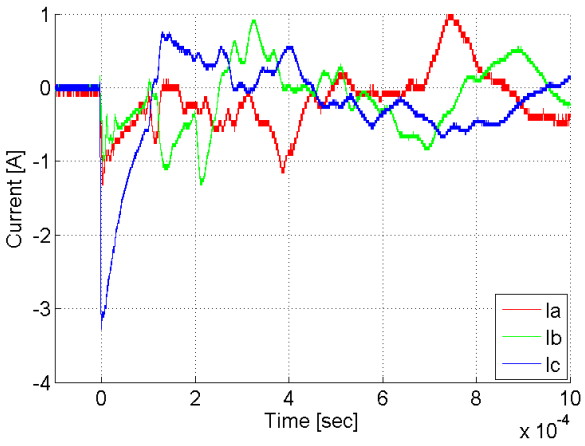

Figure F.32: Core conductor currents, impulse on screen 3, dismounted SVL in SLB.

Impulse applied to center conductor 3, for healthy screen circuit.

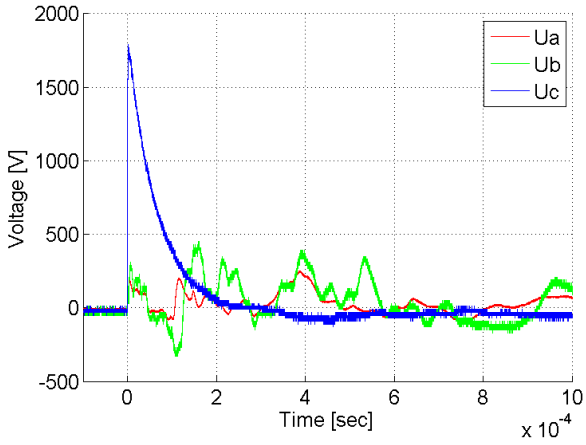

Figure F.33: Core conductor voltages, impulse on core 3, healthy screen circuit.

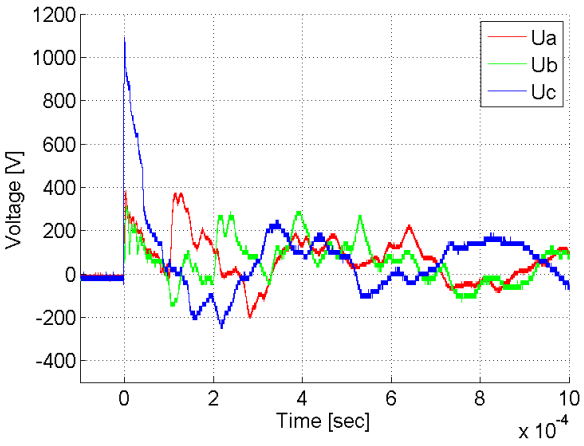

Figure F.34: Screen voltage, impulse on core 3, healthy screen circuit.

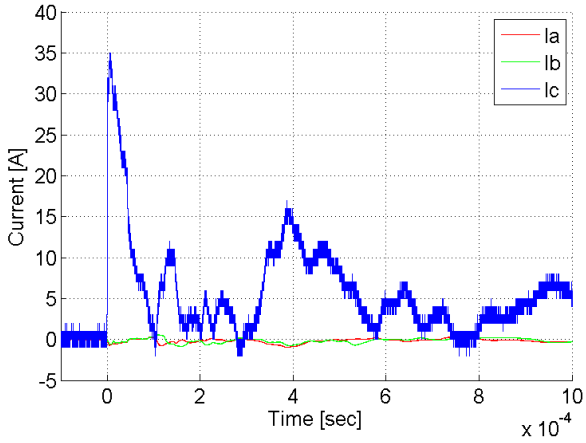

Figure F.35: Core conductor currents, impulse on core 3, healthy screen circuit.

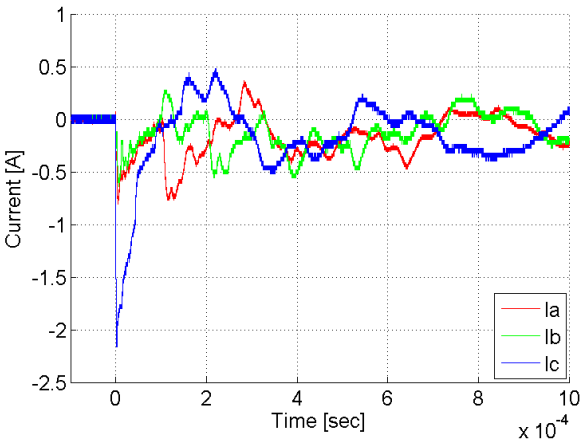

Figure F.36: Screen currents, impulse on core 3, healthy screen circuit.

F.4 Analysis of measurements

In the problem analysis, section 3.4.3, the reflection and refraction coefficients were briefly introduced. Due to the reflection coefficients, a part of the injected wave is reflected back into the media it came from. Thereby the size of the reflected wave says something about what surge impedance the wave was met by.

Figure F.37(a) shows the three screen currents when an impulse is applied to screen C and the screen circuit is in healthy state. In figure F.37(b), there is applied a Sc-Sc fault in the SLB.

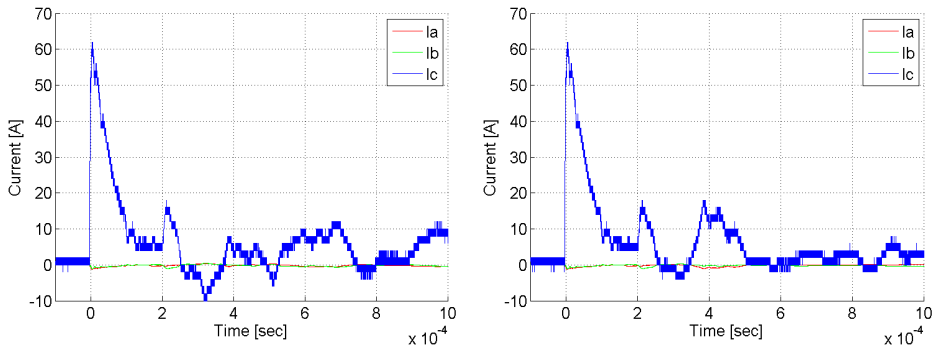

Figure F.37: (a) Screen currents, when an impulse is applied to screen 3, Healthy screen circuit. (b) Screen currents, impulse applied to Screen 3, Sc-Sc SLB (R1).

In order to detect if the screen circuit is faulty or not, it could be reasonable to do a reference measurement at the time the line is established, this could be saved used as a reference.

It might be difficult to determine the difference between the measurements in figure F.37. One way to compare two reflection measurements, is to subtract the two reflections. Thereby the instant of disagreement appear as the time the curve differs from zero. This can be seen in figure F.38, where current measurements for Sc-Sc fault in figure F.37(b) are subtracted the healthy screen currents in figure F.37(a). It may be seen that the differences appear at $\approx 160\mu s$.

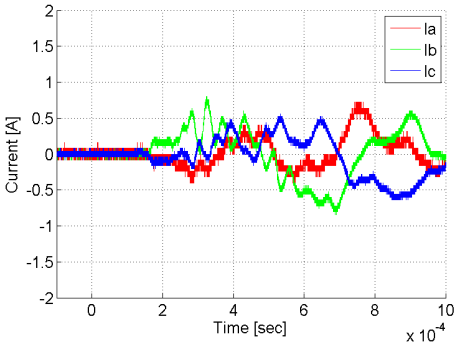

Figure F.38: Subtracted screen currents for Healthy and Sc-Sc fault in SLB. Impulse on screen 3.

From the above it may be seen that the impulse method could be used to study the condition of the link boxes. As proposed in the beginning of this chapter, here will only be giving an introduction to how the impulse method could be used. Therefore further analysis is not part of this work.

Appendix G

Link Box fault resistance

The purpose of the link box test is to study, what resistance there may be formed between the terminal, caused by water intrusion. The connection between the terminals are considered resistive due to the geometry, but is during ther test observed from the measuring equipment. Electric resistance dependent on the conducting volume: length (l) and cross section area (A), the resistivity(ρ) of the conduction material between the terminals see equation G.1 [10].

$$R = \frac{\rho \cdot l}{A} \quad [\Omega] \quad \text{(G.1)}$$

The conduction material is water, and this is present everywhere inside the box, and it is therefore not directly possible to determine the volume of the conduction material. Also the amount of water may change over time, due to penetration and vaporization of water. The current density is not homogenises because of the geometrical shape of the electrodes and therefore the length and cross section is complex to determine .

The conductivity of the water is dependent on the chemical composition. The chemical composition of the water that might penetrate into the link box may depend according to the environment in which the box is installed. The project group has therefore discussed the chemical composition of water, with engineering assistant Henrik Koch from the Section of Environmental Engineering. From this discussion it was found that rain water, is distilled water with supplements of what it had to take down through the atmosphere. The conductivity of distilled water is in the range of a few micro siemens per centimeter ($\mu S/cm$). For areas with heavy industries which high pollution the rain may pick up different material through the air and gain higher conductive. In China there have been performed measurements which indicate that in the most polluted areas the conductivity of rain water may be up to $1000 - 2000 \mu S/cm$ [47]. Another significant factor is what the rain water might be mixed with during the penetration down through the ground from the surface until it reaches the link box. Also the amount of ground water at the location at which the link box is installed may influence the water in the link box. If the box is located beneath a forest then the contribution of fertilizer may be small, compared to one installed in a farmers field. Some link boxes may be installed close to a road where there may be expected a high concentration of natrium clorid due to salting of roads. According to the environment the conductivity may be expected in a range from $10 - 2000 \mu S/cm$.

From the previous explanation it is found that some exact fault resistance in the link boxes are not possible to calculate. It is therefore decided to set up a test. A link box is borrowed from the co-operation company N1. The SVL is removed from the box and the box is filled by water as shown in figure G.1.

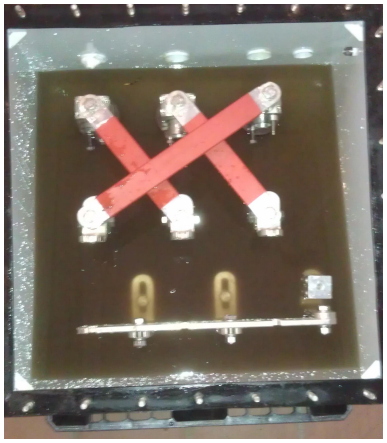

Figure G.1: Link box filled by water for fault resistance test.

G.1 Water samples

To study the variations of conductivity it is decided to collect four water from different locations in the area around AAU. To be able to measure the conductivity of water an **Cond 340i conductivity measuring instrument** is borrowed from the Section of Environmental Engineering at AAU. The instrument is shown in figure G.2. The instrument measures the conductivity and the temperature. The read conductivity is corrected to the standard conductivity of $20°C$. The water samples are all taken i February 2012.

(a) (b)

Figure G.2: Instrument used for conductivity measurement of water samples. (a) Shows the instrument and the connected sensor. (b) Shows the instrument during measuring, the sensor is placed in the water and the conductivity is read from the display.

It is expected that most link boxes are installed in farmers field and therefore a sample from a farmers field is taken. The sample is taken at sufficient distance to roads, see figure G.3. The conductivity is measured to 636$\mu S/cm$.

Figure G.3: The red arrow indicated the place at which the farmers field water sample has been taken.

The second sample is taken from a water hole placed near the university and close to a road as shown in figure G.4. It was expected that the conductivity of this is rather high, due the salting of the road. The conductivity is measured to 853$\mu S/cm$.

Figure G.4: Water hole near AAU, where second water sample is taken.

The third is taken form a lake at another place of the university, this is not close to any road see figure G.5. The conductivity of the sample is measured to 1040$\mu S/cm$.

Figure G.5: Small lake near AAU, where third water sample is taken.

The fourth sample is taken directly from the water supply see figure G.6. It is known that this may not be directly connected to the measurement from the nature, but is performed for comparable reasons. G.5. The conductivity of the sample is measured to 440$\mu S/cm$.

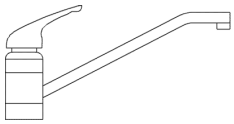

Figure G.6: Link box filled by water for fault resistance test.

The conductivity of four water samples are measured and it is found that the three taken from the nature differs from $636 - 1040 \mu S/cm$. The conductivity of the sample from the water supply is $\approx 1/2$ of the conductivity of the average of the samples in the nature. The link box is filled with water from the places shown in figure G.4 and G.5.

G.2 Performing Link box test

Voltage is applied between the earthing bus bar and one of the cross bonding terminals. It is decided to apply AC voltage because this is the situation for the actual case. The test setup is shown in figure G.7.

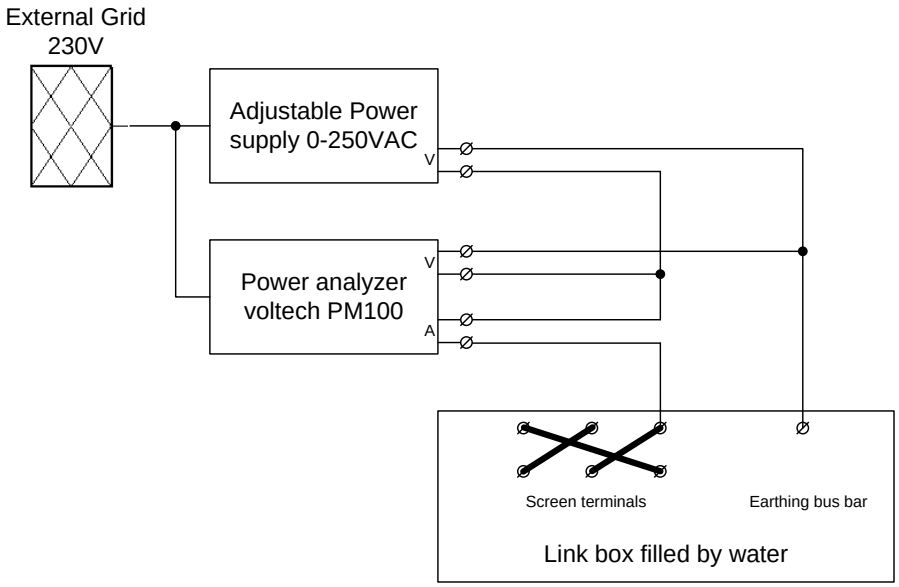

Figure G.7: Test setup used for link box measurement.

The voltage is supplied by an adjustable voltage supply $0-250VAC$. The maximum current of the supply is 3A. The supply is shown in figure G.8.

Figure G.8: Impo Power supply.

A single phase power analyser is used to measure voltage, current and phase angle. The power analyser is shown in figure G.9.

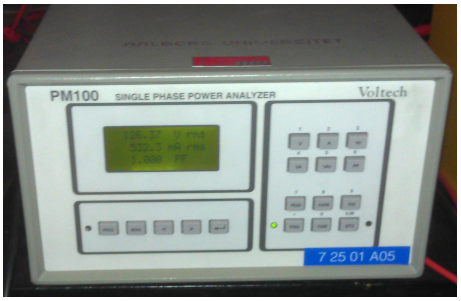

Figure G.9: Power analyser Voltech PM100.

Table G.1 include the instruments that have been used for the link box test.

Type	Producer	Model	AAU number
Adjustable power supply	Impo	-	87735
Power analyzer	Voltech	PM100	35596

Table G.1: Instruments used for link box Test.

Test 1

Figure G.10 shows the link box during test. It may be seen that the water covers a few centimeter of the terminals.

Figure G.10: Link box under test, half filled by water.

The applied voltage is increased in steps ($\approx 50, 100, 150, 200$) and the current is read after a couple of minutes when the setup has stabilized. The test is performed according to the procedure listed below.

1 $\approx$ 50V is applied and the corresponding current is read.

2 Voltage increased to $\approx$ 100V and the current is read.

3 Voltage increased to $\approx$ 150V and the current is read.

4 Voltage increased to $\approx$ 200V and the current is read.

5 Voltage decreased to $\approx$ 50V the setup is left energized until the following day.

The procedure is performed one time a day, three days after another, to study if the water should change characteristic when voltage is applied over time. Measuring results are given in table G.2, where the first day is marked $1a-4a$, the second $1b-4b$ and the third $1c-4c$. It is observed that the power factor for every measurement is 1. The corresponding resistance is calculated for each measurement directly using ohms law.

Measurement	Voltage[V]	Current[A]	Resistance[Ω]
1a	51	0.22	237.7
1b	105	0.46	227.8
1c	150	0.70	214.0
1d	217	1.02	213.8
2a	52	0.22	240.6
2b	104	0.45	230.9
2c	153	0.70	221.6
2d	210	0.99	211.4
3a	52	0.21	240.6
3b	107	0.46	230.9
3c	155	0.69	221.6
3d	208	0.97	211.4

Table G.2: Measurement from test 1.

From table G.2 it may be seen that the calculated resistance decreases as the applied voltage increases. The measurements from table G.2 are plotted in figure G.11

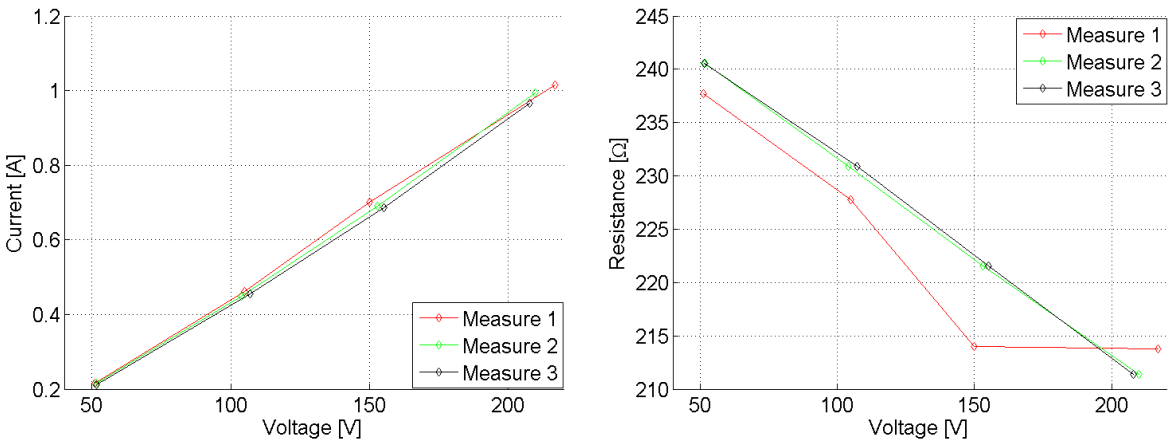

(a) (b)

Figure G.11: Link box test with water level as shown in figure G.10. (a) Shows corresponding voltage and current. (b) Shows calculated resistance as a function of applied voltage.

From figure G.11 it may be seen that the that the first measurement differs a few ohms from the two others, but sill the same trend is present, for all three measurements. It is also seen that the resistance decreases when the applied voltage is increased. The resistance is $\approx 240\Omega$ for a voltage of 50V and $\approx 210\Omega$ when the applied voltage is increased to 200V.

Test 2

After the three measurements of test 1, it is decided to increase the water level, to study if the amount of water affect the resistance. The water level is increased as shown in figure G.12 and the conductivity is measured to $892 \mu S/cm$.

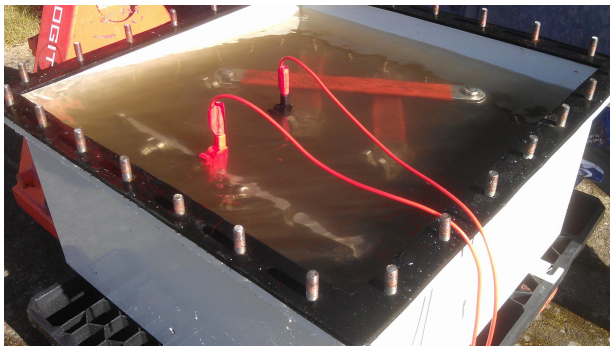

Figure G.12: Link box under test, completely filled by water.

As for the first test voltages and currents are read from the power analyzer. The results are listed in table G.3, where the resistances are calculated directly using ohms law. From the table it is seen that the resistance is decreased significantly compared to test 1. The decreased resistance make the applied voltage lower than for test 1, because the current limitation of the power supply is reached. Because of significant decreased resistance, test 2 will study both Sc-Sc and Sc-Gr fault.

The measuring results are shown in table G.3, where $a - e$ marks the five measuring points.

Measurement	Voltage[V]	Current[A]	Resistance[Ω]
Sc-sc-a	13.7	0.55	24.8
Sc-sc-b	24.5	1.00	24.4
Sc-sc-c	37.9	1.58	24.1
Sc-sc-d	49.3	2.08	23.8
Sc-sc-e	62.2	2.64	23.6
Sc-gr-a	15.0	0.53	28.8
Sc-gr-b	39.7	1.06	28.0
Sc-gr-c	42.8	1.55	27.6
Sc-gr-d	57.3	2.07	27.5
Sc-gr-e	72.0	2.65	27.2

Table G.3: Measurement from test 2.

The results from table G.3 are plotted in figure G.13.

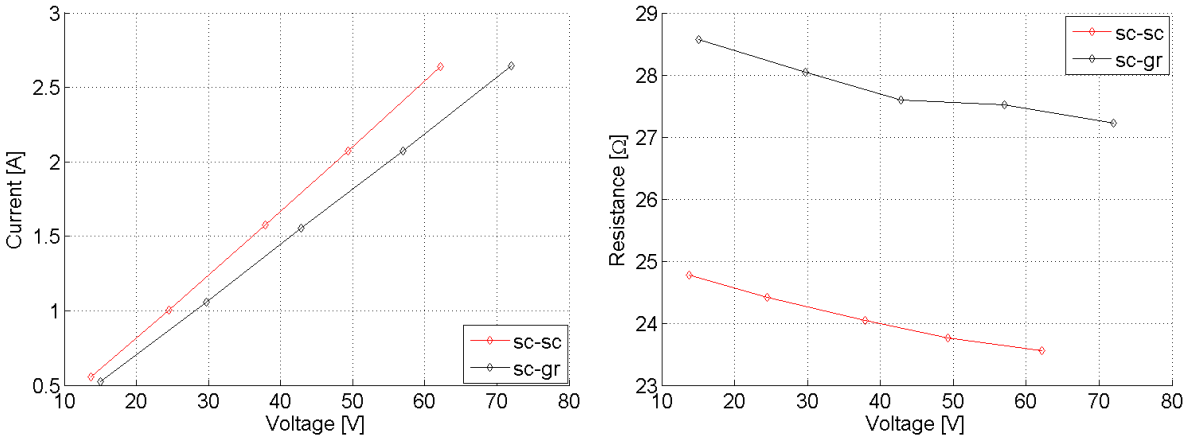

(a) (b)

Figure G.13: Link box test with completely filled box is shown in figure G.12. (a) Shows corresponding voltage and current. (b) Shows calculated resistance as a function of applied voltage.

The black line shows Sc-Gr fault and the red line shows Sc-Sc fault. It is seen that the Sc-Sc fault provide lower resistance than the Sc-Gr fault, which might be due to the shorter distance between the screen terminal than from screen terminal to earthing bus bar.

From test 2 it is observed that the resistance decreases when the applied voltage is increased, which trend is identical to test 1. The resistances are measured to $\approx 24.8\Omega$ and $\approx 28.5\Omega$ for Sc-Sc and Sc-Gr accordingly, for an applied voltage of ≈ 15V. When the applied voltage is increased to ≈ 65V the resistances has decreased to 23.5Ω and 27.2Ω for the two different fault types.

G.3 Influence of the water conductivity

As earlier explained three water samples were taken from the nature. The conductivities of the samples are within the interval $636 - 1040 \mu S/cm$. It is studied how much the conductivity interval affect the fault resistance. The study is based on equation G.1 shown in the beginning of this section. Using this equation there is calculate a value which expresses the volume of the conduction material ⅊ this constant is for this calculation named k_V see equation G.2. The matlab script may be found on the CD, in the folder: *MATLAB*.

$$R = \frac{\rho \cdot l}{A} = \rho \cdot k_V \quad [\Omega] \tag{G.2}$$

The conductivities from the three water samples are converted to resistivitys using equation G.3.

$$\frac{1}{\frac{\sigma[\mu S/cm] \cdot 10^{-6}}{100}} = \rho[\Omega m] \tag{G.3}$$

The three measured conductivities and corresponding resistivities are shown in table G.4.

Water sample	Conductivity[$\mu S/cm$]	Resistivity[Ωm]
Farmers field	636	ρ_{ff} = 157 233
Water hole	980	ρ_{wh} = 102 041
Small lake	1140	ρ_{sl} = 96 154

Table G.4: Conductivity and resistivity of the three water samples.

The conductivity of the water from the link box is converted to resistivity by G.4, based on equation G.3.

$$\frac{1}{\frac{892[\mu S \cdot 10^{-6}/cm]}{100}} = 112108[\Omega m] \tag{G.4}$$

By rearranging equation G.2, the volume constant (k_V) is calculated based on the measured conductivity and the average resistance from test 2.

$$k_V = \frac{R}{\rho} = \frac{24.14}{112108} = 21.5 \cdot 10^{-5} \tag{G.5}$$

Using the volume constant(k_V) from equation G.5 and the resistivitys from table G.4 there are calculated corresponding fault resistances from each water conductivity.

$$R_{wh} = \rho_{ff} \cdot k_V = 33.9\Omega \tag{G.6}$$

$$R_{wh} = \rho_{wh} \cdot k_V = 22.0\Omega \tag{G.7}$$

$$R_{sl} = \rho_{sl} \cdot k_V = 20.7\Omega \tag{G.8}$$

The expected fault resistances are calculated to be within the interval $20.7 - 33.9\Omega$ according to the conductivity of the water. For comparison water from the water supply would establish a resistance of 48.9Ω. Because of the relative large deviation between the upper and lower limit of the interval, it is decided not to distinguish between Sc-Sc and Sc-Gr fault. The interval according to conductivity, and the decrease according to applied voltage is illustrated in figure G.14.

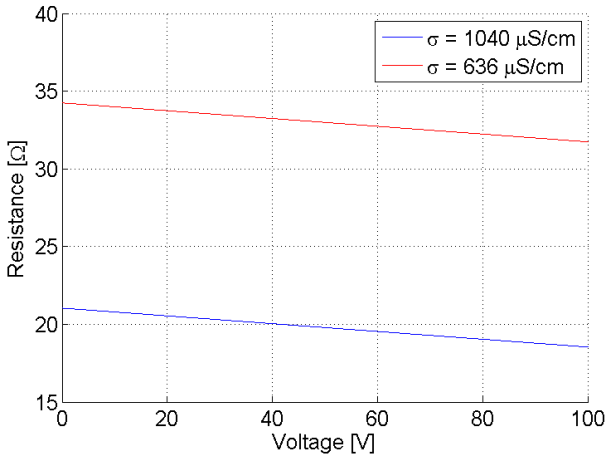

Figure G.14: Resistance interval as a function of applied voltage.

Figure G.14 shows the resistance interval, that the fault resistance is expected to be within.

G.4 Observations during the test

It was observed that there was formed a glossy layer on the water as shown in figure G.15, which might indicate that some kind of electrolysis were going on. No further attempt is done to explain the deposits on the water surface.

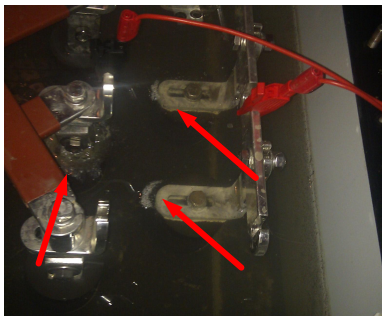

Figure G.15: Glossy surface on water during test.

G.5 Link box test summary

The link box test shown that it is very difficult to determine the size of the expected fault resistance, cause by water intrusion. The conductivity of the water may differ in a wide range according to the surrounding environment. The performed water samples from the nature differs from $636 - 1040 \mu S/cm$.

From the tests it is observed that the amount of water have great influence of the measured resistance. As earlier explained it is expected that the when a link box starts to become leaky the will may over time be completely filled by water. Therefore it is expected that the second test, where the box is filled by water, may provide the most proper results. Another term has not been taken into account, which is the size of the electrodes covered by water. From the system description in chapter 2 it is seen that during installation the button of the boxes are covered by compound, making the part of the electrodes which are in direct contact with the water smaller, than what is tested. This may increase the resistance for the actual system.

From the test it is also observed that the resistance decreases $\approx 1\Omega$ when the applied voltage is increased by 40V.

Based on the test results and the observations it is assumed that it is not unlikely that water in the link boxes forms resistance of 35Ω.

Appendix H

Calculation of resonance points

H.1 Calculation of inductance and capacitance

This appendix describes how the dominating components of the screen circuit may be calculated. The calculated parameters are compared to the domination components calculated by the DIgSILENT model of the cable line FRT-NOR, described in Appendix C. The resonance frequencies are calculated for both the calculation and the DIgSILENT model and compared. Finally the effect of using lumped parameter representation, in respect to determination of the resonance frequency, is considered.

Series inductance

The series inductance of a transposed three phased system may be calculated by equation H.1 [36]:

$$L = 2 \cdot 10^{-7} \cdot \ln \frac{D_m}{D_s} \qquad \left[\frac{\mathrm{H}}{\mathrm{m}}\right] \quad \text{(H.1)}$$

Where D_m is the geometrical mean distance between the conductors determined by equation H.2, the distances used in equation H.2 can be seen in figure H.1. D_s is the geometrical mean radius of the conductor.

$$D_m = \sqrt[3]{D_{12} \cdot D_{13} \cdot D_{23}} \quad [\mathrm{m}] \quad \text{(H.2)}$$

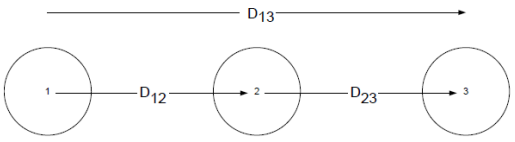

Figure H.1: Calculation of geometrical mean distance.

$$D_m = \sqrt[3]{0.3 \cdot 0.6 \cdot 0.3} = 0.38\mathrm{m} \quad \text{(H.3)}$$

Because the cable screen is a hollow conductor, the radius may be corrected. The inner radius of the cable screen is 40.1mm and the outer radius is 41.7mm. The r_2/r_1 ratio is calculated to 0.962 and used

for correction figure H.3. For the correction, the D_s/r_1 ratio is read from the graph in figure H.3 to 0.987 and thereby D_s is determined to 41.16mm.

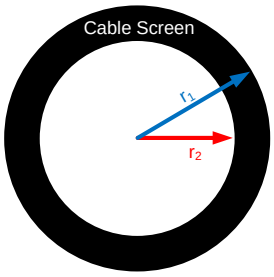

Figure H.2: Sketch of cable screen.

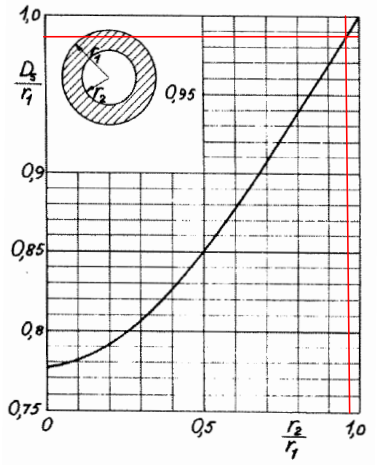

Figure H.3: Graph for correction of radius [53].

Using the calculated geometrical mean distance and mean radius, the series inductance may be calculated using equation H.1. The calculation is shown in equation H.4.

$$L = 2 \cdot 10^{-7} \cdot \ln \frac{0.38}{0.04116} = 445^{\mathrm{nH}}/_{\mathrm{m}} \tag{H.4}$$

Multiplying equation H.4 by the length of the line the total inductance may be determined see equation H.5.

$$L_{phase} = 445^{\mathrm{nH}}/_{\mathrm{m}} \cdot 11520 = 5.12\mathrm{mH} \tag{H.5}$$

Shunt capacitance

The cable screen forms two capacitances. One from the screen to the surrounding soil through the outer insulation, and another from the cable screen to the center conductor, because the center conductor is grounded during the tests. The two capacitances are shown in figure H.4.

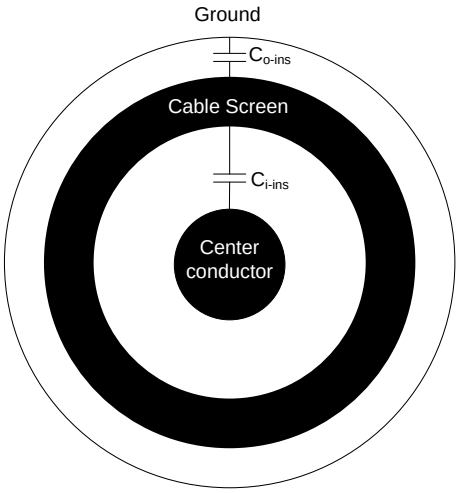

Figure H.4: HV cable forming two capacitors from the screen to ground and to center conductor.

The capacitance may be calculated by equation H.6 [36, p.29], where b is the distance from center of the inner conductor to ground potential, a is the radius of the inner conductor and ε is the permittivity of the dielectric.

$$C = \frac{2 \cdot \pi \cdot \varepsilon_0 \cdot \varepsilon_r}{ln\frac{b}{a}} \qquad [F/m] \quad \text{(H.6)}$$

The capacitance from the cable screen to the center conductor may be calculated by equation H.7 :

$$C_1 = \frac{2 \cdot \pi \cdot \varepsilon_0 \cdot 2.5}{ln\frac{41.7}{21}} = 0.20\frac{nF}{m} \qquad \text{(H.7)}$$

$$C_{i-ins} = C_1 \cdot l = 0.20\text{nF} \cdot 11520\text{m} = 2.33\mu\text{F} \qquad \text{(H.8)}$$

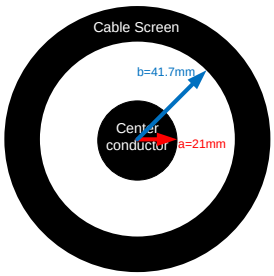

Figure H.5: Distances for calculation shunt capacitance.

The capacitance from cable screen to surrounding soil may be calculated by equation H.9:

$$C_2 = \frac{2 \cdot \pi \cdot \varepsilon}{ln\frac{b}{a}} = \frac{2 \cdot \pi \cdot \varepsilon_0 \cdot 2.3}{ln\frac{45.5}{41.7}} = 1.47\frac{nF}{m} \qquad \text{(H.9)}$$

$$C_{o-ins} = C_2 \cdot l = 1.47\text{nF} \cdot 11520\text{m} = 16.9\mu\text{F} \qquad \text{(H.10)}$$

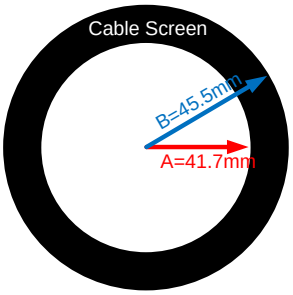

Figure H.6: Distances for calculation shunt capacitance.

From equation H.8 and H.10 it is seen that the capacitance from screen to soil is $7.3gg$ higher than the capacitance from screen to center conductor.

As it may be seen from figure H.7 the two capacitors of the cable are present as a parallel connection and therefore their capacitance may be added in order to determine the total capacitance see equation H.11.

$$C_{shunt-total} = 2.33 + 16.9 = 19.23\frac{nF}{m} \qquad \text{(H.11)}$$

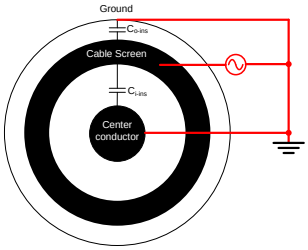

Figure H.7: Inner and outer capacitance of HV cable.

The calculated inductance and capacitance are compared with the inductance and capacitance from the DIgSILENT model of the cable line FRT-NOR, explained in Appendix C.

DIgSILENT screen impedance

The series impedance of the screen conductor is identified from the DIgSILENT cable model: $0.53\Omega/_{minorsection}$.

The inductance (L) is calculated from the series impedance, by equation H.12, for the fundamental frequency of 50Hz.

$$L_{minor-section} = \frac{X_L}{2 \cdot \pi \cdot f} = \frac{0.53}{2 \cdot \pi \cdot 50} = 1.7\text{mH} \qquad \text{(H.12)}$$

The total phase self induction is calculated by equation H.13.

$$L_{phase} = 3 \cdot 1.7 = 5.1\text{mH} \qquad \text{(H.13)}$$

DIgSILENT shunt capacitance

The shunt admittance of the cable screen is identified from the admittance matrix: $541\,{}^{\mu S}/_{km}$.

The admittance per km is multiplied by the length of the major section, and the shunt reactance is determined by equation H.14.

$$X_{C-phase} = \frac{1}{541\mu S \cdot 11.52} = 160.5\Omega \tag{H.14}$$

From the shunt reactance is calculated by equation H.15, for the fundamental frequency f of 50Hz.

$$C_{phase} = \frac{1}{X_{C-phase} \cdot 2 \cdot \pi \cdot f} = 19.8\mu F \tag{H.15}$$

The total series impedance and shunt capacitances of the calculation and from DIgSILENT are shown in table H.1. The corresponding resonance frequencies are calculated by equation H.16 and also shown in the table.

$$f_{resonance} = \frac{1}{2 \cdot \pi \sqrt{L \cdot C}} \quad [\text{Hz}] \tag{H.16}$$

Parameter	Calculated	DIgSILENT
Inductance	5.12mH	5.1mH
Capacitance	19.23µF	19.8µF
Resonance Frequency	507.2Hz	500.8Hz

Table H.1: Comparison of Inductance, capacitance and resonance frequency calculated and DIgSILENT values.

It is seen that the calculated frequencies are close to the values from DIgSILENT.

Representing a transmission line by lumped parameters may lead to inaccurate results, because for a transmission line the parameters are distributed along the line. Therefore the effect of lumped parameter representation is studied in the following.

H.1.1 Transmission line representation

To show the effect of using lumped parameters the following analysis will compare one, three and ten cascade coupled π-section. The cascade coupled π-section representation is compared to the exact π-model, which is often used as reference for validation of line models in the frequency domain [16].
The comparison is carried out for the actual screen circuit, using the parameters calculated in the previous section.

For an transmission line the series impedance and shunt admittance are uniformly distributed along the line as shown in figure H.8 [28, p.243].

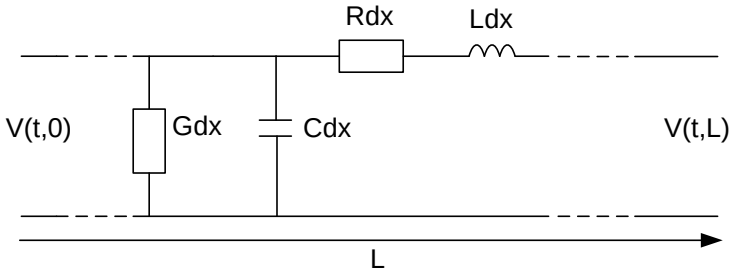

Figure H.8: Transmission line with parameters distributed along the line.

Where Rdx is the resistance per dx length, Ldx is the inductance per dx length, Cdx is the capacitance per unit length and Gdx is the conductance per unit length.

Using the approach presented in [53], the voltage and current may be expressed as equation H.17 and H.18.

$$V(x) = cosh(\gamma x)U_r + Z_c sinh(\gamma x)I_r \quad [\mathrm{V}] \quad \text{(H.17)}$$

$$I(x) = \frac{1}{Z_c} sinh(\gamma x)U_r + cosh(\gamma x)I_r \quad [\mathrm{A}] \quad \text{(H.18)}$$

Where U_r and I_r is the receiving end voltage and current. Z_c is the characteristic impedance and given in equation H.19 and γ is the propagation constant determined by equation H.20 [28, p.245].

$$Z_c = \sqrt{\frac{Z}{Y}} = \sqrt{\frac{R + j\omega L}{G + j\omega C}} \quad [\Omega] \quad \text{(H.19)}$$

$$\gamma = \sqrt{ZY} = \sqrt{(R + j\omega L)(G + j\omega C)} = \alpha + j\beta \quad [1/\mathrm{m}] \quad \text{(H.20)}$$

I order to use the transmission line model in connection with other systems, the an equivalent π-mode is typically used, this is shown in figure H.9.

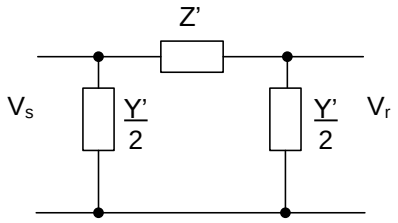

Figure H.9: π representation of the equivalent π model.

Where Z' is defined by equation H.21 and Y' by equation H.22.

$$Z' = Z\frac{sinh(\gamma x)}{\gamma L} \qquad [\Omega/\mathrm{m}] \quad \text{(H.21)}$$

$$\frac{Y'}{2} = \frac{Y}{2}\frac{tanh(\frac{\gamma L}{2})}{\frac{\gamma L}{2}} \qquad [S/\mathrm{m}] \quad \text{(H.22)}$$

Where:
$Z = (R + jx)L$. L is the total transmission line length.
$Y = (G + jB)L$. L is the total transmission line length.
L is the total length of the transmission line.
γ is the propagation constant given in equation H.20.

Using equation H.21 and H.22 result in correct calculation of voltages and currents at the cable terminations [53]. The voltage and currents, at the frequency to which the parameters are tuned, will be accurate because this lumped parameter representation are taking into account, the travelling wave theory.

Often the simplified version nominal π-model is used instead of the equivalent π-model. In the nominal π-model the series impedance and shunt admittance are not recalculated by equation H.21 and H.22. Instead the series impedance and shunt admittance per unit length is used directly for calculation of the parameters (Z and Y). This lumped representation reduces the accuracy of the model. In order to compensate for the accuracy a number of nominal π-sections may by cascade coupled, where the parameters are equal divided between all π sections.

H.1.2 Effect of lumped parameters

Figure H.10(a) shows the equivalent π-model, and the nominal π-model is shown in figure H.10(b). In both circuits there are included an load impedance Z_L which is set to 1Ω.

The input impedance of the equivalent π-model is calculated as equation H.23:

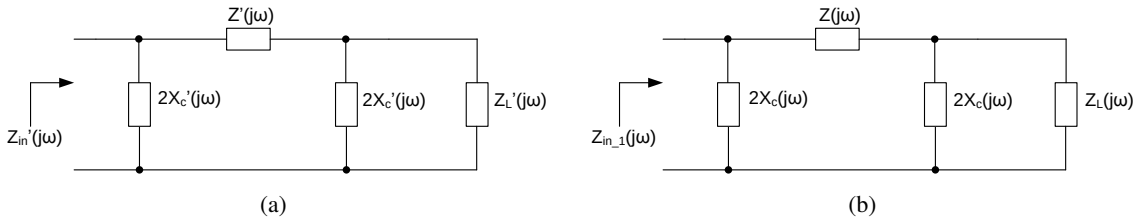

Figure H.10: (a) input impedance of equivalent π-model. (b) input impedance of nominal π model.

$$Z'_{in} = [Z'_L(j\omega)||2X'_C(j\omega) + Z'(j\omega)]||2X'_C(j\omega) \quad [\Omega] \quad \text{(H.23)}$$

Where:
$X'_C(j\omega) = \frac{1}{Y'(j\omega)}$.

The input impedance of the nominal π-model is calculated as equation H.24:

$$Z_{in,1} = [Z_L(j\omega)||2X_C(j\omega) + Z(j\omega)]||2X_C(j\omega) \quad [\Omega] \quad \text{(H.24)}$$

The input impedances of two cascade coupled nominal π-sections, are calculated by replacing Z_L in the first model by the input impedance of the second, as shown in equation H.25

$$Z_{in,2} = [Z_{in,1}(j\omega)||2X_C(j\omega) + Z(j\omega)]||2X_C(j\omega) \quad [\Omega] \quad \text{(H.25)}$$

The cascade of n π-sections are performed by repeating the above procedure n times.

The impedances are calculated for a frequency spectrum of $0-2000$Hz and shown in figure H.4. The figure compare one, three and ten nominal π-sections to the equivalent π-model. In the frequency spectrum there is also seen the result for using only the domination components of the circuit.

The input impedance of the representation by the domination components are performed using equation H.26, based on figure H.11.

$$Z_{in-D} = [Z_L(j\omega) + Z(j\omega)]||X_C(j\omega) \quad [\Omega] \quad \text{(H.26)}$$

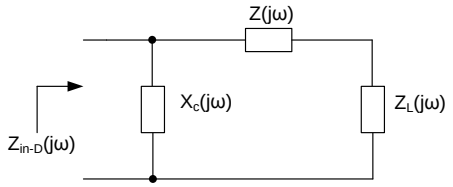

Figure H.11: Equivalent line diagram using domination components.

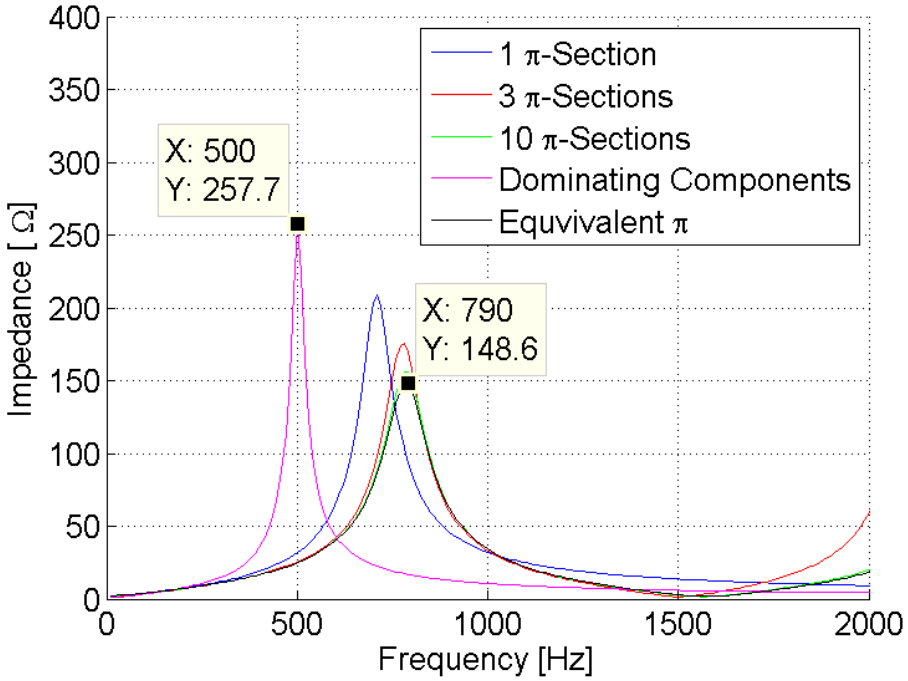

Figure H.12: Frequency spectrum of one, three, ten, equivalent pi, and domination components model.

From figure H.12 it is seen that the peak of the domination components matches well the resonance frequencies calculated in the preceding section (510Hz). It is also seen that the three cascade coupled π-sections, which is used by DIgSILENT, matches the frequency response generated by DIgSILENT in figure H.13 (800Hz).

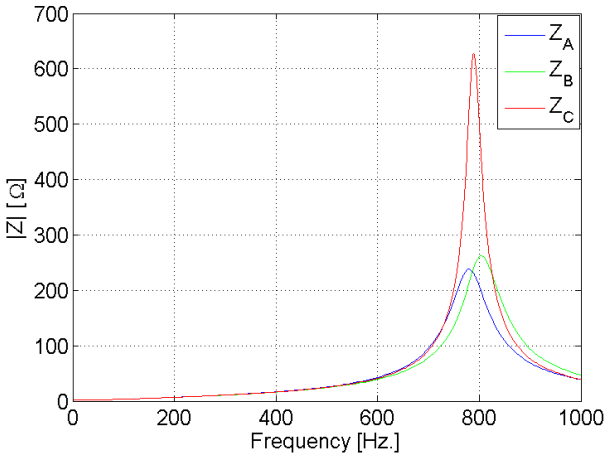

Figure H.13: DIgSILENT frequency sweep.

Therefore the exact resonance points may not be determined only based on the domination components, but an indication of the location may be obtained.